TARGETING DIABETIC VASCULAR COMPLICATIONS USING A NOVEL RAT MODEL FOR DIABETIC RETINOPATHY

By

Inesa Lelyte, MSc

A thesis submitted to

The University of Birmingham for

the degree of

DOCTOR OF PHILOSOPHY

Inflammation and Ageing

College of Medical and Dental Sciences

The University of Birmingham

February 2024

ABSTRACT

Aims

Diabetic retinopathy (DR) is a prevalent microvascular complication of diabetes, emerging as a primary cause of vision impairment and blindness in the working-age population. Many mechanisms of DR remain incompletely understood, and existing treatments are limited. Animal models serve as an invaluable tool for advancing our knowledge of DR and identifying novel interventions for this sight-threatening disease. However, current animal models fall short of reflecting the entire spectrum of DR. The aim of this PhD research project is to develop a novel rat animal model that replicates the pathophysiology of both proliferative and non-proliferative DR. The current gold standard streptozotocin (STZ)-induced DR animal model was also assessed.

Methods

A systematic literature review was performed to outline both structural and functional readouts in the rodent STZ-induced DR animal model. A follow-up experimental study was undertaken in the STZ-induced Brown Norway (BN) rats to characterize changes in the ocular structure and functional activity following injection. In the pursuit of developing a novel preclinical model relevant to DR, the feasibility of cumate-inducible lentiviral (LV) vectors mediating vascular endothelial grow factor (VEGF-A) expression was evaluated in retinal pigment epithelial cells (ARPE-19), and the tolerability of cumate was tested in Wistar rat eyes after intravitreal delivery. Finally, intravitreally injected adeno-associated virus (AAV) vectors encoding *Vegf-a* were investigated in BN rats, and the efficacy of aflibercept (Eylea®) as a therapeutic intervention was assessed within this model.

Results

Systematic literature review highlighted electroretinography (ERG) as the most consistent functional redout in rodent STZ-induced DR, revealing high risk of bias in selected studies. A detailed examination of STZ-induced BN rats revealed consistent morphological changes and visual deficits post-injection, though it primarily mirrored only the early stages of DR. Cumate-inducible LV expression of VEGF-A in ARPE-19 cells led to enhanced cell proliferation, viability, permeability, and migration in tube-like structures. However, the observed retinal toxicity following intravitreal injection of cumate in Wistar rat eyes made the use of cumate-inducible LV impractical for further *in vivo* DR studies. Intravitreal injection of AAV vectors mediating human VEGF-A expression resulted in DR-like vascular pathology in Brown Norway rat retinas, along with reduced retinal activity, and heightened immune cell reactivity. The administration of aflibercept effectively ameliorated these effects, thereby confirming the translational applicability of this newly established model.

Conclusion

The findings described in this thesis explore the prevalent STZ-induced DR animal model and successfully culminate in the development of a novel rat model replicating the main pathophysiological features of DR. The newly established easy-to-use AAV-induced rat model recapitulates several DR-related phenotypes and serves as an attractive tool to gain valuable insights into the underlying molecular mechanisms of DR pathologies and for testing novel therapeutic strategies.

ACKNOWLEDGEMENTS

The title page may say "by Inesa Lelyte" but behind the scenes, there is an incredible amount of people who played a crucial role in bringing this thesis to life.

I would like to express my deepest gratitude to my supervisors, Dr. Giedrius Kalesnykas and Prof. Dr. Zubair Ahmed, for their guidance and insightful feedback throughout the entire research process. Their expertise and encouragement played an important role in shaping both this thesis and me as a scientist. They are the ones who meticulously reviewed every sentence, answered every question, and inspired me to delve deeper.

I was fortunate to have mentors like Dr. Symantas Ragauskas and Dr. Vidhya R Rao, whose knowledge and support have been instrumental in this journey. They patiently guided me through every step, generously sharing their own experiences along the way. Not only it has been a pleasure to work with you both as well as share our life stories, but I also learned so much from you, and I will always be grateful.

I am also indebted to my colleagues at Experimentica, whose collaboration in conducting experiments helped me to bring this thesis to its final form. Kernius and Robertas, the exchange of our ideas and shared enthusiasm created a stimulating environment for me to go further. Tomas, as I told you once before, you are an excellent ERG specialist and in times my personal therapist. A special appreciation goes to Anita, my experience at Loyola University Chicago was enriched by our discussions and laughs, and I am thankful to have found a friend for a lifetime. The list of Experimentica people would go on but due to limited space, a huge thank you to all of you that I have not mentioned.

A heartfelt thank you to my mother, whose endless love and encouragement have been my anchor. Your belief in my abilities provided the strength and motivation essential to move forward in this academic journey. And of course, huge appreciation to my little sister, whose youthful yet wise perspective inspired me to strive for the best. My only wish is that I have set a good example for you.

In addition, I extend my appreciation to my friends who stood by me with humour and a listening ear during the challenging moments. Karolina and Kotryna, your friendship has been a constant source of inspiration and joy, transforming this academic path into a more enjoyable experience.

Lastly, I would like to express my gratitude to the ORBITAL Marie Sklodowska-Curie Innovation Training Network and its participants for enriching this academic experience, allowing me to conduct my research abroad, participate in various workshops, and establish valuable connections with other scientists.

LIST OF PAPERS AND ABSTRACTS

This thesis presents the following papers which correspond to the:

- **Lelyte I**, Ahmed Z, Kaja S, Kalesnykas G. Structure–Function Relationships in the Rodent Streptozotocin-Induced Model for Diabetic Retinopathy: A Systematic Review. Journal of Ocular Pharmacology and Therapeutics. 2022 May 1;38(4):271-86. (Chapter 2).
- **Lelyte I**, Cerrada-Gimenez M, Ghosh A K, Ahmed Z, Kaja S, Kalesnykas G. Structure–Function Relationships in the Brown Norway Streptozotocin-Induced Model of Diabetic Retinopathy. Manuscript in preparation (Chapter 3).
- **Lelyte I**, Rao V R, Kalesnykas G, Ragauskas S, Kaja S, Ahmed Z. Cumate-Inducible Lentivirus as a Tool for Investigating VEGF-A-Mediated Pathology in Diabetic Retinopathy: Prospects and Limitations. Scientific Reports, 2024 Jun 21;14(1):14325. (Chapter 4).
- **Lelyte I**, Ragauskas S, Paulauskas T, Litvinaviciute D, Ahmed Z, Kaja S, Kalesnykas G. AAV-Mediated Human VEGF Expression as a Novel Rat Model of Diabetic Retinopathy. Manuscript in preparation (Chapter 5).

In addition, the following abstracts arose from this thesis:

- **Lelyte I**, Cerrada-Gimenez M, Ghosh A K, Ahmed Z, Kalesnykas G, Kaja S. Structure-function relationships in the Brown Norway rat streptozotocin-induced diabetic retinopathy model. Society for Neuroscience (SfN), hosted online, November 2021.
- **Lelyte I**, Cerrada-Gimenez M, Ghosh A K, Ahmed Z, Kalesnykas G, Kaja S. Detailed characterization of vascular abnormalities in the Brown Norway rat streptozotocin-

induced diabetic retinopathy model. Retina 2021, Fighting Blindness, hosted online, November 2021.

- **Lelyte I**, Cerrada-Gimenez M, Ghosh A K, Ahmed Z, Kalesnykas G, Kaja S. Structure-function relationships in the Brown Norway rat streptozotocin-induced diabetic retinopathy model. St. Albert's Day, Loyola University Chicago, Chicago, USA, November 2021.
- **Lelyte I**, Rao VR, Ahmed Z, Kalesnykas G, Kaja S. Development of human retinal pigment epithelial cells with inducible VEGF expression. ARVO, Denver, CO, USA, May 2022. Investigative Ophthalmology & Visual Science. 2022 Jun 1;63(7):3608-A0063.
- **Lelyte I**, Ragauskas S, Paulauskas T, Ahmed Z, Kaja S, Kalesnykas G. AAV-mediated expression of human VEGF-A as a novel rat model of diabetic retinopathy. ARVO, New Orleans, LA, USA, April 2023. Investigative Ophthalmology & Visual Science. 2023 Jun 1;64(8):1820.

The following oral presentations arose from the work presented in this thesis:

- **Lelyte I**, Cerrada-Gimenez M, Ghosh A K, Ahmed Z, Kalesnykas G, Kaja S. Targeting diabetic vascular complications using a novel rat model for diabetic retinopathy. Month 18 ORBITAL-ITN Meeting, hosted online, March 2021.
- **Lelyte I**, Ragauskas S, Paulauskas T, Ahmed Z, Kaja S, Kalesnykas G. AAV-mediated expression of human VEGF-A as a novel rat model of diabetic retinopathy. Pharmaceutical drug discovery: lessons from ophthalmology. Vilnius, Lithuania, May 2023.

TABLE OF CONTENTS

LIST OF FIGURES

Chapter two:

Chapter three:

Chapter four:

Chapter five:

LIST OF TABLES

Chapter one:

Chapter two:

Chapter four:

LIST OF ABBREVIATIONS

AAV	Adeno-associated virus
AGEs	Advanced glycation end products
BN	Brown Norway
BM	Basement membrane
BRB	Blood retinal barrier
CymR	Cumate repressor
CNV	Choroidal neovascularization
CuO	Cumate operator
DAG	Diacylglycerol
DME	Diabetic macular edema
DR	Diabetic retinopathy
ECs	Endothelial cells
ERG	Electroretinography
FA	Fluoresceine angiography
FDA	Food and Drug Administration
fERG	Flash electroretinography
GCL	Ganglion cell layer
H&E	Hematoxylin and eosin

HbA1c	Hemoglobin A1c
HFD	High-fat diet
HIF-1	Hypoxia-inducible factor 1
HIV-1	Human immunodeficiency virus 1
ICAM-1	Intracellular adhesion molecule 1
IDF	International Diabetes Federation
INL	Inner nuclear layer
IPL	Inner plexiform layer
ITRs	Inverted terminal repeats
IVT	Intravitreal injection
LV	Lentivirus
LTRs	Long terminal repeats
MA	Microaneurysm
NFL	Nerve fiber layer
NPDR	Non-proliferative diabetic retinopathy
NV	Neovascularization
OCT	Optical coherence tomography
OCT-A	Optical coherence tomography angiography
OE	Ophthalmic examination

OIR	Oxygen-induced retinopathy
OPs	Oscillatory potentials
OPL	Outer plexiform layer
PDR	Proliferative diabetic retinopathy
PIGF	Placental growth factor
PKC	Protein kinase C
RGCs	Retinal ganglion cells
RPE	Retinal pigment epithelium
SD-OCT	Spectral-domain optical coherence tomography
STZ	Streptozotocin
T1D	Type one diabetes
T2D	Type two diabetes
TNF-α	Tumor necrosis factor alpha
VFP	Vitreous fluorophotometry
VEGF	Vascular endothelial growth factor
VEGFR-1	Vascular endothelial growth factor receptor 1
VEGFR-2	Vascular endothelial growth factor receptor 2
VCAM-1	Vascular cell adhesion molecule 1
VSV-G	Vesicular stomatitis virus glycoprotein G

CHAPTER 1

GENERAL INTRODUCTION

1.1 Diabetes

Diabetes has become one of the most common chronic diseases of our times, giving rise to life-threatening complications and causing a significant economic burden.[1,2] The impact extends globally, with the International Diabetes Federation (IDF) estimating a 10.5% prevalence of diabetes in 2021, affecting 536.6 million people within the age group of 20 to 79 years, and projecting an increase to 12.2% (783.2 million) by 2045.[3] In addition, the American Diabetes Association® assessed the financial burden of living with diabetes in the United States, reporting healthcare expenditures amounting to 412.9 billion USD,[4] while IDF revealed a global total of 966 billion USD associated with diabetes-related expenses, in 2021.[3] This underscores the pressing need for comprehensive global efforts to address the challenges posed by the escalating prevalence of diabetes.

Diabetes is a collection of metabolic conditions, all characterized by elevated blood glucose levels (known as hyperglycemia) resulting from issues with insulin secretion, insulin action, or both.[5] This group of conditions can be subdivided into two main categories presenting distinct characteristics: type 1 (T1D), and type 2 (T2D) diabetes. Type 1 diabetes accounts for 5% to 10% of all cases of diabetes and is a consequence of autoimmune beta (β)-cell destruction in the pancreas, resulting in complete lack of insulin production.[6] T2D, the most common type, accounting for 90% to 95% of all cases, begins when the body becomes resistant to insulin action or does not produce enough insulin to maintain glucose homeostasis.[7] In the absence of sufficient insulin, cells have difficulty taking up glucose, therefore glucose accumulates in the bloodstream, leading to hyperglycemia.

Both T1D and T2D have the potential to cause serious diabetic complications, broadly classified as macrovascular or microvascular depending on the underlying pathophysiology.

Macrovascular complications include cardiovascular, cerebrovascular, and peripheral arterial diseases. The pathophysiology of macrovascular complications in diabetes involves hyperglycemia, increased oxidative stress, and chronic inflammation, significantly contributing to the development and progression of atherosclerosis — plaque formation and the narrowing of arterial walls. Accumulation of plaque in large arteries increases the risk of cardiovascular disease, the primary cause of death in people with type 2 diabetes (> 70%).[8] In addition, atherosclerotic plaques contribute to compromised blood flow to the brain, heightening the likelihood of cerebrovascular complications, such as stroke. Diabetic patients are 3 times more susceptible to stroke than non-diabetic,[9] and poststroke outcomes are poorer in those with uncontrolled glucose levels.[10,11] Peripheral arterial disease (PAD) involves narrowing of peripheral vessels of the upper and lower limbs, which is associated with claudication (pain, ache, or discomfort that may occur while moving), impaired wound healing, and an increased risk for limb amputation.[12,13] PAD is 2- to 7-fold more prevalent in people with diabetes than in those without it.[14]

The triad of microvascular complications, diabetic neuropathy, nephropathy, and retinopathy,[15] exhibit a higher prevalence compared to the macrovascular complications.[16] Diabetic neuropathy, mediated by hyperglycemia, affects approximately 50% of people with diabetes and is classified based on the specific parts of the nervous system that are affected.[17] The most common presentation of neuropathy in diabetes is chronic sensorimotor distal polyneuropathy, involving length-dependent peripheral nerve dysfunction and resulting in sensations of numbness, tingling, and/or pain in patients' hands and lower limbs.[18,19] Another microvascular complications of hyperglycemia is diabetic nephropathy, which stands as the leading cause of end-stage renal disease worldwide, occurring in 20% to 40% of individuals with diabetes.[20,21] Early symptoms of diabetic nephropathy involve increased albumin protein excretion in the

urine (known as microalbuminuria), which can progress to persistent proteinuria (>500 mg of protein in 24 hours), potentially leading to renal failure.[22]

1.2 Diabetic retinopathy (DR)

Diabetic retinopathy is the most common microvascular complication among people with diabetes, holding the position as the primary cause of vision impairment and blindness among the working-age adult population.[23,24] It was estimated that the number of people with DR will rise from 103.12 million in 2020 to 160.50 million by the year 2045.[25] The main risk factors for DR include duration of diabetes, poor glycemic control, and the presence of hypertension. Nearly every patient diagnosed with T1D is likely to develop some degree of DR within two decades after diagnosis, while likelihood for those with type 2 diabetes is approximately 80%.[26,27] Individuals with poor glycemic control are more sensitive to DR development and progression, while glycemic management can significantly reduce the risk of the disease. Maintaining blood glucose concentrations close to the normal range decreases the risk for the development of diabetic retinopathy by 76% and slows the progression of existing retinopathy by 54%.[28] Also, it has been reported that keeping HbA1c (glycated haemoglobin A1c) levels below 7.6% as a treatment target prevents DR for up to 20 years in T1D patients.[29] In addition, elevated blood pressure is associated with DR and controlling hypertension can help manage this risk.[30,31] Antihypertensive therapy, specifically inhibitors of angiotensin-converting enzyme, slowed the progression of retinopathy in type 1 diabetic patients by 50% over a 2-year period.[32] Other risk factors such as age, sex, and hyperlipidemia (elevated level of lipids and fats in blood) were variably associated with DR.[26,30,33,34]

1.2.1 Clinical classification of DR

Diabetic retinopathy can be clinically classified into non-proliferative (NPDR) and proliferative diabetic retinopathy (PDR).[35] Depending on the presence of retinal microvasculature changes, NPDR can be categorized into mild, moderate, and severe forms. The onset and progression of DR is gradual, starting from mild NPDR, identified when at least one retinal microaneurysm (MA) appear. Moderate NPDR is characterized by multiple microaneurysms or intraretinal hemorrhages in one to three retinal quadrants (superior, nasal, temporal, or inferior), and/or the presence of cotton wool spots, hard exudates, or venous beading.[36] Severe NPDR diagnosis is made based on the "4-2-1" criteria from the Early Treatment Diabetic Retinopathy Study (ETDRS), where patient has one of the following: intraretinal microaneurysms or hemorrhages in all 4 retinal quadrants, venous beading in 2 or more quadrants, or intraretinal microvascular abnormalities (IRMA) in 1 or more quadrant.[37] During the severe NPDR stage, the risk to develop proliferative diabetic retinopathy heightens by 50% within 1 year.[38]

The most advanced and sight-threatening stage of DR is proliferative diabetic retinopathy, characterised by neovascularization (NV) on the optic nerve (new vessels at the disk) or elsewhere in the retina (new vessels elsewhere).[36] These newly formed vessels are fragile and prone to leakage and bleeding, leading to preretinal or vitreous hemorrhages, resulting in vision impairment.[39] In response to neovascularization, fibrous or scar tissue may develop, which can contract and pull the neurosensory retina from the retinal pigment epithelium (RPE) layer, leading to a condition called tractional retinal detachment, contributing to total vision loss.[40]

Another major common vision-threatening complication of DR is diabetic macular edema (DME), which involves swelling and thickening of the macular area, a consequence of intraretinal fluid accumulation due to increased vascular permeability.[41] Although DME has

three severity levels, it can be present with any level of diabetic retinopathy but appears to occur more frequently as the severity of DR increases.[42]

1.2.2 Pathological features of DR

One of the earliest pathological events in DR is alterations in the cellular structure of retina microvasculature. Endothelial cells (ECs), forming a smooth inner lining of retinal blood vessels, play a major role in the maintenance of blood vessel integrity, regulating arterial blood pressure, and controlling the exchange of nutrients and waste products between the blood and surrounding tissues.[43] ECs are connected through tight, gap and adherens junctions, creating a continuous and impermeable blood-retinal barrier (BRB) along the blood vessels. However, chronic hyperglycemic exposure during diabetes mediates the loss of endothelium integrity and dysregulation of endothelial cell-to-cell junctions, resulting in inadequate blood supply (ischemia) and insufficient oxygen supply (hypoxia) to the retina.[43,44] The BRB is divided into inner and outer parts. The inner blood–retina barrier, consisting of ECs and accompanied by pericytes, astrocytes, and Müller cells, is essential for maintaining the microenvironment of the inner layers of the retina. In contrast, the outer BRB is composed of RPE cells interconnected by tight junctions and act as a filtration system, regulating passage of solutes and nutrients from the bloodstream.[45] Hyperglycemia-induced hypoxic conditions result in structural and functional defects of the BRB, leading to both inner and outer blood-retinal barrier breakdown. Compromised BRB integrity can result in increased vascular permeability, allowing plasma and blood components to leak into the retinal tissue. This leakage contributes to the accumulation of hard exudates (lipid deposits) in the retina, and formation of retinal edema, commonly observed in DR.[46,47] Moreover, excess of glucose induces synthesis of vascular basement membrane (BM) components, contributing to vascular BM thickening.[48] In addition, inadequate blood and oxygen supply to the retina, including to the nerve fiber layer (NFL), leads to the

formation of nerve fiber infarcts known as cotton wool spots, recognized as an early sign of DR.[49] Another essential retinal cell type in the development and progression of DR is pericytes, which are mural cells of blood microvessels lying on the capillaries and separated from ECs by BM. Due to hyperglycemia-induced retinal ischemia and hypoxia, signalling pathways between ECs and pericytes are disturbed, resulting in pericytes apoptosis and the formation of pericyte "ghosts" — intramural pockets lacking normal cell contents.[50,51] Pericytes degeneration and the consequent loss of mechanical support for capillary walls lead to the development of acellular capillaries and microaneurysm[52]. MAs are hypercellular saccular outpouchings from the capillary wall that are prone to leakage. Microaneurysms are usually the earliest visible manifestation of diabetic retinopathy and serves as the hallmark in the clinical diagnosis of DR.[53] Moreover, during the progression of DR, manifestations of venous beading, involving narrowing or dilation of retinal veins, become apparent,[54] as well as vascular tortuosity — twisting of retinal blood vessels.[55]

A crucial pathological event in DR involves the growth of new blood vessels originating from existing ones, a phenomenon known as angiogenesis. The initial trigger for pathological angiogenesis in DR is ischemia and hypoxia. In response to these conditions, the retina releases multiple pro-angiogenic factors, including vascular endothelial growth factor (VEGF), placental growth factor (PIGF), angiopoietin-2, and neuropilin-1, which cooperatively promote retinal neovascularization, a characteristic feature of PDR.[56–58] Notably, the overexpression of VEGF-A has been identified as a potential mediator of NPDR, and key initiator of proliferative diabetic retinopathy.[59]

Although most of DR research focuses on the breakdown of the inner blood-retina barrier, studies have also shown that diabetes and hypoxia compromise the outer BRB as well, which is constituted by tight junctions between retinal pigment epithelium cells.[60,61] RPE is a

monolayer of pigmented cells located between the outer segments of photoreceptors and the choroid. By forming outer BRB, RPE cells are responsible for maintaining structural and functional integrity of photoreceptors, transporting nutrients, ion and water, and secreting neurotrophic factors.[62] However, diabetic retinopathy patients exhibit structural changes in the outer retina, including the thinning of the RPE layer, suggesting loss and degradation of RPE cells during the disease progression.[63,64] Additionally, both morphological[65,66] and functional[67,68] abnormalities of RPE cels have been reported in diabetic animals. To assess the significance of the outer BRB breakdown in DR, researchers injected streptozotocin-induced rodents with fluorescein isothiocyanate (FITC)-dextran and visualized retinal leakage using fluorescent microscopy.[60] This assay suggested that the outer BRB accounted for more than one-third of the total retinal leakage in diabetic retinas. Furthermore, another study found that disrupting VEGF signaling in the mouse RPE significantly reduced diabetes-induced vascular leakage and inflammation.[61] Therefore, although majority of DR research focuses on the breakdown of the inner BRB, these finding address the importance of the outer BRB and RPE cells in diabetic retinopathy.

1.2.3 Biochemical and molecular mechanisms involved in the pathogenesis of DR

Although the mechanisms driving the development of DR are complex and remain incompletely understood, it is observed that increased glucose flux and hyperglycemia-induced oxidative stress has an important role in retinal vascular damage.[69] Overproduction of mitochondrial reactive oxygen species (ROS) promotes the activation of polyol, hexosamine, and protein kinase C (PKC) pathways, as well as production of advanced glycation end-products (AGEs) and increased expression of AGE receptors.[70–72] Polyol pathway is a metabolic pathway where excess of glucose is reduced to sorbitol. Sorbitol, being a highly hydrophilic alcohol, cannot diffuse through lipid membranes, as a result, it accumulates and causes osmotic pressure,

leading to cell damage, including vascular endothelial cells in retina.[70,73] In addition, in response to hyperglycemia hexosamine pathway is activated as an alternative to the glycolysis, resulting in excess protein glycosylation that leads to alterations in protein function and gene expression, further aggravating oxidative stress, and inducing apoptosis of endothelial cells.[70,74] Furthermore, hyperglycemia results in the enhancement of diacylglycerol (DAG) synthesis, which is a critical activator of various isoforms of PKC in the cells. DAG-induced hyper-activation of PKC was found to result in cytokine activation, endothelial cell dysfunction, increased vascular permeability and abnormal angiogenesis.[75,76] Finally, chronic exposure to hyperglycemia promotes the non-enzymatic glycosylation of macromolecules, such as proteins and lipids, which leads to the formation and accumulation of advanced glycation end products.[70] It has been found that accumulation of AGEs and increased expression of AGE receptors together with their activating ligands induce endothelial cells damage and pericytes loss, elicits ROS generation, and amplifies inflammation.[77–79] All these metabolic pathways are interrelated with each other and with ROS production, creating a vicious cycle that contributes to the progression of DR.

While diabetic retinopathy is considered a microvascular disease, current research shows that chronic low-grade inflammation plays and important role in the disease's pathogenesis.[80–82] Infiltration of inflammatory cells, coupled with the expression of chemokines and cytokines, affects neuronal and vascular components of the retina, resulting in retinal edema, neovascularization or damage of retinal cells.[81] Recent studies suggest that leukocytes (white blood cells) may play an important role in the development of DR. Diabetes-induced expression of adhesion molecules, such as intracellular adhesion molecule-1 (ICAM-1), vascular cell adhesion molecule-1 (VCAM-1), and P-selectin, facilitates leukocyte-endothelial cell adhesion (leukostasis), resulting in endothelial cells damage, breakdown of BRB, and increased vascular

permeability of retinal vessels.[83,84] Moreover, hypoxia-activated retinal cells produce inflammatory chemokines and cytokines, including interleukin (IL)-1β, interleukin-6, interleukin-8, tumor necrosis factor-α, and monocyte chemoattractant protein-1, all of which have been found to be elevated in the vitreous and serum of DR patients.[85,86] Animal model showed that angiogenic responses of endothelial cells were regulated not only by growth factors (such as VEGF-A), but also by inflammatory cytokines, resulting in the development of new vessel.[87,88] In addition, findings from *in vitro* research indicate that endothelial cells respond to cytokines rather than high glucose, suggesting that diabetes-associated endothelial alterations may be attributed to glucose-induced release of cytokines, rather than direct impact of excess of glucose.[89]

Molecular analyses have become essential tools in investigating these complex biochemical and molecular mechanisms in DR. Techniques such single-cell RNA sequencing (scRNA-seq) enables to study gene expression at the level of individual cells, which can provide detailed insights into specific molecular mechanisms that contribute to DR pathogenesis and facilitate novel therapeutic approaches. For instance, by using scRNA-seq on the retinas of streptozotocin (STZ)-induced diabetic mice, Sun et al.[90] identified a distinct subpopulation of endothelial cells characterized by the activation of inflammation-associated signaling pathways, including interleukin-17, tumor necrosis factor (TNF), and necrosis factor-kappa B (NF-κB). In a separate study by Ben et al.,[91] endothelial cells were classified into three clusters, one of which being strongly associated with angiogenesis and inflammation in STZ-induced animals. Moreover, activated microglia subpopulation have been identified within the retina of STZ-induced diabetic mice, expressing IL-1β and TNF, which contribute to inflammation in early DR.[92] In addition to inflammation, a subpopulation of microglia cells have been found to release fibroblast growth factor 2, which acts on endothelial cells and induce retinal

neovascularization.[93] Other retinal cell subpopulations, such as pericytes, have been observed to express high levels of genes related to extracellular matrix remodeling in oxygen-induced neonatal mice.[94] Overall, the use of scRNA-seq has enabled researchers to identify key retinal cell subpopulations in DR, and targeting these clusters may facilitate the development of novel therapies to prevent the progression of the disease. In addition to single-cell RNA sequencing, proteomic analysis has emerged as a tool to identify DR biomarkers in patients' biofluids, including aqueous humor, vitreous humor, tear, and serum.[95] A wide range of biomarkers associated with DR has been identified, such as ICAM-1, IL-6, and VEGF.[96–100] However, a leading limitation of proteomic analysis lies in it the challenges to obtain control samples of aqueous humor and vitreous humor, as these require invasive procedures that are typically performed on patients. Furthermore, microRNAs, a major class of short (∼22 nucleotides) non-coding RNAs, have been shown to regulate gene expression and signaling pathways involved in the pathology of diabetic retinopathy.[101,102] By targeting multiple messenger RNAs (mRNAs) in the 3' untranslated region (UTR) sites of those mRNAs, microRNAs regulate gene expression, control signaling pathways and other cellular functions in DR.[103] For instance, the overexpression of microRNA-21 contributes to diabetes-induced endothelial cell disfunction and low-grade inflammation.[104] Whereas microRNA-216a showed a protective effect on endothelial cells in STZ-induced Sprague-Dawley rats.[105] Additionally, microRNA-203a-3p has been found to inhibit retinal angiogenesis an attenuate proliferative DR in an oxygen-induced retinopathy rat model by targeting VEGF-A and hypoxia-inducible factor 1 (HIF-1).[106] Circulating miRNAs in the bloodstream have also emerged as valuable blood-based biomarkers for the diagnosis of this disease. [107] Therefore, microRNAs could be considered potential biomarkers and pharmacological targets for the diagnosis and treatment of DR. However, identification of miRNAs through miRNA microarray can be costly and typically requires

validation with quantitative PCR (qPCR). Consequently, in silico analysis has become an important approach for efficiently predicting miRNA involvement in DR.[108,109] Platania et al.[109] carried out an in-silico analysis to identify a set of microRNAs that are potentially involved in diabetic retinopathy and checked those microRNAs in STZ-induced diabetic mice retinas. Eight microRNAs were significantly dysregulated in STZ-induced mice retina and serum. These microRNAs modulated VEGF, cyclic AMP response element-binding protein 1 (CREB1), brain-derived neurotrophic factor (BDNF), and peroxisome proliferator-activated receptors -α (PPAR-α) expression, in the retina of diabetic mice. Additionally, by using gene expression datasets, such as those available in the Gene Expression Omnibus (GEO) database, researchers aim to identify key genes and dysregulated biological pathways associated with diabetic retinopathy.[110–112] This approach not only enhances understanding of the mechanisms driving DR but also provides potential novel drug targets for therapeutic interventions.

1.2.4 Role of vascular endothelial growth factor (VEGF) in DR

As previously stated, vascular endothelial growth factor plays a pivotal role in the development and progression of diabetic retinopathy. VEGF proteins are a subfamily of growth factors that promote both vasculogenesis (the process by which blood vessels are formed de novo) and angiogenesis (the formation of new blood vessels from pre-existing vasculature).[113] The VEGF family includes VEGF-A, VEGF-B, VEGF-C, VEGF-D, VEGF-E, and PlGF.[114] VEGF-A, which has been studied in the context of DR the most, is a 36–46 kilodaltons glycosylated protein with a N-terminal signal sequence and heparin-binding domain.[53] Depending on the number of amino acids, five different VEGF-A isoforms have been identified: 121, 145, 165, 189, and 206, with VEGF-A isoform 165 being critical in the development and progression of DR.[115] In retina, VEGF-A is produced and secreted from various retinal cells, including ECs, pericytes, RPE cells, retinal ganglion cells (RGCs), astrocytes, and Müller cells.[113,115]

Hyperglycemia-induced ischemia and hypoxia leads to the production of a DNA binding protein HIF-1, which binds to the *Vegf-a* gene and initiates the transcription process.[116] This promotes increased *Vegf-a* mRNA transcription and decreased mRNA degradation, eventually leading to the intracellular accumulation of VEGF-A proteins. VEGF-A binds to two types of receptors: VEGF receptor 1 (VEGFR-1/Flt-1), and 2 (VEGFR-2/KDR/Flk-1) on the surface of endothelial cells.[117] VEGF-A, upon interaction with its receptors on endothelial cells, induces phosphorylation of ECs tight-junction proteins, like occludin, leading to enhanced blood vessel permeability.[118] Moreover, VEGF-A stimulates endothelial cells to release matrix metalloproteinases and urokinase-type plasminogen activator, promoting the breakdown of BRB and facilitating the migration of endothelial cells.[119] Activated endothelial cells then express integrins such as αvβ3 and αvβ5, enabling their migration through the degraded matrix, followed by proliferation of ECs.[120] Subsequently, ECs merge, organize into capillary (tuble-like) structures, and synthesize a new basement membrane. This sequence of events promoted by VEGF-A ultimately results in the formation of new capillaries. However, in hypoxic conditions, there is an overexpression of VEGF-A, leading to the accelerated formation of new vessels, which become fragile and prone to leakage, ultimately contributing to vision impairments in DR patients. High VEGF-A protein levels has been found in vitreous samples from diabetic patients, as compared to control subjects, correlating with the severity of retinopathy.[121,122]

In addition to VEGF's role in angiogenesis, it also functions as a neurotrophic factor, supporting the survival and growth of retinal neurons.[123] VEGF-A receptors are present in retinal neurons, [124,125] suggesting a functional role of VEGF-A in the neural retina. Studies have shown that VEGF-A stimulates axonal outgrowth, enhance cell survival, and proliferation in peripheral nervous system.[126,127] Moreover, VEGF-A secreted by retinal ganglion cells promotes their own

survival.[128] In contrast, inhibiting VEGF-A in healthy rat retinas can lead to significant RGC loss. [128,129] Similarly, neutralizing VEGF in healthy mice has been associated with neural cell death, evidenced by reduced thickness of the inner and outer nuclear layers and decreased retinal function.[130] These results suggest that using VEGF inhibitors for DR treatment can have both beneficial and adverse effects. While anti-VEGF therapies reduce pathological neovascularization and vascular permeability, they may also interfere with VEGF's neuroprotective effects. For instance, intravitreal injections of anti-VEGF in healthy Sprague-Dawley rats resulted in significant RGC death, as compared to vehicle-treated rats.[131] Moreover, anti-VEGF treatment in STZ-induced rats have been shown to induce RGCs, amacrine, and bipolar cells apoptosis.[132] Additionally, multiple intravitreal anti-VEGF injections (5–6 injections) in Akita diabetic mice have been associated with retinal neurodegeneration.[133] Therefore, while anti-VEGF therapy is effective in reducing vascular damage, careful considerations are needed to avoid negative impacts on retinal neurons when administering anti-VEGF treatment to treat DR.

1.2.5 Therapeutic strategies to prevent and treat DR

The National Institute for Health and Care Excellence (NICE) has set recommendations aiming to prevent the onset and progression of diabetic retinopathy. These guidelines focus on educating patients about the disease, providing dietary advice, managing blood glucose levels and blood pressure, and encouraging regular eye screenings.[134] Studies indicate that intensive glycemic control significantly reduces the risk of DR development and slows its progression.[28] For instance, reducing HbA1c levels to below 7% has been correlated with a decreased incidence of microvascular complications, including diabetic retinopathy.[29] Furthermore, studies demonstrate that controlling elevated blood pressure can help to prevent DR in diabetic patients.[30,31] Additionally, early detection through regular eye screening is an essential

preventive measure of DR. Notably, establishing a national screening programme for diabetic retinopathy in England, has successfully reduced its prevalence, such that it is no longer the leading cause of blindness in the country.[135]

For patients with severe non-proliferative diabetic retinopathy to early PDR, therapeutic intervention are proposed, including pan-retinal photocoagulation (PRP), during which non-perfusion areas are destroyed using laser burns, which in turn reduces retinal neovascularization, VEGF production, and the progression of DR.[136–138] PRP has been shown to reduce the risk of severe visual loss by more than 50% in DR patients. However, long-term patient studies have identified peripheral vision loss, delayed dark adaptation, as well as severe pain during the procedure, as notable limitations of PRP.[139–141] This led to an interest in targeted retinal photocoagulation (TRP), a technique involving selective photocoagulation of retinal vascular occlusion areas. TRP has been reported to induce earlier regression of PDR and to be less painful than PRP.[142] However, recent studies suggest that combining laser photocoagulation (whether PRP or TRP) with anti-VEGF therapy may be more effective in reducing neovascularization and delaying vision loss associated with DR, compared to either PRP or TRP monotherapy.[143,144]

Recognition of the VEGF pathway as a pivotal regulator of pathological angiogenesis has led to the development of VEGF-targeted therapeutic interventions. Bevacizumab (Avastin®, Genentech Inc., San Francisco, CA), approved by the US Food and Drug Administration (FDA) to treat specific types of cancer, has been used off-label for the treatment of DR.[145,146] Bevacizumab is a full-length antibody which binds to circulating VEGF-A, thereby inhibiting VEGF-A binding to its receptors. Bevacizumab has been found to be successful in neovascularization regression and resolution of vitreous hemorrhage of PDR patients.[147] In

addition, about three times smaller molecule — ranibizumab (Lucentis®, Genentech Inc., San Francisco, CA) was introduced for treatment of DR. Ranibizumab is an antibody fragment that binds to the receptor-binding site of active VEGF-A, preventing the interaction of VEGF-A with its receptors on endothelial cells. This interference disrupts the VEGF-mediated signaling pathway, consequently suppressing abnormal ECs function and neovascularization.[148] Ranibizumab was approved by the US FDA for the treatment of DR, with a recommended dose of 0.3 mg as an intravitreal injection (IVT) once a month. On the other hand, aflibercept (Eylea®, Regeneron Pharmaceuticals Inc., Tarrytown, NY and the Sanofi-aventis Inc., Paris, France) is a dimeric glycoprotein that acts as a soluble protein decoy for VEGF receptors (VEGFR-1 and VEGFR-2). While ranibizumab and bevacizumab primarily targets VEGF-A, aflibercept binds to VEGF-A and PlGF, inhibiting pathologic angiogenesis, retinal leakage, and inflammation.[149,150] Aflibercept was approved by the US FDA for the treatment of DR, requiring less frequent IVT injections (2 mg administered intravitreally every month for the first 5 injections, followed by 2 mg once every 2 months). However, all presented drugs might cause adverse effects, including eye irritation, temporary blurred vision, ocular pressure, hemorrhage, and vitreous or retinal detachment.[151–154] Therefore, considering the side effects of these drugs, variability in patient response, and the need for frequent injections, encourages further exploration of novel anti-VEGF-A therapies.

1.2.6 Structure – function relationships in the pathogenesis of DR

In addition to vascular alterations, the neurosensory retina undergoes profound changes in diabetic retinopathy. The proper functioning of retinal neurons relies heavily on blood vessels, which supply essential nutrients and oxygen while removing metabolic wastes and carbon dioxide.[155] Therefore, any disturbance in the integrity of the retinal vascular unit can adversely affect the structure and function of retinal neurons, potentially leading to visual impairments.[156]

Although visual deficits in DR typically manifests in the later stages when vascular changes are evident, in some cases, neuronal damage was observed in diabetic patients who showed no signs of vascular alterations.[157–159] Therefore, considering diabetic retinopathy more broadly, as a neurovascular disease, may lead to an improved understanding of the mechanisms underlying vision loss. Neurons (RGCs, bipolar cells, horizontal cells, amacrine cells, and photoreceptors), glial cells (microglia, astrocytes, and Müller cells), and blood vessels together form neurovascular unit, and their coordinated activity is essential for normal vision.[160] Retinal neurons and vasculature are organized in layered structure, with the superficial vascular plexus located in the NFL and GCL (ganglion cell layer), the intermediate vascular plexus between the IPL (inner plexiform layer) and INL (inner nuclear layer), and deep vascular plexus lining the outer surface of the INL, while choroid supplies blood to the outer layers of the retina, including the OPL (outer plexiform layer) and ONL (outer nuclear layer).[155]

Significant deficits during diabetes are found in the inner retina, which consists of bipolar cells, amacrine cells, and RGCs.[161] Additionally, while photoreceptors of the outer retina have not traditionally been considered significant in the pathogenesis of DR (likely due to the spatial separation between photoreceptors and the retinal microvasculature affected during DR), emerging evidence suggests that hyperglycemia-induced changes can indeed lead to structural and functional changes of these cells.[162] Inner and outer retina neurons play a crucial role in visual processing and the transmission of visual information from the retina to the brain. Therefore, disfunction of these cells during DR contributes to visual impairment in the disease.[163] Oxidative stress, hypoxia and inflammation collectively contribute to the impairment of retinal neuron function and eventual loss.[162,164–166]

In addition, Müller cells, the primary glial cell types found in the retina,[167] play a major role in regulating physiological responses in healthy retina and pathological responses during DR.[168] Müller cells spans the whole retina, making contact with the majority of retinal cell types, making them ideally positioned to carry out essential functions in the retina such as maintaining retinal metabolism, supplying nutrients for the retina, regulating blood flow, and maintaining the integrity of the blood-retinal barrier.[168–170] During DR, in high glucose environments, Müller cells start to express glial fibrillary acidic protein, a molecular marker indicating Müller cells injury and reactive gliosis.[171] Activated Müller cells result in abnormal water and potassium transport, leading to swelling of the Müller cells, decreased fluid removal, retinal thickening, and impaired visual function.[170,172] In addition to this, Müller cell-derived VEGF plays an important role during pathologic conditions. It was observed that diabetic mice with knockout VEGF in Müller cells had reduced leukostasis, inflammation, acellular capillaries, and vascular leakage, as compared to diabetic control mice.[173] Similarly, disruption of Müller cell-derived VEGF inhibited ischemia-induced retinal neovascularization and vascular leakage, and attenuated ischemia-induced breakdown of the BRB.[174] In addition to growth factors, Müller cells also secrete various inflammatory cytokines and chemokines, including interleukin-1β, including interleukin-8, and tumor necrosis factor-α, amplifying diabetic retinal inflammation.[175,176] Moreover, upregulation of cell adhesion molecules in Müller cells further disrupts vascular permeability during DR.[177]Additionally, Müller cells play a fundamental role in the survival of retinal neurons by secreting neurotrophins and degrading glutamate during high glucose environment.[178] However, with the progression of DR, imbalance in the expression of neuroprotective factors and failed transport of excessive glutamate can lead to retinal neuronal degeneration in the retina. [179]

Functional deficits in DR patients can be measured using the electroretinogram (ERG) and behavioral visual testing. Focusing on the inner retina, the activity of bipolar cells is reflected by flash ERG (fERG) b-wave amplitude responses, which are found to be decreased in patients with early-stage DR.[180] In patients with advanced DR, b-wave abnormalities become more apparent.[181,182] The ERG oscillatory potentials (OPs) reflect the amacrine cells and their interaction with bipolar cells. Numerous studies indicate that alterations in OPs appear in diabetic patients even before DR-related vascular changes,[183,184] and that reduced or slowed OPs can be correlated with later DR development.[185] Pattern-ERG, which captures RGCs activity, have been found to be attenuated in type 2 diabetics without signs of DR,[186] and in NPDR patients.[187] A decrease in the activity of outer retina photoreceptors (rods and cones) have been observed in individuals with newly diagnosed TD2, even in the absence of visible vascular retinopathy, as assessed through the analysis of ERG a-wave amplitudes.[188] Visual behavioral measurements, including visual acuity and contrast sensitivity tests, which reflect the integration of information in the whole retina, have been found to be affected in patients with DR.[189,190] In addition, loss of color vision and difficulty adjusting to dark environments were present in DR patients,[64,191] or in diabetic patients prior to signs of retinopathy.[192] These results indicate that DR involves not only vascular abnormalities but also dysfunction in multiple types of retinal neurons, and the interplay between structure and function underscores the need for a comprehensive understanding of the mechanisms leading to visual impairment in DR. Additionally, the recognition of early changes in neurosensory retina may act as potential biomarkers for timely detection and intervention in DR.

1.3 Animal models of diabetic retinopathy

While many mechanisms of diabetic retinopathy are still not fully understood and current treatments face resistance in some patients, animal models serve as an invaluable tool for

advancing our knowledge and discovering effective interventions for this vision-threatening condition. Various animal species, including mice, rats, rabbits, cats, dogs, and nonhuman primates, have been used to recapitulate DR-related features. Cats did not develop cataracts upon diabetes, allowing visualization of the fundus via fluoresceine angiography (FA) throughout the study, however DR phenotypes were found to be inconsistent.[193,194] While DR induced in dogs closely mimics human disease, high maintenance cost and long-term follow-up period makes this model less commonly used.[195,196] Nonhuman primates are considered as a potential model in DR research since their eye structure resembles humans, especially the presence of a macula. However, the absence of advanced retinopathies, coupled with high costs, prolonged study durations, and ethical concerns, makes DR investigations in nonhuman primates impractical.[197,198] Rabbits mimic vascular changes observed in DR, including vascular leakage and angiogenesis. Nevertheless, their retinal vasculature differs from those in other species (the optic artery branches into major blood vessels bidirectionally in a horizontal manner), and the duration of DR phenotypes are temporary.[199,200]

Rodent models are commonly chosen in DR investigations due to their cost-effectiveness, shorter lifespan, rapid breeding rates, and ability to develop retinopathies within a relatively short timeframe.[198,201,202] Additionally, particular rodent strains, like Brown Norway (BN) rats, are exceptionally suited for studying DR-related phenotypes such as vascular leakage and neovascularization, due to their pronounced retinal vascularity.[203,204] However, there is no single animal model currently that would replicate the entire spectrum of vascular and neural complications observed in human DR. Various methodologies have been created to induce different stages of DR, including pharmacologic inductions, environmental exposures, as well as genetic and VEGF manipulations, each with its own set of advantages and disadvantages (Table 1).

1.3.1 Pharmacologically induced animal models of DR

By 1942, it was discovered that a single injection of alloxan can induce diabetes in laboratory animals.[205] Alloxan acts directly on insulin-producing beta cells of the pancreas by inhibiting glucokinase, a key enzyme in the glucose-insulin pathway.[206] In alloxan-induced mice, DR-related changes, including formation of acellular capillaries and pericyte ghosts, gliosis of Müller cells, and RGCs loss, occurred within 7 days of induction.[207] Pronounced vascular proliferation and formation of microaneurysms were evident by day 21.[207] Additionally, three months after diabetes onset alloxan-induced mice exhibited a reduction in neuronal cells activity as measured by ERG, and changes in microglia morphology.[208] However, retinal fundus and vessels remained unchanged in this investigation. Similar to the phenotypes observed in mice, alloxan-induced rats develop pericyte ghosts and acellular capillaries, although these manifestations become evident only 18 months after the induction.[209] In addition, alloxan administration in rats led to BRB breakdown and endothelial cells damage.[210,211] However, a significant drawback of alloxan is its toxicity to the liver and kidneys, resulting in less frequent use and prompting a shift towards the use of streptozotocin.[212]

To this day the streptozotocin-induced animal model remains the gold standard agent in inducing DR *in vivo*. Administration of STZ leads to the loss of β-cells in the pancreas, ultimately resulting in insulin deficiency and hyperglycemia. The chemical structure of streptozotocin closely resembles that of glucose and N-acetyl glucosamine, causing beta-cells to take up STZ through the low-affinity glucose transporter 2, leading to cell loss via DNA fragmentation.[201] Streptozotocin is now commonly preferred over alloxan, as it is a more stable compound, and produces more predictable and consistent results.[212,213] Hyperglycemia induced by STZ in mice typically manifests within 2 weeks following induction, achieved through 1 to 5 doses, with a total STZ dosage ranging from 150 to 400 mg/kg.[198] Vascular pathogenesis

observed in STZ mice includes increased vascular permeability detected within eight days of hyperglycemia,[214] while neovascularization was reported 17 weeks post-STZ injection.[215] As diabetes progresses (six to nine months), the retina of STZ-induced mice exhibits acellular capillaries and pericyte ghosts.[216] Additionally, apoptosis of RGCs is identified starting at 6 weeks after STZ administration,[217] along with thinning of retinal layers, including INL, OPL, and ONL between 8 to 12 weeks of hyperglycemia.[217–219] Four to eight weeks post-STZ-induction, a decline in both a- and b-waves is observed in diabetic mice, indicating decreased retinal activity.[218,220,221] Increased leukocyte number and retinal leukostasis was found 8 weeks after the first STZ injection in mice.[222,223] Moreover, STZ-induced diabetic mice exhibits retinal gliosis, macrophage infiltration, microglia reactivity, and the presence of pro-inflammatory cytokines within the period of 4 to 8 weeks of hyperglycemia.[221,224,225]

In contrast to mice, rats require lower doses of STZ to develop diabetes, typically necessitating a single injection of STZ ranging from 40 to 65 mg/kg. The onset of DR-related phenotypes may vary among rat strains, but BRB breakdown was found to start as early as two weeks post-STZ injection.[226,227] Additionally, after 8 weeks of hyperglycemia, increased acellular capillaries and decreased numbers of both pericytes and endothelial cells were found.[228] Elevated levels of VEGF-A and its receptors (VEGFR1 and VEGFR2) expression were associated with neovascularization in STZ-induced rats, at 2, 3 and 4 months following the onset of diabetes.[229] Moreover, decreased retinal thickness in GCL, IPL, INL, and ONL layers has been detected between 4 and 24 weeks post-STZ injections in rats.[230–232] Retinal cell loss and functional changes in diabetic rats have been reported at weeks 2 to 24 post-STZ.[232]

While the STZ model reproduces features related to human DR, it comes with several limitations, including STZ toxicity leading to compromised well-being and elevated mortality

rates among the animals.[233] Additionally, studies have demonstrated that STZ has a neurotoxic effect on neurons.[234,235] This can lead to non-specific neuronal damage in the retina and brain, exaggerating neurodegeneration beyond what would be observed in human DR. Moreover, the STZ-induced DR model generally mirrors early stages of the disease, whereas late-stage DR, characterized by retinal leakage, and vascular tortuosity, may occur after an extended period of time or not be present at all. The reliability and consistency of neovascularization in STZ models vary across the literature. Typically, STZ models mimic the early to intermediate stages of DR, but they often fail to consistently produce robust neovascularization or use unreliable methods to confirm its presence. While some studies report the development of neovascularization in STZ models, the methods chosen to confirm its presence are often inadequate. For instance, hematoxylin and eosin staining, though useful for general tissue morphology, lacks the specificity needed to accurately identify and differentiate new blood vessel formation.[236] Others studies indicate that the model more reliably replicates retinal inflammation and capillary changes (such as the formation of acellular capillaries and pericyte loss) rather than significant neovascularization. [222,223,216] Consequently, while the STZ model is reliable for studying early retinal changes in DR, it is less consistent for replicating neovascularization, prompting researchers to consider alternative models for this pathology. Additionally, prolonged STZ-induced hyperglycemia might lead to cataract formation, restricting the applicability of *in vivo* imaging techniques such as FA, optical coherence tomography (OCT), and the use of ERG.[237] Notably, streptozotocin-induced hyperglycemia is gender-dependent, with male mice exhibiting a higher vulnerability to STZ-induced pancreatic damage compared to females, because the female hormone estrogen potentially inhibiting STZ.[238]

1.3.2 Environmentally induced rodent models of DR

To study late-stage DR vascular changes, including retinal neovascularization and vascular leakage, the use of oxygen-induced retinopathy (OIR) animal model has been proposed. Initially developed to explore retinopathy of prematurity in newborns, the OIR model was later adapted for studying angiogenesis, resembling PDR. Fluctuations between hyperoxia (excess of oxygen) and hypoxia (lack of oxygen) in OIR model leads to compensatory neovascularization.[201] The mouse OIR model is generated when neonatal mice are introduced into a high-oxygen environment (75%) at postnatal day 7 (P7), leading to retinal vessel growth inhibition and significant vessel loss, resulting in avascular areas. Five days later (P12), mice are returned to standard environment, where retina becomes hypoxic, triggering vessel regrowth (revascularization) and pathological neovascular response (neovascularization).[239] Hypoxia results in the rapid increase of HIF-1, leading to the release of VEGF-A that triggers angiogenesis, which had been suppressed during the hyperoxia phase.[240] Additionally, hypoxia promotes retinal blood vessels to sprout towards the vitreous, forming "preretinal tufts" prone to leakage.[239] Neovascularization reaches its peak at P17, followed by spontaneous regression, and the retina reaches resolution by P25.[241] Oxygen-induced neovascularization in mice is accompanied by the emergence of microaneurysms, usually observed within 5 days following exposure.[242] Moreover, reduced retinal thickness is found in OIR mice between P17 and P19, possibly attributed to arrested retinal development or cell apoptosis.[243] Functional deficits were reported both in a-wave and in b-wave amplitudes in OIR mice at P26-27.[244,245] In addition, oxygen-induced mice exhibit retinal gliosis.[244]

Rat OIR conditions are more variable, with higher incidence and severity of neovascularization reported when rats were subjected to 50% oxygen (hyperoxia) and 10% oxygen (hypoxia), cycling every 12 hours for the first 14 days (P0-P14).[246] Increased neovascularization and

impaired pericyte-endothelial interactions were found in oxygen-induced rat retinas as early as P18.[247] Furthermore, preretinal tufts sprouting above the retinal surface were observed in rat OIR, along with changes in retinal thickness from P15 to P24.[248] ERG analysis confirmed retinal dysfunction in OIR rats, showing a significant decrease in both a- and b-wave amplitudes at P30 and P60.[249] While oxygen-induced retinopathy recapitulates PDR features as observed in human patients, its limitation lies in the spontaneous regression of neovascularization, restricting its utility in therapeutic drug research. In addition, since most DR therapeutic interventions are administered via intravitreal or subretinal injections, it becomes challenging to perform them on rodent pups. Another major drawback of OIR is the absence of chronic hyperglycemia, limiting the studies of DR progression from NPRD to PDR.

Diet-induced hyperglycemia is an alternative method to recapitulate the metabolic changes of diabetes and imitate DR progression. Standard animal chow, typically providing around 11% of calories from fat, is replaced with a high-fat diet (HFD) containing approximately 50% of fat caloric intake. C57BL/6 mice fed with HFD (60% kcal from fat) for a duration of 12 months exhibited increased body weight and decreased insulin sensitivity, however, hyperglycemia was not observed.[250] By the 6-month mark, a reduction in both a-wave and b-wave amplitudes was observed, accompanied with increased vascular leakage by the end of 12-month period. Meanwhile, HFD containing 42% fat calories administered to the same species induced insulin resistance by month six, along with increased vascular permeability, formation of pericyte ghosts, and reduction in OP amplitudes by month 12.[251] In another study, the Swiss mice fed with HFD (35% calories from fat) displayed elevated body weight, decreased insulin tolerance, and diminished OP responses by week eight, while significantly increased levels of VEGF were found 16 weeks after the start of HFD.[252] However, in most cases, rodents fed with HFD do not develop hyperglycemia and exhibit mild vascular changes resembling human DR, only after

extended periods of HFD consumption. Therefore, a model using HFD combined with STZ injection has been proposed. Mice fed with a HFD (17.9% calories from fat) for 12 weeks along with intraperitoneal administration of STZ (30 mg/kg) for 7 consecutive days presented key features of NPDR, including formation of acellular capillaries, loss of pericytes, increased vascular leakage, and chronic inflammation.[253] High-fat diet (10% calories from fat) combined with only one STZ injection (30 mg/kg) in Sprague–Dawley rats resulted in abnormal b-wave and OP responses, as well as decreased ONL and total retinal thickness.[254] Although rodents can develop diet-induced early-stage DR features, pharmacologically induced and genetic animal models are more frequently used due to their faster onset of the disease.

1.3.3 Genetic animal models of DR

Genetic rodent models of DR have been designed to study the disease through the deletion or alteration of genes associated with diabetes or the regulation of pathways involved in DR development. Genetic mice models of DR include Akita ($Ins2^{Akita}$) and nonobese diabetic (NOD) mice developing type 1 diabetes, db/db ($Lepr^{db}$) developing T2D, and mice genetically modified to overexpress VEGF (Kimba and Akimba). The $Ins2^{Akita}$ mice have a spontaneous point mutation in the *insulin2* gene, which results in conformational change in the insulin protein that accumulates in pancreatic β-cells, leading to cell dysfunction and death.[255] Akita mice typically exhibit hyperglycemia as early as 4 weeks of age, and early signs of DR start to appear around week 8.[256] Retinal vascular changes in Akita mice include increased leukocytes count at week 8, compromised vascular permeability at week 12, and early signs of microaneurysms are observed in 6-month-old $Ins2^{Akita}$ mice.[256,257] In addition, reduction in the thickness of IPL and GCL have been observed in Akita mice by week 22,[256] with dendrites of RGCs undergoing morphologic changes after 3 months of hyperglycemia.[258] Moreover, functional deficits were observed via ERG at 9 months of age.[257,259] The Akita mice model is

useful for studying the early progression of DR. However, observations via OCT and FA showed no disruption of retinal architecture or vascular changes in $Ins2^{Akita}$ mice up to 6 months of age, suggesting that this model is limited to accurately reflect vascular changes observed in human DR.[260]

Non-obese diabetic (NOD) mice are an alternative to Akita mice, in which autoimmune process by the $CD4^+$ and $CD8^+$ cells destroy pancreatic β-cells, resulting in type 1 diabetes at 12 weeks of age. Diabetes-induced retinal alterations in NOD mice include apoptosis of pericytes, endothelial cells, and RGCs, alongside with thickening of basement membrane, observed as early as 4 weeks into hyperglycemia.[261] In addition, increased levels of VEGF expression are detected in both serum and retina of NOD mice by week 12.[261] However, NOD model is gender specific, with diabetes developing in 80% of female mice and only 20% of male mice, potentially due to the protective role of the female hormone.[262] Therefore, the NOD model is less commonly employed.

The db/db ($Lepr^{db}$) mice develop type 2 diabetes, due to the mutation in the leptin receptor, leading to obesity and hyperglycemia. BRB breakdown, loss of pericytes, apoptosis of neuronal cells, glial reactivation, and proliferation of retinal capillaries were reported in 15-month-old db/db mice.[263] Additionally, reduction of RGCs number and decreased thickness of INL, photoreceptor layer and total retina were identified starting after 6 weeks of hyperglycemia.[264] However, db/db mice model tends to represent early stages of DR rather than more advanced stages observed in PDR patients. Moreover, challenges in maintaining a stable and productive breeding population, makes the use of db/db mice for studying DR less favored.

In the absence of late-stage DR phenotypes in genetic mice, transgenic mouse models that overexpress VEGF have been developed. Kimba (tr029VEGF), a transgenic mouse model that

is genetically modified to overexpress VEGF-A in the rhodopsin-expressing cells, mimics NPDR and mild PDR.[265] Within the first week of life, Kimba mice exhibit a decrease in GCL, INL, ONL, and the overall retinal thickness.[265] By day 28, alterations in retinal microvasculature, such as microaneurysms and vascular leakage, become apparent.[265] Increased number of adhered leukocytes along with increased acellular capillaries were identified at the 6-week mark. Additionally, vessel tortuosity and pericytes loss was observed in 9-week-old Kimba mice.[266] Although Kimba mice are valuable for treatment development, it has several limitations. Early disease development and rapid progression evident at birth limits DR progression research. Additionally, a lack of hyperglycemia is a notable drawback. Therefore, the hybrid Akimba mouse line was generated by crossing $Ins2^{Akita}$ mice and Kimba mice, resulting in both hyperglycemia and significant retinal neovascularization.[267] Akimba mice exhibit various retinal vascular changes, including microaneurysms, vascular leakage, hemorrhages, neovascularization, venous beading, and vascular tortuosity, by 8 weeks of age. Furthermore, there is a noticeable decrease in photoreceptors, and reduced retinal thickness of IPL, INL, ONL, and total retina at week 8, which escalates with age.[267] Moreover, as Akimba mice ages and disease progresses, increased persistence of edema and retinal detachment were observed. However, Akimba mice lack retinal neovascularization, possibly due to the VEGF-A overexpression occurring primarily in photoreceptors rather than in inner retinal layers.[268] As a result, the model tends to exhibit neovascularization in outer nuclear layers or choroid. This limitation raises concerns about the model's relevance to human DR, where neovascularization typically occurs in the inner retina, suggesting that the Akimba model may not fully replicate the pathological human condition. Additionally, Akimba mice primarily manifest photoreceptor loss, while DR patients often experience loss of RGCs and amacrine cells.[269]

Six genetic rat models (BB, ZDF, WBN/Kob, OLETF, SDT and GK) have been created to study diabetes and its complications. Biobreeding (BB) rats, similary to NOD mice, spontaneously develop autoimmune type 1 diabetes between the age of 40 and 140 days, during which the pancreatic beta-cells are selective destroyed.[270] BB rats exhibit loss of pericytes, thickening of the basement membrane, and capillary degeneration after 8 to 11 months of hyperglycemia.[270,271] However, limited studies involving BB rats have been reported in the context of DR, therefore there is a lack of information for its suitability.

Zucker diabetic fatty (ZDF) rats carry gene mutation leading to compromised glucose tolerance and insulin resistance. ZDF rats develop type 2 diabetes between 6 and 7 weeks of age.[272] Some studies demonstrated pericytes and ECs loss, thickening of the BM, and increased number of acellular capillaries in ZDF rats upon 5-6 months of diabetes.[273,274] However, ZDF rats do not exhibit severe retinal vascular damage, even after 42 weeks of sustained hyperglycemia, making this model less frequent in DR research.[275]

WBN/Kob rat is a spontaneously type 2 diabetic strain, in which hyperglycemia occurs at nine months of age.[276] Retinal changes in this model include intraretinal angiopathy, however, neovascularization has not been confirmed.[277] Moreover, retinal thickness of OPL and ONL was found to be decreased in the retinas of 11-month-old WBN/Kob rats.[276] While 15-month-old WBN/Kob rats manifested thickening of the basement membrane and irregular capillaries, however, microaneurysms were not observed.[278]

Another T2D rat model is Otsuka Long-Evans Tokushima fatty (OLETF), which was created by the selective breeding of Long-Evans rats. OLETF caries a mutation in *G-protein-coupled receptor 10* that leads to obesity and hyperglycemia.[279] Elevated blood glucose levels in OLETF rats are observed at month six.[280] Leukocytes trapped in the retinal microcirculation have been

found in OLETF rats by week 6 after the onset of hyperglycemia.[281] 14-month-old OLETF rats exhibited thickening of the BM, damaged endothelial cells and pericytes loss.[282] Nevertheless, this model is limited in DR investigation due to delayed onset of diabetes and the absence of a common feature observed in DR pathology.

The Goto-Kakizaki (GK) rat is a spontaneous model of non-insulin-dependent T2D, without obesity. GK rats, generated by multiple inbreeding crosses from glucose-intolerant Wistar rats, exhibit chronic hyperglycemia from 4 to 6 weeks of age.[283] GK rats are characterized by reduced retinal blood flow without changes in retinal vessel diameters.[284] Increased BRB permeability is observed in 3-month-old GK rats.[285] Although this model may have potential in studying microcirculatory changes in the retina, however, it does not replicate the common hallmarks observed in DR pathology.

Spontaneously diabetic Torii (SDT) rat, an inbred strain of Sprague-Dawley rat, was established as a non-obese type 2 diabetes model. Glucose intolerance and impaired insulin secretion in SDT rats lead to hyperglycemia at 5 months of age.[286] Vascular lesions, including acellular capillaries and pericytes loss were observed in SDT rats.[287] Moreover, retinal deficits in SDT rats were observed after 24 weeks of hyperglycemia, manifesting as reduced a-wave, b-wave, and OP amplitudes.[288] Additionally, SDT rats exhibits proliferative DR features, such as retinal hemorrhages and vascular tortuosity.[289,290] A distinct feature of SDT in the context of DR, is the appearance of vascular leakage around the optic disc and large retinal folds, mimicking tractional retinal detachment observed in PDR patients.[287] Amongst the genetic rat models mentioned above, the SDT rat is the only one exhibiting severe ocular complication which mimic those observed in human DR. However, one limitation of the SDT rats is the lack of

microaneurysms and neovascularization. In addition, similar to NOD mice, SDT model is gender specific, with 100% of males developing diabetes, compared to 33% of females.[290]

1.3.4 VEGF-induced animal models of DR

Upregulation of VEGF-A, a pivotal occurrence in diabetic retinopathy, prompted the development of recombinant VEGF-A-induced animal models, as they provide a platform to study the underlying molecular mechanisms of VEGF-mediated pathologies and to test novel anti-VEGF treatments. Intravitreal injections of recombinant VEGF-A were initially introduced in non-humane primates (Macaca fascicularis).[199] Animals receiving varying doses of VEGF-A, ranging from 0.25 μg to 1.25 μg, exhibited vessel dilation, vascular tortuosity, and leakage. Additionally, in an individual animal subjected to three IVT injections every 3 days, venous beading, intraretinal hemorrhage, and microaneurysm appeared. Histopathologic examination revealed dilated vessels, intraretinal hemorrhage, and edema, along with the increased proliferation of endothelial cells. This study shows that intravitreal VEGF-A, injected in amounts resembling those measured in human eyes with neovascularization, is sufficient to produce retinal vascular abnormalities in the adult nonhuman primates, however, it does not replicate DR-like retinal neovascularization, and short half-life of VEGF-A require frequent IVT injections. Recombinant human VEGF-A administered intravitreally to Dutch Belt rabbits, resulted in breakdown of the blood–retinal barrier and vascular leakage 48 hours post-injection with a dose of 500 ng.[200] Other effects of VEGF-A included vessel dilation and tortuosity, along with inner retinal edema. However, these VEGF-mediated features were transient, returning to baseline within one week.

Additionally, a method involving intraocular implantation of VEGF-A-releasing pellets has been introduced, where a polymeric pellet containing 30 μg of human recombinant VEGF-A

was implanted into the vitreous cavity of albino rabbits.[291] By day 14, rabbits exhibited vessel dilation and tortuosity. Between days 14 and 21 an increase in retinal leakage, as evident in FA, was observed. Additionally, numerous small, tortuous blood vessels were present, indicating the initiation of neovascularization. Nevertheless, these vascular changes stopped and nearly completely regressed after 35 days of pellets implementation. Although immunohistochemical analysis revealed severe breakdown of the BRB and vessel dilation, retinal neovascularization could not be identified.

Another study group generated a similar model, in which polymeric pellets contained both 20 μg of human recombinant VEGF-A and 20 μg of human recombinant basic fibroblast growth factor.[292] Intravitreal implantation of sustained-release pellets, performed on Dutch belted rabbits, resulted in similar vascular alterations, but required less time to develop then when compared to VEGF-A-releasing pellets described above. Additionally, retinal hemorrhages and traction retinal detachment were observed. Nevertheless, vascular leakage in this study was also transient. Therefore, there is an urgent need for novel VEGF-A-induced animal model development, where the presence of VEGF-A is sustained, and DR-related phenotypes are prolonged.

Table 1. Overview of existing animal models used to study DR

Animal model	DR-related features			Disadvantages
	Cellular	**Vascular**	**Functional**	
Pharmacologically induced animal models of DR				
Alloxan injection	- Pericyte ghosts[207,209] - Gliosis of Müller cells[207] - RGCs loss[207,208] - Endothelial cells damage[210,211]	- Acellular capillaries[207] - Vascular proliferation[207] - Microaneurysms[207] - BRB breakdown[210,211]	- Decrease in b-wave/a-wave amplitude ratio[208]	- Toxic to the liver and kidneys - Elevated mortality rates among the animals
STZ injection	- Pericyte ghosts[216] - Decreased number of pericytes[228] - Decreased number of endothelial cells[228] - RGCs loss[217]	- BRB breakdown[226,227] - Increased vascular permeability[214] - Acellular capillaries[216,228] - Increased leukocyte number[222,223] - Leukostasis[222,223]	- Decrease in a- and b-wave amplitudes[218,220,221]	- Toxic to animals -Toxic to retinal neurons - Elevated mortality rates among the animals - Fails to consistently produce robust neovascularization or use

	- Reduced thickness of GCL, IPL, INL, OPL, ONL[217–219,230–232] - Retinal gliosis[224,225] - Macrophage infiltration[224] - Microglia reactivity[224] - Pro-inflammatory cytokines[225]	- Elevated levels of VEGF[229]		unreliable methods to confirm its presence - Mirrors only early stages of DR - Formation of cataracts - Gender-dependent
Environmentally induced rodent models of DR				
Oxygen-induced retinopathy (OIR)	- Reduced retinal thickness[243,248] - Retinal gliosis[244] - Impaired pericyte-endothelial interactions[247]	- Neovascularization[239,247] - Elevated levels of HIF-1 and VEG[240] - Formation of preretinal tufts[239,248] - Microaneurysms[242]	- Decrease in a- and b-wave amplitudes[244,245,249]	- Spontaneous regression of neovascularization - Challenging to perform intravitreal and subretinal injections

				- Absence of chronic hyperglycemia
High-fat diet (HFD)	- Pericyte ghosts[251] - Reduced thickness of ONL and total retina (High-fat diet + STZ injection)[254]	- Vascular leakage[250] - Increased vascular permeability[251] - Elevated levels of VEGF[252]	- Decrease in OP amplitudes[251,252] - Abnormal b-wave and OP responses (High-fat diet+ STZ injection)[254]	- Not all animals develop hyperglycemia - Mirrors only mild vascular changes of DR
Genetic animal models of DR				
Akita ($Ins2^{Akita}$) mice	- Reduced thickness of IPL, GCL[256] - RGCs morphologic changes[258]	- Leukostasis[256] - Increased vascular permeability[256] - Early signs of microaneurysms[257]	- Decrease in a- and b-wave amplitudes[257,259] - Increase in a- and b-wave implicit time[259] - Reduction of the b/a wave ratio[259] - Increase in OPs implicit time[259]	- Mirrors only mild vascular changes of DR

Non-obese diabetic (NOD) mice	- Apoptosis of pericytes[261] - RGCs loss[261] - Apoptosis of endothelial cells[261]	- Thickening of basement membrane[261] - Elevated levels of VEGF[261]	—	- Gender specific, with diabetes developing in 80% of female mice and only 20% of male mice
db/db (Lepr^{db}) mice	- Loss of pericytes[263] - Apoptosis of neuronal cells[263] - Glial reactivation[263] - RGCs loss[264] - Reduced thickness of INL, photoreceptor layer and total retina[264]	- BRB breakdown[263] - Proliferation of retinal capillaries[263]	—	- Mirrors only early stages of DR - Challenges in maintaining a stable and productive breeding population
Kimba (tr029VEGF) mice	- Reduced thickness of RGC, INL, ONL and the overall retina[265] - Pericytes loss[266]	- Microaneurysms[265] - Vascular leakage[265] - Adhered leukocytes[265] - Acellular capillaries[265]	—	- Early disease development and rapid progression limits DR progression research

		- Vessel tortuosity[266]		- Absence of chronic hyperglycemia
Akimba mice	- Loss of photoreceptors [267]	- Microaneurysms[267] - Vascular leakage[267] - Retinal hemorrhages[267] - Venous beading[267] - Vascular tortuosity[267] - Retinal detachment[267]	—	- Lack retinal neovascularization - Lack loss of RGCs and amacrine cells
Biobreeding (BB) rats	- Loss of pericytes[270,271]	- Thickening of the basement membrane[270,271] - Capillary degeneration[270,271]	—	- Limited number of studies in the context of DR
Zucker diabetic fatty (ZDF) rats	- Apoptosis of pericytes[274] - Apoptosis of endothelial cells[274]	- Thickening of the basement membrane[273] - Acellular capillaries[274]	—	- Lack of retinal vascular damage

WBN/Kob rats	- Reduced thickness of OPL, ONL[276]	- Intraretinal angiopathy [277] - Irregular capillaries[278] - Thickening of the basement membrane[278]	—	- Mirrors only early stages of DR
Otsuka Long-Evans Tokushima fatty (OLETF) rats	- Loss of pericytes[282] - Damage of endothelial cells[282]	- Trapped leukocytes[281] - Thickening of the basement membrane[282]	—	- Delayed onset of diabetes - Absence of a common feature observed in DR pathology
The Goto-Kakizaki (GK) rats	—	- Reduced retinal blood flow[285] - BRB breakdown[285]	—	- Absence of a common feature observed in DR pathology

Spontaneously diabetic Torii (SDT) rats	- Loss of pericytes[287]	- Acellular capillaries[287] - Retinal hemorrhages[290] - Vascular tortuosity[290] - Vascular leakage around the optic disc[287] - Large retinal folds[287]	- Decrease in a- and b-wave amplitudes - Decrease in OP amplitudes[288]	- Lack of microaneurysms and neovascularization - Gender specific, with 100% of males developing diabetes, compared to 33% of females
VEGF-induced animal models of DR				
Intravitreal injections of recombinant VEGF-A	- Increased proliferation of endothelial cells[199]	- Vessel dilation[199,200] - Vascular tortuosity[199,200] - Vascular leakage[199,200] - Venous beading[199] - Intraretinal hemorrhage[199] - Microaneurysm[199] - Retinal edema[199,200] - BRB breakdown[200]	—	- Does not replicate DR-like retinal neovascularization - VEGF-mediated features are transient

Implantation of VEGF-A-releasing pellets	—	- Vessel dilation[291] - Vascular tortuosity[291] - Vascular leakage[291] - Initiation of neovascularization[291] - BRB breakdown[291] - Retinal hemorrhages (pallets with VEGF-A and bFGF)[292] - Traction retinal detachment (pallets with VEGF-A and bFGF)[292]	—	- VEGF-mediated features are transient

1.4 Viral vectors in DR

Viral vectors are widely employed in DR gene therapy and biomedical research due to their efficiency in delivering genes to specific cells and tissues. Their use can both mitigate and enhance phenotypes associated with DR. In the realm of gene therapy to treat DR, the primary focus is on the inhibition of neovascularization and protection of neurovascular degeneration in the retina[293–296]. Conversely, viral vectors employed in the creation of DR-related phenotypes focus on the overexpression or knock down of genes that promote neovascularization, inflammation, or neurovascular degeneration. This allows researchers to replicate key features of the disease, enabling them to study the underlying mechanisms and test potential therapeutic strategies.

1.4.1 Lentiviral vectors (LV)

Lentiviral vectors are derived from the human immunodeficiency virus (HIV-1), which belongs to the *Retroviridae* family.[297] These viruses possess the unique capability to infect both dividing and non-dividing cells, promoting interest in the development of recombinant lentiviral vectors for gene transfer. LV contains a single-stranded RNA that is reverse-transcribed into DNA and integrated into the host cell genome. Several viral genes of HIV-1 are modified, deleted, or replaced to enhance safety of lentiviral vectors. Three generations of recombinant lentiviral packaging systems have been developed, with the first generation no longer being in use due to biosafety risks. In this latest, 3rd generation of lentiviral vectors, the viral genome is split into three separate plasmids, which are co-transfected with the transgene plasmid into the producer cell line[298]. The packaging plasmid exclusively carries essential HIV-1 packaging genes (*gag* and *pol*), crucial for viral assembly and integration.[299] A regulatory plasmid contains only one gene — *rev*, necessary for viral transcription. An envelope plasmid holds *env* gene, responsible for surface glycoproteins determining tropism and facilitating entry to the cells.[299] The HIV-1

env glycoprotein can be replaced with the envelope glycoprotein G from the vesicular stomatitis virus (VSV-G), to widen the range of cells types that the lentiviral vector can bind to.[300] Lastly, the transgene, carrying the gene of interest, is flanked by long terminal repeats (LTRs) on both sides, which are modified during the creation of lentiviral vectors. Deletions into the 3'LTR create self-inactivating (SIN) system, disturbing the promoter/enhancer activity of the LTR, and further improving safety of LV vector.[301] Lentiviral vectors are well-known for their stable integration into the host genome, long-term expression of transgene, broad tropism, and low immunogenicity, along with a capability to deliver transgene fragments up to 8 kilobases (kb).[302,303]

Among the diverse range of lentiviral products, inducible lentivectors have brought attention due to their capacity to regulate gene expression in a controlled and tunable manner. In the inducible lentivector system, the gene of interest is activated only in the presence of an inducer, giving researchers full control over the timing and extent of gene expression. Lentivirus incorporated with tetracycline-inducible expression system offers an opportunity to regulate gene expression based on the presence or absence of tetracycline or one of its analog — doxycycline.[304] However, tetracycline-controlled system come with specific limitations, including leaky gene expression in the absence of the inducer.[305] A more recent addition to this field is the cumate-inducible lentivector system, where transgene is expressed upon exposure to cumate, a small non-toxic molecule.[306] The lentivector includes hybrid promoter, which is regulated by strong binding of the cumate repressor (CymR) to the cumate operator site (CuO).[306,307] In the absence of cumate, CymR binds to CuO, and prevents RNA polymerase from effectively transcribing the gene. In contrast, addition of cumate relieves the repression and drives gene activation.[306] *In vitro* studies demonstrate that cumate-inducible LV can be used as a system for regulated gene expression in mammalian, chinese hamster ovary (CHO), and

human embryonic kidney (HEK293) cells.[306,308,309] The main advantage of cumate-inducible LV system is that gene expression can be titratable by adjusting the concentration of cumate. In the experiment involving the transduction of mammalian cells with cumate-inducible LV expressing the fluorescent protein GFP, varying concentrations of cumate revealed a dose-dependent increase in fluorescence.[306] In addition, gene expression in cumate-inducible system can be reversed by depleting cumate, allowing for repeated inductions. Therefore, cumate-inducible LV can be employed to achieve controlled expression of specific genes associated diabetic retinopathy, to induced DR-related phenotypes. Despite this potential, there is a lack of research utilizing cumate-inducible lentiviral vectors in *in vivo* studies, particularly in the context of DR investigations.

1.4.2 Adeno-associated viral (AAV) vectors

Adeno-associated virus belongs to the *Parvoviridae* family, and its replication is dependent on the presence of a helper virus, typically adenovirus.[310] AVV is composed of an icosahedral protein capsid (approximately 26nm in diameter) and a single-stranded DNA genome of ~4.7 kb, which is flanked by two T-shaped inverted terminal repeats (ITRs).[311] The capsid is made up of 60 protein subunits, organized into three structural proteins: VP1, VP2, and VP3. The AAV genome is composed of *Rep* and *Cap* genes, required for the AAV life cycle and production of capsid proteins, respectively.[311] AAV viral vectors contain the same capsid structure as found in wild-type AAV, however the viral DNA is completely replaced with the therapeutic gene of interest. The only retained elements of the wild-type AVV genome are ITRs, which are necessary for genome replication and packaging during vector production.[310] Therefore, maximizing the packaging capacity of AAV vector (up to 5 kb) and contributing to their low immunogenicity and cytotoxicity. The production of AAV vector, usually in HEK293 cells, includes co-transduction of a plasmid containing original AAV genes (*Rep* and *Cap*),

helper genes from adenovirus (*E4*, *E2a* and *VA*), and a transgene.[312] More than 100 AAV serotypes have been identified from different animal species, with AAV serotype 2 (AAV2) being best characterized and most commonly used.[313] The primary differences among AAV serotypes lie in their capsid proteins, which contribute to variations in tissue tropism. Majority of AAV vectors do not integrate into host cells' genome, because of their episomal DNA.[314] Nonetheless, AAV vectors are recognized for their ability to sustain long-term transgene expression and exhibit low pathogenicity.[315] Additionally, in the context of diabetic retinopathy, AAVs show a promise as therapeutic strategies. Intravitreally administered AAV vectors are used to deliver transgenes aimed to inhibit the VEGF-signaling cascade or alternative pathways.[294]

In the development of animal models, AAV vectors have been introduced as well, where the induction of neovascularization was achieved through the overexpression of VEGF-A. Subretinal injections of AAV2 carrying *Vegf-a* under an RPE-specific promotor resulted in the induction of choroidal neovascularization (CNV) in rats, 6-9 weeks post-transduction.[316] Activation of macrophages and microglia were also detected. In addition, in eyes treated with bevacizumab, CNV lesion thickness significantly decreased one week after administration. Another study involving subretinal injections of AAV-VEGF in rats demonstrated persistent choroidal neovascularization for more than 20 months.[317] During this period, a- and b-wave amplitudes significantly decreased, while histological analysis revealed photoreceptor degeneration, and RPE proliferation. Both studies suggest that subretinal injection of AAV-VEGF provides an effective model for evaluating the long-term effects of choroidal neovascularization.

In contrast, intravitreal injections of AAV-VEGF in nonhuman primates were found to be associated with both iris and local regions of retinal neovascularization within 7 days of AAV injection.[318] However, leakage of fluorescein from the iris neovascularization and a vascularized pupillary membrane limited the ability to conduct detailed *in vivo* investigations, such as FA or OCT. Histological evaluation revealed neovascularization of the optic disk and an increase in inflammatory cells. In a more recent study, AAV-mediated expression of human VEGF-A in the murine retina resulted in neovascularization 3 to 6 weeks after the injection.[319] Additionally, AAV-VEGF led to focally dilated or constricted vessels and vascular leakage one week after the injection in 50% of the mice, while the rest developed more severe pathologies, such as retinal detachment. However, their analysis was limited to neuronal damage and retinal function assessments.

1.5 Aims and hypotheses

1.5.1 Aims

The goal of this project was to develop a novel rat model that recapitulates the pathophysiology of DR. Firstly, a systematic literature review was conducted to summarize published morphological and functional changes in the most popular and widely used streptozotocin-induced rat DR model. This step was necessary to have a better understanding if a combination of rat strain, induction protocol, and study design could lead to more robust manifestation of DR-related changes after STZ induction. A follow-up experimental study was an attempt to refine STZ model in Brown Norway rats based on the information collected during the systematic review. The results of the experimental study led to the conclusion that novel methods should be used to induce DR-related changes in the rat eye. Thus, cumate-inducible LV vectors encoding *Vegf-a* gene and having a capability to control VEGF-A expression were employed. Successful use of cumate LV vectors in *in vitro* studies was promising. However,

preliminary *in vivo* testing revealed cumate's toxicity after intravitreal injections. In the last study, stable and long-lasting VEGF-A overexpression was achieved using intravitreal delivery of AAVs. Induced DR-like phenotype was well characterized and tested in the therapeutic paradigm using clinically approved aflibercept (Eylea®).

1.5.2 Hypotheses

1. A systematic literature review will reveal a combination of factors, which in the follow-up study could lead to a more robust manifestation of DR-like phenotype.

2. Cumate-inducible LV vectors could be effectively used to titrate the expression of VEGF-A both *in vitro* and *in vivo*.

3. AAV vectors encoding *Vegf-a* induce stable and long-lasting VEGF-A overexpression leading to the development of DR-like phenotype.

1.6 Experimental approach

To investigate these hypotheses, (1) a systematic search in PubMed and EMBASE, selecting articles on rodent STZ-induced DR with both functional and structural readouts, was performed. The risk of bias was assessed, and qualitative data were analyzed in the selected studies (presented in chapter 2). In addition, a follow-up experimental study was performed on Brown Norway rats which received a single STZ injection, and retinal structural changes were monitored using vitreous fluorophotometry (VFP), spectral domain optical coherence tomography (SD-OCT), FA, and histological analysis. Functional pathologic processes of STZ-induced BN rats were assessed via flash ERG (presented in chapter 3). Hypothesis 2 was tested by transducing ARPE-19 cells with cumate-inducible LV vectors carrying *Vegf-a*. This involved evaluating VEGF-A expression levels, as well as investigating the effects of LV-mediated VEGF-A expression on ARPE-19 cell proliferation, viability, motility, and permeability. To

bring this approach *in vivo*, the tolerability of cumate in Wistar rat eyes delivered via IVT was evaluated by SD-OCT, fERG, ophthalmic examination (OE), and immunohistochemistry analysis (presented in chapter 4). Hypothesis 3 was tested by intravitreally injecting AAV vectors mediating VEGF-A expression in BN rats, and monitoring retinal pathology using SD-OCT, FA, VFP, fERG, and immunohistochemistry. Aflibercept injections were performed to attenuate AAV-induced pathology (presented in chapter 5).

1.7 References

1. Fowler MJ. Microvascular and Macrovascular Complications of Diabetes. Clinical Diabetes. 2011 Jul 1;29(3):116–22.

2. O'Connell JM, Manson SM. Understanding the Economic Costs of Diabetes and Prediabetes and What We May Learn About Reducing the Health and Economic Burden of These Conditions. Diabetes Care. 2019 Sep;42(9):1609–11.

3. Sun H, Saeedi P, Karuranga S, Pinkepank M, Ogurtsova K, Duncan BB, et al. IDF Diabetes Atlas: Global, regional and country-level diabetes prevalence estimates for 2021 and projections for 2045. Diabetes Research and Clinical Practice. 2022 Jan 1;183:109119.

4. Parker ED, Lin J, Mahoney T, Ume N, Yang G, Gabbay RA, et al. Economic Costs of Diabetes in the U.S. in 2022. Diabetes Care. 2023 Nov 1;dci230085.

5. Diagnosis and Classification of Diabetes Mellitus. Diabetes Care. 2010 Jan;33(Suppl 1):S62–9.

6. Mobasseri M, Shirmohammadi M, Amiri T, Vahed N, Hosseini Fard H, Ghojazadeh M. Prevalence and incidence of type 1 diabetes in the world: a systematic review and meta-analysis. Health Promot Perspect. 2020 Mar 30;10(2):98–115.

7. Deshpande AD, Harris-Hayes M, Schootman M. Epidemiology of Diabetes and Diabetes-Related Complications. Phys Ther. 2008 Nov;88(11):1254–64.

8. Laakso M. Cardiovascular Disease in Type 2 Diabetes From Population to Man to Mechanisms. Diabetes Care. 2010 Feb;33(2):442–9.

9. Beckman J, Creager M, Libby P. Diabetes and Atherosclerosis. JAMA : the journal of the American Medical Association. 2002 Jun 1;287:2570–81.

10. Yang S, Boudier-Revéret M, Kwon S, Lee MY, Chang MC. Effect of Diabetes on Post-stroke Recovery: A Systematic Narrative Review. Front Neurol. 2021 Dec 14;12:747878.

11. Lau L, Lew J, Borschmann K, Thijs V, Ekinci EI. Prevalence of diabetes and its effects on stroke outcomes: A meta-analysis and literature review. J Diabetes Investig. 2019 May;10(3):780–92.

12. Foussard N, Dari L, Ducasse E, Rigalleau V, Mohammedi K, Caradu C. Lower-limb peripheral arterial disease and amputations in people with diabetes: Risk factors, prognostic value and management. La Presse Médicale. 2023 Mar 1;52(1):104164.

13. Thiruvoipati T, Kielhorn CE, Armstrong EJ. Peripheral artery disease in patients with diabetes: Epidemiology, mechanisms, and outcomes. World J Diabetes. 2015 Jul 10;6(7):961–9.

14. Soyoye DO, Abiodun OO, Ikem RT, Kolawole BA, Akintomide AO. Diabetes and peripheral artery disease: A review. World J Diabetes. 2021 Jun 15;12(6):827–38.

15. Vithian K, Hurel S. Microvascular complications: pathophysiology and management. Clin Med (Lond). 2010 Oct;10(5):505–9.

16. Papatheodorou K, Banach M, Bekiari E, Rizzo M, Edmonds M. Complications of Diabetes 2017. Journal of Diabetes Research. 2018 Mar 11;2018:e3086167.

17. Tesfaye S, Boulton AJM, Dickenson AH. Mechanisms and Management of Diabetic Painful Distal Symmetrical Polyneuropathy. Diabetes Care. 2013 Aug 13;36(9):2456–65.

18. Callaghan BC, Price RS, Feldman EL. Diagnostic and Therapeutic Advances: Distal Symmetric Polyneuropathy. JAMA. 2015 Nov 24;314(20):2172–81.

19. Boulton AJM, Vinik AI, Arezzo JC, Bril V, Feldman EL, Freeman R, et al. Diabetic Neuropathies: A statement by the American Diabetes Association. Diabetes Care. 2005 Apr 1;28(4):956–62.

20. Samsu N. Diabetic Nephropathy: Challenges in Pathogenesis, Diagnosis, and Treatment. BioMed Research International. 2021 Jul 9;2021:e1497449.

21. Gheith O, Farouk N, Nampoory N, Halim MA, Al-Otaibi T. Diabetic kidney disease: world wide difference of prevalence and risk factors. J Nephropharmacol. 2015 Oct 9;5(1):49–56.

22. Natesan V, Kim SJ. Diabetic Nephropathy – a Review of Risk Factors, Progression, Mechanism, and Dietary Management. Biomol Ther (Seoul). 2021 Jul 1;29(4):365–72.

23. Kropp M, Golubnitschaja O, Mazurakova A, Koklesova L, Sargheini N, Vo TTKS, et al. Diabetic retinopathy as the leading cause of blindness and early predictor of cascading complications—risks and mitigation. EPMA J. 2023 Feb 13;14(1):21–42.

24. Sivaprasad S, Gupta B, Crosby-Nwaobi R, Evans J. Prevalence of Diabetic Retinopathy in Various Ethnic Groups: A Worldwide Perspective. Survey of Ophthalmology. 2012 Jul 1;57(4):347–70.

25. Teo ZL, Tham YC, Yu M, Chee ML, Rim TH, Cheung N, et al. Global Prevalence of Diabetic Retinopathy and Projection of Burden through 2045. Ophthalmology. 2021 Nov;128(11):1580–91.

26. Zegeye AF, Temachu YZ, Mekonnen CK. Prevalence and factors associated with Diabetes retinopathy among type 2 diabetic patients at Northwest Amhara Comprehensive Specialized Hospitals, Northwest Ethiopia 2021. BMC Ophthalmology. 2023 Jan 5;23(1):9.

27. Keenan HA, Costacou T, Sun JK, Doria A, Cavellerano J, Coney J, et al. Clinical Factors Associated With Resistance to Microvascular Complications in Diabetic Patients of Extreme Disease Duration: The 50-year Medalist Study. Diabetes Care. 2007 Aug 1;30(8):1995–7.

28. Diabetes Control and Complications Trial Research Group, Nathan DM, Genuth S, Lachin J, Cleary P, Crofford O, et al. The effect of intensive treatment of diabetes on the development and progression of long-term complications in insulin-dependent diabetes mellitus. N Engl J Med. 1993 Sep 30;329(14):977–86.

29. Nordwall M, Abrahamsson M, Dhir M, Fredrikson M, Ludvigsson J, Arnqvist HJ. Impact of HbA1c, followed from onset of type 1 diabetes, on the development of severe retinopathy and nephropathy: the VISS Study (Vascular Diabetic Complications in Southeast Sweden). Diabetes Care. 2015 Feb;38(2):308–15.

30. Liu Y, Yang J, Tao L, Lv H, Jiang X, Zhang M, et al. Risk factors of diabetic retinopathy and sight-threatening diabetic retinopathy: a cross-sectional study of 13 473 patients with type 2 diabetes mellitus in mainland China. BMJ Open. 2017 Sep 1;7(9):e016280.

31. Simó-Servat O, Hernández C, Simó R. Diabetic Retinopathy in the Context of Patients with Diabetes. Ophthalmic Research. 2019 May 24;62(4):211–7.

32. Chaturvedi N, Sjolie AK, Stephenson JM, Abrahamian H, Keipes M, Castellarin A, et al. Effect of lisinopril on progression of retinopathy in normotensive people with type 1 diabetes. The EUCLID Study Group. EURODIAB Controlled Trial of Lisinopril in Insulin-Dependent Diabetes Mellitus. Lancet. 1998 Jan 3;351(9095):28–31.

33. Lima VC, Cavalieri GC, Lima MC, Nazario NO, Lima GC. Risk factors for diabetic retinopathy: a case–control study. International Journal of Retina and Vitreous. 2016 Sep 12;2(1):21.

34. Bryl A, Mrugacz M, Falkowski M, Zorena K. The Effect of Hyperlipidemia on the Course of Diabetic Retinopathy—Literature Review. J Clin Med. 2022 May 13;11(10):2761.

35. Kusuhara S, Fukushima Y, Ogura S, Inoue N, Uemura A. Pathophysiology of Diabetic Retinopathy: The Old and the New. Diabetes Metab J. 2018 Oct;42(5):364–76.

36. Singh R, Ramasamy K, Abraham C, Gupta V, Gupta A. Diabetic retinopathy: An update. Indian J Ophthalmol. 2008;56(3):179–88.

37. Wu L, Fernandez-Loaiza P, Sauma J, Hernandez-Bogantes E, Masis M. Classification of diabetic retinopathy and diabetic macular edema. World J Diabetes. 2013 Dec 15;4(6):290–4.

38. Klein R, Klein BEK, Moss SE. Epidemiology of Proliferative Diabetic Retinopathy. Diabetes Care. 1992 Dec 1;15(12):1875–91.

39. Viswanath K, McGavin DDM. Diabetic Retinopathy: Clinical Findings and Management. Community Eye Health. 2003;16(46):21–4.

40. Mishra C, Tripathy K. Retinal Traction Detachment. In: StatPearls [Internet]. Treasure Island (FL): StatPearls Publishing; 2023 [cited 2024 Jan 2]. Available from: http://www.ncbi.nlm.nih.gov/books/NBK558952/

41. Musat O, Cernat C, Labib M, Gheorghe A, Toma O, Zamfir M, et al. Diabetic Macular Edema. Rom J Ophthalmol. 2015;59(3):133–6.

42. Gangnon RE, Davis MD, Hubbard LD, Aiello LM, Chew EY, Ferris FL III, et al. A Severity Scale for Diabetic Macular Edema Developed from ETDRS Data. Investigative Ophthalmology & Visual Science. 2008 Nov 1;49(11):5041–7.

43. Mrugacz M, Bryl A, Zorena K. Retinal Vascular Endothelial Cell Dysfunction and Neuroretinal Degeneration in Diabetic Patients. J Clin Med. 2021 Jan 25;10(3):458.

44. Biswas S, Chakrabarti S. Pathogenetic Mechanisms in Diabetic Retinopathy: From Molecules to Cells to Tissues. In: Kartha CC, Ramachandran S, Pillai RM, editors. Mechanisms of Vascular Defects in Diabetes Mellitus [Internet]. Cham: Springer International Publishing; 2017 [cited 2024 Jan 4]. p. 209–47.

45. Vinores SA. Breakdown of the Blood–Retinal Barrier. Encyclopedia of the Eye. 2010;216–22.

46. Zhang X, Zeng H, Bao S, Wang N, Gillies MC. Diabetic macular edema: new concepts in patho-physiology and treatment. Cell & Bioscience. 2014 May 14;4(1):27.

47. Rudraraju M, Narayanan SP, Somanath PR. Regulation of blood-retinal barrier cell-junctions in diabetic retinopathy. Pharmacol Res. 2020 Nov;161:105115.

48. Roy S, Kim D. Retinal Capillary Basement Membrane Thickening: Role in the Pathogenesis of Diabetic Retinopathy. Prog Retin Eye Res. 2021 May;82:100903.

49. Chihara E, Matsuoka T, Ogura Y, Matsumura M. Retinal nerve fiber layer defect as an early manifestation of diabetic retinopathy. Ophthalmology. 1993 Aug;100(8):1147–51.

50. Geraldes P, Hiraoka-Yamamoto J, Matsumoto M, Clermont A, Leitges M, Marette A, et al. Activation of PKC-δ and SHP-1 by hyperglycemia causes vascular cell apoptosis and diabetic retinopathy. Nat Med. 2009 Nov;15(11):1298–306.

51. Robison WG, McCaleb ML, Feld LG, Michaelis OE, Laver N, Mercandetti M. Degenerated intramural pericytes ('ghost cells') in the retinal capillaries of diabetic rats. Curr Eye Res. 1991 Apr;10(4):339–50.

52. Hammes HP, Lin J, Renner O, Shani M, Lundqvist A, Betsholtz C, et al. Pericytes and the pathogenesis of diabetic retinopathy. Diabetes. 2002 Oct;51(10):3107–12.

53. Witmer AN, Vrensen GFJM, Van Noorden CJF, Schlingemann RO. Vascular endothelial growth factors and angiogenesis in eye disease. Prog Retin Eye Res. 2003 Jan;22(1):1–29.

54. Pearce E, Sivaprasad S, Broadgate S, Kiire C, Downes SM, Halford S, et al. Intraretinal Microvascular Abnormalities and Venous Beading Have Different Genetic Profiles in Caucasian Patients with Non-Proliferative Diabetic Retinopathy. Vision. 2023 Mar;7(1):18.

55. Sasongko MB, Wong TY, Nguyen TT, Cheung CY, Shaw JE, Wang JJ. Retinal vascular tortuosity in persons with diabetes and diabetic retinopathy. Diabetologia. 2011 Sep;54(9):2409–16.

56. Takagi H, Oh H, Otani A, Suzuma K, Suzuma I, Ohashi H, et al. Molecular mechanisms of retinal neovascularization in diabetic retinopathy. International Congress Series. 2004 May 1;1262:160–3.

57. Whitehead M, Osborne A, Widdowson PS, Yu-Wai-Man P, Martin KR. Angiopoietins in Diabetic Retinopathy: Current Understanding and Therapeutic Potential. J Diabetes Res. 2019 Aug 14;2019:5140521.

58. Wang J, Wang S, Li M, Wu D, Liu F, Yang R, et al. The Neuropilin-1 Inhibitor, ATWLPPR Peptide, Prevents Experimental Diabetes-Induced Retinal Injury by Preserving Vascular Integrity and Decreasing Oxidative Stress. PLoS One. 2015;10(11):e0142571.

59. Aiello LP, Wong JS. Role of vascular endothelial growth factor in diabetic vascular complications. Kidney International. 2000 Sep 1;58:S113–9.

60. Xu HZ, Le YZ. Significance of outer blood-retina barrier breakdown in diabetes and ischemia. Invest Ophthalmol Vis Sci. 2011 Apr 5;52(5):2160–4.

61. Xu HZ, Song Z, Fu S, Zhu M, Le YZ. RPE barrier breakdown in diabetic retinopathy: seeing is believing. J Ocul Biol Dis Infor. 2011 Dec 31;4(1–2):83–92.

62. Simó R, Villarroel M, Corraliza L, Hernández C, Garcia-Ramírez M. The Retinal Pigment Epithelium: Something More than a Constituent of the Blood-Retinal Barrier—Implications for the Pathogenesis of Diabetic Retinopathy. BioMed Research International. 2010;2010(1):190724.

63. Boynton GE, Stem MS, Kwark L, Jackson GR, Farsiu S, Gardner TW. Multimodal characterization of proliferative diabetic retinopathy reveals alterations in outer retinal function and structure. Ophthalmology. 2015 May;122(5):957–67.

64. Bavinger JC, Dunbar GE, Stem MS, Blachley TS, Kwark L, Farsiu S, et al. The Effects of Diabetic Retinopathy and Pan-Retinal Photocoagulation on Photoreceptor Cell Function as Assessed by Dark Adaptometry. Invest Ophthalmol Vis Sci. 2016 Jan;57(1):208–17.

65. Aizu Y, Katayama H, Takahama S, Hu J, Nakagawa H, Oyanagi K. Topical instillation of ciliary neurotrophic factor inhibits retinal degeneration in streptozotocin-induced diabetic rats. Neuroreport. 2003 Nov 14;14(16):2067–71.

66. Aizu Y, Oyanagi K, Hu J, Nakagawa H. Degeneration of retinal neuronal processes and pigment epithelium in the early stage of the streptozotocin-diabetic rats. Neuropathology. 2002 Sep;22(3):161–70.

67. Pautler EL, Ennis SR. The effect of induced diabetes on the electroretinogram components of the pigmented rat. Invest Ophthalmol Vis Sci. 1980 Jun;19(6):702–5.

68. Rimmer T, Linsenmeier RA. Resistance of diabetic rat electroretinogram to hypoxemia. Invest Ophthalmol Vis Sci. 1993 Nov;34(12):3246–52.

69. Madsen-Bouterse S, Zhong Q, Mohammad G, Ho Y, Kowluru R. Oxidative damage of mitochondrial DNA in diabetes and its protection by manganese superoxide dismutase. Free Radic Res. 2010 Mar;44(3):313–21.

70. Kang Q, Yang C. Oxidative stress and diabetic retinopathy: Molecular mechanisms, pathogenetic role and therapeutic implications. Redox Biol. 2020 Nov 13;37:101799.

71. Wei L, Sun X, Fan C, Li R, Zhou S, Yu H. The pathophysiological mechanisms underlying diabetic retinopathy. Front Cell Dev Biol. 2022 Aug 30;10:963615.

72. Giacco F, Brownlee M. Oxidative stress and diabetic complications. Circ Res. 2010 Oct 29;107(9):1058–70.

73. Safi SZ, Qvist R, Kumar S, Batumalaie K, Ismail ISB. Molecular Mechanisms of Diabetic Retinopathy, General Preventive Strategies, and Novel Therapeutic Targets. Biomed Res Int. 2014;2014:801269.

74. Wang Y, Eshwaran R, Beck SC, Hammes HP, Wieland T, Feng Y. Contribution of the hexosamine biosynthetic pathway in the hyperglycemia-dependent and -independent breakdown of the retinal neurovascular unit. Molecular Metabolism. 2023 Jul 1;73:101736.

75. Das Evcimen N, King GL. The role of protein kinase C activation and the vascular complications of diabetes. Pharmacological Research. 2007 Jun 1;55(6):498–510.

76. Noh H, King GL. The role of protein kinase C activation in diabetic nephropathy. Kidney International. 2007 Aug 1;72:S49–53.

77. Sharma Y, Saxena S, Mishra A, Saxena A, Natu SM. Advanced glycation end products and diabetic retinopathy. J Ocul Biol Dis Infor. 2013 Apr 19;5(3–4):63–9.

78. Yamagishi S ichi, Amano S, Inagaki Y, Okamoto T, Takeuchi M, Makita Z. Beraprost sodium, a prostaglandin I2 analogue, protects against advanced gycation end products-induced injury in cultured retinal pericytes. Mol Med. 2002 Sep;8(9):546–50.

79. Yamagishi S ichi, Inagaki Y, Amano S, Okamoto T, Takeuchi M, Makita Z. Pigment epithelium-derived factor protects cultured retinal pericytes from advanced glycation end product-induced injury through its antioxidative properties. Biochem Biophys Res Commun. 2002 Aug 30;296(4):877–82.

80. Gomułka K, Ruta M. The Role of Inflammation and Therapeutic Concepts in Diabetic Retinopathy—A Short Review. Int J Mol Sci. 2023 Jan 5;24(2):1024.

81. Rübsam A, Parikh S, Fort PE. Role of Inflammation in Diabetic Retinopathy. Int J Mol Sci. 2018 Mar 22;19(4):942.

82. Tang J, Kern TS. Inflammation in Diabetic Retinopathy. Prog Retin Eye Res. 2011 Sep;30(5):343–58.

83. Noda K, Nakao S, Ishida S, Ishibashi T. Leukocyte Adhesion Molecules in Diabetic Retinopathy. Journal of Ophthalmology. 2011 Nov 2;2012:e279037.

84. Chibber R, Ben-Mahmud B, Chibber S, Kohner E. Leukocytes in Diabetic Retinopathy. CDR. 2007 Feb 1;3(1):3–14.

85. Koleva-Georgieva DN, Sivkova NP, Terzieva D. Serum inflammatory cytokines IL-1beta, IL-6, TNF-alpha and VEGF have influence on the development of diabetic retinopathy. Folia Med (Plovdiv). 2011;53(2):44–50.

86. Maier R, Weger M, Haller-Schober EM, El-Shabrawi Y, Wedrich A, Theisl A, et al. Multiplex bead analysis of vitreous and serum concentrations of inflammatory and proangiogenic factors in diabetic patients. Mol Vis. 2008 Mar 27;14:637–43.

87. Tsutsumi C, Sonoda KH, Egashira K, Qiao H, Hisatomi T, Nakao S, et al. The critical role of ocular-infiltrating macrophages in the development of choroidal neovascularization. J Leukoc Biol. 2003 Jul;74(1):25–32.

88. Sakurai E, Taguchi H, Anand A, Ambati BK, Gragoudas ES, Miller JW, et al. Targeted disruption of the CD18 or ICAM-1 gene inhibits choroidal neovascularization. Invest Ophthalmol Vis Sci. 2003 Jun;44(6):2743–9.

89. Busik JV, Mohr S, Grant MB. Hyperglycemia-Induced Reactive Oxygen Species Toxicity to Endothelial Cells Is Dependent on Paracrine Mediators. Diabetes. 2008 Jul;57(7):1952–65.

90. Sun L, Wang R, Hu G, Liu H, Lv K, Duan Y, et al. Single cell RNA sequencing (scRNA-Seq) deciphering pathological alterations in streptozotocin-induced diabetic retinas. Exp Eye Res. 2021 Sep;210:108718.

91. Ben S, Ma Y, Bai Y, Zhang Q, Zhao Y, Xia J, et al. Microglia-endothelial cross-talk regulates diabetes-induced retinal vascular dysfunction through remodeling inflammatory microenvironment. iScience [Internet]. 2024 Mar 3;27(3).

92. Lv K, Ying H, Hu G, Hu J, Jian Q, Zhang F. Integrated multi-omics reveals the activated retinal microglia with intracellular metabolic reprogramming contributes to inflammation in STZ-induced early diabetic retinopathy. Front Immunol. 2022;13:942768.

93. He C, Liu Y, Huang Z, Yang Z, Zhou T, Liu S, et al. A specific RIP3+ subpopulatin of microglia promotes retinopathy through a hypoxia-triggered necroptotic mechanism. Proc Natl Acad Sci U S A. 2021 Mar 16;118(11):e2023290118.

94. Xia M, Jiao L, Wang XH, Tong M, Yao MD, Li XM, et al. Single-cell RNA sequencing reveals a unique pericyte type associated with capillary dysfunction. Theranostics. 2023;13(8):2515–30.

95. Youngblood H, Robinson R, Sharma A, Sharma S. Proteomic Biomarkers of Retinal Inflammation in Diabetic Retinopathy. Int J Mol Sci. 2019 Sep 25;20(19):4755.

96. Sharma S, Purohit S, Sharma A, Hopkins D, Steed L, Bode B, et al. Elevated Serum Levels of Soluble TNF Receptors and Adhesion Molecules Are Associated with Diabetic Retinopathy in Patients with Type-1 Diabetes. Mediators Inflamm. 2015;2015:279393.

97. Jain A, Saxena S, Khanna VK, Shukla RK, Meyer CH. Status of serum VEGF and ICAM-1 and its association with external limiting membrane and inner segment-outer segment junction disruption in type 2 diabetes mellitus. Mol Vis. 2013;19:1760–8.

98. Srividya G, Jain M, Mahalakshmi K, Gayathri S, Raman R, Angayarkanni N. A novel and less invasive technique to assess cytokine profile of vitreous in patients of diabetic macular oedema. Eye (Lond). 2018 Apr;32(4):820–9.

99. Kaviarasan K, Jithu M, Arif Mulla M, Sharma T, Sivasankar S, Das UN, et al. Low blood and vitreal BDNF, LXA4 and altered Th1/Th2 cytokine balance are potential risk factors for diabetic retinopathy. Metabolism. 2015 Sep;64(9):958–66.

100. Cavusoglu AC, Bilgili S, Alaluf A, Doğan A, Yilmaz F, Aslanca D, et al. Vascular endothelial growth factor level in the serum of diabetic patients with retinopathy. Ann Ophthalmol (Skokie). 2007;39(3):205–8.

101. Mastropasqua R, Toto L, Cipollone F, Santovito D, Carpineto P, Mastropasqua L. Role of microRNAs in the modulation of diabetic retinopathy. Prog Retin Eye Res. 2014 Nov;43:92–107.

102. Gong Q, Su G. Roles of miRNAs and long noncoding RNAs in the progression of diabetic retinopathy. Biosci Rep. 2017 Dec 22;37(6):BSR20171157.

103. Smit-McBride Z, Morse LS. MicroRNA and diabetic retinopathy—biomarkers and novel therapeutics. Ann Transl Med. 2021 Aug;9(15):1280.

104. Roy D, Modi A, Khokhar M, Sankanagoudar S, Yadav D, Sharma S, et al. MicroRNA 21 Emerging Role in Diabetic Complications: A Critical Update. Curr Diabetes Rev. 2021;17(2):122–35.

105. Liu Y, Xiao J, Zhao Y, Zhao C, Yang Q, Du X, et al. microRNA-216a protects against human retinal microvascular endothelial cell injury in diabetic retinopathy by suppressing the NOS2/JAK/STAT axis. Exp Mol Pathol. 2020 Aug;115:104445.

106. Han N, Xu H, Yu N, Wu Y, Yu L. MiR-203a-3p inhibits retinal angiogenesis and alleviates proliferative diabetic retinopathy in oxygen-induced retinopathy (OIR) rat model via targeting VEGFA and HIF-1α. Clin Exp Pharmacol Physiol. 2020 Jan;47(1):85–94.

107. de Ronde MWJ, Ruijter JM, Moerland PD, Creemers EE, Pinto-Sietsma SJ. Study Design and qPCR Data Analysis Guidelines for Reliable Circulating miRNA Biomarker Experiments: A Review. Clin Chem. 2018 Sep;64(9):1308–18.

108. Xiong F, Du X, Hu J, Li T, Du S, Wu Q. Altered Retinal MicroRNA Expression Profiles in Early Diabetic Retinopathy: An In Silico Analysis. Current Eye Research. 2014 Jul 1;39(7):720–9.

109. Platania CBM, Maisto R, Trotta MC, D'Amico M, Rossi S, Gesualdo C, et al. Retinal and circulating miRNA expression patterns in diabetic retinopathy: An in silico and in vivo approach. Br J Pharmacol. 2019 Jul;176(13):2179–94.

110. Platania CBM, Leggio GM, Drago F, Salomone S, Bucolo C. Computational systems biology approach to identify novel pharmacological targets for diabetic retinopathy. Biochem Pharmacol. 2018 Dec;158:13–26.

111. Rajendran S, Seetharaman S, Vetrivel U, Kuppan K. Integrative study of gene expression datasets in retinal samples of Diabetic Retinopathy. Experimental Eye Research. 2022 Oct 1;223:109194.

112. Gong MT, Li WX, Zhang Q, Lv WW, He ZH, Zhou SL, et al. Comprehensive analysis of gene expression profiles associated with proliferative diabetic retinopathy. Experimental and Therapeutic Medicine. 2018 Oct 1;16(4):3539–45.

113. Gupta N, Mansoor S, Sharma A, Sapkal A, Sheth J, Falatoonzadeh P, et al. Diabetic Retinopathy and VEGF. Open Ophthalmol J. 2013 Feb 1;7:4–10.

114. Shibuya M. Vascular Endothelial Growth Factor (VEGF) and Its Receptor (VEGFR) Signaling in Angiogenesis. Genes Cancer. 2011 Dec;2(12):1097–105.

115. Penn JS, Madan A, Caldwell RB, Bartoli M, Caldwell RW, Hartnett ME. Vascular Endothelial Growth Factor in Eye Disease. Prog Retin Eye Res. 2008 Jul;27(4):331–71.

116. Levy AP, Levy NS, Goldberg MA. Post-transcriptional regulation of vascular endothelial growth factor by hypoxia. J Biol Chem. 1996 Feb 2;271(5):2746–53.

117. Shibuya M, Claesson-Welsh L. Signal transduction by VEGF receptors in regulation of angiogenesis and lymphangiogenesis. Exp Cell Res. 2006 Mar 10;312(5):549–60.

118. Antonetti DA, Barber AJ, Hollinger LA, Wolpert EB, Gardner TW. Vascular endothelial growth factor induces rapid phosphorylation of tight junction proteins occludin and zonula occluden 1. A potential mechanism for vascular permeability in diabetic retinopathy and tumors. J Biol Chem. 1999 Aug 13;274(33):23463–7.

119. Mignatti P, Rifkin DB. Plasminogen activators and matrix metalloproteinases in angiogenesis. Enzyme Protein. 1996;49(1–3):117–37.

120. Weis SM, Cheresh DA. αv Integrins in Angiogenesis and Cancer. Cold Spring Harb Perspect Med. 2011 Sep;1(1):a006478.

121. Wang X, Wang G, Wang Y. Intravitreous vascular endothelial growth factor and hypoxia-inducible factor 1a in patients with proliferative diabetic retinopathy. Am J Ophthalmol. 2009 Dec;148(6):883–9.

122. Selim KM, Sahan D, Muhittin T, Osman C, Mustafa O. Increased levels of vascular endothelial growth factor in the aqueous humor of patients with diabetic retinopathy. Indian J Ophthalmol. 2010;58(5):375–9.

123. Zachary I. Neuroprotective role of vascular endothelial growth factor: signalling mechanisms, biological function, and therapeutic potential. Neurosignals. 2005;14(5):207–21.

124. Kim I, Ryan AM, Rohan R, Amano S, Agular S, Miller JW, et al. Constitutive expression of VEGF, VEGFR-1, and VEGFR-2 in normal eyes. Invest Ophthalmol Vis Sci. 1999 Aug;40(9):2115–21.

125. Gilbert RE, Vranes D, Berka JL, Kelly DJ, Cox A, Wu LL, et al. Vascular endothelial growth factor and its receptors in control and diabetic rat eyes. Lab Invest. 1998 Aug;78(8):1017–27.

126. Sondell M, Lundborg G, Kanje M. Vascular Endothelial Growth Factor Has Neurotrophic Activity and Stimulates Axonal Outgrowth, Enhancing Cell Survival and Schwann Cell Proliferation in the Peripheral Nervous System. J Neurosci. 1999 Jul 15;19(14):5731–40.

127. Sondell M, Sundler F, Kanje M. Vascular endothelial growth factor is a neurotrophic factor which stimulates axonal outgrowth through the flk-1 receptor. Eur J Neurosci. 2000 Dec;12(12):4243–54.

128. Froger N, Matonti F, Roubeix C, Forster V, Ivkovic I, Brunel N, et al. VEGF is an autocrine/paracrine neuroprotective factor for injured retinal ganglion neurons. Sci Rep. 2020 Jul 24;10(1):12409.

129. Nishijima K, Ng YS, Zhong L, Bradley J, Schubert W, Jo N, et al. Vascular endothelial growth factor-A is a survival factor for retinal neurons and a critical neuroprotectant during the adaptive response to ischemic injury. Am J Pathol. 2007 Jul;171(1):53–67.

130. Saint-Geniez M, Maharaj ASR, Walshe TE, Tucker BA, Sekiyama E, Kurihara T, et al. Endogenous VEGF Is Required for Visual Function: Evidence for a Survival Role on Müller Cells and Photoreceptors. PLOS ONE. 2008 Nov 3;3(11):e3554.

131. Martínez-Vacas A, Di Pierdomenico J, Gómez-Ramirez AM, Vidal-Sanz M, Villegas-Pérez MP, García-Ayuso D. Dose-Related Side Effects of Intravitreal Injections of Humanized Anti-Vascular Endothelial Growth Factor in Rats: Glial Cell Reactivity and Retinal Ganglion Cell Loss. Investigative Ophthalmology & Visual Science. 2024 Apr 4;65(4):10.

132. Park HYL, Kim JH, Park CK. Neuronal Cell Death in the Inner Retina and the Influence of Vascular Endothelial Growth Factor Inhibition in a Diabetic Rat Model. The American Journal of Pathology. 2014 Jun 1;184(6):1752–62.

133. Hombrebueno JR, Ali IH, Xu H, Chen M. Sustained intraocular VEGF neutralization results in retinal neurodegeneration in the Ins2Akita diabetic mouse. Sci Rep. 2015 Dec 16;5(1):18316.

134. Sibal L, Home PD. Management of type 2 diabetes: NICE guidelines. Clin Med (Lond). 2009 Aug;9(4):353–7.

135. Scanlon PH. The English National Screening Programme for diabetic retinopathy 2003–2016. Acta Diabetol. 2017;54(6):515–25.

136. Tomita Y, Lee D, Tsubota K, Negishi K, Kurihara T. Updates on the Current Treatments for Diabetic Retinopathy and Possibility of Future Oral Therapy. J Clin Med. 2021 Oct 12;10(20):4666.

137. Gozawa M, Takamura Y, Miyake S, Matsumura T, Morioka M, Yamada Y, et al. Photocoagulation of the Retinal Nonperfusion Area Prevents the Expression of the Vascular Endothelial Growth Factor in an Animal Model. Invest Ophthalmol Vis Sci. 2017 Nov 1;58(13):5946–53.

138. Aiello LP, Avery RL, Arrigg PG, Keyt BA, Jampel HD, Shah ST, et al. Vascular Endothelial Growth Factor in Ocular Fluid of Patients with Diabetic Retinopathy and Other Retinal Disorders. N Engl J Med. 1994 Dec;331(22):1480–7.

139. Sims LM, Stoessel K, Thompson JT, Hirsch J. Assessment of visual-field changes before and after focal photocoagulation for clinically significant diabetic macular edema. Ophthalmologica. 1990;200(3):133–41.

140. Seiberth V, Alexandridis E, Feng W. Function of the diabetic retina after panretinal argon laser coagulation. Graefes Arch Clin Exp Ophthalmol. 1987;225(6):385–90.

141. Denadai L, Mozetic V, Moore RA, Yamada VH, Riera R. Pain control during panretinal photocoagulation for diabetic retinopathy. Cochrane Database Syst Rev. 2022 Jun 9;2022(6):CD014927.

142. Nikkhah H, Ghazi H, Razzaghi MR, Karimi S, Ramezani A, Soheilian M. Extended targeted retinal photocoagulation versus conventional pan-retinal photocoagulation for proliferative diabetic retinopathy in a randomized clinical trial. Int Ophthalmol. 2018 Feb;38(1):313–21.

143. Zhang W, Geng J, Sang A. Effectiveness of Panretinal Photocoagulation Plus Intravitreal Anti-VEGF Treatment Against PRP Alone for Diabetic Retinopathy: A Systematic Review With Meta-Analysis. Front Endocrinol (Lausanne). 2022 Mar 29;13:807687.

144. Lee E, Hubschman JP, Gonzales C, Schwartz S. Combination Therapy: Targeted Retinal Photocoagulation (TRP) and Anti-VEGF Treatment for Retinal Vascular Macular Edema. Investigative Ophthalmology & Visual Science. 2008 May 14;49(13):3494.

145. Ferrara N, Hillan KJ, Gerber HP, Novotny W. Discovery and development of bevacizumab, an anti-VEGF antibody for treating cancer. Nat Rev Drug Discov. 2004 May;3(5):391–400.

146. Arevalo JF, Sanchez JG, Lasave AF, Wu L, Maia M, Bonafonte S, et al. Intravitreal Bevacizumab (Avastin) for Diabetic Retinopathy: The 2010 GLADAOF Lecture. J Ophthalmol. 2011;2011:584238.

147. Spaide RF, Fisher YL. Intravitreal bevacizumab (Avastin) treatment of proliferative diabetic retinopathy complicated by vitreous hemorrhage. Retina. 2006 Mar;26(3):275–8.

148. Blick SKA, Keating GM, Wagstaff AJ. Ranibizumab. Drugs. 2007;67(8):1199–206; discussion 1207-1209.

149. Babiuch AS, Wykoff CC, Srivastava SK, Talcott K, Zhou B, Hach J, et al. R retinal leakage index dynamics on ultra-widefield fluorescein angiography in eyes treated with intravitreal aflibercept for proliferative diabetic retinopathy in the recovery study. Retina. 2020 Nov;40(11):2175–83.

150. Lazzara F, Fidilio A, Platania CBM, Giurdanella G, Salomone S, Leggio GM, et al. Aflibercept regulates retinal inflammation elicited by high glucose via the PlGF/ERK pathway. Biochem Pharmacol. 2019 Oct;168:341–51.

151. Bressler SB, Almukhtar T, Bhorade A, Bressler NM, Glassman AR, Huang SS, et al. Repeated intravitreous ranibizumab injections for diabetic macular edema and the risk of sustained elevation of intraocular pressure or the need for ocular hypotensive treatment. JAMA Ophthalmol. 2015 May;133(5):589–97.

152. Wang W, Zhang X. Systemic Adverse Events after Intravitreal Bevacizumab versus Ranibizumab for Age-Related Macular Degeneration: A Meta-Analysis. PLoS One. 2014 Oct 16;9(10):e109744.

153. Ha D, Choi SR, Kwon Y, Park HH, Shin JY. Pattern of adverse events induced by aflibercept and ranibizumab. Medicine (Baltimore). 2019 Aug 16;98(33):e16785.

154. Wu L, Martínez-Castellanos MA, Quiroz-Mercado H, Arevalo JF, Berrocal MH, Farah ME, et al. Twelve-month safety of intravitreal injections of bevacizumab (Avastin): results of the Pan-American Collaborative Retina Study Group (PACORES). Graefes Arch Clin Exp Ophthalmol. 2008 Jan;246(1):81–7.

155. Nian S, Lo ACY, Mi Y, Ren K, Yang D. Neurovascular unit in diabetic retinopathy: pathophysiological roles and potential therapeutical targets. Eye and Vision. 2021 May 1;8(1):15.

156. Fu Z, Sun Y, Cakir B, Tomita Y, Huang S, Wang Z, et al. Targeting Neurovascular Interaction in Retinal Disorders. International Journal of Molecular Sciences. 2020 Jan;21(4):1503.

157. Jonsson KB, Frydkjaer-Olsen U, Grauslund J. Vascular Changes and Neurodegeneration in the Early Stages of Diabetic Retinopathy: Which Comes First? Ophthalmic Res. 2016;56(1):1–9.

158. Salvi L, Plateroti P, Balducci S, Bollanti L, Conti FG, Vitale M, et al. Abnormalities of retinal ganglion cell complex at optical coherence tomography in patients with type 2 diabetes: a sign of diabetic polyneuropathy, not retinopathy. J Diabetes Complications. 2016 Apr;30(3):469–76.

159. Sohn EH, van Dijk HW, Jiao C, Kok PHB, Jeong W, Demirkaya N, et al. Retinal neurodegeneration may precede microvascular changes characteristic of diabetic retinopathy in diabetes mellitus. Proceedings of the National Academy of Sciences. 2016 May 10;113(19):E2655–64.

160. Stem MS, Gardner TW. Neurodegeneration in the Pathogenesis of Diabetic Retinopathy: Molecular Mechanisms and Therapeutic Implications. Curr Med Chem. 2013;20(26):3241–50.

161. Eggers ED, Carreon TA. The effects of early diabetes on inner retinal neurons. Vis Neurosci. 2020 Sep 16;37:E006.

162. Kern TS, Berkowitz BA. Photoreceptors in diabetic retinopathy. J Diabetes Investig. 2015 Jul;6(4):371–80.

163. Ebbinghaus B, Sorenson CM, Sheibani N, Hoon M. Early effects of diabetes on retinal ganglion cell morphology and synaptic connectivity. Investigative Ophthalmology & Visual Science. 2021 Jun 21;62(8):3035.

164. Kaur C, Rathnasamy G, Foulds WS, Ling EA. Cellular and Molecular Mechanisms of Retinal Ganglion Cell Death in Hypoxic-Ischemic Injuries. J Neurol Exp Neurosci. 2015.

165. Kim SJ, Yoo WS, Choi M, Chung I, Yoo JM, Choi WS. Increased O-GlcNAcylation of NF-κB Enhances Retinal Ganglion Cell Death in Streptozotocin-induced Diabetic Retinopathy. Curr Eye Res. 2016;41(2):249–57.

166. Cui Y, Xu N, Xu W, Xu G. Mesenchymal stem cells attenuate hydrogen peroxide-induced oxidative stress and enhance neuroprotective effects in retinal ganglion cells. In Vitro Cell Dev Biol Anim. 2017 Apr;53(4):328–35.

167. Vecino E, Rodriguez FD, Ruzafa N, Pereiro X, Sharma SC. Glia-neuron interactions in the mammalian retina. Prog Retin Eye Res. 2016 Mar;51:1–40.

168. Coughlin BA, Feenstra DJ, Mohr S. Müller Cells and Diabetic Retinopathy. Vision Res. 2017 Oct;139:93–100.

169. Reichenbach A, Bringmann A. New functions of Müller cells. Glia. 2013;61(5):651–78.

170. Yang S, Qi S, Wang C. The role of retinal Müller cells in diabetic retinopathy and related therapeutic advances. Front Cell Dev Biol. 2022 Dec 2;10:1047487.

171. Sanchez MC, Chiabrando GA. Multitarget Activities of Müller Glial Cells and Low-Density Lipoprotein Receptor-Related Protein 1 in Proliferative Retinopathies. ASN Neuro. 2022;14:17590914221136365.

172. Hassan I, Luo Q, Majumdar S, Dominguez JM, Busik JV, Bhatwadekar AD. Tumor Necrosis Factor Alpha (TNF-α) Disrupts Kir4.1 Channel Expression Resulting in Müller Cell Dysfunction in the Retina. Invest Ophthalmol Vis Sci. 2017 May 1;58(5):2473–82.

173. Wang J, Xu X, Elliott MH, Zhu M, Le YZ. Müller cell-derived VEGF is essential for diabetes-induced retinal inflammation and vascular leakage. Diabetes. 2010 Sep;59(9):2297–305.

174. Bai Y, Ma J xing, Guo J, Wang J, Zhu M, Chen Y, et al. Müller cell-derived VEGF is a significant contributor to retinal neovascularization. J Pathol. 2009 Dec;219(4):446–54.

175. Schmalen A, Lorenz L, Grosche A, Pauly D, Deeg CA, Hauck SM. Proteomic Phenotyping of Stimulated Müller Cells Uncovers Profound Pro-Inflammatory Signaling and Antigen-Presenting Capacity. Front Pharmacol. 2021;12:771571.

176. Liu X, Ye F, Xiong H, Hu D, Limb GA, Xie T, et al. IL-1β Upregulates IL-8 Production in Human Müller Cells Through Activation of the p38 MAPK and ERK1/2 Signaling Pathways. Inflammation. 2014 Oct;37(5):1486–95.

177. Taghavi Y, Hassanshahi G, Kounis NG, Koniari I, Khorramdelazad H. Monocyte chemoattractant protein-1 (MCP-1/CCL2) in diabetic retinopathy: latest evidence and clinical considerations. J Cell Commun Signal. 2019 Dec;13(4):451–62.

178. Fu S, Dong S, Zhu M, Sherry DM, Wang C, You Z, et al. Müller Glia Are a Major Cellular Source of Survival Signals for Retinal Neurons in Diabetes. Diabetes. 2015 Oct;64(10):3554–63.

179. Wang L, Deng QQ, Wu XH, Yu J, Yang XL, Zhong YM. Upregulation of glutamate-aspartate transporter by glial cell line-derived neurotrophic factor ameliorates cell apoptosis in neural retina in streptozotocin-induced diabetic rats. CNS Neurosci Ther. 2013 Dec;19(12):945–53.

180. Gualtieri M, Feitosa-Santana C, Lago M, Nishi M, Ventura DF. Early visual changes in diabetic patients with no retinopathy measured by color discrimination and electroretinography. Psychol Neurosci. 2013;6:227–34.

181. Chen H, Zhang M, Huang S, Wu D. The photopic negative response of flash ERG in nonproliferative diabetic retinopathy. Doc Ophthalmol. 2008 Sep;117(2):129–35.

182. Jansson RW, Raeder MB, Krohn J. Photopic full-field electroretinography and optical coherence tomography in type 1 diabetic retinopathy. Graefes Arch Clin Exp Ophthalmol. 2015 Jul;253(7):989–97.

183. Luu CD, Szental JA, Lee SY, Lavanya R, Wong TY. Correlation between retinal oscillatory potentials and retinal vascular caliber in type 2 diabetes. Invest Ophthalmol Vis Sci. 2010 Jan;51(1):482–6.

184. Parisi V, Uccioli L, Monticone G, Parisi L, Manni G, Ippoliti D, et al. Electrophysiological assessment of visual function in IDDM patients. Electroencephalogr Clin Neurophysiol. 1997 Mar;104(2):171–9.

185. Kizawa J, Machida S, Kobayashi T, Gotoh Y, Kurosaka D. Changes of oscillatory potentials and photopic negative response in patients with early diabetic retinopathy. Jpn J Ophthalmol. 2006;50(4):367–73.

186. Tabl MA. Early detection of neurodegeneration in type 2 diabetic patients without diabetic retinopathy using electroretinogram and spectral-domain optical coherence tomography. Journal of the Egyptian Ophthalmological Society. 2020 Mar;113(1):26.

187. Park JC, Chau FY, Lim JI, McAnany JJ. Electrophysiological and pupillometric measures of inner retina function in nonproliferative diabetic retinopathy. Doc Ophthalmol. 2019 Oct;139(2):99–111.

188. Tyrberg M, Lindblad U, Melander A, Lövestam-Adrian M, Ponjavic V, Andréasson S. Electrophysiological studies in newly onset type 2 diabetes without visible vascular retinopathy. Doc Ophthalmol. 2011 Dec;123(3):193–8.

189. Attia Ali Ahmed M, Shawkat Abdelhaleem A. Evaluation of Microvascular and Visual Acuity Changes in Patients with Early Diabetic Retinopathy: Optical Coherence Tomography Angiography Study. OPTH. 2022 Feb;Volume 16:429–40.

190. Silva-Viguera MC, García-Romera MC, López-Izquierdo I, De-Hita-Cantalejo C, Sánchez-González MC, Bautista-Llamas MJ. Contrast Sensitivity Assessment in Early Diagnosis of Diabetic Retinopathy: A Systematic Review. Seminars in Ophthalmology. 2023 May 19;38(4):319–32.

191. Wolff BE, Bearse MA, Schneck ME, Dhamdhere K, Harrison WW, Barez S, et al. Color vision and neuroretinal function in diabetes. Doc Ophthalmol. 2015 Apr;130(2):131–9.

192. Feitosa-Santana C, Paramei GV, Nishi M, Gualtieri M, Costa MF, Ventura DF. Color vision impairment in type 2 diabetes assessed by the D-15d test and the Cambridge Colour Test. Ophthalmic Physiol Opt. 2010 Sep;30(5):717–23.

193. Hatchell DL, Toth CA, Barden CA, Saloupis P. Diabetic retinopathy in a cat. Exp Eye Res. 1995 May;60(5):591–3.

194. Mansour SZ, Hatchell DL, Chandler D, Saloupis P, Hatchell MC. Reduction of basement membrane thickening in diabetic cat retina by sulindac. Invest Ophthalmol Vis Sci. 1990 Mar 1;31(3):457–63.

195. Kobayashi T, Kubo E, Takahashi Y, Kasahara T, Yonezawa H, Akagi Y. Retinal vessel changes in galactose-fed dogs. Arch Ophthalmol. 1998 Jun;116(6):785–9.

196. Kador PF, Takahashi Y, Wyman M, Ferris F. Diabeteslike proliferative retinal changes in galactose-fed dogs. Arch Ophthalmol. 1995 Mar;113(3):352–4.

197. Tso MO, Kurosawa A, Benhamou E, Bauman A, Jeffrey J, Jonasson O. Microangiopathic retinopathy in experimental diabetic monkeys. Trans Am Ophthalmol Soc. 1988;86:389–421.

198. Lai AKW, Lo ACY. Animal Models of Diabetic Retinopathy: Summary and Comparison. J Diabetes Res. 2013;2013:106594.

199. Tolentino MJ, Miller JW, Gragoudas ES, Jakobiec FA, Flynn E, Chatzistefanou K, et al. Intravitreous injections of vascular endothelial growth factor produce retinal ischemia and microangiopathy in an adult primate. Ophthalmology. 1996 Nov;103(11):1820–8.

200. Edelman JL, Lutz D, Castro MR. Corticosteroids inhibit VEGF-induced vascular leakage in a rabbit model of blood-retinal and blood-aqueous barrier breakdown. Exp Eye Res. 2005 Feb;80(2):249–58.

201. Olivares AM, Althoff K, Chen GF, Wu S, Morrisson MA, DeAngelis MM, et al. Animal Models of Diabetic Retinopathy. Curr Diab Rep. 2017;17(10):93.

202. Quiroz J, Yazdanyar A. Animal models of diabetic retinopathy. Ann Transl Med. 2021 Aug;9(15):1272.

203. Gao G, Li Y, Fant J, Crosson CE, Becerra SP, Ma J xing. Difference in Ischemic Regulation of Vascular Endothelial Growth Factor and Pigment Epithelium--Derived Factor in Brown Norway and Sprague Dawley Rats Contributing to Different Susceptibilities to Retinal Neovascularization. Diabetes. 2002 Apr 1;51(4):1218–25.

204. Zhang SX, Ma JX, Sima J, Chen Y, Hu MS, Ottlecz A, et al. Genetic difference in susceptibility to the blood-retina barrier breakdown in diabetes and oxygen-induced retinopathy. Am J Pathol. 2005 Jan;166(1):313–21.

205. McLetchie NG. Alloxan diabetes: a discovery, albeit a minor one. J R Coll Physicians Edinb. 2002;32(2):134–42.

206. Dixon KC, King AJ, Malinin T. Pprotein in dying β-cells of the pancreatic islets. Quarterly Journal of Experimental Physiology and Cognate Medical Sciences. 1960;45(2):202–12.

207. Weerasekera LY, Balmer LA, Ram R, Morahan G. Characterization of Retinal Vascular and Neural Damage in a Novel Model of Diabetic Retinopathy. Investigative Ophthalmology & Visual Science. 2015 Jun 5;56(6):3721–30.

208. Gaucher D, Chiappore JA, Pâques M, Simonutti M, Boitard C, Sahel JA, et al. Microglial changes occur without neural cell death in diabetic retinopathy. Vision Research. 2007 Mar 1;47(5):612–23.

209. Kern TS, Engerman RL. Comparison of retinal lesions in alloxan-diabetic rats and galactose-fed rats. Current Eye Research. 1994 Jan 1;13(12):863–7.

210. Schröder S, Palinski W, Schmid-Schönbein GW. Activated monocytes and granulocytes, capillary nonperfusion, and neovascularization in diabetic retinopathy. Am J Pathol. 1991 Jul;139(1):81–100.

211. Doczi-Keresztesi Z, Jung J, Kiss I, Mezei T, Szabo L, Ember I. Retinal and renal vascular permeability changes caused by stem cell stimulation in alloxan-induced diabetic rats, measured by extravasation of fluorescein. In Vivo. 2012;26(3):427–35.

212. Sadikan MZ, Abdul Nasir NA, Lambuk L, Mohamud R, Reshidan NH, Low E, et al. Diabetic retinopathy: a comprehensive update on in vivo, in vitro and ex vivo experimental models. BMC Ophthalmology. 2023 Oct 19;23(1):421.

213. Szkudelski T. The mechanism of alloxan and streptozotocin action in B cells of the rat pancreas. Physiol Res. 2001;50(6):537–46.

214. Kim JH, Kim JH, Yu YS, Cho CS, Kim KW. Blockade of angiotensin II attenuates VEGF-mediated blood-retinal barrier breakdown in diabetic retinopathy. J Cereb Blood Flow Metab. 2009 Mar;29(3):621–8.

215. Su L, Ji J, Bian J, Fu Y, Ge Y, Yuan Z. Tacrolimus (FK506) prevents early retinal neovascularization in streptozotocin-induced diabetic mice. Int Immunopharmacol. 2012 Dec;14(4):606–12.

216. Feit-Leichman RA, Kinouchi R, Takeda M, Fan Z, Mohr S, Kern TS, et al. Vascular damage in a mouse model of diabetic retinopathy: relation to neuronal and glial changes. Invest Ophthalmol Vis Sci. 2005 Nov;46(11):4281–7.

217. Martin PM, Roon P, Van Ells TK, Ganapathy V, Smith SB. Death of Retinal Neurons in Streptozotocin-Induced Diabetic Mice. Investigative Ophthalmology & Visual Science. 2004 Sep 1;45(9):3330–6.

218. Piano I, Novelli E, Della Santina L, Strettoi E, Cervetto L, Gargini C. Involvement of Autophagic Pathway in the Progression of Retinal Degeneration in a Mouse Model of Diabetes. Front Cell Neurosci. 2016 Feb 19;10:42.

219. Ren X, Li C, Liu J, Zhang C, Fu Y, Wang N, et al. Thioredoxin plays a key role in retinal neuropathy prior to endothelial damage in diabetic mice. Oncotarget. 2017 May 24;8(37):61350–64.

220. Chang JYA, Yu F, Shi L, Ko ML, Ko GYP. Melatonin Affects Mitochondrial Fission/Fusion Dynamics in the Diabetic Retina. J Diabetes Res. 2019 Apr 11;2019:8463125.

221. Liao YR, Li ZJ, Zeng P, Lan YQ. TLR7 deficiency contributes to attenuated diabetic retinopathy via inhibition of inflammatory response. Biochemical and Biophysical Research Communications. 2017 Nov 18;493(2):1136–42.

222. Kubota S, Ozawa Y, Kurihara T, Sasaki M, Yuki K, Miyake S, et al. Roles of AMP-Activated Protein Kinase in Diabetes-Induced Retinal Inflammation. Investigative Ophthalmology & Visual Science. 2011 Nov 24;52(12):9142–8.

223. Li G, Tang J, Du Y, Lee CA, Kern TS. Beneficial effects of a novel RAGE inhibitor on early diabetic retinopathy and tactile allodynia. Mol Vis. 2011 Dec 6;17:3156–65.

224. Sergeys J, Etienne I, Van Hove I, Lefevere E, Stalmans I, Feyen JHM, et al. Longitudinal In Vivo Characterization of the Streptozotocin-Induced Diabetic Mouse Model: Focus on Early Inner Retinal Responses. Investigative Ophthalmology & Visual Science. 2019 Feb 27;60(2):807–22.

225. Kumar S, Zhuo L. Longitudinal in vivo imaging of retinal gliosis in a diabetic mouse model. Experimental Eye Research. 2010 Oct;91(4):530–6.

226. Rungger–Brändle E, Dosso AA, Leuenberger PM. Glial Reactivity, an Early Feature of Diabetic Retinopathy. Investigative Ophthalmology & Visual Science. 2000 Jun 1;41(7):1971–80.

227. Zhang J, Wu Y, Jin Y, Ji F, Sinclair SH, Luo Y, et al. Intravitreal injection of erythropoietin protects both retinal vascular and neuronal cells in early diabetes. Invest Ophthalmol Vis Sci. 2008 Feb;49(2):732–42.

228. Li L, Li YL, Zhou YF, Ge ZY, Wang LL, Li ZQ, et al. Jiangtang Xiaozhi Recipe () prevents diabetic retinopathy in streptozotocin-induced diabetic rats. Chin J Integr Med. 2017 Jun;23(6):425–32.

229. Gong CY, Lu B, Hu QW, Ji LL. Streptozotocin induced diabetic retinopathy in rat and the expression of vascular endothelial growth factor and its receptor. Int J Ophthalmol. 2013 Oct 18;6(5):573–7.

230. Park SH, Park JW, Park SJ, Kim KY, Chung JW, Chun MH, et al. Apoptotic death of photoreceptors in the streptozotocin-induced diabetic rat retina. Diabetologia. 2003 Sep 1;46(9):1260–8.

231. Shruthi K, Reddy SS, Reddy GB. Ubiquitin-proteasome system and ER stress in the retina of diabetic rats. Archives of Biochemistry and Biophysics. 2017 Aug 1;627:10–20.

232. Feng Y, Wang R, Xu J, Sun J, Xu T, Gu Q, et al. Hydrogen-Rich Saline Prevents Early Neurovascular Dysfunction Resulting from Inhibition of Oxidative Stress in STZ-Diabetic Rats. Current Eye Research. 2013 Mar;38(3):396–404.

233. Wang YJ, Xie XS, Feng SG, Long QX, Ai N, Wang BF. [Causes of death in STZ-induced rat models of diabetes mellitus]. Sichuan Da Xue Xue Bao Yi Xue Ban. 2014 Jul;45(4):691–5.

234. Genrikhs EE, Stelmashook EV, Golyshev SA, Aleksandrova OP, Isaev NK. Streptozotocin causes neurotoxic effect in cultured cerebellar granule neurons. Brain Res Bull. 2017 Apr;130:90–4.

235. Shoham S, Bejar C, Kovalev E, Weinstock M. Intracerebroventricular injection of streptozotocin causes neurotoxicity to myelin that contributes to spatial memory deficits in rats. Exp Neurol. 2003 Dec;184(2):1043–52.

236. Jiang N, Chen XL, Yang HW, Ma YR. Effects of nuclear factor κB expression on retinal neovascularization and apoptosis in a diabetic retinopathy rat model. Int J Ophthalmol. 2015 Jun 18;8(3):448–52.

237. Bahmani F, Bathaie SZ, Aldavood SJ, Ghahghaei A. Glycine therapy inhibits the progression of cataract in streptozotocin-induced diabetic rats. Mol Vis. 2012;18:439–48.

238. Paik SG, Michelis MA, Kim YT, Shin S. Induction of insulin-dependent diabetes by streptozotocin. Inhibition by estrogens and potentiation by androgens. Diabetes. 1982 Aug;31(8 Pt 1):724–9.

239. Vähätupa M, Järvinen TAH, Uusitalo-Järvinen H. Exploration of Oxygen-Induced Retinopathy Model to Discover New Therapeutic Drug Targets in Retinopathies. Front Pharmacol. 2020 Jun 11;11:873.

240. Stahl A, Connor KM, Sapieha P, Chen J, Dennison RJ, Krah NM, et al. The Mouse Retina as an Angiogenesis Model. Invest Ophthalmol Vis Sci. 2010 Jun;51(6):2813–26.

241. Connor KM, Krah NM, Dennison RJ, Aderman CM, Chen J, Guerin KI, et al. Quantification of oxygen-induced retinopathy in the mouse: a model of vessel loss, vessel regrowth and pathological angiogenesis. Nat Protoc. 2009 Nov;4(11):1565–73.

242. Zhang P, Wang H, Cao H, Xu X, Sun T. Insulin-Like Growth Factor Binding Protein-Related Protein 1 Inhibit Retinal Neovascularization in the Mouse Model of Oxygen-Induced Retinopathy. J Ocul Pharmacol Ther. 2017;33(6):459–65.

243. Mezu-Ndubuisi OJ, Wanek J, Chau FY, Teng P yu, Blair NP, Reddy NM, et al. Correspondence of retinal thinning and vasculopathy in mice with oxygen-induced retinopathy. Experimental Eye Research. 2014 May 1;122:119–22.

244. Villacampa P, Menger KE, Abelleira L, Ribeiro J, Duran Y, Smith AJ, et al. Accelerated oxygen-induced retinopathy is a reliable model of ischemia-induced retinal neovascularization. PLoS One. 2017 Jun 26;12(6):e0179759.

245. Nakamura S, Imai S, Ogishima H, Tsuruma K, Shimazawa M, Hara H. Morphological and Functional Changes in the Retina after Chronic Oxygen-Induced Retinopathy. PLoS One. 2012 Feb 14;7(2):e32167.

246. Madan A, Penn JS. Animal models of oxygen-induced retinopathy. Front Biosci. 2003 May 1;8:d1030-1043.

247. Downie LE, Pianta MJ, Vingrys AJ, Wilkinson-Berka JL, Fletcher EL. AT1 receptor inhibition prevents astrocyte degeneration and restores vascular growth in oxygen-induced retinopathy. Glia. 2008;56(10):1076–90.

248. Kim Y, Hong H kyoung, Park JR, Koh Y, Choi W, Woo SJ, et al. Vascular change in oxygen-induced retinopathy rat model observed using retinal optical coherence tomography angiography. Investigative Ophthalmology & Visual Science. 2017 Jun 23;58(8):4878.

249. Dembinska O, Rojas LM, Varma DR, Chemtob S, Lachapelle P. Graded Contribution of Retinal Maturation to the Development of Oxygen-Induced Retinopathy in Rats. Investigative Ophthalmology & Visual Science. 2001 Apr 1;42(5):1111–8.

250. Asare-Bediako B, Noothi SK, Li Calzi S, Athmanathan B, Vieira CP, Adu-Agyeiwaah Y, et al. Characterizing the Retinal Phenotype in the High-Fat Diet and Western Diet Mouse Models of Prediabetes. Cells. 2020 Feb 18;9(2):464.

251. Rajagopal R, Bligard GW, Zhang S, Yin L, Lukasiewicz P, Semenkovich CF. Functional Deficits Precede Structural Lesions in Mice With High-Fat Diet–Induced Diabetic Retinopathy. Diabetes. 2016 Apr;65(4):1072–84.

252. Dátilo MN, Sant'Ana MR, Formigari GP, Rodrigues PB, de Moura LP, da Silva ASR, et al. Omega-3 from Flaxseed Oil Protects Obese Mice Against Diabetic Retinopathy Through GPR120 Receptor. Sci Rep. 2018 Sep 25;8:14318.

253. Cheng Y, Yu X, Zhang J, Chang Y, Xue M, Li X, et al. Pancreatic kallikrein protects against diabetic retinopathy in KK Cg-Ay/J and high-fat diet/streptozotocin-induced mouse models of type 2 diabetes. Diabetologia. 2019 Jun;62(6):1074–86.

254. Zhang Q, Xiao X, Zheng J, Li M, Yu M, Ping F, et al. Compound Danshen Dripping Pill Inhibits Retina Cell Apoptosis in Diabetic Rats. Front Physiol. 2018;9:1501.

255. Wang J, Takeuchi T, Tanaka S, Kubo SK, Kayo T, Lu D, et al. A mutation in the insulin 2 gene induces diabetes with severe pancreatic beta-cell dysfunction in the Mody mouse. J Clin Invest. 1999 Jan;103(1):27–37.

256. Barber AJ, Antonetti DA, Kern TS, Reiter CEN, Soans RS, Krady JK, et al. The Ins2Akita Mouse as a Model of Early Retinal Complications in Diabetes. Investigative Ophthalmology & Visual Science. 2005 Jun 1;46(6):2210–8.

257. Han Z, Guo J, Conley SM, Naash MI. Retinal Angiogenesis in the Ins2Akita Mouse Model of Diabetic Retinopathy. Invest Ophthalmol Vis Sci. 2013 Jan;54(1):574–84.

258. Gastinger MJ, Kunselman AR, Conboy EE, Bronson SK, Barber AJ. Dendrite Remodeling and Other Abnormalities in the Retinal Ganglion Cells of Ins2Akita Diabetic Mice. Investigative Ophthalmology & Visual Science. 2008 Jun 1;49(6):2635–42.

259. Hombrebueno JR, Chen M, Penalva RG, Xu H. Loss of synaptic connectivity, particularly in second order neurons is a key feature of diabetic retinal neuropathy in the Ins2Akita mouse. PLoS One. 2014;9(5):e97970.

260. McLenachan S, Chen X, McMenamin PG, Rakoczy EP. Absence of clinical correlates of diabetic retinopathy in the Ins2Akita retina. Clin Exp Ophthalmol. 2013 Aug;41(6):582–92.

261. Li CR, Sun SG. VEGF expression and cell apoptosis in NOD mouse retina. Int J Ophthalmol. 2010 Sep 18;3(3):224–7.

262. Makino S, Kunimoto K, Muraoka Y, Mizushima Y, Katagiri K, Tochino Y. Breeding of a non-obese, diabetic strain of mice. Jikken Dobutsu. 1980 Jan;29(1):1–13.

263. Cheung AKH, Fung MKL, Lo ACY, Lam TTL, So KF, Chung SSM, et al. Aldose reductase deficiency prevents diabetes-induced blood-retinal barrier breakdown, apoptosis, and glial reactivation in the retina of db/db mice. Diabetes. 2005 Nov;54(11):3119–25.

264. Tang L, Zhang Y, Jiang Y, Willard L, Ortiz E, Wark L, et al. Dietary wolfberry ameliorates retinal structure abnormalities in db/db mice at the early stage of diabetes. Exp Biol Med (Maywood). 2011 Sep;236(9):1051–63.

265. Van Eeden PE, Tee LBG, Lukehurst S, Lai CM, Rakoczy EP, Beazley LD, et al. Early Vascular and Neuronal Changes in a VEGF Transgenic Mouse Model of Retinal Neovascularization. Investigative Ophthalmology & Visual Science. 2006 Oct 1;47(10):4638–45.

266. Shen WY, Lai CM, Graham CE, Binz N, Lai YKY, Eade J, et al. Long-term global retinal microvascular changes in a transgenic vascular endothelial growth factor mouse model. Diabetologia. 2006 Jul 1;49(7):1690–701.

267. Rakoczy EP, Rahman ISA, Binz N, Li CR, Vagaja NN, de Pinho M, et al. Characterization of a Mouse Model of Hyperglycemia and Retinal Neovascularization. Am J Pathol. 2010 Nov;177(5):2659–70.

268. Van Hove I, De Groef L, Boeckx B, Modave E, Hu TT, Beets K, et al. Single-cell transcriptome analysis of the Akimba mouse retina reveals cell-type-specific insights into the pathobiology of diabetic retinopathy. Diabetologia. 2020 Oct 1;63(10):2235–48.

269. Simó R, Stitt AW, Gardner TW. Neurodegeneration in diabetic retinopathy: does it really matter? Diabetologia. 2018 Sep 1;61(9):1902–12.

270. Sima AA, Chakrabarti S, Garcia-Salinas R, Basu PK. The BB-rat--an authentic model of human diabetic retinopathy. Curr Eye Res. 1985 Oct;4(10):1087–92.

271. Sima AA, Garcia-Salinas R, Basu PK. The BB Wistar rat: an experimental model for the study of diabetic retinopathy. Metabolism. 1983 Jul;32(7 Suppl 1):136–40.

272. Danis RP, Yang Y. Microvascular retinopathy in the Zucker diabetic fatty rat. Invest Ophthalmol Vis Sci. 1993 Jun;34(7):2367–71.

273. Yang YS, Danis RP, Peterson RG, Dolan PL, Wu YQ. Acarbose partially inhibits microvascular retinopathy in the Zucker Diabetic Fatty rat (ZDF/Gmi-fa). J Ocul Pharmacol Ther. 2000 Oct;16(5):471–9.

274. Behl Y, Krothapalli P, Desta T, DiPiazza A, Roy S, Graves DT. Diabetes-Enhanced Tumor Necrosis Factor-α Production Promotes Apoptosis and the Loss of Retinal Microvascular Cells in Type 1 and Type 2 Models of Diabetic Retinopathy. Am J Pathol. 2008 May;172(5):1411–8.

275. Caolo V, Roblain Q, Lecomte J, Carai P, Peters L, Cuijpers I, et al. Resistance to retinopathy development in obese, diabetic and hypertensive ZSF1 rats: an exciting model to identify protective genes. Sci Rep. 2018 Aug 9;8(1):11922.

276. Miyamura N, Amemiya T. Lens and Retinal Changes in the WBN/Kob Rat (Spontaneously Diabetic Strain): Electron-Microscopic Study. Ophthalmic Research. 1998 Jun 12;30(4):221–32.

277. Tsuji N, Matsuura T, Ozaki K, Sano T, Narama I. Diabetic retinopathy and choroidal angiopathy in diabetic rats (WBN/Kob). Exp Anim. 2009 Oct;58(5):481–7.

278. Bhutto IA, Miyamura N, Amemiya T. Vascular architecture of degenerated retina in WBN/Kob rats: corrosion cast and electron microscopic study. Ophthalmic Res. 1999;31(5):367–77.

279. Watanabe TK, Suzuki M, Yamasaki Y, Okuno S, Hishigaki H, Ono T, et al. Mutated G-protein-coupled receptor GPR10 is responsible for the hyperphagia/dyslipidaemia/obesity locus of Dmo1 in the OLETF rat. Clin Exp Pharmacol Physiol. 2005;32(5–6):355–66.

280. Lu ZY, Bhutto IA, Amemiya T. Retinal changes in Otsuka long-evans Tokushima Fatty rats (spontaneously diabetic rat)--possibility of a new experimental model for diabetic retinopathy. Jpn J Ophthalmol. 2003;47(1):28–35.

281. Miyamoto K, Hiroshiba N, Tsujikawa A, Ogura Y. In vivo demonstration of increased leukocyte entrapment in retinal microcirculation of diabetic rats. Invest Ophthalmol Vis Sci. 1998 Oct;39(11):2190–4.

282. Miyamura N, Bhutto IA, Amemiya T. Retinal capillary changes in Otsuka Long-Evans Tokushima fatty rats (spontaneously diabetic strain). Electron-microscopic study. Ophthalmic Res. 1999;31(5):358–66.

283. Goto Y, Suzuki K, Ono T, Sasaki M, Toyota T. Development of diabetes in the non-obese NIDDM rat (GK rat). Adv Exp Med Biol. 1988;246:29–31.

284. Miyamoto K, Ogura Y, Nishiwaki H, Matsuda N, Honda Y, Kato S, et al. Evaluation of retinal microcirculatory alterations in the Goto-Kakizaki rat. A spontaneous model of non-insulin-dependent diabetes. Invest Ophthalmol Vis Sci. 1996 Apr;37(5):898–905.

285. Carmo A, Cunha-Vaz JG, Carvalho AP, Lopes MC. Nitric oxide synthase activity in retinas from non-insulin-dependent diabetic Goto-Kakizaki rats: correlation with blood-retinal barrier permeability. Nitric Oxide. 2000 Dec;4(6):590–6.

286. Sasase T, Ohta T, Masuyama T, Yokoi N, Kakehashi A, Shinohara M. The spontaneously diabetic torii rat: an animal model of nonobese type 2 diabetes with severe diabetic complications. J Diabetes Res. 2013;2013:976209.

287. Kakehashi A, Saito Y, Mori K, Sugi N, Ono R, Yamagami H, et al. Characteristics of diabetic retinopathy in SDT rats. Diabetes Metabolism Res. 2006 Nov;22(6):455–61.

288. Okuno T, Oku H, Sugiyama T, Ikeda T. Electroretinographic study of spontaneously diabetic Torii rats. Doc Ophthalmol. 2008 Nov;117(3):191–6.

289. Yamada H, Yamada E, Higuchi A, Matsumura M. Retinal neovascularisation without ischaemia in the spontaneously diabetic Torii rat. Diabetologia. 2005 Aug;48(8):1663–8.

290. Shinohara M, Masuyama T, Shoda T, Takahashi T, Katsuda Y, Komeda K, et al. A new spontaneously diabetic non-obese Torii rat strain with severe ocular complications. Int J Exp Diabetes Res. 2000;1(2):89–100.

291. Ozaki H, Hayashi H, Vinores SA, Moromizato Y, Campochiaro PA, Oshima K. Intravitreal Sustained Release of VEGF Causes Retinal Neovascularization in Rabbits and Breakdown of the Blood– Retinal Barrier in Rabbits and Primates. Experimental Eye Research. 1997 Apr;64(4):505–17.

292. Wong CG, Rich KA, Liaw LHL, Hsu HT, Berns MW. Intravitreal VEGF and bFGF produce florid retinal neovascularization and hemorrhage in the rabbit. Current Eye Research. 2001 Jan;22(2):140–7.

293. Jiang J, Xia XB, Xu HZ, Xiong Y, Song WT, Xiong SQ, et al. Inhibition of retinal neovascularization by gene transfer of small interfering RNA targeting HIF-1α and VEGF. Journal of Cellular Physiology. 2009;218(1):66–74.

294. Wang JH, Roberts GE, Liu GS. Updates on Gene Therapy for Diabetic Retinopathy. Curr Diab Rep. 2020 May 16;20(7):22.

295. Biswal MR, Prentice HM, Dorey CK, Blanks JC. A hypoxia-responsive glial cell-specific gene therapy vector for targeting retinal neovascularization. Invest Ophthalmol Vis Sci. 2014 Nov 6;55(12):8044–53.

296. Gong Y, Chang ZP, Ren RT, Wei SH, Zhou HF, Chen XF, et al. Protective Effects of Adeno-associated Virus Mediated Brain-derived Neurotrophic Factor Expression on Retinal Ganglion Cells in Diabetic Rats. Cell Mol Neurobiol. 2012 Apr;32(3):467–75.

297. Gutierrez-Guerrero A, Cosset FL, Verhoeyen E. Lentiviral Vector Pseudotypes: Precious Tools to Improve Gene Modification of Hematopoietic Cells for Research and Gene Therapy. Viruses. 2020 Sep;12(9):1016.

298. Gándara C, Affleck V, Stoll EA. Manufacture of Third-Generation Lentivirus for Preclinical Use, with Process Development Considerations for Translation to Good Manufacturing Practice. Human Gene Therapy Methods. 2018 Feb;29(1):1–15.

299. Stripecke R, Kasahara N. Lentiviral and Retroviral Vector Systems. In: Hunt KK, Vorburger SA, Swisher SG, editors. Gene Therapy for Cancer [Internet]. Totowa, NJ: Humana Press; 2007 [cited 2024 Jan 10]. p. 39–71. (Cancer Drug Discovery and Development). Available from: http://link.springer.com/10.1007/978-1-59745-222-9_3

300. Burns JC, Friedmann T, Driever W, Burrascano M, Yee JK. Vesicular stomatitis virus G glycoprotein pseudotyped retroviral vectors: concentration to very high titer and efficient gene transfer into mammalian and nonmammalian cells. Proc Natl Acad Sci U S A. 1993 Sep 1;90(17):8033–7.

301. Fesnak A, O'Doherty U. Clinical Development and Manufacture of Chimeric Antigen Receptor T cells and the Role of Leukapheresis. European Oncology & Haematology. 2017 Jan 1;13:28.

302. Munis AM. Gene Therapy Applications of Non-Human Lentiviral Vectors. Viruses. 2020 Sep 29;12(10):1106.

303. Abordo-Adesida E, Follenzi A, Barcia C, Sciascia S, Castro MG, Naldini L et al. Stability of Lentiviral Vector-Mediated Transgene Expression in the Brain in the Presence of Systemic Antivector Immune Responses. Hum Gene Ther. 2005 Jun;16(6):741–51.

304. Rommereim L, Akhade AS, Germain RN, Fraser IDC, Subramanian N. Lentivirus-mediated Conditional Gene Expression. Bio Protoc. 2021 Nov 5;11(21):e4205.

305. Costello A, Lao NT, Gallagher C, Capella Roca B, Julius LAN, Suda S, et al. Leaky Expression of the TET-On System Hinders Control of Endogenous miRNA Abundance. Biotechnol J. 2019 Mar;14(3):e1800219.

306. Mullick A, Xu Y, Warren R, Koutroumanis M, Guilbault C, Broussau S, et al. The cumate gene-switch: a system for regulated expression in mammalian cells. BMC Biotechnology. 2006 Nov 3;6(1):43.

307. Eaton RW. p-Cymene catabolic pathway in Pseudomonas putida F1: cloning and characterization of DNA encoding conversion of p-cymene to p-cumate. J Bacteriol. 1997 May;179(10):3171–80.

308. Gaillet B, Gilbert R, Broussau S, Pilotte A, Malenfant F, Mullick A, et al. High-level recombinant protein production in CHO cells using lentiviral vectors and the cumate gene-switch. Biotech & Bioengineering. 2010 Jun;106(2):203–15.

309. Qi Z, Wilkinson MN, Chen X, Sankararaman S, Mayhew D, Mitra RD. An optimized, broadly applicable piggyBac transposon induction system. Nucleic Acids Res. 2017 Apr 20;45(7):e55.

310. Wang D, Tai PWL, Gao G. Adeno-associated virus vector as a platform for gene therapy delivery. Nat Rev Drug Discov. 2019 May;18(5):358–78.

311. Naso MF, Tomkowicz B, Perry WL, Strohl WR. Adeno-Associated Virus (AAV) as a Vector for Gene Therapy. BioDrugs. 2017;31(4):317–34.

312. Kimura T, Ferran B, Tsukahara Y, Shang Q, Desai S, Fedoce A, et al. Production of adeno-associated virus vectors for in vitro and in vivo applications. Sci Rep. 2019 Sep 19;9(1):13601.

313. Hammond SL, Leek AN, Richman EH, Tjalkens RB. Cellular selectivity of AAV serotypes for gene delivery in neurons and astrocytes by neonatal intracerebroventricular injection. PLOS ONE. 2017 Dec 15;12(12):e0188830.

314. Penaud-Budloo M, Le Guiner C, Nowrouzi A, Toromanoff A, Chérel Y, Chenuaud P, et al. Adeno-Associated Virus Vector Genomes Persist as Episomal Chromatin in Primate Muscle. J Virol. 2008 Aug;82(16):7875–85.

315. Daya S, Berns KI. Gene Therapy Using Adeno-Associated Virus Vectors. Clin Microbiol Rev. 2008 Oct;21(4):583–93.

316. Liu S, Biesemeier AK, Tschulakow AV, Thakkar HV, Julien-Schraermeyer S, Schraermeyer U. A new rat model of treatment-naive quiescent choroidal neovascularization induced by human VEGF165 overexpression. Biol Open. 2020 Jun 11;9(6):bio048736.

317. Wang F, Rendahl KG, Manning WC, Quiroz D, Coyne M, Miller SS. AAV-Mediated Expression of Vascular Endothelial Growth Factor Induces Choroidal Neovascularization in Rat. Investigative Ophthalmology & Visual Science. 2003 Feb 1;44(2):781–90.

318. Lebherz C, Maguire AM, Auricchio A, Tang W, Aleman TS, Wei Z, et al. Nonhuman Primate Models for Diabetic Ocular Neovascularization Using AAV2-Mediated Overexpression of Vascular Endothelial Growth Factor. Diabetes. 2005 Apr 1;54(4):1141–9.

319. Weigelt CM, Fuchs H, Schönberger T, Stierstorfer B, Strobel B, Lamla T, et al. AAV-Mediated Expression of Human VEGF, TNF-α, and IL-6 Induces Retinal Pathology in Mice. Transl Vis Sci Technol. 2021 Sep 14;10(11):15.

CHAPTER 2

Structure–Function Relationships in the Rodent Streptozotocin-Induced Model for Diabetic Retinopathy: A Systematic Review

Inesa Lelyte,[1,2] Zubair Ahmed,[2,3] Simon Kaja,[4,5] and Giedrius Kalesnykas[1,6]

[1]Research and Development Division, Experimentica Ltd., Kuopio, Finland.

[2]Institute of Inflammation and Ageing, and [3]Center for Trauma Sciences Research, University of Birmingham, Birmingham, United Kingdom.

[4]Departments of Ophthalmology and Molecular Pharmacology and Neuroscience, Stritch School of Medicine, Loyola University Chicago, Maywood, Illinois, USA.

[5]Experimentica Ltd., Research and Development Division, Forest Park, Illinois, USA.

[6]Experimentica Ltd., Research and Development Division, Vilnius, Lithuania.

A version of this manuscript has been published in

Journal of Ocular Pharmacology and Therapeutics

2.1 Abstract

The streptozotocin (STZ)-induced rodent model is one of the most commonly employed models in preclinical drug discovery for diabetic retinopathy (DR). However, standardization and validation of experimental readouts are largely lacking. The aim of this systematic review was to identify and compare the most useful readouts of STZ-induced DR and provide recommendations for future study design based on our findings. We performed a systematic search using 2 major databases, PubMed and EMBASE. Only articles describing STZ-induced DR describing both functional and structural readouts were selected. We also assessed the risk of bias and analyzed qualitative data in the selected studies. We identified 21 studies that met our inclusion/exclusion criteria, using either rats or mice and study periods of 2 to 24 weeks. Glucose level thresholds used to define hyperglycemia were inconsistent between studies, however, most studies used either 250 or 300.6 mg/dL as a defining criterion for hyperglycemia. All included studies performed electroretinography (ERG) and reported a reduction in a-, b-, or c-wave and/or oscillatory potential amplitudes. Spectral-domain optical coherence tomography and fluorescein angiography, as well as immunohistochemical and histopathological analyses showed reductions in retinal thickness, vascular changes, and presence of inflammation. Risk of bias assessment showed that all studies had a high risk of bias due to lack of reporting or correctly following procedures. Our systematic review highlights that ERG represents the most consistent functional readout in the STZ model. However, due to the high risk of bias, caution must be used when interpreting these studies.

2.2 Introduction

Diabetic retinopathy (DR) occurs in more than one-third of individuals with diabetes and is one of the leading causes of blindness in individuals 24 to 74 years of age.[1] With increasing human life expectancy and rising numbers of diabetics, it is estimated that the number of people with DR worldwide will grow from 126.6 million diagnosed in 2010 to 191.0 million cases by 2030.[2] Almost all patients who are diagnosed with type I diabetes will develop some degree of DR within 2 decades after diagnosis; for type II diabetes this probability increases up to 80% at 20 years after disease onset.[3] Hyperglycemia, oxidative stress, anemia, pericyte loss, apoptosis of endothelial cells, thickening of the basement membrane, and other mechanisms are considered to play an important role in the pathogenesis of DR.[4] If DR is left untreated, it results in diabetic macular edema (DME) and proliferative DR (PDR), which leads to total loss of vision.[1] Thus, there is an urgent need for novel therapeutics that can slow down the progression of disease and prevent the development of end-stage DR, especially DME and PDR.

Animal models that mimic the pathophysiology of DR have contributed significantly to the understanding of the etiology and progression of this condition and validated and standardized models are required for drug discovery and development. Historically, DR animal model studies have relied primarily on histological and immunohistochemical readouts.[5,6]

In addition, various molecular and biochemical techniques, including quantitative polymerase chain reaction (qPCR), single-cell RNA sequencing, western blot, TUNEL assay, as well as protein, enzyme, and cytokine assays are carried out to study the development of DR in diabetic animals.[7–9] Research shows that fluorescein angiography (FA), spectral-domain optical coherence tomography (SD-OCT), and electroretinography (ERG) in animal models of DR could potentially help to detect early changes of DR, and could aid in developing novel, more potent drugs for an early treatment of DR.[10–15]

The most commonly used rodent model in drug discovery utilizes streptozotocin (STZ) administration to induce chronic hyperglycemia and DR by causing pancreatic β cell loss.[16] DR phenotypes observed in STZ-induced rodents include thinning of retinal layers,[17,18] loss of retinal cells,[19] and increased inflammation.[20] Historically, preclinical studies relied on morphological changes as detected using *post mortem* tissue processing, histological and immunohistochemical staining, and morphometric analyses.

With advancement in functional assessments and, in particular, adaptation of clinically used *in vivo* imaging modalities, detection of early phenotypes reminiscent of subclinical and/or non-PDR is now possible in rodents. However, both functional and imaging modalities rely on a clear optical path and measurements can be confounded or even become impossible as animals develop diabetic cataracts. Therefore, accurate and early detection of DR-related changes by noninvasive techniques requires strict validation to identify the optimal balance between disease progression, accuracy of assessment of structure–function relationships and magnitude of the therapeutic window for drug discovery.

These considerations are of particular importance as early phenotypes in the STZ model that can be studied using in life imaging modalities and electrophysiological recordings identify and assess mostly subclinical pathological changes. Furthermore, while OCT and FA, and more recently, optical coherence tomography angiography (OCT-A) are routinely used to diagnose the various disease stages of DR, electrophysiology is not typically used in ophthalmic practice.

Despite rapid development of noninvasive methods and their applications, the STZ-induced DR model lacks standardized experimental paradigms and readouts. Moreover, the reliability and consistency of neovascularization in STZ models vary across the literature. Typically, STZ models are often used to replicate early to intermediate stages of DR, however, they frequently

fail to reliably induce significant neovascularization or employ dependable methods to verify its presence. Although some research indicates neovascularization in STZ models, the techniques used to confirm it are often insufficient. For example, hematoxylin and eosin staining, though beneficial for overall tissue morphology, lacks the precision to accurately identify and distinguish new blood vessel growth.[21] Therefore, the goal of this study is to perform systematic literature review of the literature in search of standardized readouts or experimental paradigms, which would be useful in future STZ studies.

2.3 Methods

Literature search

We followed a comprehensive search strategy to obtain published articles by using the recommendations for the Preferred Reporting Items for Systematic Reviews and MetaAnalyses (PRISMA) reporting guidelines.[22] Two major databases, PubMed and EMBASE, were investigated to identify articles suitable to STZ-induced DR animal model, from inception to 14th of August 2020. The searched items were used in combination: STZ OR streptozotocin AND diabetic retinopathy OR FA OR fluorescence angiography OR OCT OR optical coherence tomography OR ERG OR electroretinogram OR VFP OR vitreofluorophotometry. Search terms were queried in both databases.

Inclusion and exclusion criteria

Records were included in this systematic review if they met the following inclusion criteria: (1) studies in English, (2) published in the last 10 years (starting 2010), (3) articles in peer-reviewed scientific journals, and (4) studies conducted on rodents only. We excluded the following: (1) Meta-analysis, review and systematic review articles, (2) clinical and *in vitro* studies, and (3) studies in languages other than English.

Data collection

Two reviewers (I.L. and Z.A.) independently conducted the literature search based on the titles and abstracts. Any discrepancies were resolved by discussion and if needed, consultation with a third reviewer (S.K). Relevant articles had to meet the above inclusion/exclusion criteria. Records were imported into Excel, duplicates removed, titles and abstracts searched manually, and full text of potential studies was retrieved.

Data extraction and synthesis

The following data are extracted: (1) study characteristics; (2) induction of DR; and (3) outcome measures in studies.

Risk of bias assessment

To assess bias in the included studies, we used the SYRCLE risk of bias tool for animal studies, which is based on the Cochrane Collaboration's tool for assessing risk bias in randomized controlled trials.[23,24] Bias assessments were carried out by 2 independent reviewers (I.L. and Z.A) and any discrepancies were resolved after discussion. Risk of bias was assessed using 10 criteria in the SYRCLE risk of bias tool that is related to 6 types of bias: selection bias, performance bias, detection bias, attrition bias, reporting bias, and other sources of bias.[23]

Statistical analysis

Descriptive statistics were used to characterize included studies. The kappa statistic was used to assess interrater agreement between the 2 reviewers. Since included studies did not contain sufficient quantitative data, a meta-analysis was not possible and hence a qualitative comparison between studies was performed.

2.4 Results

Study selection

A systematic search according to our strategy identified a total of 622 studies obtained from PubMed and EMBASE (Fig. 1). After removing duplicates, 434 studies were screened by title and abstract and 356 were excluded. Seventy-eight articles were considered acceptable, of which 51 studies were excluded after full-text screening due to either a long follow-up time (*n* = 4) or lack of structure–function relationship readouts (*n* = 51). Ultimately, 21 studies were included in the qualitative synthesis. Section may be divided by subheadings. It should provide a concise and precise description of the experimental results, their interpretation, as well as the experimental conclusions that can be drawn.

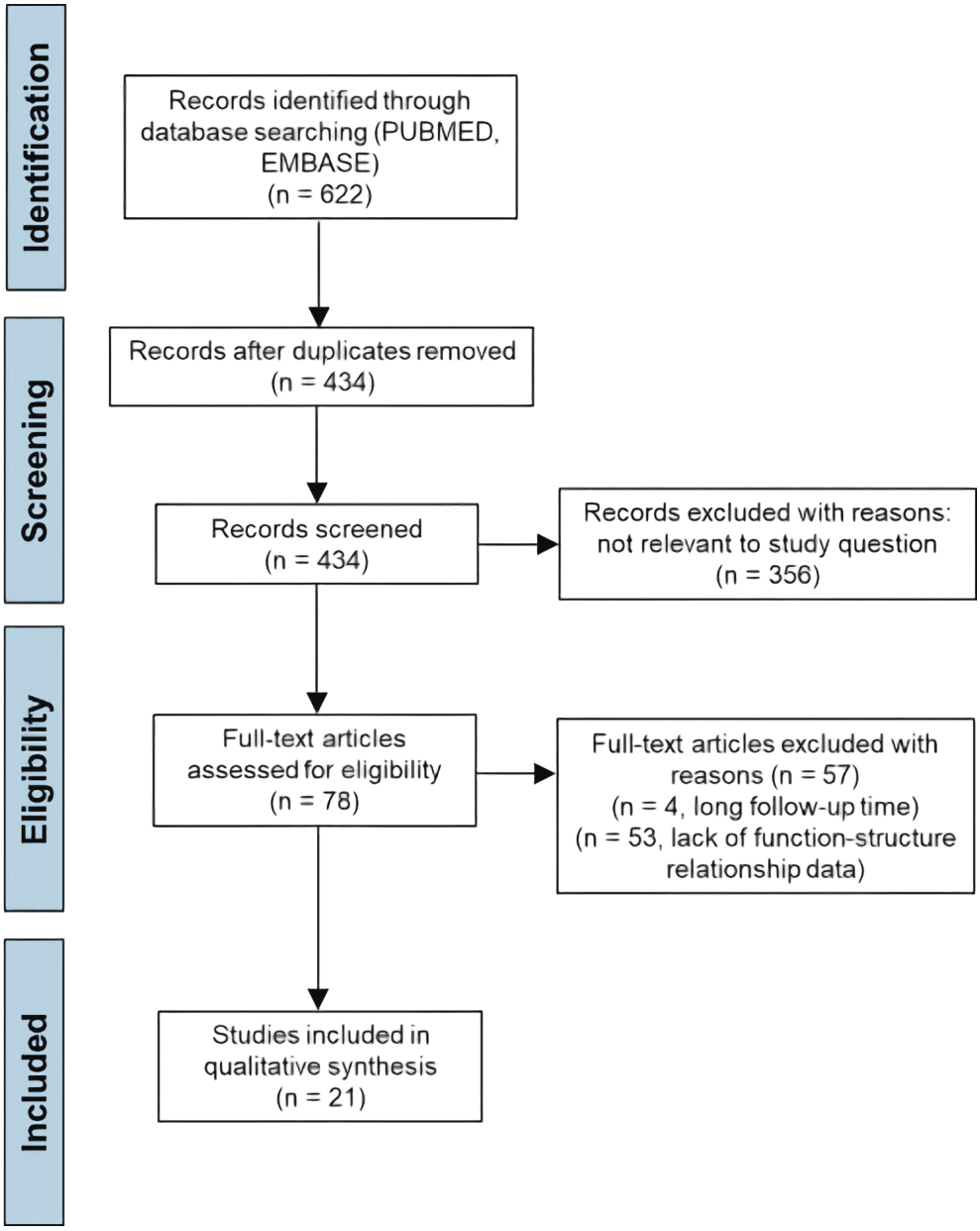

FIG. 1. Prisma flow chart illustrating the process of literature search.

Study characteristics

From the included studies, 11 were conducted in rats (8 in Sprague-Dawley rats, 2 in Wistar rats, 1 study in Brown Norway rats), whereas the remaining studies were conducted in mice (3 in C57BL6, 4 in C57BL6/J; 2 in BALB/c, 1 in B6.129S4) (Table 1). Although all studies used STZ to induce DR, each one considered different glucose levels as diabetic. In addition, follow-up times also varied from 2 to 24 weeks post-DR induction.

STZ injection

The majority of included studies with rats used single STZ injection to induce DR. Only Nagai et al.[25] and Deguchi et al.[26] used 2 STZ injections on 2 consecutive days. However, the amount of administered STZ for rats varied from 30 to 100 mg/kg. As for the type of injections, almost in all studies, researchers performed intraperitoneal injections, except Hernández et al.[27] and Yee et al.,[28] who administered STZ through the rat's tail vein. In contrast, the number of STZ injections in mice studies were more variable. From collected studies, 4 of them had 5 STZ injections, 3 studies had 3 injections, and 2 single STZ injections. The volume of STZ injections for mice varied from 50 to 150 mg/kg. All STZ injections to mice were performed intraperitoneally.

Glucose level considered as diabetic

Out of all included articles, 8 studies considered rodents as diabetic, which had equal or greater than 250 mg/dL of glucose.[27,29–34] While Zhang et al.[35] considered a threshold of 199.8 mg/dL (the equivalent of 11.1 mmol/L) of glucose as diabetic for Sprague-Dawley rats. However, for Nagai et al.[25] and Yee et al.[28] glucose level had to rise more than 250 mg/dL to consider rats as diabetic, 267.6 and 270 mg/dL (the equivalent of 15 mmol/L), respectively. Other 7 research groups considered rodents with induced diabetes with equal or greater than 300.6 mg/dL (the

equivalent of 16.7 mmol/L) of glucose.[36–43] While for Qiu et al.[44] glucose level in animals had to hit 350 mg/dL, to be considered as diabetic. Only Deguchi et al.[26] and Liao et al.[31] presented no data of glucose level in rodents.

Functional readouts

All studies used either flash electroretinography or full-field ERG, direct-coupled electroretinography (DC-ERG) or visual evoked potentials (VEP).

In vivo imaging

From included articles, six[31,32,37,38,43,44]performed OCT to observe structural changes of the retinas and to evaluate total retinal thickness and the thickness of individual retinal layers. The other 5 studies[29,31,32,40,44] used FA to monitor morphological and pathological changes in the eye fundus. Liao et al.[31] and Liao et al.[33] performed fundus photography (FP) in addition to FA. The rest of included articles did not use any *in vivo* imaging.

Postmortem analysis

The included studies used a number of different postmortem analyses, including Hematoxylin and Eosin (H&E) and Toluidine Blue staining to quantify retinal thickness, western blot assays, and enzyme-linked immunosorbent assay to detect specific proteins in retina; qPCR to evaluate gene expression, leukostasis assays to count the number of adherent leukocytes, Evans Blue extravasation to quantify blood–retinal barrier breakdown, and to measure retinal vascular permeability, trypsin-digested retinal whole mounts for quantification of acellular capillaries and pericyte loss, as well as TUNEL and MTT assays to assess viability of retina cells.

Table 1. Characteristics of the Included Studies

Study	*Species (animal number)*	*STZ injection*	*Follow-up time in weeks*	*Glucose level considered as diabetic (mg/dL)*	*Functional readouts*	In vivo *imaging*	*Postmortem analyses*
He et al.[37,a]	Sprague-Dawley rats (*n* = 30)	Single intraperitoneal injection of STZ (60 mg/kg) +high-fat and high-calorie diet	4	300.6	Full-field ERG	OCT	Antioxidant parameters: the concentration of antioxidant SOD; Inflammatory parameters: levels of proinflammatory cytokines (TNF-α and IL-6); Immunofluorescence and western blot assay: expression VEGF-A,

							ALDH2, and expression of Nrf2 and Sirt1.
Qiu et al.[44]	Brown Norway rats (*n* = 48)	Single intraperitoneal injection of STZ (50 mg/kg)	8	>350	Flash ERG	OCT	Evans Blue extravasation: retinal vascular permeability; Leukostasis assay: number of adherent leukocytes; Western blot analysis: levels of VEGF, ICAM-1, and β-actin.
Sergeys et al.[32]	C57BL/6J mice (*n* varies from 4 to 18 depending on the readout)	5 sequential daily intraperitoneal injections of STZ (50 mg/kg)	24	>250	Full-field ERG	FA, OCT	Leukostasis assay: number of adherent leukocytes;

							H&E staining: observation of general retinal and the optic nerve head morphology; Neurodegeneration: number of RGC (RBPMS) and cholinergic amacrine cell (ChAT); Inflammation and Gliosis: number of macrophages (F4/80); and Muller cell (vimentin).

Liao et al.[31,b]	C57BL/6 mice (n = 25)	5 sequential daily intraperitoneal injections of STZ (55 mg/kg) + whole-body hypoxia (10% O_2)	4	>250	Flash ERG	OCT, FA, FP	H&E staining: morphology of the retina; TUNEL assay: morphology of the retina, number of INL and ONL cells; Western blot analysis: expression of inflammatory and junction proteins (BAX, COX-2, iNOS); MTT assay: viability of RPE cells.
Chang et al.[29]	C57BL/6J mice (n = 37)	3 sequential daily intraperitoneal	12	>250	Flash ERG	FA	Immunofluorescent staining:

		injections of STZ (100 mg/kg)					observation of mitochondrial processes with DRP1, MFN2, and MCU
Feng et al.[30]	Sprague-Dawley rats (*n* = 90)	Single intraperitoneal injection of STZ (60 mg/kg)	4	>250	Full-field ERG	No data	BRB breakdown: extravasation of albumin; H&E staining: thicknesses of the IPL, INL and ONL, number of RGC; ELISA: activities of antioxidant enzyme (SOD, GSHPx, GSSGRed, and GSHTrans); and

							examination of oxidative stress (levels of 4-HNE and 8-OhdG); Western blot analysis: levels of BDNF and synaptophysin.
Tarchick et al.[34,c]	Mice with inactivated insulin receptor (IR) B6.129S4 (FVB)-Insrtm1Khn/J (*n* varies from 9 to 18 depending on the readout)	3 sequential daily intraperitoneal injections of STZ (55 mg/kg)	4	>250	Flash ERG	No data	Light micrographs: the distance from OLM to ILM, the length of OS, IS, and ONL, and thickness of RPE was measured. DHE staining: measurement of

							reactive oxygen species.
Nagai et al.[25]	Wistar rats (n = 7)	2 sequential daily intraperitoneal injections of STZ (100 mg/kg)	6	267.6	Flash ERG	No data	ELISA: level of VEGF; H&E staining: the distance between RGC to the outer granule layer.
Deguchi et al.[26]	Wistar rats (n = 6)	2 sequential daily intraperitoneal injections of STZ (100 mg/kg)	2	No data	Flash ERG	No data	H&E staining: distance between the GCL and the distal border of the ONL.
Hernández et al.[27]	Sprague-Dawley rats (n = 24)	Single injection of STZ (60 mg/kg) into the tail vein	2	>250	Flash ERG	No data	Assessment of glial activation: expression of GFAP; TUNEL assay: assessment of apoptosis

							(number of retinal apoptotic cells); Western blot analysis: observation of proapoptotic and survival signaling; Real-time PCR, immunohistochemistry: expression of GLAST.
Wang et al.[42]	C57BL/6 mice (n = 36)	3 sequential daily intraperitoneal injections of STZ (75 mg/kg)	5	300.6	Focal ERG	FA	Leukostasis: number of adherent leukocytes, and vascular endothelial cells; Western blot analysis: Levels of GFAP, VEGF and ICAM-1 levels;

							BRB breakdown: extravasation of albumin; DHE assay: measurement of MDA, SOD, and ROS formation.
Tarchick et al.[34]	C57BL/6J mice ($n \geq 10$)	3 sequential daily intraperitoneal injections of STZ (30 mg/kg)	4	≥250	dc-ERG	No data	Light microscopy: length of the inner segment, outer segment, and ONL; thickness of RPE; PNA staining: Number of rod and cone photoreceptor nuclei per column.

Lv et al.[39]	BALB/c mice (n = 25)	5 sequential daily intraperitoneal injections of STZ (50 mg/kg)	2	≥300.6	Full-field ERG	No data	H&E staining: the thickness of GCL, INL, ONL, and total retina.
Zhang et al.[35]	Sprague-Dawley rats (n = 24)	Single STZ injection of STZ (30 mg/kg)	12	>199.8	Flash ERG	No data	H&E staining: thickness of total retina, thickness of INL and ONL layers, and cell number in the INL and ONL; TUNEL assay: apoptosis assessment; Immunohistochemistry: expression of Bcl-2, Bax.

He et al.[38]	Sprague-Dawley rats (n = 40)	Single intraperitoneal injection of STZ (35 mg/kg)	10.2	>300.6	Full-field ERG	OCT	Western blot analysis: expression of VEGF, GFAP, and VCAM-1; Levels of GLU, TC, and TG; Levels of GSH-Px, SOD, and CAT.
Liao et al.[33]	C57/BL6 mice (n = 40)	5 sequential daily intraperitoneal injections of STZ (55 mg/kg)	5	No data	Flash ERG	FA + FP	Trypsin-digested retinal whole mounts: number of acellular capillaries; H&E staining: number of preretinal neovascular cells; Thicknesses of the IPL, INL, OPL, and ONL; RT-qPCR and western

							blot analysis: expressions of VEGF; levels of proinflammatory cytokines, including TNF-a, IL-1b, IL-6, IL-18, and IL-12.
Goharinia et al.[36]	Sprague-Dawley rats (*n* = 8)	Single intraperitoneal injection of STZ (60 mg/kg)	8	300	Flash ERG	No data	H&E staining: number of RGCs.
Ren et al.[41]	BALB/c mice (*n* = 20)	Single intraperitoneal injection of STZ (80 mg/kg)	4	≥300.6	Full-field ERG	No data	H&E staining: the thickness of the whole retina, ONL, INL, and RGC layer; Trx expression.

Piano et al.[40]	C57BL/6J mice (*n* = 20)	Single intraperitoneal injection of STZ (150 mg/kg)	12	≥300.6	Flash ERG	No data	Cryosections: total retinal thickness; Vascular area: deep plexus vessels; neovascularization; Western blot analysis: rhodopsin and cone-opsin content; TUNEL staining: apoptosis of rod photoreceptors; Western blot analysis: level of Caspase-3 and GAPDH.
Yee et al.[28,d]	Sprague-Dawley rats (*n* = 56)	Single injection of STZ (53	20	270	Flash ERG	No data	Toluidine Blue staining: thickness of ONL, INL,

		mg/kg) into the tail vein + specific fish oil or safflower oil diet					IPL layers, and total retina; Retinal fatty acid analysis: identification of fatty acids in retina; Immunolabeling: level of GFAP.
Wang et al.[43]	Sprague-Dawley rats (n = 16)	Single intraperitoneal injection of STZ (35 mg/kg) + high-sucrose/high-fat diet	17	300.6	fVEP	OCT	H&E staining: number of RGC; Expressions of GFAP and number of activated astrocytes; PAS assessment: retinal microvascular changes, ghost pericytes.

Reasons for study exclusions:

[a]No control group (only a group with STZ).

[b]STZ administration was combined with whole-body hypoxia (10% O2) for quicker diabetes induction.

[c]Mice with inactivated insulin receptor.

[d]STZ administration with specific oil diet.

BAX, Bcl-2-associated X protein; BRB, blood–retinal barrier; ChAT, choline acetyltransferase; COX-2, cyclooxygenase-2; DHE, dihydroethidium; DR, diabetic retinopathy; ELISA, enzymelinked immunosorbent assays; ERG, electroretinography; FA, fluorescein angiography; fVEP, functional visually evoked potentials; GAPDH, glyceraldehyde 3-phosphate dehydrogenase; GCL, ganglion cell layer; GFAP, glial fibrillary acidic protein; H&E, Hematoxylin and Eosin; ICAM-1, intercellular adhesion molecule-1; IL, interleukin; INL, inner nuclear layer; iNOS, inducible nitric oxide synthases; IPL, inner plexiform layer; MCU, mitochondrial calcium uniporter; OCT, optical coherence tomography; ONL, outer nuclear layer; OPL, outer plexiform layer; PAS, Periodic acid–Schiff; PCR, polymerase chain reaction; RGC, retinal ganglion cell; RT-qPCR, reverse transcription quantitative polymerase chain reaction; SOD, superoxide dismutase; STZ, streptozotocin; TNF-a, tumor necrosis factor-a; VCAM-1, vascular cell adhesion molecule-1; VEGF, vascular endothelial growth factor.

Subgroup analysis

We grouped all of the selected studies into 4 subgroups based on the follow-up time after STZ administration: subgroup 1 had a follow-up time of 2–4 weeks, subgroup 2 had a follow-up time of 5–8 weeks, subgroup 3 had a follow-up time of 8–12 weeks, and subgroup 4 had a follow-up time of 13–24 weeks (Fig. 2). All studies in subgroup 1 considered 150–250 mg/dL glucose levels as diabetic, while studies in subgroups 2–4 considered glucose levels of 250–350 mg/dL as diabetic. Although some studies fell into subgroup 1 with respect to follow-up time, they considered 300 mg/dL of glucose levels as diabetic. In one study[26] no data for glucose levels were reported. Insulin was administered only in the study by Tarchick et al.[45] every other day. The study by Liao et al.[33] fell into subgroup 2 but did not report glucose levels they considered to be diabetic. The study by Zhang et al.[35] fell into subgroup 3 because of follow-up time, but they considered glucose levels of 198.6 mg/dL as diabetic.

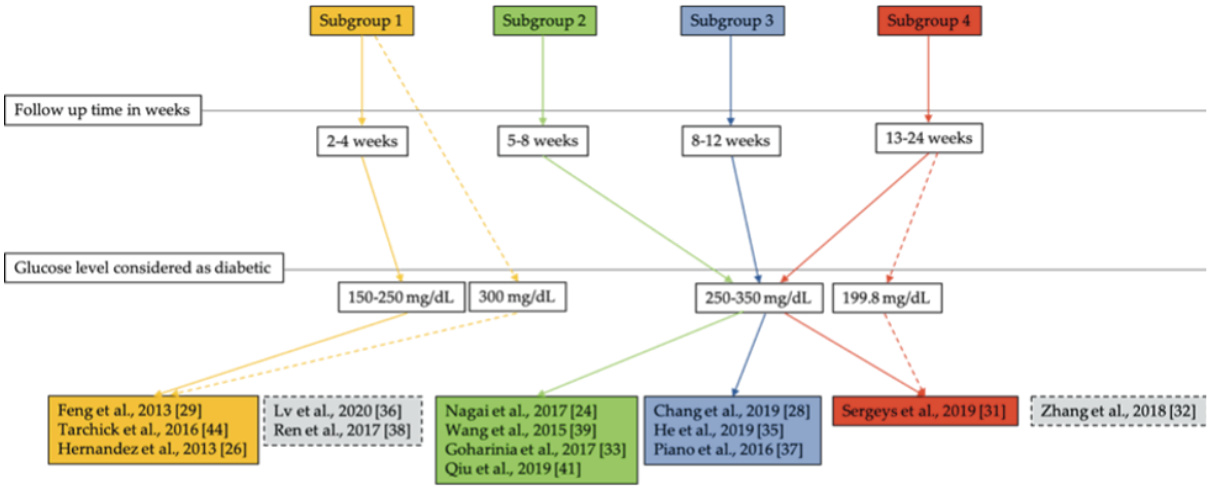

FIG. 2. Overview of subgroup analysis. The majority of the studies fell into subgroups 1–4 based on follow-up time (*solid arrows*). However, some studies fell into specific subgroups, although the authors of those studies considered different levels of blood glucose as diabetic (*dotted arrows*).

Outcomes of selected studies

Glucose levels and body weights. All studies reported an increase in glucose levels in STZ-induced animals[25–27,29,30,32–36,38–44] (Table 2). However, only 4 studies provided raw numbers of glucose levels. The increase in glucose levels in those studies was species dependent. In Sprague-Dawley rats, the glucose level increased by fourfold after a single STZ administration,[30,36] whereas a threefold increase was found in C57BL/6J mice after single STZ administration,[40] and after 5 sequential daily intraperitoneal injections of STZ31 (Table 2).

Body weight of STZ-induced animals decreased in the majority of studies[25,26,30,32,33,35,36,40,42,45] (Table 2). However, in 2 studies, the authors found body weight gains in diabetic C57BL/6J mice as compared with healthy control groups.[29,42] Similarly, as with blood glucose level data, one mouse study[32] and 2 rat studies[30,36] reported raw body weight data showing almost a twofold reduction in body weight after STZ injections, whereas others did not reveal any raw data,[25,26,29,33–35,40,42] or did not record body weight changes at all[27,38,39,41,43,44] (Table 2).

Visual function: ERG and VEP. All studies showed deterioration of visual function in STZ animals as compared with healthy controls either in amplitude reduction in a-, b-, c-wave and/or oscillatory potential (OP) as assessed by ERG, or in decrease of N and P wave amplitudes in VEP measurements. However, only 2 studies provided numerical values of a-wave, b-wave, and OP amplitudes expressed as percentage decrease in STZ-injected animals in comparison with healthy control animals (50% for a-wave, 70%–80% for b-wave, and 50%–60% for OP amplitudes)[38,39] (Table 3).

Table 2. Outcomes of Studies: Glucose Levels and Body Weights

Study	*Species*	*Glucose level (mg/dL)*	*Body weight (g)*
Chang et al.[29]	C57BL/6J mice	Increased (no raw data)	Increased (no raw data)
Deguchi et al.[26]	Wistar rats	Increased (no raw data)	Decreased (no raw data)
Feng et al.[30]	Sprague-Dawley rats	Increased (Healthy control rat 93.6 ± 23.4, and STZ induced 390.6 ± 55.8)	Decreased (Healthy control rat 289.9 ± 5.2 and STZ induced 171.9 ± 14.5)
Goharinia et al.[36]	Sprague-Dawley rats	Increased (Healthy control rat 112 ± 4 and STZ induced 443 ± 24)	Decreased (Healthy control rat 268 ± 9 and STZ induced 178 ± 7)
He et al.[38]	Sprague-Dawley rats	Increased (no raw data)	N/A
Hernández et al.[27]	Sprague-Dawley rats	Increased (no raw data)	N/A
Liao et al.[33]	C57BL/6J mice	Increased (no raw data)	Decreased (no raw data)
Lv et al.[39]	BALB/c mice	Increased (no raw data)	N/A
Nagai et al.[25]	Wistar rats	Increased (no raw data)	Decreased (no raw data)
Piano et al.[40]	C57BL/6J mice	Increased (Healthy control mice 135 ± 7.2 and STZ induced 502.2 ± 27)	Decreased (no raw data)
Qiu et al.[44]	Brown Norway rats	Increased (no raw data)	N/A

Ren et al.[41]	BALB/c mice	Increased (no raw data)	N/A
Sergeys et al.[32]	C57BL/6J mice	Increased (Healthy control mice 180 ± 8 and STZ induced 477 ± 29)	Decreased (Healthy control mice 30.8 ± 0.7 and STZ induced 22.7 ± 0.5)
Tarchick et al.[34]	C57BL/6J mice	Increased (no raw data)	Decreased (no raw data)
Wang et al.[42]	C57BL/6J mice	Increased (no raw data)	Increased (no raw data)
Wang et al.[43]	Sprague-Dawley rats	Increased (no raw data)	N/A
Zhang et al.[35]	Sprague-Dawley rats	Increased (no raw data)	Decreased (no raw data)

N/A, data not available.

Table 3. Outcomes of Studies: Electroretinography and Visually Evoked Potential Measurements

Study	*Species*	*a-wave amplitude*	*b-wave amplitude*	*c-wave amplitude*	*OPs amplitude*	*VEP: amplitude of N and P waves*
Chang et al.[29]	C57BL/6J mice	Decreased (no raw data)	Decreased (no raw data)			
Deguchi et al.[26]	Wistar rats	Decreased (no raw data)	Decreased (no raw data)		Decreased (no raw data)	
Feng et al.[30]	Sprague-Dawley rats		Decreased (no raw data)		Decreased (no raw data)	
Goharinia et al.[36]	Sprague-Dawley rats		Decreased (no raw data)		Decreased (no raw data)	
He et al.[38]	Sprague-Dawley rats		Decreased (70–80%)		Decreased (50%–60%)	
Hernández et al.[27]	Sprague-Dawley rats		Decreased (no raw data)			

Liao et al.[33]	C57BL/6J mice	Decreased (no raw data)	Decreased (no raw data)			
Lv et al.[39]	BALB/c mice	Decreased (50%)				
Nagai et al.[25]	Wistar rats	Decreased (no raw data)	Decreased (no raw data)		Decreased (no raw data)	
Piano et al.[40]	C57BL/6J mice	Decreased (no raw data)	Decreased (no raw data)		Decreased (no raw data)	
Qiu et al.[44]	Brown Norway rats	Decreased (no raw data)	Decreased (no raw data)			
Ren et al.[41]	BALB/c mice	Decreased (no raw data)	Decreased (no raw data)			
Sergeys et al.[32]	C57BL/6J mice	Decreased (no raw data)	Decreased (no raw data)		Decreased (no raw data)	
Tarchick et al.[34]	C57BL/6J mice	Decreased (no raw data)		Decreased (no raw data)	Decreased (no raw data)	

Wang et al.[42]	C57BL/6J mice		Decreased (no raw data)			
Wang and Lo[4]	Sprague-Dawley rats					Decreased (no raw data)
Zhang et al.[35]	Sprague-Dawley rats	Decreased (no raw data)	Decreased (no raw data)		Decreased (no raw data)	

OPs, oscillatory potentials.

Total retinal thickness and thickness of individual retinal layers. The majority of selected studies reported retinal thinning after induction of DR[30–32,38–41,44,45] (Table 4). For example, a decrease of total retinal thickness was assessed either using in vivo imaging (OCT) or histology (H&E staining).[32,35,38–41] However, in 2 studies,[26,44] an increase in total retinal thickness was found, which authors hypothesized to be caused by retinal edema. In some studies, a decrease of thickness was found in the outer nuclear layer (ONL),[33,35,39–41] outer plexiform layer,[33,38,40] inner nuclear layer (INL),[30,33,35,39,41] inner plexiform layer (IPL),[30,33,38,40] and ganglion cell layer (GCL)[32,38,39,41] (Table 4). Zhang et al.[35] were the only group that reported no changes in IPL thickness in STZ-induced rats, although ONL and INL showed a marked decrease.

The raw data were presented by Deguchi et al.[26] and the decrease in retinal thickness expressed in percentages was shown in other 2 studies.[40,41] The rest of studies did not provide any raw data (Table 4). Four studies reported a decrease in retinal ganglion cell (RGC) number.[30,32,36,43] In 2 studies, Sergeys et al.[32] and Goharinia et al.,[36] the decrease in RGC number was expressed in percentages (20% and 27%, respectively), whereas other studies[30,43] did not provide any raw data. In addition, a decrease of cholinergic amacrine cells by 44%,[32] a lower number of cells in ONL[35] or lower rhodopsin expression[40] were separately reported in diabetic animals.

Retinal vascular changes. Most of selected studies used either FA, Evans Blue extravasation, extravasation of albumin, or trypsin-digested retinal whole mounts to detect vascular changes in DR-induced rodents[29,30,32,40,42–45] (Table 5). An increase in vascular permeability was found in the majority of studies.[29,30,42,44,45] An increase in vascular endothelial growth factor (VEGF) levels were detected in STZ-injected animals of 5 studies.[25,33,38,42,44] Others reported retinal vascular changes, such as an increased formation of acellular capillaries,[29,33] increased number of vascular endothelial cells,[42] and an increase of ghost pericytes in diabetic

retina.[41] However, only Nagai et al.[25] presented raw data from described vascular changes (Table 5). Although neovascularization is a hallmark of proliferative diabetic retinopathy (PDR), none of the selected studies were able to identify its presence in STZ-induced animals.

Retinal inflammation and neurodegeneration. The majority of selected studies reported an increase of retinal inflammation and neurodegeneration markers in STZ-injected rodents[27,30,32,38,40,42–45] (Table 6). For example, 3 studies showed an increase of adherent leukocytes in diabetic retina.[32,42,44] Sergeys et al.[32] specified a 2.5-fold increase of adherent leukocytes, 3.1-fold increase of macrophages, and 2.7-fold increase of reactive gliosis as assessed by immunohistochemistry at 8 weeks after STZ injections in C57BL/6J mice. Similarly, a significant increase in the levels of proinflammatory cytokines [tumor necrosis factora (TNF-a), interleukin (IL)-1b, IL-6, IL-18, and IL-12] was observed in one study that used C57BL/6J mice.[44]

At mRNA or protein level an increased expression of glial fibrillary acidic protein (GFAP), which is a marker for reactive gliosis in retina, was observed in 4 studies[27,38,42,43] and increased expression of vascular cell adhesion molecule-1 (VCAM-1) and intercellular adhesion molecule1 (ICAM-1) was found in diabetic animals of other 3 studies.[38,42,44] No changes in Müller glia of diabetic C57BL/6J mice as studied by GFAP immunohistochemistry from retinal sections were reported by Piano et al.[40] A decreased expression of BDNF as assessed by Western blotting was found in STZ-diabetic Sprague-Dawley rats.[30]

Table 4. Outcomes of Studies: Total Retinal Thickness and Thickness of Individual Retinal Layers

Study	*Species*	*ONL*	*OPL*	*INL*	*IPL*	*GCL*	*Total retinal thickness*
Deguchi et al.[26]	Wistar rats						Increased (Healthy control rat 71.0 ± 3.57μm and STZ induced 130.6 ± 5.46 μm)
Feng et al.[30]	Sprague-Dawley rats			Decreased (no raw data)	Decreased (no raw data)		
He et al.[38]	Sprague-Dawley rats		Decreased (no raw data)		Decreased (no raw data)	Decreased (no raw data)	Decreased (no raw data)
Liao et al.[33]	C57/BL6 mice	Decreased (no raw data)	Decreased (no raw data)	Decreased (no raw data)	Decreased (no raw data)		
Lv et al.[39]	BALB/c mice	Decreased (no raw data)		Decreased (no raw data)		Decreased (no raw data)	Decreased (no raw data)

Piano et al.[40]	C57/BL6 mice	Decreased (no raw data)	Decreased (no raw data)		Decreased (no raw data)		Decreased (no raw data)
Qiu et al.[44]	Brown Norway rats						Increased (no raw data)
Ren et al.[41]	BALB/c mice	Decreased (10%)		Decreased (10%)		Decreased (10%)	Decreased (10%)
Sergeys et al.[32]	C57/BL6 mice					Decreased (4%)	Decreased (4%)
Zhang et al.[35]	Sprague-Dawley rats	Decreased (no raw data)		Decreased (no raw data)	Decreased (no raw data)		

Table 5. Outcomes of Studies: Retinal Vascular Changes

Study	*Species*	*Vascular permeability*	*Neovascularization*	*Preretinal neovascular cells*	*VEGF*	*Acellular capillaries*	*Vascular endothelial cells*	*Ghost pericyte*
Chang et al.[29]	C57BL/6J mice	Increased (no raw data)				Increased (no raw data)		
Feng et al.[30]	Sprague-Dawley rats	Increased (no raw data)						
He et al.[38]	Sprague-Dawley rats				Increased (no raw data)			
Liao et al.[33]	C57BL/6 mice	Increased (no raw data)		Increased (no raw data)	Increased (no raw data)	Increased (no raw data)		

Nagai et al.[25]	Wistar rats				Increased (9.26-fold higher than in controls)			
Piano et al.[40]	C57BL/6 mice		No changes (no raw data)					
Qiu et al.[44]	Brown Norway rats	Increased (no raw data)	No changes (no raw data)		Increased (no raw data)			
Sergeys et al.[32]	C57BL/6 mice	No changes (no raw data)						
Wang et al.[42]	C57BL/6 mice	Increased (no raw data)			Increased (no raw data)		Increased (no raw data)	

Wang et al.[43]	Sprague-Dawley rats							Increased (no raw data)

Table 6. Outcomes of Studies: Retinal Inflammation and Neurodegeneration

Study	*Adherent leukocytes*	*Macrophages*	*Müller cell gliosis*	*Pro-inflammatory cytokines*	*VCAM-1 expression*	*ICAM-1 expression*	*GFAP expression*	*BDNF expression*
Feng et al.[30]								Decreased (to 0.52 ± 0.1-fold)
He et al.[38]					Increased (no raw data)		Increased (no raw data)	
Hernández et al.[27]							Increased (GFAP score 1–3)	
Liao et al.[33]				Increased (TNF-a, IL-1b, IL-6, IL-				

				18, IL-12) (no raw data)				
Piano et al.[40]			No changes (no raw data)					
Qiu et al.[44]	Increased (no raw data)					Increased (no raw data)		
Sergeys et al.[32]	Increased (2.5-fold)	Increased (3.1-fold)	Increased (2.7-fold)					
Wang et al.[42]	Increased (no raw data)					Increased (no raw data)	Increased (no raw data)	
Wang et al.[43]							Increased (no raw data)	

Risk of bias. All articles specified both the primary outcomes and the baseline characteristics of the study, with sufficient methodological details (Fig. 3). However, only 5% of studies detailed the correct timing of randomization and 24% of studies reported random sequence generation of test subjects. In addition, only 5% of studies reported random outcome assessment and blinding of experiments, but the methodologies were unknown or insufficient to establish suitability. It should be noted that descriptions of methodology did not provide other important parameters of bias, such as sample size calculations, random housing of animals, allocation concealment, or whether gathered data were incomplete and how the researchers dealt with that during the study (Fig. 3).

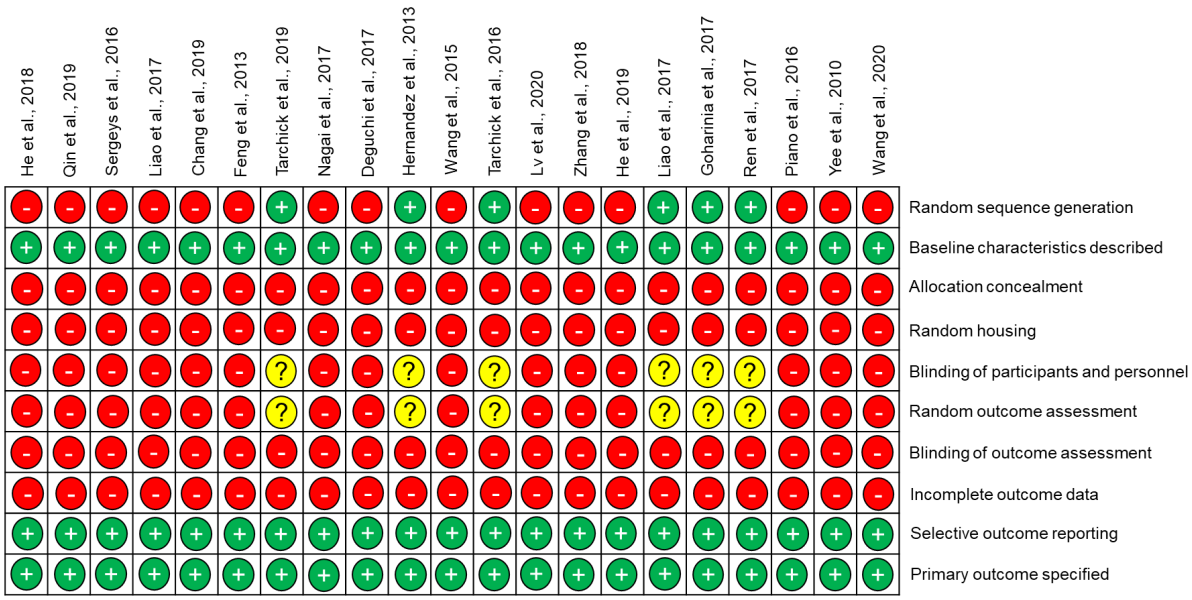

FIG. 3. Overview of bias assessment in included studies using the SYRCLE risk of bias tool for animal studies.

2.5 Discussion

In this study, we systematically reviewed the literature and included 21 articles that met our inclusion criteria. In all studies, STZ injections were used to induce a phenotype that is

reminiscent of DR in rodents. Although the majority of analyzed studies used a single STZ injection, the dose of STZ varied from 30 to 100 mg/kg in rats and from 50 to 150 mg/kg in mice. Furthermore, the follow-up times and study periods varied from 2 to 24 weeks. Glucose level thresholds used to define hyperglycemia were not consistent between studies. However, most studies used either 250 or 300.6 mg/dL blood glucose level as defining criterion. The majority of studies reported a decrease in body weight, whereas only 2 studies[29,43] found an increase of body weight in diabetic mice; however, the reported body weight gains were lower compared with control groups. Functional decline of the inner retina is a hallmark of early DR both in humans and in animal models mimicking DR.[46,47] These early functional deficits can be detected using noninvasive ERG measurement. In this systematic analysis, we found that all analyzed studies reported a deterioration of visual function as assessed either locally using ERG or at the level of occipital cortex using VEP. However, only 2 studies reported a percentage change in which a-wave, b-wave, and OP amplitudes decreased after DR induction compared with healthy control animals.[38,39] Other studies did not provide raw data. Therefore, we could not compare and conclude on the magnitude of visual function decrease in our analysis.

Reduced total retinal thickness or reduced thickness of individual retinal layers in DR suggests neuronal degeneration. Our systematic review revealed that the majority of included studies reported a decrease in total retinal thickness. Interestingly, total retinal thickness was increased in 2 studies on Wistar[26] and Brown Norway rats,[44] which most likely indicates retinal edema. Similarly, as with functional data, only 2 studies provided raw data on the total retinal thickness or individual retinal layers, which were expressed as percentage.

DR is characterized as a vascular disease that is manifested by endothelial cell proliferation, increased vascular permeability,[48,49] and inflammatory response.[50] In this systematic review we

found that the majority of analyzed studies used either FA, Evans Blue extravasation, extravasation of albumin, or trypsin-digested retinal whole mounts to detect vascular changes in DR-induced rodents.

Selected studies detected various vascular changes in STZ rodents, including increased vascular permeability, increase in VEGF levels, appearance of acellular capillaries, vascular endothelial cells, and ghost pericytes. Despite neovascularization being a defining feature of PDR, none of the selected studies reported evidence of its occurrence. This absence of neovascularization highlights a limitation in the model to mirror the pathological neovascularization observed in human PDR. Vascular changes were accompanied with inflammatory events: increased number of leukocytes, increased reactive gliosis of Müller cells, release of inflammatory cytokines and increased number of macrophages, and increased expression of endothelial cell adhesion molecules, such as ICAM-1 and VCAM-1.

Our detailed risk of bias analysis revealed that only less than one-third of studies (29%) reported the use of randomization and random sequence generation to assign the interventions. Furthermore, methods of blinding were inadequate or not reported at all. To confound this further, random housing of animals or treatment allocation concealment was also missing from all studies. Whether this is due to inadequate reporting or a lack of use of these methods when performing animal experiments is not clear. However, a failure to carry out these methods when conducting animal experiments is concerning, since randomization is essential for obtaining comparable study groups and may confound study findings.[51,52]

The inadequate number of studies reporting correct timing of randomization is also worrying since the lack of randomization together with the lack of allocation concealment, particularly

in unblinded studies, could lead to variations in the preintervention study conditions and potentially affect the outcomes.

The lack of blinding in the majority of studies (71%) is a fundamental shortcoming and raises doubts about data validity.[51,53] Random outcome assessment was again missing in the majority of the studies (71%) and the methodology was unknown or insufficient. In addition, attrition bias was difficult to assess in these studies since none of the studies specifically reported on this aspect of the risk of bias tool. Hence, we left this as not reported to highlight the issue and the potential bias that this could introduce. Finally, none of the studies reported sample size calculations, which is another confounder introducing bias into these studies. For example, too few animals may not be sufficient to detect treatment effects (e.g., binary outcomes such as survival, etc.), whereas the use of too few and too many animals are regarded as an unethical waste of resources.[54,55]

Especially given the utility of the STZ model for drug discovery for DR, we urge researchers to adhere to a minimum reporting standard, for example by adhering to the ‘‘Animal Research: Reporting of *In Vivo* Experiments’’ (ARRIVE) and ARRIVE 2.0 guidelines and reporting the ‘‘ARRIVE Essential 10,’’ which are the recommended minimum requirement for reporting animal experiments.[56,57] The ‘‘ARRIVE Essential 10’’ include a detailed description of study design, sample size, inclusion and exclusion criteria, blinding, outcome measures, statistics, identification of experimental animals, description of experimental procedures, as well as recommendations for how to report and present the results.[56,57] Consideration of these recommendations in the reporting of STZ studies would mitigate many of the reporting shortcomings of the studies reviewed herein.

2.6 Limitations

The leading limitation of this study was that due to the lack of quantitative data in the included studies, meta-analysis was not possible to perform. The lack of quantitative data for all of the outcome measures in the majority of the studies significantly hampers the interpretation of obtained results. Simply reporting that the values ‘‘decreased’’ or ‘‘increased’’ in diabetic animals does not provide helpful insight on the magnitude of changes. Quantitative data would have been easier to compare and would provide more information on determining the efficacy of a particular outcome in DR. A possible limitation could also arise from differences in follow-up times ranging from 2 to 24 weeks, and a wide range (150–350 mg/dL) of blood glucose levels, which were used to classify animals into diabetic and nondiabetic.

2.7 Conclusions

This systematic review demonstrates that the most consistent reported readout in the STZ model is the functional assessment of visual function by ERG. Specifically, amplitudes of a-wave, b-wave, and OP correlated with DR-related pathology. However, a significant concern is the relatively high risk of bias in the reviewed studies, either due to the lack of reporting or lack of correctly following procedures to reduce bias, thereby limiting the potential usefulness of these studies. Stricter adherence to the ARRIVE guidelines are recommended in future studies. Our review, therefore, highlights a need for further studies, considering the risk of bias, to validate that ERG is the most useful readout in preclinical studies of DR.

2.8 Future Directions

The systematic review offered insights that will enhance the design of our future STZ study (Chapter 3). First, within this extensive research, only one investigation was conducted in pigmented rats, specifically Brown Norway rats. Comparative studies have shown, STZ-

induced BN rats demonstrate greater vessel hyperpermeability and express higher levels of VEGF, compared to non-pigmented rats,[58,59] therefore, we plan to focus on Brown Norway rats in our future STZ study. In addition, by analyzing 21 studies, we noted a range of STZ doses (30-100 mg/kg) to induce diabetes and will select a dose within this range to ensure model efficacy. We will also adopt a glucose threshold consistent with other rat studies (e.g., >250 mg/dL for Sprague-Dawley rats). In addition to this, with follow-up durations ranging from 2 to 12 weeks in the selected studies, we will select a timeframe within this range and include several timepoint measurements to ensure thorough observation of diabetic complications. Additionally, the review highlighted that STZ models mimic early vascular changes, including increased vascular permeability, pericyte loss, and acellular capillary formation, observed via Evans Blue extravasation assay, and trypsin-digested retinal flat mounts, which we plan to incorporate in our future STZ study. Moreover, the review indicates that while most studies observed reduced retinal thickness, some studies indicated increased retinal thickness due to the presence of retinal edema. This insight allows us to anticipate potential outcomes and incorporate both inner and outer retinal thickness measurements in our future STZ study. As the systematic review emphasizes the importance of functional assessments, this encourages us to incorporate ERG measurements and evaluate visual function in our future STZ model as well. Additionally, the review's discussion on bias and reporting standards highlights the importance of adhering to ARRIVE guidelines in our future experiments. Finally, the noticed lack of quantitative data in the included studies encourages us to report quantitative data in our future research.

2.9 Authors' Contributions

The project was conceptualized by Z.A., S.K., and G.K. Literature search based on the titles and abstracts was performed by I.L. and Z.A. Any discrepancies were resolved by discussion

and if needed, consultation with S.K. Risk of bias assessment was performed by both I.L. and Z.A. Review of articles, and original draft preparation was performed by I.L. Review and editing process involved contributions from I.L., Z.A., S.K., and G.K. Supervision of the project was handled by Z.A., S.K., and G.K. All authors have read and agreed to the published version of the article.

2.10 Author Disclosure Statement

Employment: G.K. and I.L. (Experimentica Ltd.); Stock/ equity ownership: G.K. and S.K. (Experimentica Ltd.); S.K. (K&P Scientific LLC). S.K. conducts academic research in areas of interest similar to the business interests of Experimentica Ltd and K&P Scientific LLC. The terms of this arrangement have been reviewed and approved by Loyola University Chicago in accordance with its conflict-of interest policy. The funders had no role in the design of the study; in the collection, analyses, or interpretation of data; in the writing of the article, or in the decision to publish the results. Z.A. declares no conflicts of interest.

2.11 Funding Information

This research was funded, in part, by the European Union's Horizon 2020 research and innovation program under the Marie Sklodowska-Curie Actions, grant agreement—No. 813440 (ORBITAL—Ocular Research by Integrated Training and Learning). Additional funding by the Dr. John P. and Therese E. Mulcahy Endowed Professorship in Ophthalmology (S.K.) is gratefully acknowledged.

2.12 References

1. Lee R, Wong TY, Sabanayagam C. Epidemiology of diabetic retinopathy, diabetic macular edema and related vision loss. Eye Vis (Lond) 2015;2:17; doi: 10.1186/s40662-015-0026-2.

2. Zheng Y, He M, Congdon N. The worldwide epidemic of diabetic retinopathy. Indian J Ophthalmol 2012;60(5):428–431; doi: 10.4103/0301-4738.100542.

3. Stitt AW, Curtis TM, Chen M, et al. The progress in understanding and treatment of diabetic retinopathy. Prog Retin Eye Res 2016;51:156–186; doi: 10.1016/j.preteyeres.2015.08.001.

4. Wang W, Lo ACY. Diabetic Retinopathy: Pathophysiology and Treatments. Int J Mol Sci 2018;19(6):1816; doi: 10.3390/ijms19061816.

5. Feit-Leichman RA, Kinouchi R, Takeda M, et al. Vascular damage in a mouse model of diabetic retinopathy: relation to neuronal and glial changes. Invest Ophthalmol Vis Sci 2005;46(11):4281–4287; doi: 10.1167/iovs.04-1361.

6. Hammes HP, Lin J, Bretzel RG, et al. Upregulation of the vascular endothelial growth factor/vascular endothelial growth factor receptor system in experimental background diabetic retinopathy of the rat. Diabetes 1998;47(3):401–406; doi: 10.2337/diabetes.47.3.401.

7. Giebel SJ, Menicucci G, McGuire PG, et al. Matrix metalloproteinases in early diabetic retinopathy and their role in alteration of the blood-retinal barrier. Lab Invest 2005;85(5):597–607; doi: 10.1038/labinvest.3700251.

8. Zhang SX, Wang JJ, Gao G, et al. Pigment epithelium-derived factor (PEDF) is an endogenous antiinflammatory factor. FASEB J 2006;20(2):323–325; doi: 10.1096/fj.05-4313fje.

9. Martin PM, Roon P, Van Ells TK, et al. Death of Retinal Neurons in Streptozotocin-Induced Diabetic Mice. Investigative Ophthalmology & Visual Science 2004;45(9):3330–3336; doi: 10.1167/iovs.04-0247.

10. Nguyen TT, Wang JJ, Sharrett AR, et al. Relationship of retinal vascular caliber with diabetes and retinopathy: the Multi-Ethnic Study of Atherosclerosis (MESA). Diabetes Care 2008;31(3):544–549; doi: 10.2337/dc07-1528.

11. Rogers SL, Tikellis G, Cheung N, et al. Retinal arteriolar caliber predicts incident retinopathy: the Australian Diabetes, Obesity and Lifestyle (AusDiab) study. Diabetes Care 2008;31(4):761–763; doi: 10.2337/dc07-1622.

12. Carpineto P, Toto L, Aloia R, et al. Neuroretinal alterations in the early stages of diabetic retinopathy in patients with type 2 diabetes mellitus. Eye (Lond) 2016;30(5):673–679; doi: 10.1038/eye.2016.13.

13. Chhablani J, Sharma A, Goud A, et al. Neurodegeneration in Type 2 Diabetes: Evidence From Spectral-Domain Optical Coherence Tomography. Invest Ophthalmol Vis Sci 2015;56(11):6333–6338; doi: 10.1167/iovs.15-17334.

14. Gundogan FC, Akay F, Uzun S, et al. Early Neurodegeneration of the Inner Retinal Layers in Type 1 Diabetes Mellitus. Ophthalmologica 2016;235(3):125–132; doi: 10.1159/000442826.

15. Luu CD, Szental JA, Lee S-Y, et al. Correlation between retinal oscillatory potentials and retinal vascular caliber in type 2 diabetes. Invest Ophthalmol Vis Sci 2010;51(1):482–486; doi: 10.1167/iovs.09-4069.

16. Olivares AM, Althoff K, Chen GF, et al. Animal Models of Diabetic Retinopathy. Curr Diab Rep 2017;17(10):93; doi: 10.1007/s11892-017-0913-0.

17. Naderi A, Zahed R, Aghajanpour L, et al. Long term features of diabetic retinopathy in streptozotocin-induced diabetic Wistar rats. Exp Eye Res 2019;184:213–220; doi: 10.1016/j.exer.2019.04.025.

18. Kucukevcilioglu M, Jeong W-J, Moo Lee K, et al. Retinal thinning in mice with streptozotocin-induced diabetes mellitus. Investigative Ophthalmology & Visual Science 2014;55(13):2257.

19. Yang Y, Mao D, Chen X, et al. Decrease in retinal neuronal cells in streptozotocin-induced diabetic mice. Mol Vis 2012;18:1411–1420.

20. Paterniti I, Di Paola R, Campolo M, et al. Palmitoylethanolamide treatment reduces retinal inflammation in streptozotocin-induced diabetic rats. Eur J Pharmacol 2015;769:313–323; doi: 10.1016/j.ejphar.2015.11.035.

21. Jiang N, Chen X-L, Yang H-W, et al. Effects of nuclear factor κB expression on retinal neovascularization and apoptosis in a diabetic retinopathy rat model. Int J Ophthalmol 2015;8(3):448–452; doi: 10.3980/j.issn.2222-3959.2015.03.03.

22. Page MJ, McKenzie JE, Bossuyt PM, et al. The PRISMA 2020 statement: an updated guideline for reporting systematic reviews. BMJ 2021;372:n71; doi: 10.1136/bmj.n71.

23. Hooijmans CR, Rovers MM, de Vries RBM, et al. SYRCLE's risk of bias tool for animal studies. BMC Med Res Methodol 2014;14:43; doi: 10.1186/1471-2288-14-43.

24. Higgins JPT, Altman DG, Gøtzsche PC, et al. The Cochrane Collaboration's tool for assessing risk of bias in randomised trials. BMJ 2011;343:d5928; doi: 10.1136/bmj.d5928.

25. Nagai N, Deguchi S, Otake H, et al. Therapeutic Effect of Cilostazol Ophthalmic Nanodispersions on Retinal Dysfunction in Streptozotocin-Induced Diabetic Rats. Int J Mol Sci 2017;18(9):1971; doi: 10.3390/ijms18091971.

26. Deguchi S, Otake H, Nakazawa Y, et al. Ophthalmic Formulation Containing Nilvadipine Nanoparticles Prevents Retinal Dysfunction in Rats Injected with Streptozotocin. Int J Mol Sci 2017;18(12):2720; doi: 10.3390/ijms18122720.

27. Hernández C, García-Ramírez M, Corraliza L, et al. Topical Administration of Somatostatin Prevents Retinal Neurodegeneration in Experimental Diabetes. Diabetes 2013;62(7):2569–2578; doi: 10.2337/db12-0926.

28. Yee P, Weymouth AE, Fletcher EL, et al. A role for omega-3 polyunsaturated fatty acid supplements in diabetic neuropathy. Invest Ophthalmol Vis Sci 2010;51(3):1755–1764; doi: 10.1167/iovs.09-3792.

29. Chang JY-A, Yu F, Shi L, et al. Melatonin Affects Mitochondrial Fission/Fusion Dynamics in the Diabetic Retina. J Diabetes Res 2019;2019:8463125; doi: 10.1155/2019/8463125.

30. Feng Y, Wang R, Xu J, et al. Hydrogen-Rich Saline Prevents Early Neurovascular Dysfunction Resulting from Inhibition of Oxidative Stress in STZ-Diabetic Rats. Current Eye Research 2013;38(3):396–404; doi: 10.3109/02713683.2012.748919.

31. Liao P-L, Lin C-H, Li C-H, et al. Anti-inflammatory properties of shikonin contribute to improved early-stage diabetic retinopathy. Sci Rep 2017;7:44985; doi: 10.1038/srep44985.

32. Sergeys J, Etienne I, Van Hove I, et al. Longitudinal In Vivo Characterization of the Streptozotocin-Induced Diabetic Mouse Model: Focus on Early Inner Retinal Responses. Investigative Ophthalmology & Visual Science 2019;60(2):807–822; doi: 10.1167/iovs.18-25372.

33. Liao Y-R, Li Z-J, Zeng P, et al. TLR7 deficiency contributes to attenuated diabetic retinopathy via inhibition of inflammatory response. Biochemical and Biophysical Research Communications 2017;493(2):1136–1142; doi: 10.1016/j.bbrc.2017.08.085.

34. Tarchick MJ, Bassiri P, Rohwer RM, et al. Early Functional and Morphologic Abnormalities in the Diabetic Nyxnob Mouse Retina. Invest Ophthalmol Vis Sci 2016;57(7):3496–3508; doi: 10.1167/iovs.15-18775.

35. Zhang Q, Xiao X, Zheng J, et al. Compound Danshen Dripping Pill Inhibits Retina Cell Apoptosis in Diabetic Rats. Front Physiol 2018;9:1501; doi: 10.3389/fphys.2018.01501.

36. Goharinia M, Zareei A, Rahimi M, et al. Can allopurinol improve retinopathy in diabetic rats? Oxidative stress or uric acid; which one is the culprit? Res Pharm Sci 2017;12(5):401–408; doi: 10.4103/1735-5362.213985.

37. He M, Long P, Yan W, et al. ALDH2 attenuates early-stage STZ-induced aged diabetic rats retinas damage via Sirt1/Nrf2 pathway. Life Sci 2018;215:227–235; doi: 10.1016/j.lfs.2018.10.019.

38. He M, Long P, Guo L, et al. Fushiming Capsule Attenuates Diabetic Rat Retina Damage via Antioxidation and Anti-Inflammation. Evid Based Complement Alternat Med 2019;2019:5376439; doi: 10.1155/2019/5376439.

39. Lv J, Bao S, Liu T, et al. Sulforaphane delays diabetes-induced retinal photoreceptor cell degeneration. Cell Tissue Res 2020;382(3):477–486; doi: 10.1007/s00441-020-03267-w.

40. Piano I, Novelli E, Della Santina L, et al. Involvement of Autophagic Pathway in the Progression of Retinal Degeneration in a Mouse Model of Diabetes. Front Cell Neurosci 2016;10:42; doi: 10.3389/fncel.2016.00042.

41. Ren X, Li C, Liu J, et al. Thioredoxin plays a key role in retinal neuropathy prior to endothelial damage in diabetic mice. Oncotarget 2017;8(37):61350–61364; doi: 10.18632/oncotarget.18134.

42. Wang J, Wang S, Li M, et al. The Neuropilin-1 Inhibitor, ATWLPPR Peptide, Prevents Experimental Diabetes-Induced Retinal Injury by Preserving Vascular Integrity and Decreasing Oxidative Stress. PLoS One 2015;10(11):e0142571; doi: 10.1371/journal.pone.0142571.

43. Wang Q-C, Sheng W, Yi C-J, et al. Retrobulbarly injecting nerve growth factor attenuates visual impairment in streptozotocin-induced diabetes rats. Int Ophthalmol 2020;40(12):3501–3511; doi: 10.1007/s10792-020-01537-8.

44. Qiu F, Meng T, Chen Q, et al. Fenofibrate-Loaded Biodegradable Nanoparticles for the Treatment of Experimental Diabetic Retinopathy and Neovascular Age-Related Macular Degeneration. Molecular pharmaceutics 2019;16(5):1958; doi: 10.1021/acs.molpharmaceut.8b01319.

45. Tarchick MJ, Cutler AH, Trobenter TD, et al. Endogenous insulin signaling in the RPE contributes to the maintenance of rod photoreceptor function in diabetes. Exp Eye Res 2019;180:63–74; doi: 10.1016/j.exer.2018.11.020.

46. Hancock HA, Kraft TW. Oscillatory potential analysis and ERGs of normal and diabetic rats. Invest Ophthalmol Vis Sci 2004;45(3):1002–1008; doi: 10.1167/iovs.03-1080.

47. Kubota S, Ozawa Y, Kurihara T, et al. Roles of AMP-Activated Protein Kinase in Diabetes-Induced Retinal Inflammation. Investigative Ophthalmology & Visual Science 2011;52(12):9142–9148; doi: 10.1167/iovs.11-8041.

48. Dull RO, Yuan J, Chang YS, et al. Kinetics of placenta growth factor/vascular endothelial growth factor synergy in endothelial hydraulic conductivity and proliferation. Microvasc Res 2001;61(2):203–210; doi: 10.1006/mvre.2000.2298.

49. Shin ES, Sorenson CM, Sheibani N. Diabetes and Retinal Vascular Dysfunction. J Ophthalmic Vis Res 2014;9(3):362–373; doi: 10.4103/2008-322X.143378.

50. Rangasamy S, McGuire PG, Das A. Diabetic retinopathy and inflammation: novel therapeutic targets. Middle East Afr J Ophthalmol 2012;19(1):52–59; doi: 10.4103/0974-9233.92116.

51. Bebarta V, Luyten D, Heard K. Emergency medicine animal research: does use of randomization and blinding affect the results? Acad Emerg Med 2003;10(6):684–687; doi: 10.1111/j.1553-2712.2003.tb00056.x.

52. Hirst JA, Howick J, Aronson JK, et al. The need for randomization in animal trials: an overview of systematic reviews. PLoS One 2014;9(6):e98856; doi: 10.1371/journal.pone.0098856.

53. Bello S, Krogsbøll LT, Gruber J, et al. Lack of blinding of outcome assessors in animal model experiments implies risk of observer bias. J Clin Epidemiol 2014;67(9):973–983; doi: 10.1016/j.jclinepi.2014.04.008.

54. Cook JA, Hislop J, Altman DG, et al. Specifying the target difference in the primary outcome for a randomised controlled trial: guidance for researchers. Trials 2015;16:12; doi: 10.1186/s13063-014-0526-8.

55. Fenwick N, Griffin G, Gauthier C. The welfare of animals used in science: How the “Three Rs” ethic guides improvements. Can Vet J 2009;50(5):523–530.

56. Percie du Sert N, Ahluwalia A, Alam S, et al. Reporting animal research: Explanation and elaboration for the ARRIVE guidelines 2.0. PLoS Biol 2020;18(7):e3000411; doi: 10.1371/journal.pbio.3000411.

57. Percie du Sert N, Hurst V, Ahluwalia A, et al. The ARRIVE guidelines 2.0: Updated guidelines for reporting animal research. PLoS Biol 2020;18(7):e3000410; doi: 10.1371/journal.pbio.3000410.

58. Zhang SX, Ma J-X, Sima J, et al. Genetic difference in susceptibility to the blood-retina barrier breakdown in diabetes and oxygen-induced retinopathy. Am J Pathol 2005;166(1):313–321; doi: 10.1016/S0002-9440(10)62255-9.

59. Gao G, Li Y, Fant J, et al. Difference in Ischemic Regulation of Vascular Endothelial Growth Factor and Pigment Epithelium--Derived Factor in Brown Norway and Sprague Dawley Rats Contributing to Different Susceptibilities to Retinal Neovascularization. Diabetes 2002;51(4):1218–1225; doi: 10.2337/diabetes.51.4.1218.

CHAPTER 3

Structure-Function Relationships in the Brown Norway rat Streptozotocin-Induced Model of Diabetic Retinopathy

Inesa Lelyte[1,2], Marc Cerrada-Gimenez[3], Anita K Ghosh[4], Zubair Ahmed[1,5], Simon Kaja[6], and Giedrius Kalesnykas[3,4]

[1]Institute of Inflammation and Ageing, University of Birmingham, Edgbaston, Birmingham, B15 2TT, UK

[2]R&D Division, Experimentica Ltd., 10243 Vilnius, Lithuania

[3]R&D Division, Experimentica Ltd., Kuopio, Finland

[4]R&D Division, Experimentica Inc., Fort Worth, TX, USA

[5]Centre for Trauma Sciences Research, University of Birmingham, Edgbaston, Birmingham, B15 2TT, UK

[6]Department of Molecular Pharmacology & Neuroscience, Loyola University Chicago, Maywood, IL 60153, USA

Manuscript in preparation

3.1 Abstract

The rat streptozotocin-induced model for diabetic retinopathy (DR) remains the most-commonly used experimental paradigm for drug discovery, as it recapitulates many of the complex phenotypes observed in patients. Advances in ocular imaging and electrophysiological testing provide an opportunity to study pathological processes in this model and to establish structure-function relationships. Adult Brown Norway rats received single intraperitoneal injection of streptozotocin (STZ) and were followed *in vivo* for a period of nine weeks. Glucose levels and body weights were monitored on a weekly basis. Vitreous fluorophotometry (VFP), spectral domain optical coherence tomography (SD-OCT), and fluoresceine angiography (FA) were performed to investigate STZ-induced retinal structural changes. Ocular tissues were collected for quantification of pericyte ghosts and acellular capillaries using trypsin-digested retinal flat-mounts, and integrity of the blood-retinal barrier (BRB) was assessed through the Evans Blue (EB) extravasation assay. In addition to these structural assessments, flash electroretinography (fERG) was performed to evaluate retinal function. While anti-VEGF antibodies were administered to investigate its efficacy in ameliorating STZ-induced pathologies. While anti-VEGF antibodies (0.125 mg/ml per eye) were administered intravitreally at a volume of 5 µl in both eyes at weeks six, seven and eight following the STZ induction to investigate its efficacy in ameliorating STZ-induced pathologies. Breakdown of BRB was identified via elevated EB dye leak in diabetic rat retinas, nine weeks post-induction. This observation was confirmed by a decrease of VFP slope at weeks 7 and 9, indicating retinal leakage in rats subjected to STZ. Vascular abnormalities, such as augmentation in pericyte ghosts were identified at week 9 post-STZ injection, although no significant changes in acellular capillaries were detected. SD-OCT revealed inner retina thinning, suggesting retinal cell loss nine weeks following STZ injection, alongside thickening of outer retina, indicating retinal

swelling. FA imaging did not reveal any abnormalities in diabetic animals. Structural changes observed in diabetic retinas correlated with reductions in both a-wave and b-wave amplitudes as determined by fERG at weeks 7 and 9, confirming structure-function relationships in the Brown Norway rat STZ-induced DR model. Anti-VEGF treatment successfully reduced retinal vascular leakage and pericyte ghosts' number in STZ-injected animals, and reversed STZ-induced outer retinal thickening. However, it did not significantly impact STZ-mediated inner retinal thinning or decreased retinal function. Our data demonstrates that the STZ-induced Brown Norway model reproduces the known hallmarks of early DR. Detailed analysis of the structure-function relationship in the BN rats reveal consistent morphological changes and visual deficits post-STZ induction. While anti-VEGF treatment protects against certain diabetes-induced vascular pathologies in the retina, it may also have adverse effects on retinal neurons.

3.2 Introduction

Diabetic retinopathy (DR) is the most common microvascular complication of diabetes mellitus, contributing significantly to irreversible visual loss and blindness in the working-age population.[1] DR is characterized by vascular abnormalities such as microaneurysms[2] and retinal hemorrhages,[3] which are linked to diabetic macular edema (DME).[4] Without treatment, DR can progress to proliferative diabetic retinopathy (PDR), which manifests as neovascularization and vitreous/pre-retinal hemorrhages.[5] Many visual impairments are linked to these structural alterations, such as reduced visual acuity[6,7] and contrast sensitivity,[8] loss of color vision[9], and difficulty adjusting to dark environments.[10] Nevertheless, the exact mechanism that underlies between structural changes and functional deficits remains a subject of ongoing investigation.

Advancements in *in vivo* ocular imaging such as fluoresceine angiography (FA) and spectral domain optical coherence tomography (SD-OCT), and electrophysiological testing techniques like flash electroretinography (fERG), offer a unique opportunity to study the pathological processes in DR and to establish structure-function relationships. Understanding the connections between structure and function may help to detect early changes of DR, provide insights into how the disease progresses, and facilitate the development of novel treatments that are effective at cellular levels while also improve patients' vision.

The rat streptozotocin (STZ)-induced model of DR remains the most-commonly used experimental paradigm for drug discovery, as it recapitulates ocular complications of diabetes, including the breakdown of blood–retinal barrier,[11] increased expression of angiogenic factors,[12] and chronic inflammation.[13] We recently performed a systematic literature review that included 662 records of preclinical STZ studies conducted over the last decade, encompassing

both structural and functional assessments.[14] However, within this extensive research, only one investigation was conducted in pigmented rats, specifically Brown Norway (BN) rats.[15]

Comparative studies have shown that STZ-induced BN rats demonstrate greater vessel hyperpermeability and express higher levels of vascular endothelial growth factor (VEGF), compared to non-pigmented rats subjected to STZ.[16] Similarly, in oxygen-induced retinopathy model, vascular permeability and levels of angiogenic factors in albino rats were less in magnitude than in BN rats.[16,17] Furthermore, the presence of pigmentation in Brown Norway rats, allows the detection of potential pharmacologic effects due to melanin binding, as many drugs are known to bind to melanin, resulting in higher drug concentrations and prolonged retention in pigmented eye tissues.[18–20]

Therefore, since detailed structure-function relationship examinations in the STZ-induced DR model of Brown Norway rats are lacking, the aim of this study was to perform an extensive characterization of both structural and functional pathologic processes. First, we assessed STZ-induced retinal structural changes using non-invasive techniques such as SD-OCT, fluorescein angiography (FA), and vitreous fluorophotometry (VFP). Second, ocular tissues were collected for more in-depth analysis of vascular abnormalities. Third, fERG was performed to evaluate retinal function. Additionally, since VEGF inhibition is currently the standard therapy for DR, the efficacy of anti-VEGF antibody on the various pathologic hallmarks of DR was also studied to provide proof of concept that the diabetic STZ-induced BN rat model can be used for the evaluation of new therapeutic strategies to halt DR progression.

3.3 Materials and Methods

Animal Experiments

Brown Norway rats (BN/Crl; Charles River Laboratories, Sulzfeld, Germany) aged 9-10 weeks were housed at a constant temperature (22±1°C), relative humidity (50±10%) and in a light-controlled environment (lights on from 7 am to 7 pm) with *ad libitum* access to food and water. Experiments started after one-week of quarantine and acclimatization in the vivarium. All animals were treated in accordance with the ARVO Statement for the Use of Animals in Ophthalmic and Vision Research, the EC Directive 2010/63/EU of the European Parliament and of the Council on the Protection of animals used for Scientific Purposes, using protocols approved and monitored by the Animal Experiment Board of Finland (Experimentica Ltd. animal license number ESAVI-9520-2020). The study was performed in accordance with the ARRIVE guidelines. No power calculations were performed to determine group sizes, as it was determined based on prior experiments with similar conditions. Animals were allocated randomly to respective treatment groups, and experimenters remained blinded to the treatment conditions throughout the study. (N = 15-18 animals/group).

For all the procedures, animals were anesthetized with ketamine (30 mg/kg; Ketaminol Vet; Intervet, Unterschleissheim, Germany) and medetomidine (0.2 mg/kg; CP-Pharma; Burgdorf, Germany) mixture. The anesthesia was reversed by the α2-antagonist, atipamezole (1.0 mg/kg; CP-Pharma). At the end of the experiment, rats were euthanized by anesthesia overdose, transcardially perfused with 0.9% sodium chloride solution using peristaltic pump (120S/DV; Watson-Marlow Pumps, Marlow, UK), and eyes were enucleated. The retinas were either excised and snap-frozen in liquid nitrogen for Evan´s Blue (EB) extravasation assay (n =10-14 eyes/group), or retinal flat-mounts were prepared and fixed in 4% paraformaldehyde (PFA) for histological analysis (n =12 eyes/group).

Streptozocin (STZ)-induced DR

Diabetes was induced by single intraperitoneal (IP) injection of STZ (65 mg/kg; Sigma-Aldrich, Steinheim, Germany) in 10 mM sodium citrate buffer, pH 4.5. Prior to STZ injection all animals were fasted for four hours, weighed, and blood glucose was measured using Alpha Trak 2 (Zoetis Inc., Parsippany-Troy Hills, NJ, USA) glucose meter. After induction, rats were placed in their cages with *ad libitum* food and 10% (w/v) sucrose solution in tap water for 48 h. Four days after the first STZ injection, the success of the induction was monitored by measuring the blood glucose levels from the saphenous vein. The induction of diabetes was considered successful when the blood glucose values were equal or higher than 16 mmol/l (288 mg/dl). Animals that were not diabetic based on this criterion 96 h after the first STZ injection received a second STZ injection. Blood glucose level and body weight of STZ rats were monitored weekly during the whole follow-up period (9 weeks).

Intravitreal Injection (IVT)

All IVT injections were performed under ketamine/medetomidine anesthesia as previously outlined, using a 5 µl glass microsyringe (Hamilton Bonaduz AG, Bonaduz, Switzerland). A solution containing D-Mannitol, trisodium citrate dihydrate, sodium hydroxide, hydrochloric acid, and water, was used as vehicle group for control. The reference compound, rat anti-VEGF antibody (AF564; R&D Systems, Minneapolis, MN, USA), was dissolved in vehicle solution to achieve a final concentration of 0.125 mg/ml per eye. Both the vehicle and the anti-VEGF were administered intravitreally at a volume of 5 µl in both eyes at weeks six, seven and eight following the STZ induction.

In Vivo Imaging

STZ-mediated retinal structural changes in rat eyes were assessed using fluorescein angiography (FA) and spectral domain optical coherence tomography (SD-OCT). After

anesthesia (described above) pupils were dilated with 0.5% tropicamide solution (Santen Oy, Tampere, Finland), and the optic nerve head was aligned at the retina level using an infrared reflectance camera. Then 2% of sodium fluorescein solution (Sigma-Aldrich, Steinheim, Germany) was injected intravenously (IV) into the tail vein (50 µl/ 100 g), and images were taken 5 minutes after injection using a Spectralis HRA/OCT device (Heidelberg Engineering, Heidelberg, Germany). FA was performed at weeks 3, 5, 7, and 9 after induction. Following FA, SD-OCT imaging was conducted using the Bioptigen Envisu R2200 device (Leica Microsystems, Mannheim, Germany). The scanned area covered a 2.4 x 2.4 mm^2 region of the retina, centered around the optic nerve. Each scan consisted of 100 B-scans, each of which was composed of 1000 A-scans. SD-OCT was performed nine weeks post-STZ injection. The retinal thickness was analyzed by a convolutional neural network based on U-net architecture using transfer learning approach. The thickness results were presented as inner retina (including the nerve ganglion cell layer, inner plexiform and inner nuclear layers), and outer retina (including the outer plexiform and outer nuclear layers, inner and outer segments, retinal pigmented epithelium, and choroid).

Vitreous fluorophotometry (VFP)

Vitreous fluorophotometry (VFP) is the measurement of fluorescence across the anatomical axis of the eye, which allows to quantitatively assess retinal leakage using an FM-2 Fluorotron Master ocular fluorophotometer (OcuMetrics Inc., Mountain View, CA, USA). The presence of retinal leakage is indicated by a reduction of the VFP slope, a straight line between the highest peak in the retina region and the mid-peak in the vitreous. After FA imaging, the rats remained under anesthesia, and VFP was performed 30 minutes post-administration of the

previously described fluorescein injection. VFP was performed at weeks 7 and 9 after STZ injection.

Flash Electroretinography (fERG)

To evaluate retinal function flash electroretinography (fERG) measurements were conducted with animals dark-adapted overnight in their home cages, with *ad libitum* access to food and water, using Celeris ERG system (Diagnosys LLC, Lowell, MA, USA). All preparations for fERG were performed under dim red light. Rats were anesthetized and their pupils were dilated as described above. During recording, eyes were lubricated using 0.9% sodium chloride to maintain corneal moisture and to ensure electrical contact between the cornea and electrode. Six different light intensities were tested: 0.003, 0.01, 0.1, 1, 3 and 10 [*log* (cd.s.m^2)]. The responses to each intensity were recorded for six consecutive times, averaged, and further used to manually identify the amplitudes (μV) for both a- and b-waves. fERG was performed at weeks 3, 5, 7, and 9 after DR induction.

Evan's Blue (EB) Extravasation Assay

Prior to sacrifice, rats were administered with an intravenous injection of 4% Evans Blue dye (100 μl/100 g) via tail vein. After 2 hours, plasma samples were collected, and animals were transcardially perfused with 0.9% sodium chloride solution for a duration of 30 minutes, using peristaltic pump (120S/DV; Watson-Marlow Pumps). Post-perfusion, eyes were enucleated, the retinas excised, snap frozen in liquid nitrogen, and stored at -80 °C until further analysis. For the quantification of EB extravasation, the retinas were homogenized in formamide, centrifuged at 20,800 x *g* for 45 minutes, and the resultant supernatant was collected. Both retina and plasma samples were aliquoted in triplicate into a 384-well plate and absorbance measurements (λ = 620 nm) were conducted using a Cytation 3 plate reader (Cytation 3, BioTek Instruments Inc.,

Winooski, VT, USA). The concentration of Evans Blue in each retina sample was determined relative to the EB concentration in plasma samples.

PAS Histological Staining of Retinal Flat-mounts

Retinal flat-mounts were trypsin-digested to isolate the retinal vasculature and stained using Periodic Acid–Schiff (PAS). Retinal flat-mounts were placed in distilled water overnight and incubated with 4% Trypsin in 0.1M Tris-HCl buffer (pH 7.8) for 1.5 hours at + 37 °C. Samples were then carefully washed with distilled water to detach the retinal cell layers from the vasculature. The vascular flat-mounts were dried on a microscope slide and processed for PAS staining. Samples were oxidized, rinsed with dH2O, placed in Schiff's reagent, washed, counterstained with hematoxylin, differentiated with acid alcohol, dehydrated, and mounted with Depex. Four to six individual images obtained from a central area, and from a peripheral area of the retinal vasculature were acquired using a Leica Thunder 3D Tissue Imager (Leica Microsystems, Mannheim, Germany). The number of acellular capillaries and the number of pericyte ghosts were manually counted by an investigator blinded to the experimental group assignment.

Statistical Analysis

Statistical analysis was performed using GraphPad Prism (version 10.0.2, GraphPad Software, La Jolla, CA, USA). Data were analyzed using the Mann Whitney test, or two-way ANOVA, followed by Dunnet's or Tukey's multiple comparison test, and presented as mean ± standard error of mean (SEM). Significance was determined according to the P value: * $P < 0.05$, ** $P < 0.01$, and *** $P < 0.001$.

3.4 Results

Glycaemia and Body Weight

Successful diabetes induction was confirmed by hyperglycemia in rats, with glucose levels exceeding 16 mmol/l, within the first week post-STZ injection. These elevated glucose levels persisted consistently throughout the duration of the study. Hyperglycemic rats presented significantly reduced body weight gain compared to the naïve rats starting from week one ($P < 0.001$; Figure 1B). Throughout the study, naïve rat's body weight steadily increased, in contrast to the STZ-treated rats who showed a slight reduction from their initial body weight.

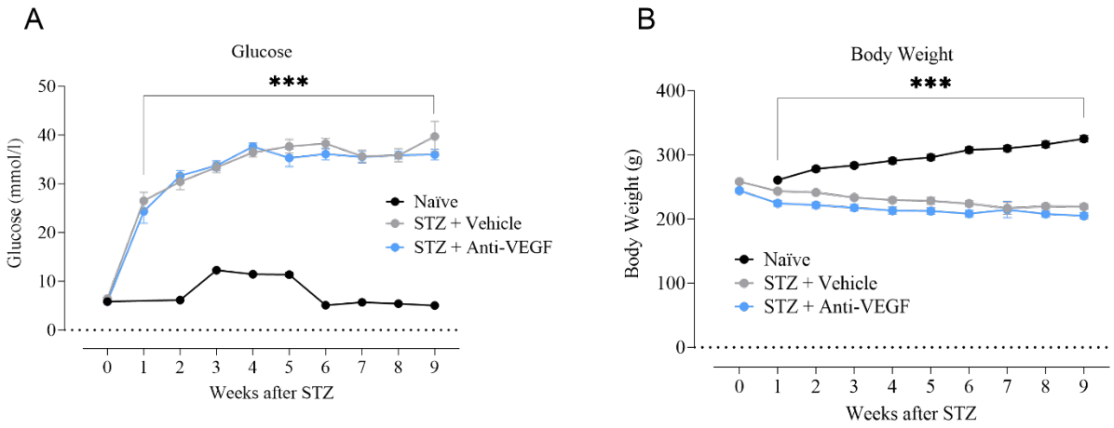

Figure 1. STZ resulted in reliable induction of hyperglycemia followed by reduced body weight gains. (**A**) Blood glucose levels (mmol/l) significantly increased in STZ-injected animals by week 1 post-induction and remained elevated throughout the entire study period, as compared to the naïve rats. *** $P < 0.001$. (**B**) Hyperglycemic rats presented significantly reduced body weight gains compared to the naïve rats starting from week 1 until the end of the study. *** $P < 0.001$. Statistical analysis was done by two-way ANOVA followed by Dunnett's multiple comparison test. Data are presented as mean ± SEM, n = 15-18 animals per group.

Increased Retinal Leakage in Diabetic Rats

Retinal vascular leakage, a key pathological feature of DR, was assessed through Evans Blue extravasation assay and vitreous fluorophotometry analysis. Nine weeks post-induction the

Evans Blue extravasation assay revealed greater than six-fold increase of EB dye leakage in the retinas of STZ-injected rats, as compared to the naïve group ($P < 0.05$; Figure 2A). Treatment with anti-VEGF antibody, significantly reduced STZ-induced EB extravasation, achieving an 82.3% reduction ($P < 0.05$; Figure 2A). Additionally, vitreous fluorophotometry analysis demonstrated significant decrease in VFP slope of diabetic rats versus naïve rats at week 7 that continued to progress to week 9 ($P < 0.0001$ and $P < 0.0001$, respectively; Figure 2B), signifying retinal leakage and corroborating the EB increased vascular permeability findings. However, on the VFP slope anti-VEGF antibody treatment failed to demonstrate effectiveness, with no significant differences noted at any timepoint when comparing anti-VEGF-treated and vehicle-treated rats. Examination with FA did not reveal any abnormalities in STZ-induced rats during the study period (images can be found in Supplemental Figure S1).

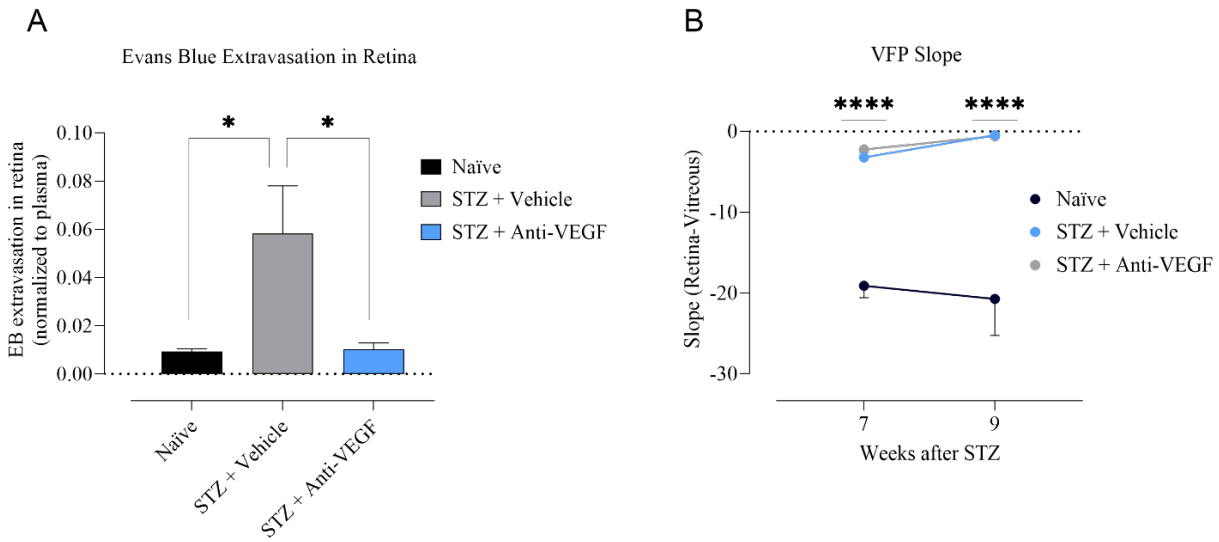

Figure 2. Significant leakage detected by EB extravasation and VFP slope measurements in diabetic retina. (**A**) EB extravasation in retina normalized to plasma. Nine weeks post-induction an approximately 6-fold increase in EB extravasation was found in diabetic rats, that was prevented by anti-VEGF antibody treatment. * $P < 0.05$. (**B**) The VFP slope between the retinal

peak and the vitreous mid-point used as the indicator of leakage. During weeks 7 and 9, a significant decrease in the VFP slope was observed in all STZ-treated rats, indicating retinal leakage. **** $P < 0.0001$. Statistical analysis was done by Mann Whitney test for EB extravasation, and two-way ANOVA followed by Tukey's multiple comparison test for VFP analysis. Data are presented as mean ± SEM, n = 10-14 eyes per group for EB extravasation, and n = 23-36 eyes per group for VFP analysis.

Vascular Abnormalities in STZ-induced Rat Retinas

To further evaluate STZ-induced vascular abnormalities, quantification of pericyte ghosts and acellular capillaries on trypsin-digested retinal flat-mounts, was performed. Analysis revealed a significant increase in the number of pericyte ghosts in the STZ-induced animals compared with naïve group, suggesting loss of healthy pericytes associated with diabetes ($P < 0.05$; Figure 3A). Anti-VEGF antibody treatment showed beneficial effects on retinal vasculature, leading to a notable reduction in the number of pericyte ghosts in comparison to vehicle-treated rats ($P < 0.01$; Figure 3A). Additionally, we quantified acellular capillaries; however no significant differences were observed between the treatment groups ($P = 0.35$; Figure 3B).

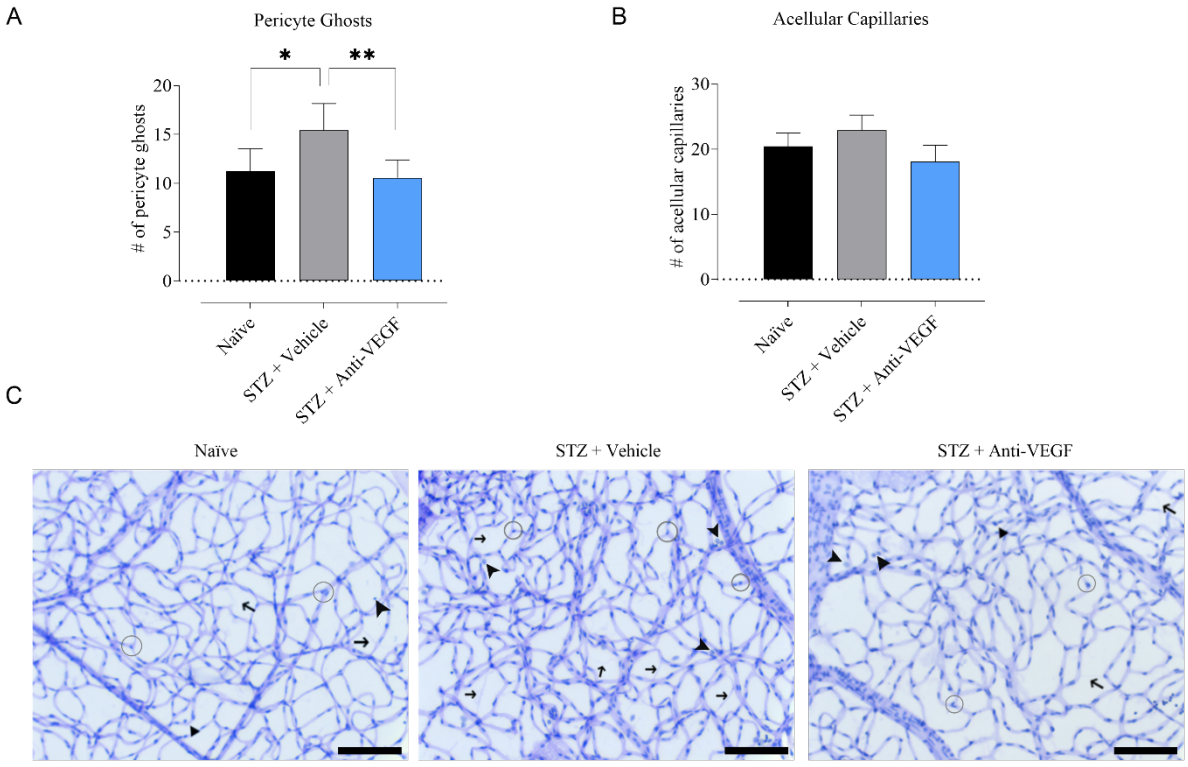

Figure 3. STZ-induced vascular abnormalities. Retinal trypsin digest analysis for the (**A**) pericyte ghosts and (**B**) acellular capillaries. Pericyte ghosts significantly increased in diabetic animals compared to naïve rats (* $P < 0.05$), with anti-VEGF antibody treatment showing significant reductions (** $P < 0.01$). No difference in acellular capillaries was observed between all treatment groups. Statistical analysis was done by one-way ANOVA followed by Tukey's multiple comparison test. Data are presented as mean ± SEM, n = 31-38 images analyzed per group from n = 6 rats per group. (**C**) Representative image of trypsin digest staining from naïve, STZ + vehicle, and STZ + anti-VEGF groups, showing acellular capillaries (*arrows*), pericytes (*circles*) and pericyte ghosts (*arrowheads*). Scale bar = 100 µm.

Diabetes-Induced Alterations in Retina Thickness

Structural changes in retinal layers were examined through SD-OCT scans, and the thickness of both inner and outer retinal layers were measured (Figure 4A). Nine weeks after the onset of

diabetes, the inner retina was approximately 6.3 % thinner in rats subjected to STZ than in nondiabetic animals, suggesting a potential loss of retinal cells ($P < 0.001$; Figure 4B). Conversely, the outer retina in these STZ-injected rats exhibited a 4.3 % increase in thickness compared to naïve rats ($P < 0.001$; Figure 4C), indicating retinal edema, possibly linked to previously described retinal leakage. Anti-VEGF antibody treatment did not significantly reverse thinning of the inner retina (naïve vs. STZ + anti–VEGF, $P < 0.01$; STZ + vehicle vs. STZ + anti–VEGF, $P = 0.93$) but did significantly reverse thickening of the outer retina caused by STZ (naïve vs. STZ + anti–VEGF, $P = 0.07$; STZ + vehicle vs. STZ + anti–VEGF, $P \leq 0.05$) (Figure 4B and C).

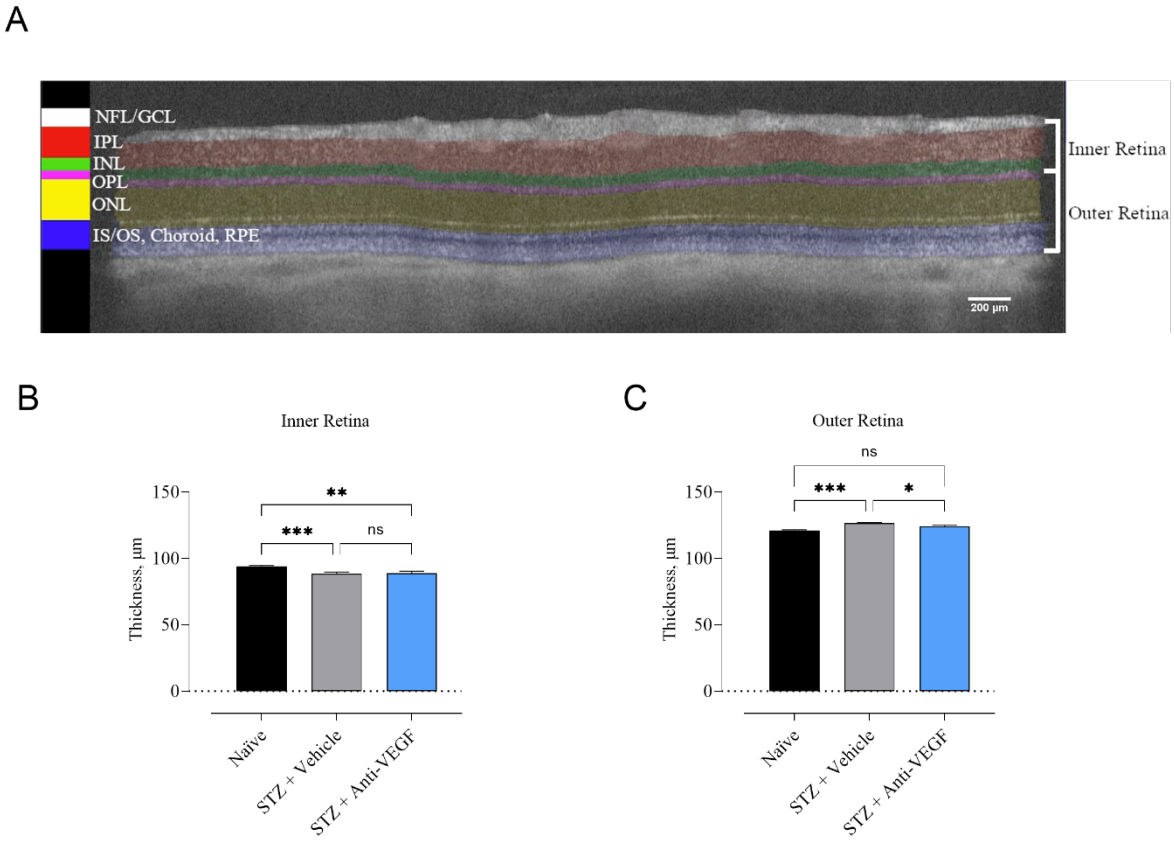

Figure 4. Inner and outer retina thickness changes in STZ-injected rats. (**B**) Diabetic animals presented thinner inner retina layers compared to naïve animals. *** $P < 0.001$; ** $P < 0.01$. In

contrast, (**C**) outer retina thickness increased in diabetic rats (naïve vs. STZ + vehicle, *** $P < 0.001$), which was restored by anti-VEGF antibody treatment (naïve vs. STZ + anti–VEGF, $P = 0.07$; STZ + vehicle vs. STZ + anti–VEGF, * $P \leq 0.05$). Statistical analysis was done by one-way ANOVA followed by Tukey's multiple comparison test. Data are presented as mean ± SEM, n = 23-36 eyes analyzed per group. (**A**) Example frame showing the six segmented layers overlayed on top of the OCT b-scan, used for inner and outer retina thickness measurements. NFL/GCL, nerve fiber layer and ganglion cell layer (white); IPL, inner plexiform layer (red); INL, inner nuclear layer (green); OPL, outer plexiform layer (purple); ONL, outer nuclear layer (yellow); IS/OS, Choroid and RPE, inner and outer segments, choroid and retinal pigmented epithelium (blue). Scale bar = 200 μm.

Reduced Retinal Activity in STZ-induced Rats

To evaluate functional deficits in STZ-induced rats, flash electroretinography (fERG) was employed. A significant reduction in a-wave amplitude was observed in diabetic rats, with a 30 % decrease at week 7 pot-induction (1 [log (cd.s.m-2)]), $P < 0.05$; Figure 5A) and a 21 % decrease by week 9, as compared to baseline measurements, indicating reduction in photoreceptor activity. Similarly, the b-wave amplitude in STZ-injected rats decreased by 23 % at week 7 ($P < 0.01$; Figure 5B), with a slight recovery to a 14% reduction by week 9, suggesting reduced bipolar and Müller cell activity. Introduction of anti-VEGF antibody did not have a significant effect on STZ-mediated a-wave and b-wave amplitude reduction at any timepoint. To the contrary, in the anti-VEGF-treated STZ group, the a-wave amplitude decreased by 61 % at week 7 (1 [log (cd.s.m-2)]), $P < 0.001$; Figure 5A), with a slight recovery to a 59% reduction by week 9 ($P < 0.001$). The b-wave amplitude in this group declined by 44 % at week 7 ($P < 0.001$; Figure 5B), which further decreased to a 48 % by week 9 ($P < 0.001$).

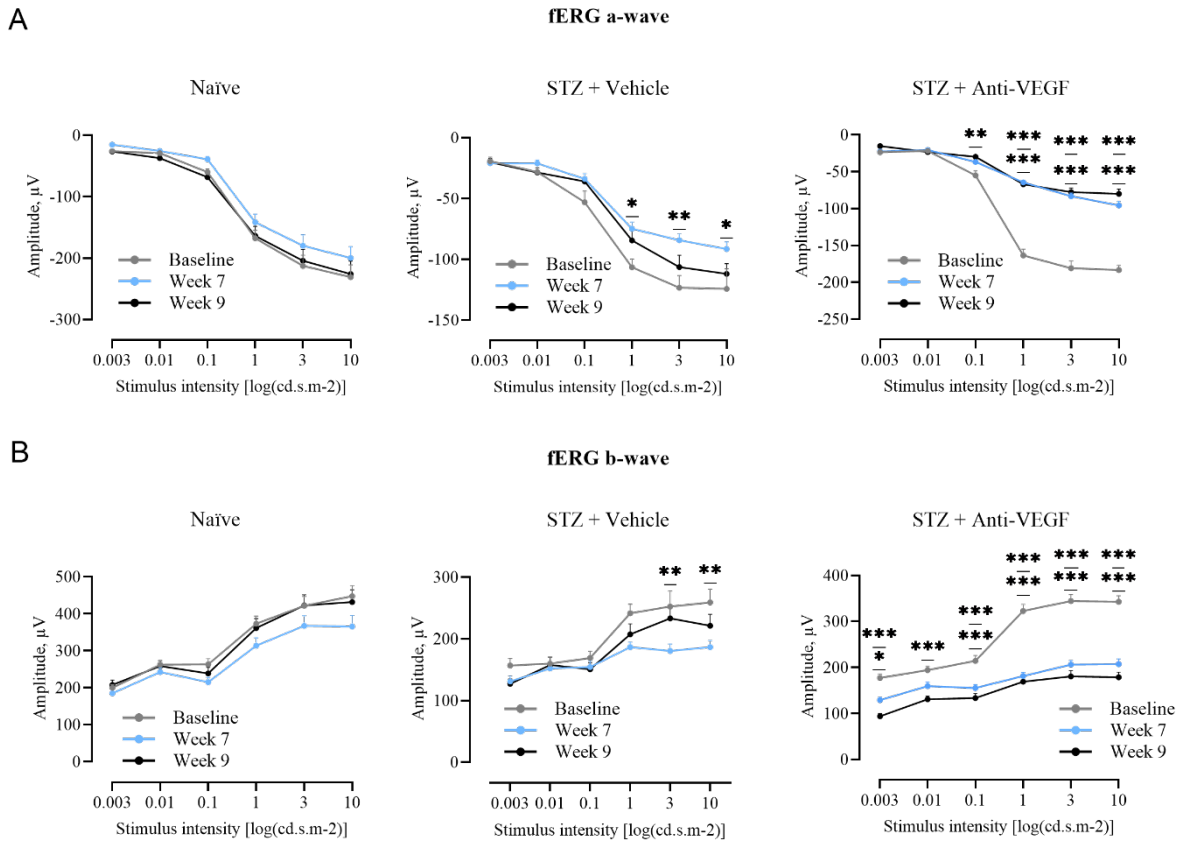

Figure 5. Reduced retinal activity in diabetic rats. Retinal function analyzed by fERG at 0.003, 0.01, 0.1, 1, 3, and 10 cd.s/m2 luminance, (**A**) a-wave, and (**B**) b-wave amplitudes. Statistical analysis was performed using two-way ANOVA followed by Šídák's multiple comparisons test. Data are presented as mean ± SEM, n = 23-36 eyes per group. *$P < 0.05$, **$P < 0.01$, *** $P < 0.001$.

3.5 Discussion

In this work we provided detailed analysis of both structural and functional pathologic processes of DR in STZ-induced Brown Norway rats. Our data demonstrates that STZ-induced Brown Norway rats exhibit key features of early DR, including the disruption of the blood-retinal barrier, vascular leakage, retinal thinning, and the presence of retinal edema. These observed structural changes were closely associated with retinal degeneration following

induction of diabetes, indicating structure-function relationship within this DR model in Brown Norway rats. Moreover, anti-VEGF treatment protected against some of the SZT-induced vascular pathologies in the BN rat retinas.

In our recent systematic literature review, which analyzed preclinical STZ studies from the past 10 years,[14] we found that only one study included both structural and functional redouts in Brown Norway (BN) rats.[15] In addition, several studies have indicated that genetic backgrounds contribute to the susceptibility to retinopathy, with BN rats being more predisposed to induction than albino rats.[16,17] Therefore, in this study, we aimed to investigate whether visual function assessed by flash ERG are related to retinal structural changes observed in STZ-induced Brown Norway rats.

Diabetes induction was achieved through a single STZ injection, leading to hyperglycemia (>16 mmol/l) week one post-STZ administration. We choose to measure blood glucose concentration to define diabetes in this model based on findings from our systematic literature review, where the onset of diabetes and diabetes related complications in rat studies were consistently observed at or above a glucose concentration of >250 mg/dL.[14] Notably, while blood glucose measurements provide immediate data, incorporating glycated hemoglobin (HbA1c) measurements, which reflect average glucose levels over the past 2-3 months, could offer additional insights into long-term rat glycemic control.[21]

Hyperglycemic rats presented significantly reduced body weight gains compared to the naïve rats, consistent with decreased body weight or attenuated weight gain commonly observed in STZ-induced albino rats.[22,23] Diabetes in BN rats caused the breakdown of blood-retinal barrier, as evidenced by increased Evans Blue dye in diabetic retina at week nine post-induction. The disruption of BRB observed in our study aligns with vascular hyperpermeability reported in

previous research in both pigmented[16,24,25] and albino[11,16,26] rats subjected to STZ. In addition, the application of VFP and the observed decrease in VFP slope further confirmed increased vascular leakage in diabetic Brown Norway rat retinas at weeks 7 and 9 post-induction.

Moreover, we assessed vascular abnormalities by quantifying pericyte ghosts and acellular capillaries on trypsin-digested retinal flat-mounts. By week 9 post-STZ the number of pericyte ghosts was significantly higher in diabetic rats, indicating loss of healthy pericytes, a finding congruent with observations in other STZ-induced rodent models.[27,28] Pericytes provide vascular stability and control endothelial cell proliferation, and the depletion of pericytes ultimately lead to the formation of acellular capillaries.[29] However, our study did not reveal any significant differences in the number of acellular capillaries. This observation can be attributed to the appearance of pericyte ghosts in the early disease course, whereas acellular capillaries tend to emerge at more advanced stages of DR.

Induction of DR did not reveal any abnormalities in FA during the study period. STZ-induced DR animal model typically mirrors early stages of disease which may not be detectable through FA imaging. Only in limited number of studies, where STZ-induced animals were assessed for an extended period of time (9 months), FA successfully visualized PDR-related vascular changes, such as extensive fluorescein leakage and vascular tortuosity.[30] However, these changes were hindered by cataract formation at one month post-diabetes, which progressed more at months 6 and 9. In our study we also observed cataract formation induced by hyperglycemia by, which became noticeable by week 6 and progressed in severity by week 9. Furthermore, the formation of new blood vessels, a hallmark of PDR, varies across the literature in STZ-induced animals. While some studies report neovascularization in STZ-induced animals, the methods used to confirm new blood vessel formation are often inadequate.[31] In our

study, the absence of significant changes observed via FA imaging further indicate that the STZ model primarily mimics the early stages of DR. To investigate late-stage DR-related phenotypes, such as neovascularization, alternative models, such as the oxygen-induced retinopathy model,[32] should be considered.

Our analysis using OCT revealed a 6.3 % decrease in inner retina thickness, and a 4.3 % increase of outer retina by week 9 post-STZ injection. Generally, STZ-induced animals present either thinning or thickening of retinal layers.[15,33,34] However, in our study, we observed consistent thinning of the inner retina and thickening of the outer retina, which might be explained by different pathophysiological mechanisms at play in different retinal layers following diabetes induction. The observed thinning of inner retinal layers is likely attributed to the loss of retinal ganglion cells, a phenomenon which is commonly observed in STZ-induced animal models[33,34] or patients with DR.[35] In contrast, thickening of outer retina can be explained by increased vascular permeability and fluid accumulation within the retina, indicating retinal edema. This finding in our study closely aligns with previous observations demonstrating retinal swelling following STZ injections in both pigmented[15] and albino rats,[36] and it parallels the manifestation of diabetic macular edema (DME) observed in DR patients.[37,38]

Together with the observed structural retinal changes in diabetic rats, a decrease in retinal activity was identified by flash electroretinography (ERG). Significant reductions were found in both a-wave and b-wave amplitudes, at weeks 7- and 9-post diabetes induction. Beyond the development of vascular pathology, DR is also a neurodegenerative disease, leading to defects in vision. These include decreased visual acuity[6,7] and contrast sensitivity, [8] impaired color vision,[9] and slowed dark adaptation,[10] commonly observed in patients with DR. Experiments involving diabetic animals have also revealed functional deficits within the retina, including

reduced retinal activity, visual acuity, and contrast sensitivity.[15,39,40] Importantly, a-wave and b-wave amplitude reduction observed in our study is consistent with vascular abnormalities and retinal thickness alterations described above, confirming the correlation between retinal structural changes and functional deficits in STZ-injected Brown Norway rats. Studying the structure-function relationship in animal models is crucial for the development and testing novel therapies, as it ensures that these therapies are not only effective at a molecular or cellular level but also translate into significant clinical improvements, ultimately enhancing patients' vision. However, it is important to consider the potential of STZ to cause neurotoxic effects on retinal neurons. Previous studies have demonstrated that streptozotocin can cause neurotoxic effect on neurons both *in vitro* and *in vivo*.[41,42] Therefore, the functional decreases observed in our study may be attributed to STZ's neurotoxic impact on neurons which could lead to retinal neuron damage and exaggerate neurodegeneration beyond what is typically observed in human DR.

Moreover, while the introduction of anti-VEGF antibody treatment ameliorated STZ-induced vascular changes, such as vascular leakage and the number of pericyte ghosts, it did not have a significant effect on STZ-mediated a-wave and b-wave amplitude reductions. To the contrary, anti-VEGF treatment in STZ-induced animals caused further retinal function decrease. This might be explained by VEGF’s function as neurotrophic factor, supporting the survival of retinal neurons.[43,44] Consequently, inhibiting VEGF with anti-VEGF therapy may interfere with its neuroprotective effects. Similar findings have been reported, where anti-VEGF treatment resulted in significant retinal neurodegeneration and decreased retinal function in diabetic animals.[45–47]Additionally, while anti-VEGF antibody administration was successful in reversing the thickening of outer retina caused by STZ, it did not show a significant effect on the inner retina thickness. Further confirming, that using VEGF inhibitors for DR treatment can

have both beneficial and adverse effects, targeting vascular changes but potentially compromising retinal neuron survival.

The presented study comes with several limitations, including a lack of IgG control and a non-treated STZ control group. Including an IgG control — an isotype-matched antibody administered at the same dose and via the same route as the anti-VEGF antibody — would account for any nonspecific effects of antibody administration. Without this control, it is challenging to distinguish between effects specific to VEGF targeting and those resulting from the injection process or antibody carrier. Similarly, a non-treated STZ control group is essential to assess the impact of STZ alone on the diabetic phenotypes, ensuring that observed DR-related features are attributed specifically to the STZ injections rather than other variables.

To conclude, our data demonstrate that the STZ-induced Brown Norway model recapitulates the known hallmarks of early DR, including the breakdown of the blood-retina barrier, vascular leakage, loss of retinal cells, retinal edema, and decreased retinal function. A detailed analysis of the structure-function relationship in these BN rats reveals concurrent morphological changes and visual deficits post-STZ induction. While anti-VEGF treatments protect against certain diabetes-induced vascular pathologies in the retina, it may also have adverse effects on retinal neurons by interfering with VEGF's neuroprotective role.

3.6 Contributions

All authors contributed to the study conceptualization and design. STZ injections were performed by I.L. Intravitreal injections were performed by M.C.G. *In vivo* imaging, VFP measurements, fERG, EB extravasation assay, and PAS histological staining were performed by both I.L, with support from M.C.G and other members of the Experimentica team (not included in the author list). Data analysis were performed by I.L. and M.C.G. The original draft

preparation was performed by I.L., while Z.A. and G.K. reviewed, edited, and supervised. All authors have read and agreed on the final manuscript.

3.7 Disclosures

Employment: G.K., I.L., M.C.G., A.K.G. (Experimentica Ltd.); Stock/equity ownership: G.K. and S.K. (Experimentica Ltd.); S.K. (K&P Scientific LLC). S.K. conducts academic research in areas of interest similar to the business interests of Experimentica Ltd and K&P Scientific LLC. The terms of this arrangement have been reviewed and approved by Loyola University Chicago in accordance with its conflict-of interest policy. Z.A. declares no conflicts of interest.

3.8 Funding

This research was funded by the European Union's Horizon 2020 research and innovation program under the Marie Sklodowska-Curie Actions, grant agreement—No. 813440 (ORBITAL — Ocular Research by Integrated Training and Learning).

3.9 Supplementary Information

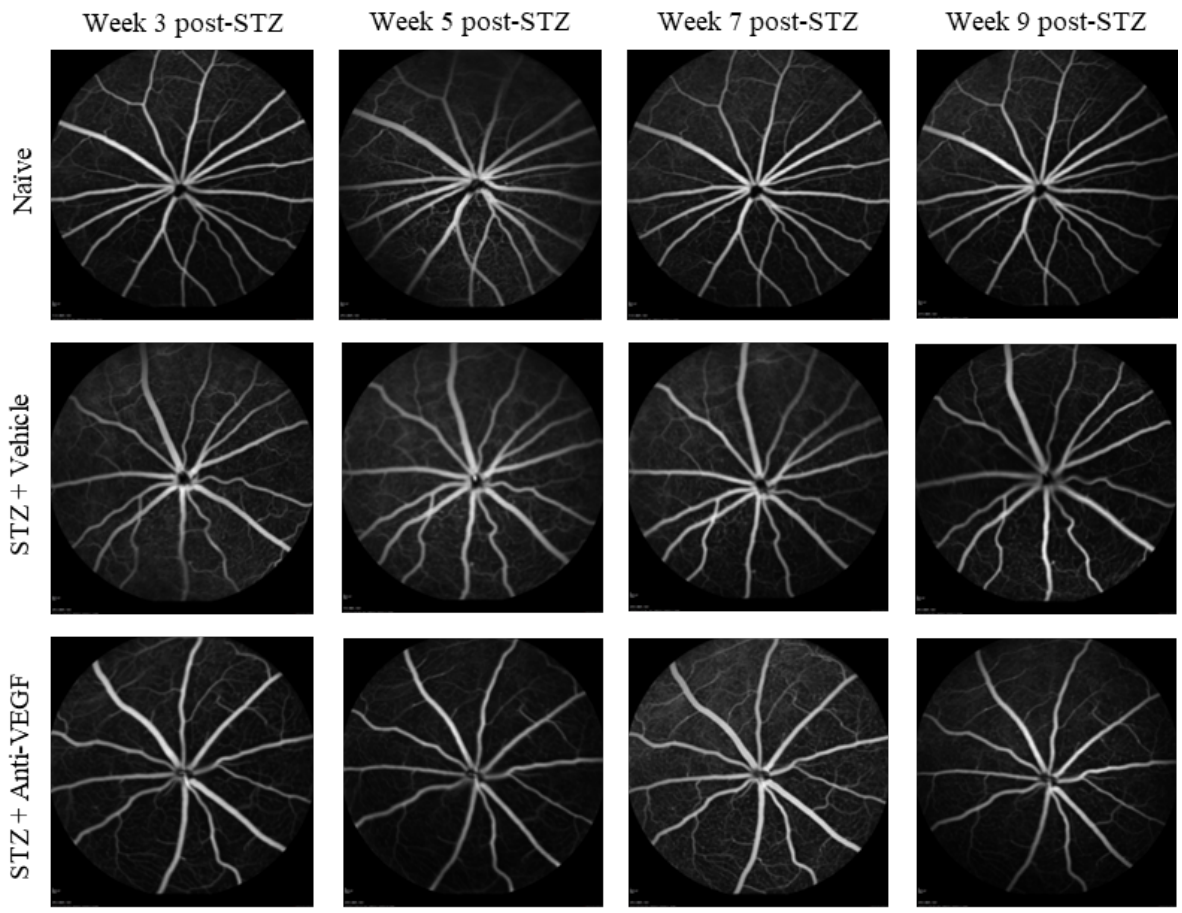

Supplemental Figure S1. No vascular abnormalities identified on FA images in diabetic retinas. Representative examples of FA scans from weeks 3, 5, 7, and 9 post-STZ of all treatment groups.

3.10 References

1. Kropp M, Golubnitschaja O, Mazurakova A, Koklesova L, Sargheini N, Vo TTKS, et al. Diabetic retinopathy as the leading cause of blindness and early predictor of cascading complications—risks and mitigation. EPMA J. 2023 Feb 13;14(1):21–42.

2. Akram MU, Khalid S, Khan SA. Identification and classification of microaneurysms for early detection of diabetic retinopathy. Pattern Recognition. 2013 Jan 1;46(1):107–16.

3. Nentwich MM, Ulbig MW. Diabetic retinopathy - ocular complications of diabetes mellitus. World J Diabetes. 2015 Apr 15;6(3):489–99.

4. Musat O, Cernat C, Labib M, Gheorghe A, Toma O, Zamfir M, et al. Diabetic Macular Edema. Rom J Ophthalmol. 2015;59(3):133–6.

5. Chaudhary S, Zaveri J, Becker N. Proliferative diabetic retinopathy (PDR). Disease-a-Month. 2021 May 1;67(5):101140.

6. Willis JR, Doan QV, Gleeson M, Haskova Z, Ramulu P, Morse L, et al. Vision-Related Functional Burden of Diabetic Retinopathy Across Severity Levels in the United States. JAMA Ophthalmol. 2017 Sep;135(9):926–32.

7. Jackson GR, Scott IU, Quillen DA, Walter LE, Gardner TW. Inner retinal visual dysfunction is a sensitive marker of non-proliferative diabetic retinopathy. Br J Ophthalmol. 2012 May;96(5):699–703.

8. Joltikov KA, de Castro VM, Davila JR, Anand R, Khan SM, Farbman N, et al. Multidimensional Functional and Structural Evaluation Reveals Neuroretinal Impairment in Early Diabetic Retinopathy. Investigative Ophthalmology & Visual Science. 2017 Sep 19;58(6):BIO277–90.

9. Wolff BE, Bearse MA, Schneck ME, Dhamdhere K, Harrison WW, Barez S, et al. Color vision and neuroretinal function in diabetes. Doc Ophthalmol. 2015 Apr;130(2):131–9.

10. Bavinger JC, Dunbar GE, Stem MS, Blachley TS, Kwark L, Farsiu S, et al. The Effects of Diabetic Retinopathy and Pan-Retinal Photocoagulation on Photoreceptor Cell Function as Assessed by Dark Adaptometry. Invest Ophthalmol Vis Sci. 2016 Jan;57(1):208–17.

11. Canovai A, Amato R, Melecchi A, Dal Monte M, Rusciano D, Bagnoli P, et al. Preventive Efficacy of an Antioxidant Compound on Blood Retinal Barrier Breakdown and Visual Dysfunction in Streptozotocin-Induced Diabetic Rats. Frontiers in Pharmacology [Internet]. 2022 [cited 2023 Nov 20];12. Available from: https://www.frontiersin.org/articles/10.3389/fphar.2021.811818

12. Lee SG, Kim JL, Lee HK, Ryu GW, Hur DY, Yun IH, et al. Simvastatin suppresses expression of angiogenic factors in the retinas of rats with streptozotocin-induced diabetes. Graefes Arch Clin Exp Ophthalmol. 2011 Mar 1;249(3):389–97.

13. Yu Z, LingWei, Gao Q, Diao L. Geraniin ameliorates streptozotocin-induced diabetic retinopathy in rats via modulating retinal inflammation and oxidative stress. Arabian Journal of Chemistry. 2023 Jan 1;16(1):104396.

14. Lelyte I, Ahmed Z, Kaja S, Kalesnykas G. Structure–Function Relationships in the Rodent Streptozotocin-Induced Model for Diabetic Retinopathy: A Systematic Review. J Ocul Pharmacol Ther. 2022 May 1;38(4):271–86.

15. Qiu F, Meng T, Chen Q, Zhou K, Shao Y, Matlock G, et al. Fenofibrate-Loaded Biodegradable Nanoparticles for the Treatment of Experimental Diabetic Retinopathy and Neovascular Age-Related Macular Degeneration. Molecular pharmaceutics. 2019 May 5;16(5):1958.

16. Zhang SX, Ma JX, Sima J, Chen Y, Hu MS, Ottlecz A, et al. Genetic difference in susceptibility to the blood-retina barrier breakdown in diabetes and oxygen-induced retinopathy. Am J Pathol. 2005 Jan;166(1):313–21.

17. Gao G, Li Y, Fant J, Crosson CE, Becerra SP, Ma J xing. Difference in Ischemic Regulation of Vascular Endothelial Growth Factor and Pigment Epithelium--Derived Factor in Brown Norway and Sprague Dawley Rats Contributing to Different Susceptibilities to Retinal Neovascularization. Diabetes. 2002 Apr 1;51(4):1218–25.

18. Bahrpeyma S, Reinisalo M, Hellinen L, Auriola S, del Amo EM, Urtti A. Mechanisms of cellular retention of melanin bound drugs: Experiments and computational modeling. Journal of Controlled Release. 2022 Aug 1;348:760–70.

19. Pitkänen L, Ranta VP, Moilanen H, Urtti A. Binding of betaxolol, metoprolol and oligonucleotides to synthetic and bovine ocular melanin, and prediction of drug binding to melanin in human choroid-retinal pigment epithelium. Pharm Res. 2007 Nov;24(11):2063–70.

20. Tanaka M, Ono C, Yamada M. Absorption, distribution and excretion of 14C-levofloxacin after single oral administration in albino and pigmented rats: binding characteristics of levofloxacin-related radioactivity to melanin in vivo. J Pharm Pharmacol. 2004 Apr;56(4):463–9.

21. Rehman H ur, Ullah K, Rasool A, Manzoor R, Yuan Y, Tareen AM, et al. Comparative impact of streptozotocin on altering normal glucose homeostasis in diabetic rats compared to normoglycemic rats. Sci Rep. 2023 May 16;13:7921.

22. Szilvássy J, Sziklai I, Horvath P, Szilasi M, Németh J, Kovacs P, et al. Feeble bronchomotor responses in diabetic rats in association with decreased sensory neuropeptide release. American journal of physiology Lung cellular and molecular physiology. 2002 Jun 1;282:L1023-30.

23. Harg J, Eggels L, Ruigrok S, Hoozemans JJM, la Fleur S, Scheper W. Neuroinflammation is not a Prerequisite for Diabetes-induced Tau Phosphorylation. Frontiers in Neuroscience. 2015 Nov 9;9.

24. Xu HZ, Le YZ. Significance of Outer Blood–Retina Barrier Breakdown in Diabetes and Ischemia. Invest Ophthalmol Vis Sci. 2011 Apr;52(5):2160–4.

25. Allen CL, Malhi NK, Whatmore JL, Bates DO, Arkill KP. Non-invasive measurement of retinal permeability in a diabetic rat model. Microcirculation. 2020;27(6):e12623.

26. Zhang H, Gao Y, Zhang J, Wang K, Jin T, Wang H, et al. The effect of total lignans from Fructus Arctii on Streptozotocin-induced diabetic retinopathy in Wistar rats. Journal of Ethnopharmacology. 2020 Jun 12;255:112773.

27. Beltramo E, Porta M. Pericyte Loss in Diabetic Retinopathy: Mechanisms and Consequences. CMC. 2013 Jul 1;20(26):3218–25.

28. Mazzoli V, Zhong LH, Dang VT, Shi Y, Werstuck GH. Characterization of Retinal Microvascular Complications and the Effects of Endoplasmic Reticulum Stress in Mouse Models of Diabetic Atherosclerosis. Investigative Ophthalmology & Visual Science. 2020 Aug 27;61(10):49.

29. Hammes HP, Feng Y, Pfister F, Brownlee M. Diabetic Retinopathy: Targeting Vasoregression. Diabetes. 2011 Jan 1;60(1):9–16.

30. Naderi A, Zahed R, Aghajanpour L, Amoli FA, Lashay A. Long term features of diabetic retinopathy in streptozotocin-induced diabetic Wistar rats. Exp Eye Res. 2019 Jul;184:213–20.

31. Jiang N, Chen XL, Yang HW, Ma YR. Effects of nuclear factor κB expression on retinal neovascularization and apoptosis in a diabetic retinopathy rat model. Int J Ophthalmol. 2015 Jun 18;8(3):448–52.

32. Villacampa P, Menger KE, Abelleira L, Ribeiro J, Duran Y, Smith AJ, et al. Accelerated oxygen-induced retinopathy is a reliable model of ischemia-induced retinal neovascularization. PLoS One. 2017 Jun 26;12(6):e0179759.

33. He M, Long P, Guo L, Zhang M, Wang S, He H. Fushiming Capsule Attenuates Diabetic Rat Retina Damage via Antioxidation and Anti-Inflammation. Evid Based Complement Alternat Med. 2019 Jul 18;2019:5376439.

34. Sergeys J, Etienne I, Van Hove I, Lefevere E, Stalmans I, Feyen JHM, et al. Longitudinal In Vivo Characterization of the Streptozotocin-Induced Diabetic Mouse Model: Focus on Early Inner Retinal Responses. Investigative Ophthalmology & Visual Science. 2019 Feb 27;60(2):807–22.

35. Sohn EH, van Dijk HW, Jiao C, Kok PHB, Jeong W, Demirkaya N, et al. Retinal neurodegeneration may precede microvascular changes characteristic of diabetic retinopathy in diabetes mellitus. Proceedings of the National Academy of Sciences. 2016 May 10;113(19):E2655–64.

36. Deguchi S, Otake H, Nakazawa Y, Hiramatsu N, Yamamoto N, Nagai N. Ophthalmic Formulation Containing Nilvadipine Nanoparticles Prevents Retinal Dysfunction in Rats Injected with Streptozotocin. Int J Mol Sci. 2017 Dec 15;18(12):2720.

37. Sánchez-Tocino H, Alvarez-Vidal A, Maldonado MJ, Moreno-Montañés J, García-Layana A. Retinal Thickness Study with Optical Coherence Tomography in Patients with Diabetes. Investigative Ophthalmology & Visual Science. 2002 May 1;43(5):1588–94.

38. Kim BY, Smith SD, Kaiser PK. Optical Coherence Tomographic Patterns of Diabetic Macular Edema. American Journal of Ophthalmology. 2006 Sep 1;142(3):405-412.e1.

39. Yee P, Weymouth AE, Fletcher EL, Vingrys AJ. A role for omega-3 polyunsaturated fatty acid supplements in diabetic neuropathy. Invest Ophthalmol Vis Sci. 2010 Mar;51(3):1755–64.

40. Aung MH, Kim MK, Olson DE, Thule PM, Pardue MT. Early Visual Deficits in Streptozotocin-Induced Diabetic Long Evans Rats. Invest Ophthalmol Vis Sci. 2013 Feb;54(2):1370–7.

41. Shoham S, Bejar C, Kovalev E, Weinstock M. Intracerebroventricular injection of streptozotocin causes neurotoxicity to myelin that contributes to spatial memory deficits in rats. Exp Neurol. 2003 Dec;184(2):1043–52.

42. Genrikhs EE, Stelmashook EV, Golyshev SA, Aleksandrova OP, Isaev NK. Streptozotocin causes neurotoxic effect in cultured cerebellar granule neurons. Brain Res Bull. 2017 Apr;130:90–4.

43. Zachary I. Neuroprotective role of vascular endothelial growth factor: signalling mechanisms, biological function, and therapeutic potential. Neurosignals. 2005;14(5):207–21.

44. Froger N, Matonti F, Roubeix C, Forster V, Ivkovic I, Brunel N, et al. VEGF is an autocrine/paracrine neuroprotective factor for injured retinal ganglion neurons. Sci Rep. 2020 Jul 24;10(1):12409.

45. Martínez-Vacas A, Di Pierdomenico J, Gómez-Ramirez AM, Vidal-Sanz M, Villegas-Pérez MP, García-Ayuso D. Dose-Related Side Effects of Intravitreal Injections of Humanized Anti-Vascular Endothelial Growth Factor in Rats: Glial Cell Reactivity and Retinal Ganglion Cell Loss. Investigative Ophthalmology & Visual Science. 2024 Apr 4;65(4):10.

46. Park HYL, Kim JH, Park CK. Neuronal Cell Death in the Inner Retina and the Influence of Vascular Endothelial Growth Factor Inhibition in a Diabetic Rat Model. The American Journal of Pathology. 2014 Jun 1;184(6):1752–62.

47. Hombrebueno JR, Ali IH, Xu H, Chen M. Sustained intraocular VEGF neutralization results in retinal neurodegeneration in the Ins2Akita diabetic mouse. Sci Rep. 2015 Dec 16;5(1):18316.

CHAPTER 4

Prospects and limitations of cumate-inducible lentivirus as a tool for investigating VEGF-A-mediated pathology in diabetic retinopathy

Inesa Lelyte[1,2,3], Vidhya R. Rao[3], Giedrius Kalesnykas[2,4], Symantas Ragauskas[2], Simon Kaja[3,5], and Zubair Ahmed[1,6]

[1]Institute of Inflammation and Ageing, University of Birmingham, Edgbaston, Birmingham, B15 2TT, UK

[2]R&D Division, Experimentica Ltd., 10243 Vilnius, Lithuania

[3]Department of Ophthalmology, Loyola University Chicago, Maywood, IL 60153, USA

[4]R&D Division, Experimentica Ltd., Kuopio, Finland, and Experimentica Inc., Fort Worth, TX, USA

[5]Department of Molecular Pharmacology & Neuroscience, Loyola University Chicago, Maywood, IL 60153, USA

[6]Centre for Trauma Sciences Research, University of Birmingham, Edgbaston, Birmingham, B15 2TT, UK

A version of this manuscript has been published in

Scientific Reports

4.1 Abstract

Diabetic retinopathy (DR) is a multifactorial disease displaying vascular-associated pathologies, including vascular leakage and neovascularization, ultimately leading to visual impairment. However, animal models accurately reflecting these pathologies all in the same model are lacking. Vascular endothelial growth factor A (VEGF-A) is an important factor in the development of micro- and macro-vascular pathology in DR. In this study, we evaluated the feasibility of using cumate-inducible lentivirus (LV) mediated expression of VEGF-A to understand DR pathology *in vitro* and *in vivo*. Retinal pigment epithelial cells (ARPE-19) were transduced with cumate-inducible LV expressing VEGF-A, with subsequent analysis of VEGF-A expression and its impact on cell proliferation, viability, motility, and permeability. Cumate tolerability in adult Wistar rat eyes was assessed as an initial step towards a potential DR animal model development, by administering cumate via intravitreal injections (IVT) and evaluating consequent effects by spectral domain optical coherence tomography (SD-OCT), flash electroretinography (fERG), ophthalmic examination (OE), and immunohistochemistry. Transduction of ARPE-19 cells with cumate-inducible LV resulted in ~2.5-fold increase in *Vegf-a* mRNA and ~3-fold increase in VEGF-A protein secretion. Transduced cells displayed enhanced cell proliferation, viability, permeability, and migration in tube-like structures. However, IVT cumate injections led to apparent retinal toxicity, manifesting as retinal layer abnormalities, hemorrhages, vitreous opacities, and significant reductions in a- and b-wave amplitudes, along with increased microglial activation and reactive gliosis. In summary, while cumate-inducible LV-mediated VEGF-A expression is valuable for *in vitro* mechanistic studies in cellular drug discovery, its use is not a feasible approach to model DR in *in vivo* studies due to cumate-induced retinal toxicity.

4.2 Introduction

Diabetic retinopathy (DR) is the leading cause of preventable blindness in the world and the primary cause of vision loss among working-age adults[1]. DR primarily results in microvascular changes, including pericyte loss[2], increased vascular permeability[3] and formation of acellular capillaries[4]. Prolonged duration of diabetes results in the appearance of microaneurysms and hemorrhages, associated with vascular leakage and neovascularization[5]. In the absence of intervention, diabetic retinopathy (DR) may progress to diabetic macular edema (DME) and proliferative diabetic retinopathy (PDR), ultimately culminating in complete vision loss. Animal models which recapitulate vascular pathophysiology of DR are essential for studying and understanding the underlying molecular mechanisms, as well as developing and testing novel therapies to treat the disease.

Vascular endothelial growth factor-A (VEGF-A) is highly upregulated in DR and induces the progression of various events characterizing the disease, including vascular leakage, neovascularization, and DME.[6] VEGF antagonists are currently in clinical use for treating vascular abnormalities,[6] but such therapies require repeated intraocular injections. To study the role of VEGF-A and develop novel anti-VEGF-A treatments, VEGF-A-induced animal models of DR have been generated. Intravitreal injections of recombinant VEGF-A have been shown to mimic many of the complex DR mechanisms, including vascular leakage and neovascularization in rodents[7] and rabbits[8]. However, VEGF-A-induced effects are transient due to the short half-life of injected peptides. To overcome this drawback, gene transfer models which mediate long-term expression of VEGF-A have been established. For instance, adeno-associated virus (AAV) based VEGF-A mouse model resembled several pathologies characteristic of proliferative DR, including vascular leakage, neovascularization, and vitreous hemorrhage.[9] However, stable expression systems do not offer the ability to temporally control

transgene expression. For this, inducible gene expression systems have been purposed, offering titratable and finely tuned control over gene expression. Furthermore, compared to stable expression systems, they typically demonstrate greater efficiency and cause fewer side effects.[10] Various inducible platforms, such as the rapamycin-inducible system[11] and light-sensitive protein-protein interaction systems,[12] have been developed. However, these systems come with specific limitations, including metabolic disruption in the rapamycin-inducible system,[13] and oxidative stress in light-sensitive systems.[14,15] The tetracycline (Tet)-inducible system,[16] another widely used platform, also faces challenges, such as leaky expression in the absence of an inducer.[17] Recently, cumate-inducible gene expression system have shown promise for regulated gene expression across various cell lines,[18–21] but to our knowledge, it have not been applied in ophthalmic research.

Therefore, the aim of this study was to evaluate the feasibility of using cumate-inducible LV constructs for controlling retinal transgene expression, with the ultimate goal of generating a preclinical model with controllable VEGF-A expression with relevance to DR. For this, our initial step involved the testing of an inducible VEGF-A expression vector within ARPE-19 cells. Subsequently, we aimed to employ this cumate-inducible VEGF-A vector to establish a DR model in adult rats *in vivo*.

4.3 Methods

Cell line and cell culture

Retinal pigment epithelial cells, ARPE-19 (CRL-2302TM, American Tissue Type Collection, ATTC, Manassas, VA, USA), were chosen for this study as they are an established and easy-to-work-with cell line, that was readily available in the laboratory. Although RPE cells are not the primary focus in diabetic retinopathy studies, ARPE-19 cells offered a valuable platform to assess the efficacy of lentiviral vectors to promote VEGF-A expression and demonstrate that

produced VEGF-A is indeed biologically active. ARPE-19 were cultured in a 1:1 mixture of Dulbecco's modified Eagles medium (DMEM) and Ham's F12 medium (F12 medium) (containing 1.2 g/L sodium bicarbonate, 2.5 mM L-glutamine, 15 mM HEPES and 0.5 mM sodium pyruvate) and fetal bovine serum to a final concentration of 10% and cultured at 37 ºC in an atmosphere of 5% CO^2/95% humidity. Cell cultures were supplemented with penicillin/streptomycin to a final concentration of 100 U/ml and were used for experiments between passages 7 to 10.

ARPE-19 were maintained in T75 tissue culture flasks (TPP Techno Plastic Products AG, Trasadingen, Switzerland) and seeded into clear, flat bottom 6, 12, or 96 well plates (TPP®; Midwest Scientific, Fenton, MO, USA) at a density of 6900 cells/well to 200,000 cells/well. For permeability experiments, cells were seeded in transwell inserts (150,000 cells/well; 12 mm Transwell® with 0.4 μm Pore Polyester Membrane Inserts [Corning; Corning, NY, USA]).

ARPE-19 cell transduction with cumate-inducible lentivirus (LV)

ARPE-19 cells were incubated at 37°C with 5% CO_2 overnight so that the cells would be 10 – 30% confluent at the time of infection. TransDuxTM (System Biosciences, Palo Alto, CA, USA) was added to cell medium to a final concentration of 1X, for efficient transduction of cells. Immediately after, ARPE-19 cells were transduced with lentivirus (LV) expressing a SparQTM all-in-one cumate-inducible plasmids (QM800A-$VEGFA_{165A}$, 1.14 x 109 ifus/ml [System Biosciences]) expressing VEGF-A 165 isoform (VEGF-A_{165}) at a multiplicity of infection (MOI) of 0, 10, and 20. Media was changed 72 hours post-transduction and cumate (30 μg/ml [System Biosciences]) was added to induce VEGF-A expression, and cells were incubated for a further 48 hours. MOI 0 condition served as cumate control where no lentivirus was added, only cumate.

RNA isolation and real-time quantitative PCR (RT-qPCR)

Total RNA from transduced ARPE-19 cell lysates were isolated using the commercially available Total RNA Purification Plus Kit (Norgen, Biotek, Ontario, Canada), according to the manufacturer's protocol, and quantified using a NanoDrop spectrophotometer (ThermoFisher Scientific Inc, Wilmington, DE, USA). An equal amount of RNA (92 ng) from each sample was used to synthesize single-stranded complementary DNA (cDNA) via reverse transcription (High-Capacity RNA-to-cDNA Kit, Thermo Fisher Scientific, Waltham, MA, USA). The resulting cDNA was then subjected to real-time quantitative PCR (RT-qPCR) (AriaMx Real-time PCR System; Agilent Technologies, Santa Clara, CA, USA) for VEGF-A (Hs00900055_m1) expression. Human GAPDH (GAPDH, 4326317E) was used as the endogenous control for gene expression normalization. All qPCR probe sets, Taqman Gene Expression Assay kit and Taqman fast advanced Master Mix were acquired from Applied Biosystems (Thermo Fisher Scientific). The assays were conducted in triplicates for each sample. (N = 3/group).

Enzyme-linked immunosorbent assay (ELISA)

Transduced ARPE-19 cell supernatant samples were prepared, and VEGF-A protein levels were determined by an investigator masked to the treatment conditions, using a commercial VEGF-A ELISA kit (R&D Systems, Minneapolis, MN, USA). The assay procedure was performed according to the manufacturer’s instructions, with the modification of a 1:5 dilution of the samples in RD5K diluent. To determine VEGF-A concentrations, a range of standards (31.3, 62.5, 125, 250500, and 1000 pg/ml) were used. Absorbance was measured at 450 nm using a Cytatation 5 microplate reader (BioTek Instruments Inc., Winooski, VT, USA), with subtraction of the absorbance of blank wells at 540 nm as a reference. (N = 4/group).

Scratch assays

The effects of LV-mediated VEGF-A expression on ARPE-19 cell motility were assessed through scratch assays. Cells transduced with LV at MOI 0, 10, and 20 were incubated for 72 hours after a scratch was created using a 10 µl pipette tip. These cells were cultured in a serum-free F12/DMEM medium at 5% CO2/95%, 37°C, in the presence of cumate (30 µg/ml). Images were taken immediately after the wound was made, then at 24, 48, and 72 hours. Initial wound dimensions and wound healing were evaluated using Image J software (v1.46r, National Institute of Health, USA) by an investigator masked to the treatment conditions. (N = 4/group).

MTT assay

ARPE-19 cell viability was evaluated by 3-(4,5-dimethylthiazol-2-yl)-2,5-diphenyltetrazolium bromide (MTT) uptake assay. Conditioned media of LV- VEGF-A-treated cells at MOI 0, 10, and 20 was added to ARPE-19 cells seeded in 96-well plate. In 48 hours, media was aspirated from the cells and replaced with 100 µl of 1.2 mM MTT in Hanks' Balanced Salt solution (HBSS) with calcium and magnesium (Lonza, Walkersville, MD, USA) supplemented with 10 mM 4-(2-Hydroxyethyl) pi-perazine-1-ethanesulfonic acid (HEPES; Sigma Aldrich, St Louis, USA). Plates then were incubated at 37 °C for 2 hours. Media was aspirated, and cells were lysed with 100 µl dimethylsulfoxide (DMSO) and gentle shaken, to lyse the cells. Absorbance was measured at 570 nm using a Cytatation 5 microplate reader (BioTek Instruments Inc.). Absorbance values were corrected for background and normalized to the control condition (MOI 0). (N = 4/group).

Cell permeability

To examine possible changes in ARPE-19 cell permeability, cells were grown to 70-90% confluency in transwell inserts. Cells were then treated with conditioned media of LV- VEGF-A-treated cells at MOI 0, 10, and 20 for 48 h. To assess permeability, the apical to basolateral movement of the low-permeability dye, 6-carboxyfluorescein (6-CF; ThermoFisher Scientific) was quantified, using an excitation 490 nm/emission 520 nm, and a microplate reader (Cytatation 5; BioTek Instruments Inc.). (N = 3/group).

Animal experiments

All animals were approved and monitored by the Animal Welfare Ethical Board of Lithuania (Experimentica UAB animal license number G2-136). Animals were also treated in accordance with the ARVO Statement for the Use of Animals in Ophthalmic and Vision Research and the EC Directive 2010/63/EU for animal experiments. No power calculations were performed to determine group sizes but were based on previous experiments in similar designs. Animals were randomly assigned to treatment groups and experimenters were masked to the treatment conditions. The study was reported in accordance with ARRIVE guidelines.

For cumate tolerability experiments, seven-weeks old male Wistar rats (Janvier Labs, Le Genest-Saint-Isle, France) (weight, 220–250 g) were housed at a constant temperature (22±1°C) in a light-controlled environment (lights on from 7 am to 7 pm) with *ad libitum* access to food and water. For all the procedures, animals were anesthetized with ketamine (45 mg/kg; Ketamidor, Richter Pharma, Wels, Austria) and medetomidine (0.6 mg/kg; Sedator, Eurovet Animal Health, Bladel, Netherlands) mixture. Anesthesia was reversed by the α2-antagonist for medetomidine, atipamezole (2.5 mg/kg; Atipam; Eurovet Animal Health). At the end of the study rats were euthanized by cervical dislocation under non-recovery deep anesthesia, and

eyes were enucleated and prepared for immunohistochemical staining (as described below). (N = 4-12 eyes/group).

Intravitreal injections

Water-soluble cumate solution (10,000 x, System Biosciences) was administered by a single bilateral intravitreal injection (IVT) into both eyes of randomly selected rats. Four distinct doses of cumate were administrated: 0.1 mg/2 µL (6 eyes), 0.2 mg/2 µL (4 eyes), 0.6 mg/2 µL (10 eyes), and 1.5 mg/5 µL (12 eyes). As for control group, 5 µL of saline was administrated. These doses of cumate were selected based on our *in vitro* studies and the prior literature indicating the efficacy of cumate at these doses for binding to the cumate repressor and inducing VEGF-A expression. For dose selection, we took also into account cumate half-life, the dilution of cumate into the rat vitreous and the need for biodistribution from the vitreous into the retina. The injections were carried out on day 0 of the study using a 5 µl glass micro syringe (Hamilton Bonaduz AG, Bonaduz, Switzerland).

Spectral domain optical coherence tomography (SD-OCT)

Cumate tolerability was assessed using spectral domain optical coherence tomography (SD-OCT) imaging obtained with an image-guided OCT system (Envisu R2210, Bioptigen Inc./Leica Microsystems, Mannheim, Germany). SD-OCT scans were conducted prior to the IVT injections (day 0), on day 3, and the final experimental day (day 7). The scanned area covered a 1.8 x 1.8 mm of the retina centered around the optic nerve. Each scan was composed of 100 B-scans, each one composed of 1000 A-scans.

Ophthalmic examination (OE)

Ophthalmic examinations (OE) were performed using slit lamp (SL-9900, C.S.O srl, Scandicci, Italy). Prior to the examinations, a 10 mg/ml tropicamide (Polfa S.A, Warsaw, Poland) solution was administered onto the cornea to dilute pupils. Rats were then placed under the slit lamp, and both eyes were examined, with images captured at both cornea and fundus levels. Ophthalmic examinations were conducted on day 0 before the intravitreal injections of cumate and then on days 3 and 7 post-injection.

Flash electroretinography (fERG)

All flash electroretinography (fERG) measurements were conducted with animals dark-adapted overnight in their home cages, with *ad libitum* access to food and water. Rats were anesthetized as described above and their pupils were dilated using a 10 mg/ml tropicamide solution (Polfa S.A). Oftagel (Santen Oy, Tampere, Finland) at a concentration of 2.5 mg/g was applied to keep the eyes moist during recording. Recordings were performed on both eyes under complete darkness. An AC/DC differential amplifier (Model 3000; A-M Systems, Sequim, WA, USA), analogue filters set to bandpass of 0.1 Hz to 1 kHz, and a data acquisition interface (C.E.D., Power140, Cambridge, UK) were used for the recordings. Light flash stimuli (3ms in duration) of five different intensities were used, in ascending order: -3.6; -2.6; -0.6; 0.4 and 0.6 [log (cd.s.m-2)], with an interstimulus interval of 5s for the two lowest intensities and 10s for the rest. The response to each intensity were recorded for ten consecutive times, averaged, and further used to manually identify the amplitudes (μV) for both a- and b-waves. fERG measurements were performed prior IVT injections (day 0) and at the termination of the study (day 7).

Eye cup cross-sections

Whole eyes were enucleated and fixed in 4% paraformaldehyde (PFA) for an over-night period at 4°C. Following fixation, the tissues underwent a 15-minute wash in 1x Tris-Buffered Saline (TBS) at room temperature, and eye cups were then carefully prepared. To prevent the formation of ice crystals, the tissues were further rinsed in a series of sucrose solutions at concentrations of 10%, 20%, and 30%. Eye cups then were placed in optimal cutting temperature (O.C.T.) compound (SAK4583, Sakura, Torrance, CA, USA), frozen, and sectioned at 7 μm thickness. Hematoxylin and eosin (H&E) staining was performed on these sections, and images were captured using an upright microscope (DM6 B, Leica Microsystems).

Immunohistochemistry of retinal flat-mounts

The eyes were enucleated and fixed in 4% PFA solution for 30 minutes at room temperature. Subsequently, retinas were dissected using fine forceps and four radial incisions were made to flatten the retina. The flattened retinas were then fixed in 4% PFA overnight at 4°C. After fixation, the tissues were washed in 1x TBS for a duration of 5-6 hours at 4°C and subjected to blocking with a solution containing 10% goat serum and 0.5% Triton in 1x TBS. After blocking retinal flat-mounts were washed with washing solution (1% goat serum + 0.1% Triton in 1x TBS) and incubated with following primary antibodies: rabbit anti-Iba-1 (dilution 1:200, cat. no. 019-19741, Thermo Fisher Scientific), and mouse anti-glial fibrillary acidic protein (GFAP) (1:1000, G3893, Sigma Aldrich) overnight at 4°C. On the next day the tissues were washed with washing solution and incubated with secondary antibodies: anti rabbit Alexa Fluor (AF) 594 (1:500, A32740, Invitrogen) and anti-mouse AF488 (1:500, A21121, Invitrogen). Flat-mounts were washed again with washing solution and counter-stained with DAPI (1:10 000, 6843.1, Carl Roth), washed and mounted with Fluoroshield (F6937-20ML, Sigma Aldrich).

Slides were imaged using an upright microscope (DM6 B, Leica Microsystems). For Iba-1 analysis twelve images were taken from each retinal flat-mount at 12 different locations (4 in periphery, 4 in middle and 4 in the central part). Iba-1-positive cells with hypertrophic cell bodies and retracted processes were identified as activated microglia, while Iba-1-positive cells with small cell bodies and extended processes were classified as silent microglia. Both Iba-1 active and silent cells were manually counted for each image, using Image J software (v1.46r, National Institute of Health, USA). GFAP-positive cells were qualitatively assessed by visual inspection of stained flat-mount images.

Data analysis

Statistical analysis was performed using GraphPad Prism (version 10.0.2, GraphPad Software, La Jolla, CA, USA). Data were analyzed using one-way or two-way ANOVA followed by Dunnett's or Šídák's multiple comparisons tests and presented as mean ± standard error of mean (SEM). Significance was determined according to the p value: * $p < 0.05$, ** $p < 0.01$, *** $p < 0.001$, and **** $p < 0.0001$.

4.4 Results

Increased VEGF-A Expression in ARPE-19 Cells

Lentivirus transduced ARPE-19 cell lysates were collected, and *Vegf-a* mRNA expression was assessed using qPCR. The results demonstrated a substantial increase in *Vegf-a* mRNA levels, with approximately a 2.5-fold elevation in cells infected with LV at MOI 10 ($p < 0.01$) and nearly a 3-fold increase at MOI 20 ($p < 0.01$) when compared to MOI 0 (Fig. 1a). Additionally, the concentration of secreted VEGF-A in cell supernatants was quantified via ELISA. Elevated levels of secreted VEGF-A were detected in cells transduced with lentivirus at MOI 10 (1,896.60 ± 104.6 pg/ml) compared to MOI 0 (1,165.57 ± 192 pg/ml). Notably, a higher

multiplicity of infection (MOI 20) resulted in a significant increase in VEGF-A protein secretion levels in ARPE-19 cells (2,005.60 ± 270.6 pg/ml, $p < 0.05$) compared to non-transduced cells (1,165.57 ± 192 pg/ml) (Fig. 1b).

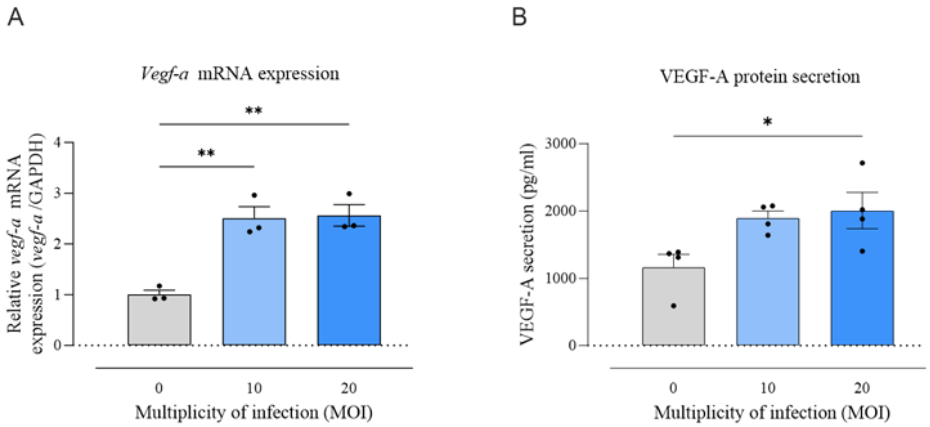

Figure 1. Vegf-a mRNA expression and VEGF-A protein secretion levels in ARPE-19 cells transduced with lentivirus at MOI 0, 10, and 20 and treated with cumate (30 µg/ml) for 48 hours. (**a**) qPCR showed an increase of *Vegf-a* mRNA expression in cells infected with LV at MOI 10 and 20 (** $p < 0.01$ and ** $p < 0.01$, respectively) compared with MOI 0. (N = 3/group). (**b**) Significantly increased VEGF-A protein secretion levels were detected by ELISA in cell supernatants transduced with lentivirus (LV) at MOI 20 (* $p < 0.05$) compared to MOI 0. (N = 4/group). Statistical analysis was performed using one-way ANOVA followed by Dunnett's multiple comparisons test. Data are presented as mean ± SEM.

Effects of Lentivirus-mediated Expression of VEGF-A on ARPE-19 Cells

Further, we wanted to evaluate the effects of lentivirus-mediated expression of VEGF-A on ARPE-19 cells. The introduction of VEGF-A through lentivirus resulted in notable enhancements in the proliferation, motility, viability, and permeability of ARPE-19 cells. For cell proliferation assessment, ARPE-19 cells were initially seeded in 12-well plates at a density

of 3,000 cells per well, followed by transduction with LV and treatment with cumate (30 µg/ml) for 48 hours. Consequently, a significant increase in the number of cells following lentivirus transduction was found at both MOI 10 (959,750 ± 200.004, $p < 0.05$) and MOI 20 (1,086,750 ± 101.268, $p < 0.01$) in comparison to MOI 0 (321,000 ± 51,828) (Fig. 2a). Furthermore, impact of VEGF-A expression on ARPE-19 cell motility was assessed through scratch assays. A substantial reduction in scratch-wound size, indicating enhanced cell migration, was evident in cells transduced with LV at MOI 10 (40.64 ± 4.22%, $p < 0.001$) and MOI 20 (33.84 ± 6.83%, $p < 0.001$) 48 hours after creating the scratch, in comparison to MOI 0 (67.67 ± 1.6%) (Fig. 2b). In addition, we observed the formation of tube-like structures by ARPE-19 cells (indicated by arrows, Fig. 2c).

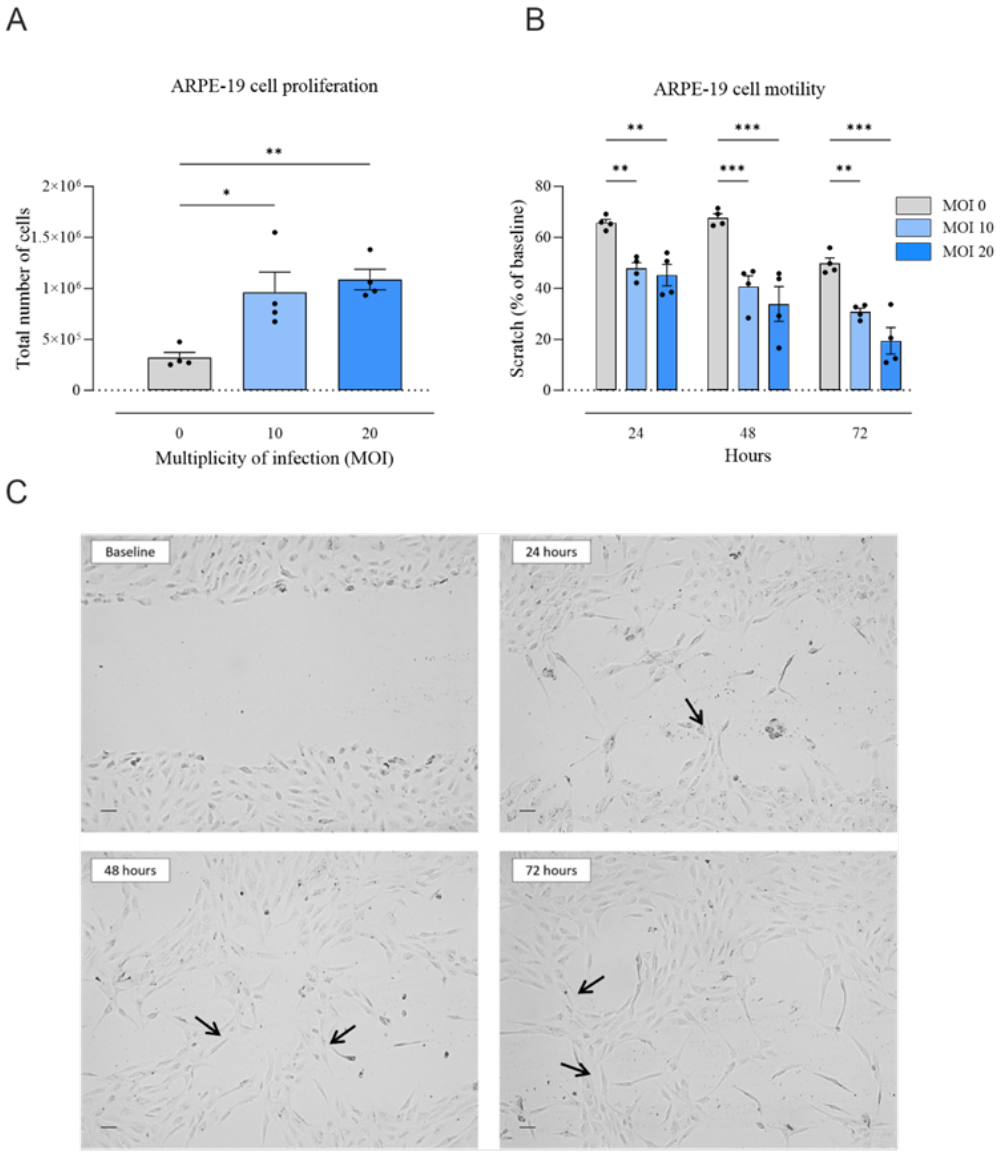

Figure 2. Effects of LV-mediated VEGF-A expression on ARPE-19 cell proliferation and motility. (**a**) There was a significant increase in total number of ARPE-19 cells when transduced with LV at MOI 10 and 20 (* $p < 0.05$ and ** $p < 0.01$, respectively) compared with MOI 0 (n = 4/group). (**b**) There was a significant decrease in wounds suggesting an increase in cell motility when transduced with LV at MOI 10 and 20 at 24 hours (** $p < 0.01$ and ** $p < 0.01$, respectively), 48 hours (*** $p < 0.001$ and *** $p < 0.001$, respectively) and 72 hours (** $p < 0.01$ and *** $p < 0.001$, respectively) compared with MOI 0. Statistical analysis was done by one-way and two-way ANOVA followed by Dunnett's multiple comparisons test. Data are

presented as mean ± SEM (n = 4). (**c**) Representative images of ARPE-19 cells infected with LV at MOI 20. The images were taken immediately after the scratches had been made (baseline) and then after 24 hours, 48 hours and 72 hours. Scratch assays showed increased motility of LV infected cells, as well as these cells forming tube-like structures, indicated by arrows. Scale bar = 100 µm.

To assess changes in cell viability, MTT assay was performed on ARPE-19 cells that were at a 70-90% confluence. Conditioned media from cells previously transduced with lentivirus and treated with cumate (30 µg/ml) for 48 hours were added. After 48 hours of exposure to conditioned media, the MTT assay showed significantly increased number of viable cells with conditioned media of LV at MOI 20 (115,73 ± 5.21 %, $p < 0.05$), compared with MOI 0 (100 ± 1,55 %) (Fig. 3a). Moreover, permeability significantly increased in cells treated with conditioned media of LV at MOI 10 ($p < 0.05$) and MOI 20 ($p < 0.05$) compared to MOI 0 (apparent permeability coefficients Papp, 10(-5) cm s-1 for RhoB were 2,08 ± 0.16, 1,80 ± 0.40, and 0,66 ± 0.07, respectively) (Fig. 3b). Our *in vitro* data are consistent with the anticipated effects of VEGF-A overexpression in ARPE-19 cells.

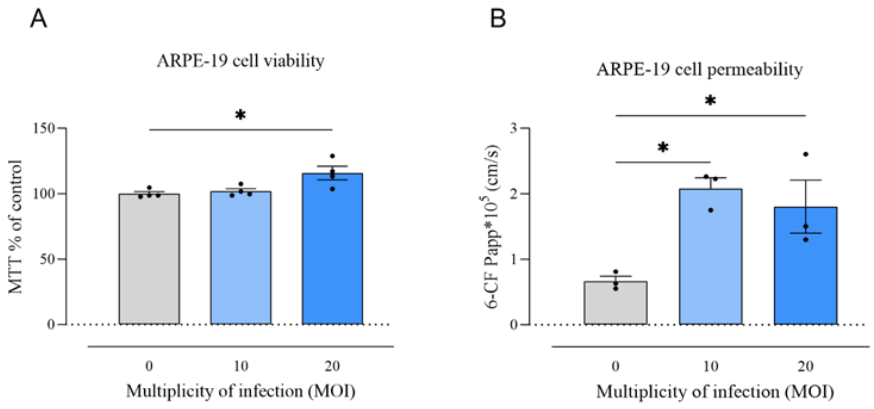

Figure 3. ARPE-19 cell viability and permeability after treatment with conditioned media of LV at MOI 10 and 20. (**a**) MTT assay showed significantly increased number of viable cells

treated with conditioned media of LV at MOI 20 (* $p < 0.05$) compared with MOI 0 (n = 4/group). (**b**) Cell permeability significantly increased in cells treated with conditioned media of LV at MOI 10 and 20 (* $p < 0.05$ and * $p < 0.05$, respectively) compared with MOI 0 (n = 3/group). Statistical analysis was performed using one-way ANOVA followed by Dunnett's multiple comparisons test. Data are presented as mean ± SEM.

Toxic Effect of Cumate IVT Injections on Retina of Wistar Rats

Our next objective was to assess the feasibility of utilizing cumate-inducible lentiviral (LV) constructs to establish inducible gene expression in an *in vivo* setting. Given the lack of *in vivo* data on cumate, we conducted an evaluation to determine cumate's tolerability introduced via intravitreal injections. Following IVT injection of cumate (administered at doses 1 mg/2 µL, 0.2 mg/2 µL, 0.6 mg/2 µL, or 1.5 mg/5 µL), the rat eyes exhibited immediate cloudiness, indicating adverse reactions to cumate. SD-OCT scans revealed noticeable changes in the retinal layers (indicated by arrows in Fig. 4), as well as the accumulation of fluid within retinal layers and retinal hemorrhage (indicated by arrowheads in Fig. 4). Additionally, in majority of SD-OCT scans from rats receiving the highest dose of cu-mate (1.5 mg/5 µL), the observations were obscured due to cumate-induced vitreous opacities that cast shadows on the retina (bottom row of Fig. 4).

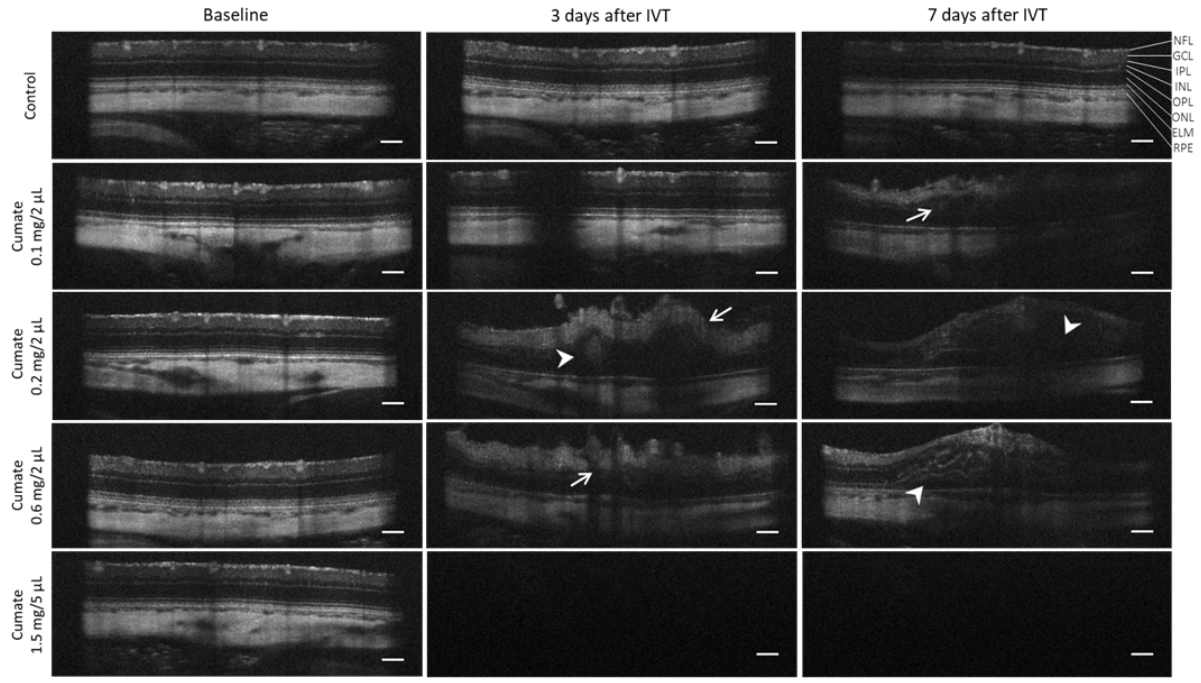

Figure 4. IVT injection of cumate induced retinal degeneration in rat eyes. Cumate (administered at doses of 0.1 mg/2 µL; 0.2 mg/2 µL; 0.6 mg/2 µL, and 1.5 mg/5 µL) resulted in pathological retinal layering (arrows), accumulation of fluid or retinal hemorrhages (arrowheads) within retinal layers, and the presence of vitreous opacities (bottom row) which completely prevented SD-OCT imaging on day 3 and day 7 post-IVT injection. NFL = nerve fiber layer; GCL = ganglion cell layer; IPL = inner plexiform layer; INL = inner nuclear layer; OPL = outer plexiform layer; ONL = outer nuclear layer; ELM = external limiting membrane; RPE = retinal pigmented epithelium. Scale bar = 200 µm.

Further, ophthalmic examinations revealed vascular abnormalities in rat eyes, both 3- and 7-days post-administration of cumate (at doses 0.1 mg/2 µL; 0.2 mg/2 µL; 0.6 mg/2 µL, or 1.5 mg/5 µL). Intravitreal injections of cumate induced distinct alterations in retinal blood vessels, characterized by either vessel enlargement or constriction (highlighted by white arrows in Figure 5). The fundus images provided further evidence of retinal hemorrhages, which were consistent with observations in SD-OCT scans 3- and 7-days after cumate administration

(indicated by arrowheads in Fig. 5). Additionally, ophthalmic examinations identified vitreous opacities, likely caused by the presence of cumate suspended within the vitreous (denoted by black arrows in Fig. 5).

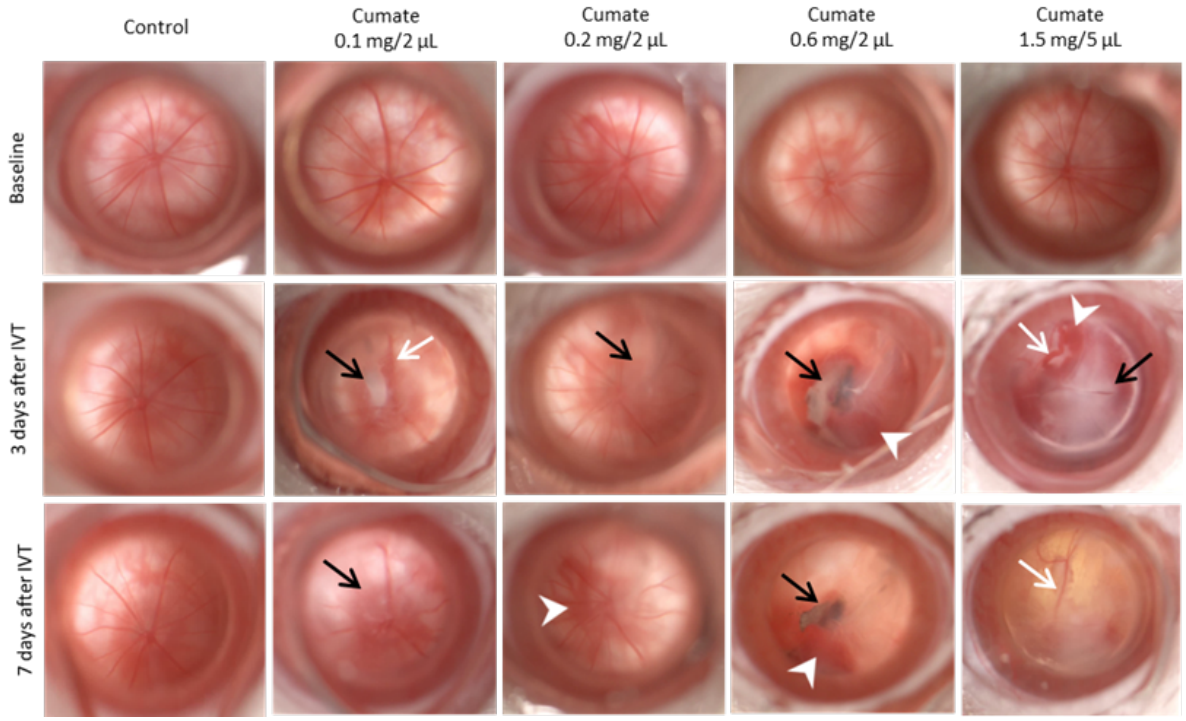

Figure 5. Administration of cumate (at doses 0.1 mg/2 µL; 0.2 mg/2 µL; 0.6 mg/2 µL, and 1.5 mg/5 µL) resulted in vascular pathologies in rat eyes. Enlarged or constricted blood vessels were noticed during fundus observations (white arrows) 3- and 7-days post-IVT-administration. Retinal hemorrhages were detected 3 days post-IVT which persisted until Day 7 (white arrowheads). Vitreous opacities were observed at 3 days and at 7 days after cumate administration (black arrows).

Flash electroretinography (fERG) was performed to determine the impact of cumate IVT injections on rat retinal function. Seven days after cumate administration (0.6 mg/2 µL), a-wave amplitude decreased by 22%, and b-wave amplitude by 39% (0.6 [log (cd.s.m-2)] stimulus intensity, $p < 0.05$ and $p < 0.001$, respectively; Fig. 6). Higher cumate concentrations (1.5 mg/5

µL) resulted in a more substantial reduction, with a 94% decline in a-wave amplitude and a 95% decrease in b-wave amplitude by day 7 (0.6 [log (cd.s.m-2)] stimulus intensity, $p < 0.001$ and $p < 0.001$, respectively; Fig. 6). However, it is important to note that these a- and b-wave amplitude decreases might be due to cumate-induced toxicity to the retina, vitreous opacities, or a combination of both factors (all fERG a-wave and b-wave absolute values can be found in Supplemental Table S1).

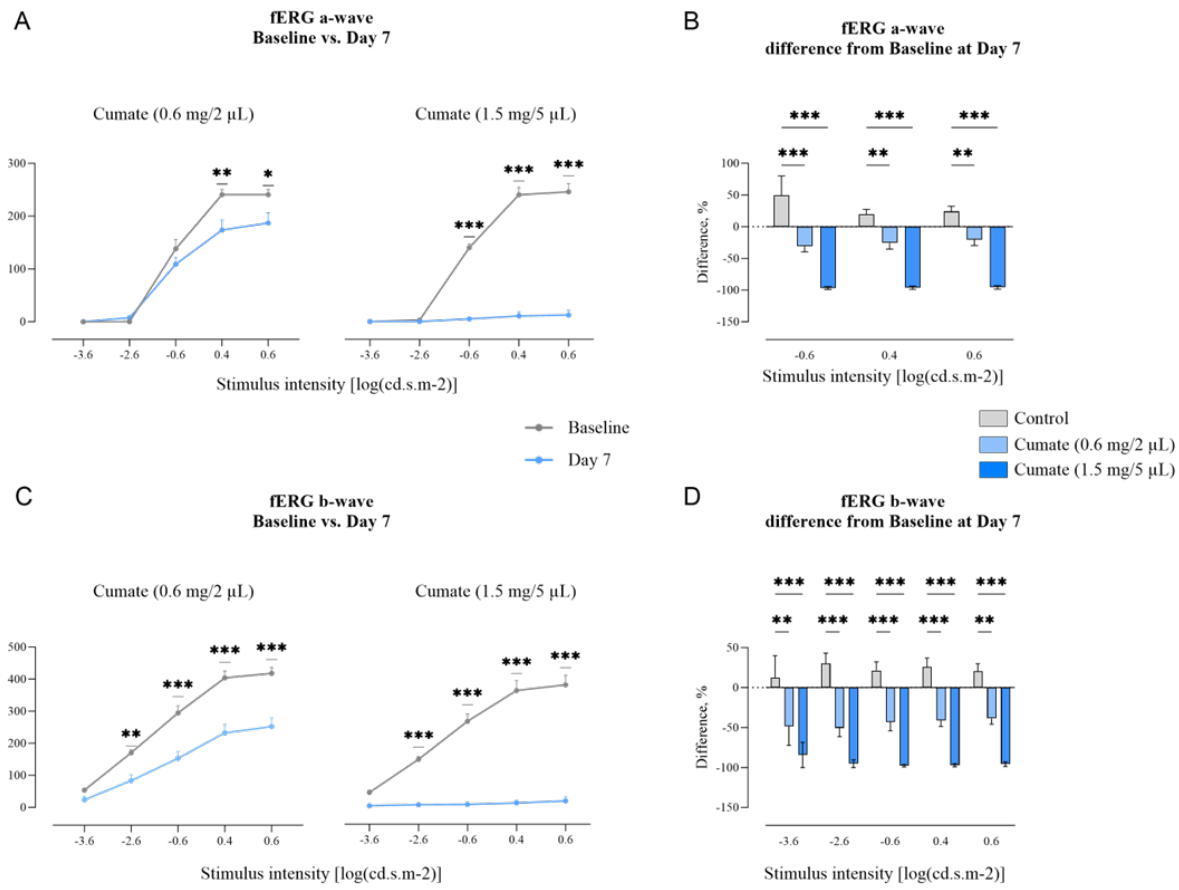

Figure 6. Cumate IVT injections (at doses 0.6 mg/2 µL and 1.5 mg/5 µL) led to decreased retinal activity. Retinal function analyzed by fERG at stimulus intensities -3.6, -2.6, -0.6, 0.4, 0.6 [log (cd.s.m-2)]. (**a**) a-wave amplitudes at baseline and day 7, and (**a**) difference from baseline at day 7 in different treatment groups. (**c**) b-wave amplitudes at baseline and day 7, and (**d**) difference from baseline at day 7 in different treatment groups. Statistical analysis was

done by two-way ANOVA followed by Šídák's or Dunnett's multiple comparisons test * $p < 0.05$, ** $p < 0.01$, *** $p < 0.001$. Data are presented as mean ± SEM, n = 8-12 eyes/group.

Next, retinas exposed to cumate were immunostained with Iba-1 and GFAP antibodies to assess the activation of microglia and the presence of reactive gliosis, respectively. Seven days after IVT injection of cumate (0.6 mg/2 µL or 1.5 mg/5 µL), retinas were largely disorganized, and $GFAP^+$ astrocytes were significantly increased across the full retina (top panel in Fig. 7a). Moreover, significantly increased number of total Iba-1-labeled cells were detected within the retinal tissue following IVT injection of cumate at doses of 0.6 mg/2 µL (944 ± 106 cells/mm², $p < 0.05$) and 1.5 mg/5 µL (1397 ± 123 cells/mm², $p < 0.001$) in comparison to control rat retinas (379 ± 33 cells/mm², Fig. 7b),), suggesting microglial activation. In-depth analysis of cellular morphology revealed that the majority of Iba-1-immunoreactive cells had hypertrophic cell bodies and nearly complete disappearance of cellular processes, indicating microglial activation (Figure 7 c). Notably, an increased number of activated Iba-1+ microglia was found in the highest dose of cumate group (1.5 mg/5 µL) (807 ± 118 cells/mm^2 compared to 47 ± 11 cells/mm^2 in control group, $p < 0.001$). Additionally, cumate (at a dose of 1.5 mg/5 µL) resulted in markedly reduced active Iba-1 to silent Iba-1 ratio (1: 0.7) in comparison to control rats (1: 7), indicating that higher proportion of Iba-1^+ cells were in an active state than silent (Fig. 7d).

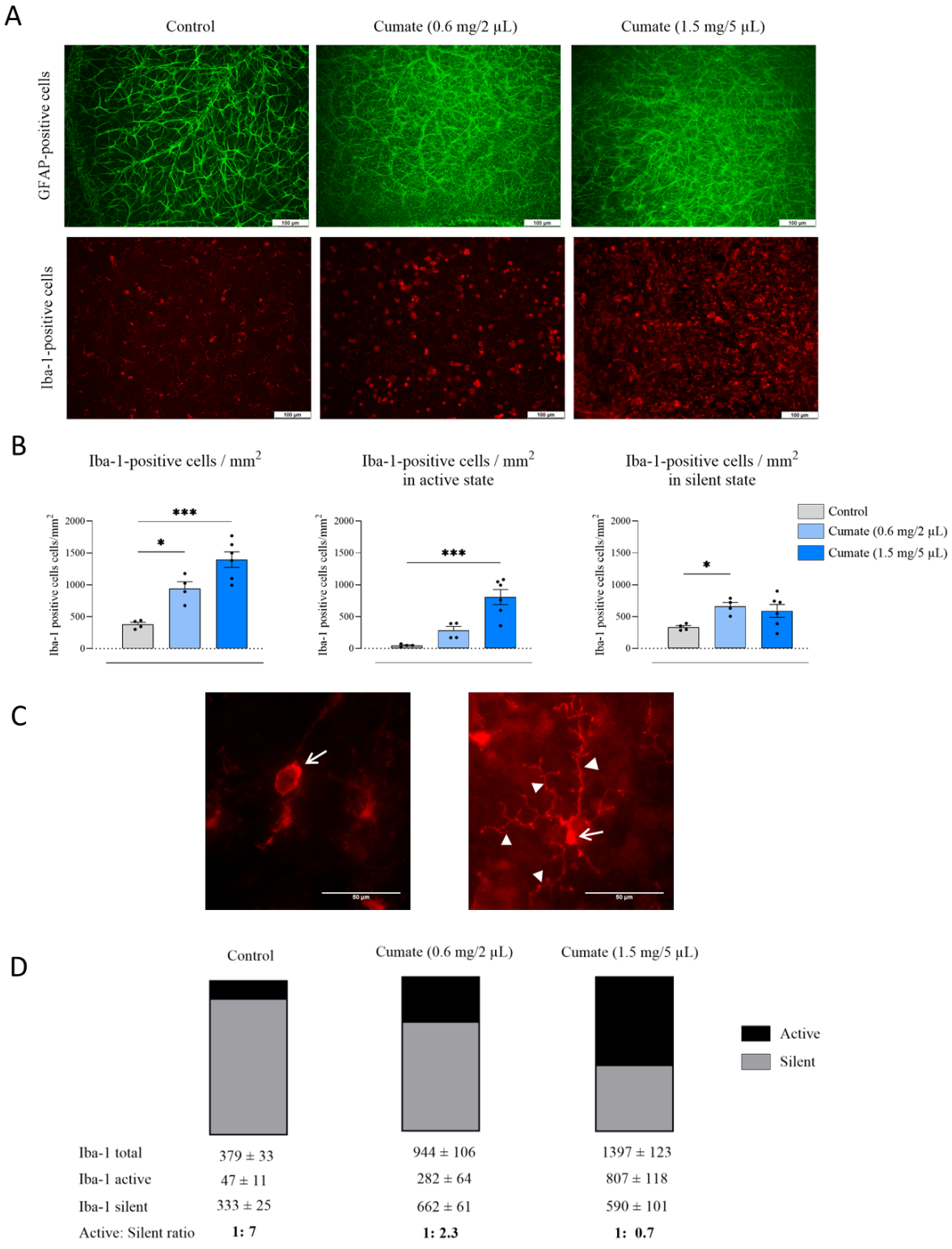

Figure 7. Assessment of immune cell activation in cumate-injected (0.6 mg/2 µL or 1.5 mg/5 µL) eyes. (**a**) Representative images of retinal flat-mounts from cumate-treated eyes stained for GFAP and Iba-1. (**b**) The count of Iba-1^{+} cell numbers per 1 mm^{2}. Significant increases in total,

active and silent Iba-1$^+$ cell numbers were observed in eyes treated with cumate (one-way ANOVA followed by Dunnet's multiple comparisons test * $p < 0.05$, *** $p < 0.001$). (**c**) Representative images of activated Iba-1 cells with hypertrophic cell body (arrow) and retracted cellular processes, and silent microglia with small cellular body (arrow) and long cellular processes (arrowheads). (**d**) Ratio between silent and active Iba-1$^+$ cells across all treatment groups. Data are presented as mean ± SEM, n = 4-6 eyes/group.

To verify cumate-induced toxicity histologically, eye cup cross-sections of injected eyes were evaluated (Fig. 8). Hematoxylin and eosin (H&E) staining revealed normal architecture of the retina in control eye (Fig. 8a) whilst distinct indications of retinal degeneration were evident at seven days after IVT injection (Fig. 8b). Notably, retinal hemorrhages (indicated by black arrows in Fig. 8b), as well as anomalous morphology of various retinal layers (e.g., ganglion cell layer (GCL), inner plexiform layer (IPL), and outer nuclear layers (ONL), Fig. 8b) were evident in the cumate-injected eyes. These findings were in alignment with our prior observations from SD-OCT scans and ophthalmic examinations. Collectively, all four administered doses of cumate (0.1 mg/2 µL, 0.2 mg/2 µL, 0.6 mg/2 µL, and 1.5 mg/5 µL) were associated with varying degrees of retinal degeneration when compared to the control group that received a 5 µL of saline injection.

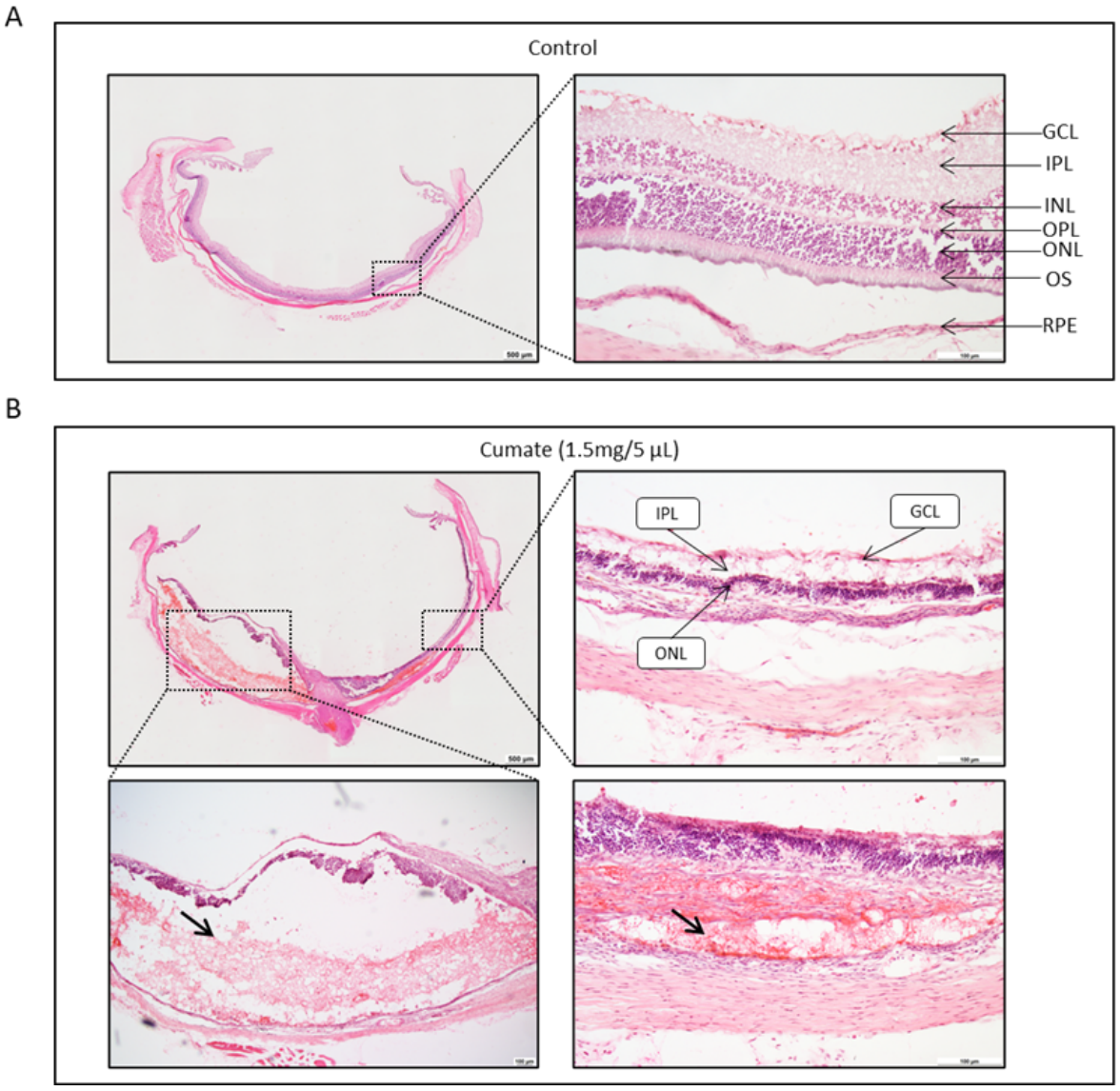

Figure 8. Hematoxylin and eosin (H&E) staining of eye cup cross-sections of (**a**) control and (**b**) cumate (1.5 mg/5 µL)-injected eyes. Retinal hemorrhages (black arrows), irregular retinal layers and retinal degeneration (e.g., IPL, ONL, and GCL) were observed seven days after cumate administration. Scale bars: 100 µm and 500 µm. GCL = ganglion cell layer; IPL = inner plexiform layer; INL = inner nuclear layer; OPL = outer plexiform layer; ONL = outer nuclear layer; OS = outer segments of photoreceptor cells; RPE = retinal pigmented epithelium.

4.5 Discussion

The aim of our study was to evaluate the feasibility of using cumate-inducible LV constructs for controlling retinal transgene expression, with the ultimate goal to generate a DR preclinical model with controllable VEGF-A expression. Transduction of ARPE-19 cells with cumate-inducible LV led to elevated *Vegf-a* mRNA and VEGF-A protein secretion levels. Transduced cells displayed enhanced cell proliferation, viability, permeability, and migration in tube-like structures. However, IVT cumate injections led to evident retinal toxicity, manifesting as retinal layer abnormalities, hemorrhages, vitreous opacities, and significant reductions in a- and b-wave amplitudes, along with increased microglial activation and reactive gliosis.

The primary advantage of inducible gene expression systems over non-inducible constructs lies in their ability to offer titratable and finely tuned control over gene expression. For instance, protein-protein interaction-based chimeric systems like the rapamycin-inducible system, offer tunable and temporal control of gene expression.[11] However, rapamycin or its analogs inhibit mammalian target of rapamycin complex 1 (mTORC1), which is essential for regulating cellular metabolism and growth, consequently disrupting metabolic status of cells.[13] Another inducible system, based on light sensitive protein-protein interactions, allows rapid on and off cycle and provides spatial regulation through selective illumination.[12] Nevertheless, prolonged exposure to blue light has been shown to induce oxidative stress in cells.[14,15] A widely used tetracycline (Tet)-inducible expression system, which, like the cumate-inducible system, offers controlled gene expression, easiness of their handling, and high efficiency.[16] In Ohno-Matsui et al. study,[22] transgenic mice with reverse tetracycline transactivator (rtTA) inducible promoter system promoting *Vegf* transgene expression, showed evidence of severe proliferative retinopathy along with retinal detachment. Yet, the Tet system poses specific challenges such as leaky expression in the absence of the inducer[17] or the loss of inducibility in

some cell lines.[23] Studies demonstrate that cumate-inducible gene expression vectors have been successfully used for regulated gene expression in mammalian,[18] human embryonic kidney,[24] and other cell lines.[20,21,19] However, to our knowledge, cumate-inducible gene expression vectors have not yet been used for ophthalmic discoveries in *in vivo* systems. Therefore, this study aimed to explore the potential of the cumate-inducible system for controlled VEGF-A expression, with the ultimate goal of generating a preclinical DR.

Our initial experimental step involved the transduction of ARPE-19 cells with cumate-inducible LV expressing VEGF-A at varying multiplicity of infection (MOI) levels, including MOI 0, 10, and 20. We chose ARPE-19 cells for this study for several reasons. First, ARPE-19 cells are an established and easy-to-work-with cell line, that was readily available in the laboratory. Second, ARPE-19 cells offered a valuable platform to assess the efficacy of lentiviral vectors to promote VEGF-A expression and demonstrate that produced VEGF-A is indeed biologically active. Finally, while most of DR research focuses on the breakdown of the inner blood-retina barrier (BRB),[25] studies have demonstrated that the outer BRB is compromised during DR as well.[26,27] The outer BRB is formed by tight junctions between retinal pigment epithelial cells, and both morphological and functional abnormalities of RPE have been reported in diabetic animals.[28–31] While RPE secreted VEGF-A is well recognized for promoting choroidal neovascularization in age-related macular degeneration (AMD),[32,33] disrupting VEGF signalling in the mouse RPE significantly reduced diabetes-induced vascular leakage and inflammation, suggesting that VEGF expressed by RPE may play an important role in diabetic retinopathy as well.[27]

In our study, qPCR showed an increase of *Vegf-a* mRNA expression within cells infected with LV at MOI 10 and 20, compared to MOI 0. Furthermore, significantly increased VEGF-A protein secretion levels into the cell supernatant were detected by ELISA upon transduction

with LV at MOI 20 as compared to MOI 0. These results demonstrate that the cumate-inducible system effectively induces VEGF-A expression in ARPE-19 cells. Additionally, we aimed to demonstrate that the produced VEGF-A is biologically active in ARPE-19 cells. VEGF-A is recognized for stimulating excessive proliferation of RPE cells,[34,35] similarly in our study transduced ARPE-19 cells showed heightened proliferation. Furthermore, our MTT assay indicated a substantial increase in ARPE-19 viable cells when exposed to conditioned media from lentivirus transduced at MOI 20, supporting the literature that VEGF-A enhances RPE survival.[36,37] These observation aligns with previous studies where VEGF-A expression driven by bidirectional tetracycline-inducible system was shown to promote cancer cell survival and proliferation[38] Similarly, VEGF expression regulated by an erythropoietin enhancer under hypoxic conditions has been demonstrated to enhance endothelial cell proliferation.[39] Moreover, prior research has indicated that the activation of VEGF receptors located on the apical surface of RPE cells are responsible for the VEGF-induced elevation in cell permeability. [40] Our study findings corroborate these observations, as we found a significant increase in permeability among ARPE-19 cells transduced with conditioned media of LV at both MOI 10 and MOI 20. In terms of cell motility, our scratch-wound assays revealed a notable reduction in scratch-wound size, indicating increased migratory capacity of ARPE-19 cells upon induction, supporting the literature that VEGF-A enhances RPE motility.[41] Interestingly, in our study we observed LV-transduced ARPE-19 cells forming tube-like structures, similarly to endothelial cells in angiogenesis studies,[42,43] however further research involving tube formation assay would be necessary to confirm this observation.

However, a key limitation of this study is the absence of both a negative control and a no-treatment group. The inclusion of a negative control, where a cumate-inducible lentiviral vector with a non-functional sequence is used instead of the *Vegf-a* gene would help ensure that any

observed effects are specifically due to VEGF-A expression and not attributable to the vector or the transduction process itself. Additionally, including a no-treatment group would provide a baseline comparison for assessing the natural behaviour of ARPE-19 cells without inducible system or cumate treatment.

Additionally, it is important to mention that while GAPDH is one of the most commonly used reference genes,[44,45] its expression can be influenced by experimental conditions, leading to inaccurate results. GAPDH gene is directly involved in cellular metabolism,[46] therefore its expression may be modulated in response to changes in metabolic pathways induced by VEGF-A expression. To ensure reliable normalization, it is important to experimentally validate GAPDH specifically in ARPE-19 cells under VEGF-A expression conditions. Moreover, incorporating additional reference genes would provide greater accuracy of normalization.[47] For instance, the use reference genes like HPRT1, GUSB and PPIA has been found to be the most suitable reference genes for ARPE-19 cells gene expression experiments subjected to diabetic conditions.[48]

Taken together, while increased proliferation, permeability, and motility of ARPE-19 cells is not directly relevant to the clinical manifestation of diabetic retinopathy, our findings demonstrate that VEGF-A expression is induced, and the produced VEGF-A is indeed biologically active. Additionally, the use of this cumate-inducible system on ARPE-19 cells highlights its potential for studying other ocular pathologies, such as age related macular degeneration, where VEGF-A expression in RPE cells is known to drive choroidal neovascularization.[32,33] Notably, one of cumate-inducible system advantages is that gene expression can be reversed by removing cumate, allowing for repeated inductions. Consequently, further research would be needed to evaluate the effectiveness of this system for

multiple inductions. Additionally, generation of stably expressing cell line could offer potential applications for VEGF-related *in vitro* studies.

Our data demonstrated that cumate-inducible lentivirus is a flexible tool to study the function of VEGF-A *in vitro*. Consequently, next, we aimed to evaluate cumate-inducible LV *in vivo*. In this system, inducible *Vegf-a* gene expression is induced through the binding of cumate to the cumate repressor (CymR), with expression levels of VEGF-A being tightly regulated by cumate concentration. Therefore, this *in vivo* study focused on assessing the tolerability of intravitreally injected cumate in Wistar rat eyes. Unfortunately, cumate administration was not well tolerated, resulting in significant retinal toxicity, including abnormalities in retinal layers, hemorrhages, vitreous opacities, and reductions in a- and b-wave amplitudes. Additionally, cumate administration led to microglial activation and increased reactive gliosis.

In contrast, our *in vitro* studies did not show any cellular toxicity, as LV-transduced APRE-19 cells remained proliferative and viable. Similarly, other *in vitro* studies,[18,20,24] using cumate-inducible gene expression vectors either reported no cell toxicity or did not address it. Park et al.[21] observed that cumate-GFP transduced quail (QM7) cells exhibited cellular toxicity, whereas chicken (DF1) cells remained viable in the presence of cumate. Interestingly, recent work has elegantly demonstrated that oral administration of cumate is safe and feasible.[49] Nevertheless, it remains unclear whether cumate can effectively cross the retinal-blood barrier and/or blood-brain barrier, which is crucial for delivering cumate to the eye and brain.

Given the observed toxicity of cumate following intravitreal injection in this study, our future research may investigate the pharmacokinetic properties of cumate in ocular sub-tissues and evaluate the feasibility of using lower concentrations to initiate VEGF-A expression. Lower concentrations may offer insights into the optimal dosage for achieving VEGF-A expression

while minimizing potential adverse effects. However, it is likely that this approach may require multiple low-dose intravitreal injections to achieve relevant tissue levels of cumate to initiate transgene expression.

In summary, our study demonstrates that the cumate-inducible VEGF-A expression system offers a valuable tool for investigating the effects of VEGF-A on ARPE-19 cells. However, the observed retinal damage induced by cumate in rat eyes precludes its use via intravitreal injections. This limitation prevents us from developing an easy-to-use inducible DR rat model and from gaining insights into the pathology of diabetic retinopathy using a cumate-inducible lentivirus expressing *vegf-a*.

4.6 Acknowledgments

This work was funded, in part, by the European Union's Horizon 2020 Research and Innovation Programme under the Mari Sklodowska-Curie Actions (grant agreement – No 813440). Additional funding from the Dr. John P. and Therese E. Mulcahy Endowed Professorship in Ophthalmology (to SK) and the Richard A. Perritt M.D. Charitable Foundation (to SK) is gratefully acknowledged.

4.7 Contributions

The project was conceptualized by I.L, Z.A., S.K., and G.K. ARPE-19 cell transduction with LV, RNA isolation and qPCR, ELISA, Scratch assays, MTT assays, and cell permeability experiments were performed by I.L with support from V.R.R.. Intravitreal injections were performed by S.R. SD-OCT, OE, and fERG were performed by I.L, with support from S.R. and other members of the Experimentica team (not included in the author list). Histology and immunohistochemistry analysis were performed by I.L with support from members of the Experimentica team (not included in the author list). Data analysis was performed by I.L.

Original draft was written by I.L. Work was reviewed, edited, and supervised by G.K., Z.A., and S.K.

4.8 Ethics Declarations

Competing interests

Employment: G.K., S.R. and I.L. (Experimentica Ltd.); Stock/equity ownership: G.K. (Experimentica Ltd.) and S.K. (K&P Scientific LLC). S.K. conducts academic research in areas of interest like the business interests of K&P Scientific LLC. The terms of this arrangement have been reviewed and approved by Loyola University Chicago in accordance with its conflict-of-interest policy. The funders had no role in the study. Z.A. and V.R.R. declare no conflicts of interest.

4.9 Supplementary Information

Supplementary Table S1. fERG a-wave and b-wave amplitude absolute values, difference and Šídák's multiple comparisons test results of all treatment groups at stimulus intensities -3.6, -2.6, -0.6, 0.4, 0.6 [*log* (cd.s.m-2)] (baseline *vs.* day 7). Data are presented as mean ± SEM.

a-wave amplitude, µV					
Stimulus intensity	-3.6	-2.6	-0.6	0.4	0.6
Control					
Baseline			123.97 ± 14.32	231.95 ± 12.31	233.55 ± 14.62
Day 7			157.2 ± 7.69	270.73 ± 7.52	282.29 ± 10.78

Difference, µV			33.23	38.78	48.74
Difference %			26.80	16.72	20.87
Summary			ns	*	**
p value			0.07	**<0.05**	**<0.01**
Cumate 0.6 mg/2 µL					
Baseline			138.31 ± 16.79	240.56 ± 9.49	240.75 ± 9.68
Day 7			108.91 ± 12.51	173.8 ± 18.94	187.19 ± 18.85
Difference, µV			-29.4	-66.76	-53.56
Difference %			-21.26	-27.75	-22.25
Summary			ns	**	*
p value			0.48	**<0.01**	**<0.05**
Cumate 1.5 mg/5 µL					
Baseline			139.07 ± 6.88	238.45 ± 13.56	244.12 ± 15.41
Day 7			5.04 ± 3.62	10.76 ± 7.31	12.4 ± 8.45
Difference, µV			-134.03	-227.69	-231.72
Difference %			-96.38	-95.49	-94.92
Summary			***	***	***

p value			**<0.001**	**<0.001**	**<0.001**
b-wave amplitude, µV					
Stimulus intensity	**-3.6**	**-2.6**	**-0.6**	**0.4**	**0.6**
Control					
Baseline	56.91 ± 3.81	157.16 ± 13.9	291.01 ± 24.32	398.25 ± 30.19	433.7 ± 27.17
Day 7	61.41 ± 11.79	195.96 ± 13.69	340.83 ± 24.41	483.33 ± 29.81	508.56 ± 24.62
Difference, µV	4.5	38.8	49.82	85.08	74.86
Difference %	7.91	24.69	17.12	21.36	17.26
Summary	ns	ns	ns	*	ns
p value	>0.99	0.62	0.35	**<0.05**	0.06
Cumate 0.6 mg/2 µL					
Baseline	53.95 ± 6.04	170.66 ± 8.91	294.53 ± 21.89	404 ± 21.27	418.38 ± 17.88
Day 7	24.01 ± 9.95	83.64 ± 17.71	153.08 ± 20.83	232.72 ± 26	252.02 ± 26.41
Difference, µV	-29.94	-87.02	-141.45	-171.28	-166.36
Difference %	-55.50	-50.99	-48.03	-42.40	-39.76
Summary	ns	**	***	***	***
p value	0.78	**<0.01**	**<0.001**	**<0.001**	**<0.001**

Cumate 1.5 mg/5 µL					
Baseline	54.57 ± 9.71	181.03 ± 10.8	325.63 ± 27.47	443.16 ± 37.16	464.7 ± 35.8
Day 7	4.38 ± 4.38	7.86 ± 7.86	9.06 ± 6.33	14.51 ± 9.82	22.69 ± 15.36
Difference, µV	-50.19	-173.17	-316.57	-428.65	-442.01
Difference %	-91.97	-95.66	-97.22	-96.73	-95.12
Summary	ns	***	***	***	***
p value	0.26	**<0.001**	**<0.001**	**<0.001**	**<0.001**

4.10 References

1. Yau, J.W.Y., Rogers, S.L., Kawasaki, R., Lamoureux, E.L., Kowalski, J.W., Bek, T., Chen, S.-J., Dekker, J.M., Fletcher, A., Grauslund, J., et al. (2012). Global Prevalence and Major Risk Factors of Diabetic Retinopathy. Diabetes Care *35*, 556–564. https://doi.org/10.2337/dc11-1909.

2. Beltramo, E., and Porta, M. (2013). Pericyte Loss in Diabetic Retinopathy: Mechanisms and Consequences. CMC *20*, 3218–3225. https://doi.org/10.2174/09298673113209990022.

3. Antonetti, D.A., VanGuilder, H.D., and Mao-Lin, C. (2008). Vascular Permeability in Diabetic Retinopathy. In Diabetic Retinopathy Contemporary Diabetes., E. J. Duh, ed. (Humana Press), pp. 333–352. https://doi.org/10.1007/978-1-59745-563-3_14.

4. Hammes, H.-P., Feng, Y., Pfister, F., and Brownlee, M. (2011). Diabetic Retinopathy: Targeting Vasoregression. Diabetes *60*, 9–16. https://doi.org/10.2337/db10-0454.

5. Shin, E.S., Sorenson, C.M., and Sheibani, N. (2014). Diabetes and Retinal Vascular Dysfunction. J Ophthalmic Vis Res *9*, 362–373. https://doi.org/10.4103/2008-322X.143378.

6. Gupta, N., Mansoor, S., Sharma, A., Sapkal, A., Sheth, J., Falatoonzadeh, P., Kuppermann, B., and Kenney, M. (2013). Diabetic Retinopathy and VEGF. Open Ophthalmol J *7*, 4–10. https://doi.org/10.2174/1874364101307010004.

7. Clermont, A.C., Murugesan, N., and Aiello, L.P. (2020). Vascular endothelial growth factor (VEGF) induces retinal edema and neuroretinal dysfunction in diabetic rats. Investigative Ophthalmology & Visual Science *61*, 1385.

8. Edelman, J.L., Lutz, D., and Castro, M.R. (2005). Corticosteroids inhibit VEGF-induced vascular leakage in a rabbit model of blood–retinal and blood–aqueous barrier breakdown. Experimental Eye Research *80*, 249–258. https://doi.org/10.1016/j.exer.2004.09.013.

9. Weigelt, C.M., Fuchs, H., Schönberger, T., Stierstorfer, B., Strobel, B., Lamla, T., Ciossek, T., Bakker, R.A., and Redemann, N.H. (2021). AAV-Mediated Expression of Human VEGF, TNF-α, and IL-6 Induces Retinal Pathology in Mice. Transl Vis Sci Technol *10*, 15. https://doi.org/10.1167/tvst.10.11.15.

10. Kallunki, T., Barisic, M., Jäättelä, M., and Liu, B. (2019). How to Choose the Right Inducible Gene Expression System for Mammalian Studies? Cells *8*, 796. https://doi.org/10.3390/cells8080796.

11. Rivera, V.M., Clackson, T., Natesan, S., Pollock, R., Amara, J.F., Keenan, T., Magari, S.R., Phillips, T., Courage, N.L., Cerasoli, F., et al. (1996). A humanized system for pharmacologic control of gene expression. Nat Med *2*, 1028–1032. https://doi.org/10.1038/nm0996-1028.

12. Yamada, M., Suzuki, Y., Nagasaki, S.C., Okuno, H., and Imayoshi, I. (2018). Light Control of the Tet Gene Expression System in Mammalian Cells. Cell Rep *25*, 487-500.e6. https://doi.org/10.1016/j.celrep.2018.09.026.

13. Abu-Remaileh, M., Wyant, G.A., Kim, C., Laqtom, N.N., Abbasi, M., Chan, S.H., Freinkman, E., and Sabatini, D.M. (2017). Lysosomal metabolomics reveals V-ATPase- and mTOR-dependent regulation of amino acid efflux from lysosomes. Science *358*, 807–813. https://doi.org/10.1126/science.aan6298.

14. Nakashima, Y., Ohta, S., and Wolf, A.M. (2017). Blue light-induced oxidative stress in live skin. Free Radic Biol Med *108*, 300–310. https://doi.org/10.1016/j.freeradbiomed.2017.03.010.

15. Lee, J.-B., Kim, S.-H., Lee, S.-C., Kim, H.-G., Ahn, H.-G., Li, Z., and Yoon, K.C. (2014). Blue light-induced oxidative stress in human corneal epithelial cells: protective effects of ethanol extracts of various medicinal plant mixtures. Invest Ophthalmol Vis Sci *55*, 4119–4127. https://doi.org/10.1167/iovs.13-13441.

16. Gossen, M., and Bujard, H. (1992). Tight control of gene expression in mammalian cells by tetracycline-responsive promoters. Proc Natl Acad Sci U S A *89*, 5547–5551. https://doi.org/10.1073/pnas.89.12.5547.

17. Costello, A., Lao, N.T., Gallagher, C., Capella Roca, B., Julius, L.A.N., Suda, S., Ducrée, J., King, D., Wagner, R., Barron, N., et al. (2019). Leaky Expression of the TET-On System Hinders Control of Endogenous miRNA Abundance. Biotechnol. J. *14*, 1800219. https://doi.org/10.1002/biot.201800219.

18. Mullick, A., Xu, Y., Warren, R., Koutroumanis, M., Guilbault, C., Broussau, S., Malenfant, F., Bourget, L., Lamoureux, L., Lo, R., et al. (2006). The cumate gene-switch: a system for regulated expression in mammalian cells. BMC Biotechnology *6*, 43. https://doi.org/10.1186/1472-6750-6-43.

19. Poulain, A., Perret, S., Malenfant, F., Mullick, A., Massie, B., and Durocher, Y. (2017). Rapid protein production from stable CHO cell pools using plasmid vector and the cumate gene-switch. Journal of Biotechnology *255*, 16–27. https://doi.org/10.1016/j.jbiotec.2017.06.009.

20. Choi, J.S., Kim, K., Lee, D.H., Cho, S., Ha, J.D., Park, B.C., Kim, S., Park, S.G., and Kim, J.-H. (2016). cIAPs promote the proteasomal degradation of mutant SOD1 linked to familial amyotrophic lateral sclerosis. Biochemical and Biophysical Research Communications *480*, 422–428. https://doi.org/10.1016/j.bbrc.2016.10.065.

21. Park, T.S., Kim, S.W., and Lee, J.H. (2017). Efficient transgene expression system using a cumate-inducible promoter and Cre-loxP recombination in avian cells. Asian-Australas J Anim Sci *30*, 886–892. https://doi.org/10.5713/ajas.16.0698.

22. Ohno-Matsui, K., Hirose, A., Yamamoto, S., Saikia, J., Okamoto, N., Gehlbach, P., Duh, E.J., Hackett, S., Chang, M., Bok, D., et al. (2002). Inducible Expression of Vascular Endothelial Growth Factor in Adult Mice Causes Severe Proliferative Retinopathy and Retinal Detachment. Am J Pathol *160*, 711–719.

23. Ackland-Berglund, C.E., and Leib, D.A. (1995). Efficacy of tetracycline-controlled gene expression is influenced by cell type. Biotechniques *18*, 196–200.

24. Qi, Z., Wilkinson, M.N., Chen, X., Sankararaman, S., Mayhew, D., and Mitra, R.D. (2017). An optimized, broadly applicable piggyBac transposon induction system. Nucleic Acids Res *45*, e55. https://doi.org/10.1093/nar/gkw1290.

25. Rudraraju, M., Narayanan, S.P., and Somanath, P.R. (2020). Regulation of blood-retinal barrier cell-junctions in diabetic retinopathy. Pharmacol Res *161*, 105115. https://doi.org/10.1016/j.phrs.2020.105115.

26. Xu, H.-Z., and Le, Y.-Z. (2011). Significance of Outer Blood–Retina Barrier Breakdown in Diabetes and Ischemia. Invest Ophthalmol Vis Sci *52*, 2160–2164. https://doi.org/10.1167/iovs.10-6518.

27. Xu, H.-Z., Song, Z., Fu, S., Zhu, M., and Le, Y.-Z. (2011). RPE barrier breakdown in diabetic retinopathy: seeing is believing. J Ocul Biol Dis Infor *4*, 83–92. https://doi.org/10.1007/s12177-011-9068-4.

28. Aizu, Y., Oyanagi, K., Hu, J., and Nakagawa, H. (2002). Degeneration of retinal neuronal processes and pigment epithelium in the early stage of the streptozotocin-diabetic rats. Neuropathology *22*, 161–170. https://doi.org/10.1046/j.1440-1789.2002.00439.x.

29. Aizu, Y., Katayama, H., Takahama, S., Hu, J., Nakagawa, H., and Oyanagi, K. (2003). Topical instillation of ciliary neurotrophic factor inhibits retinal degeneration in streptozotocin-induced diabetic rats. Neuroreport *14*, 2067–2071. https://doi.org/10.1097/00001756-200311140-00012.

30. Pautler, E.L., and Ennis, S.R. (1980). The effect of induced diabetes on the electroretinogram components of the pigmented rat. Invest Ophthalmol Vis Sci *19*, 702–705.

31. Rimmer, T., and Linsenmeier, R.A. (1993). Resistance of diabetic rat electroretinogram to hypoxemia. Invest Ophthalmol Vis Sci *34*, 3246–3252.

32. Wang, H., Han, X., Wittchen, E.S., and Hartnett, M.E. (2016). TNF-α mediates choroidal neovascularization by upregulating VEGF expression in RPE through ROS-dependent β-catenin activation. Mol Vis *22*, 116–128.

33. Spilsbury, K., Garrett, K.L., Shen, W.Y., Constable, I.J., and Rakoczy, P.E. (2000). Overexpression of vascular endothelial growth factor (VEGF) in the retinal pigment epithelium

leads to the development of choroidal neovascularization. Am J Pathol *157*, 135–144. https://doi.org/10.1016/S0002-9440(10)64525-7.

34. Kehler, A.K., Andersen, C., Andreasen, J.R., Vohra, R., Junker, N., Poulsen, K.A., and Kolko, M. (2012). Interaction between VEGF and calcium-independent phospholipase A2 in proliferation and migration of retinal pigment epithelium. Curr Eye Res *37*, 500–507. https://doi.org/10.3109/02713683.2012.663855.

35. Tsujinaka, H., Itaya-Hironaka, A., Yamauchi, A., Sakuramoto-Tsuchida, S., Ota, H., Takeda, M., Fujimura, T., Takasawa, S., and Ogata, N. (2015). Human retinal pigment epithelial cell proliferation by the combined stimulation of hydroquinone and advanced glycation end-products via up-regulation of *VEGF* gene. Biochemistry and Biophysics Reports *2*, 123–131. https://doi.org/10.1016/j.bbrep.2015.05.005.

36. Ford, K.M., Saint-Geniez, M., Walshe, T., Zahr, A., and D'Amore, P.A. (2011). Expression and Role of VEGF in the Adult Retinal Pigment Epithelium. Invest Ophthalmol Vis Sci *52*, 9478–9487. https://doi.org/10.1167/iovs.11-8353.

37. Byeon, S.H., Lee, S.C., Choi, S.H., Lee, H.-K., Lee, J.H., Chu, Y.K., and Kwon, O.W. (2010). Vascular endothelial growth factor as an autocrine survival factor for retinal pigment epithelial cells under oxidative stress via the VEGF-R2/PI3K/Akt. Invest Ophthalmol Vis Sci *51*, 1190–1197. https://doi.org/10.1167/iovs.09-4144.

38. Liang, L., Yue, Z., Du, W., Li, Y., Tao, H., Wang, D., Wang, R., Huang, Z., He, N., Xie, X., et al. (2017). Molecular Imaging of Inducible VEGF Expression and Tumor Progression in a Breast Cancer Model. Cell Physiol Biochem *42*, 407–415. https://doi.org/10.1159/000477485.

39. Lee, M., Rentz, J., Bikram, M., Han, S., Bull, D.A., and Kim, S.W. (2003). Hypoxia-inducible VEGF gene delivery to ischemic myocardium using water-soluble lipopolymer. Gene Ther *10*, 1535–1542. https://doi.org/10.1038/sj.gt.3302034.

40. Ablonczy, Z., and Crosson, C.E. (2007). VEGF Modulation of Retinal Pigment Epithelium Resistance. Exp Eye Res *85*, 762–771. https://doi.org/10.1016/j.exer.2007.08.010.

41. Hollborn, M., Stathopoulos, C., Steffen, A., Wiedemann, P., Kohen, L., and Bringmann, A. (2007). Positive Feedback Regulation between MMP-9 and VEGF in Human RPE Cells. Investigative Ophthalmology & Visual Science *48*, 4360–4367. https://doi.org/10.1167/iovs.06-1234.

42. Yadav, U.C., Srivastava, S., and Ramana, K. (2012). Prevention of VEGF-induced growth and tube formation in human retinal endothelial cell by aldose reductase inhibition. J Diabetes Complications *26*, 369–377. https://doi.org/10.1016/j.jdiacomp.2012.04.017.

43. Jin, J., Yuan, F., Shen, M., Feng, Y., and He, Q. (2013). Vascular endothelial growth factor regulates primate choroid-retinal endothelial cell proliferation and tube formation through PI3K/Akt and MEK/ERK dependent signaling. Mol Cell Biochem *381*, 267–272. https://doi.org/10.1007/s11010-013-1710-y.

44. Kozera, B., and Rapacz, M. (2013). Reference genes in real-time PCR. J Appl Genet *54*, 391–406. https://doi.org/10.1007/s13353-013-0173-x.

45. González-Bermúdez, L., Anglada, T., Genescà, A., Martín, M., and Terradas, M. (2019). Identification of reference genes for RT-qPCR data normalisation in aging studies. Sci Rep *9*, 13970. https://doi.org/10.1038/s41598-019-50035-0.

46. Seidler, N.W. (2013). GAPDH and intermediary metabolism. Adv Exp Med Biol *985*, 37–59. https://doi.org/10.1007/978-94-007-4716-6_2.

47. Bustin, S.A., Benes, V., Garson, J.A., Hellemans, J., Huggett, J., Kubista, M., Mueller, R., Nolan, T., Pfaffl, M.W., Shipley, G.L., et al. (2009). The MIQE Guidelines: Minimum Information for Publication of Quantitative Real-Time PCR Experiments. Clinical Chemistry *55*, 611–622. https://doi.org/10.1373/clinchem.2008.112797.

48. Liu, X., Xie, J., Liu, Z., Gong, Q., Tian, R., and Su, G. (2016). Identification and validation of reference genes for quantitative RT-PCR analysis of retinal pigment epithelium cells under hypoxia and/or hyperglycemia. Gene *580*, 41–46. https://doi.org/10.1016/j.gene.2016.01.001.

49. Azad, T., Rezaei, R., Singaravelu, R., Pelin, A., Boulton, S., Petryk, J., Onsu, K.A., Martin, N.T., Hoskin, V., Ghahremani, M., et al. (2023). Synthetic virology approaches to improve the safety and efficacy of oncolytic virus therapies. Nat Commun *14*, 3035. https://doi.org/10.1038/s41467-023-38651-x.

CHAPTER 5

AAV-Mediated Human VEGF Expression as a Novel Rat Model of Diabetic Retinopathy

Inesa Lelyte[1,2], Symantas Ragauskas[2], Tomas Paulauskas[2], Dovile Litvinaviciute[2], Zubair Ahmed[1,3], Simon Kaja[4], and Giedrius Kalesnykas[2,5]

[1]Institute of Inflammation and Ageing, University of Birmingham, Edgbaston, Birmingham, B15 2TT, UK

[2]R&D Division, Experimentica Ltd., 10243 Vilnius, Lithuania

[3]Centre for Trauma Sciences Research, University of Birmingham, Edgbaston, Birmingham, B15 2TT, UK

[4]Department of Molecular Pharmacology & Neuroscience, Loyola University Chicago, Maywood, IL 60153, USA

[5]R&D Division, Experimentica Ltd., Kuopio, Finland, and Experimentica Inc., Fort Worth, TX, USA

Manuscript in preparation

5.1 Abstract

Purpose. Diabetic retinopathy (DR) is a complex condition displaying diverse vascular-associated complications, including upregulation of vascular endothelial growth factor (VEGF)-A165, vascular leakage, and neovascularization. However, current VEGF-induced animal models fall short in replicating vascular-pathologies, underscoring the necessity for improved models that can sustain VEGF-A expression and provide insight into the disease's progression and potential treatments. Therefore, we evaluated the efficacy of adeno-associated virus (AAV)-mediated long-term expression of VEGF-A to establish angiogenic DR-related phenotypes in Brown Norway rats and then assessed the effect of aflibercept (Eylea®) as therapeutic intervention, aiming at determining the translational potential of this novel rat DR model.

Methods. Adult Brown Norway rats received a single unilateral intravitreal (IVT) injection of Müller-glia specific AAV vector encoding human *Vegf-a*. The progression of retinal pathology was monitored weekly via spectral-domain optical coherence tomography (SD-OCT) and fluorescein angiography (FA) for six weeks post-injection. At weeks three and six, retinal leakage was quantitatively assessed by vitreous fluorophotometry (VFP), and visual function was evaluated using flash electroretinography (fERG) at six weeks post-injection. IVT injections of aflibercept (Eylea®) were performed at weeks 2 and 3, to attenuate AAV-induced retinal pathology. Ocular tissues were collected, and a novel artificial intelligence (AI) framework was applied for autonomous quantification of retinal angiogenesis in Isolectin B4-stained retinal flat-mounts. Additionally, assessment of microglial activation and reactive gliosis, as well as identification of endothelial cells was performed.

Results. Intravitreal injection of AAV-hVEGF resulted in successful human *Vegf-a* mRNA expression within 2 to 6 weeks in rat retinas. AAV-mediated VEGF-A expression resulted in DR-like vascular pathology, appearing as vascular tortuosity, dilatation, or constriction of retinal vessels, microaneurysms, increased retinal angiogenesis and progressive vascular leakage commencing at week 2. Additionally, AAV-hVEGF injection led to increased retinal thickness — suggestive of retinal edema, accompanied by reduced retinal activity and heightened immune cell reactivity. Moreover, implementation of AI analysis delivered reliable quantitative assessments of retinal angiogenesis in AAV-hVEGF-injected eyes: increases in vascular area and total vessel length, higher number of branch points were found 6 weeks post-injection as compared to non-injected contralateral eyes. These effects were ameliorated by the administration of aflibercept (Eylea®), confirming the translational applicability of this novel rat DR model.

Conclusions. AAV-mediated expression of human VEGF-A in rat retinas, coupled with the observed therapeutic effects of aflibercept (Eylea®), demonstrates an easy-to-use model that recapitulates several aspects of DR pathology and serves as an attractive approach to gain valuable insights into the underlying molecular mechanisms of VEGF-mediated pathologies and for testing novel anti-angiogenic therapies.

5.2 Introduction

Diabetic retinopathy (DR) constitutes a significant global health burden, being a leading cause of vision impairment and blindness among the working-age adult population.[1] The pathogenesis of DR begins as non-proliferative diabetic retinopathy (NPDR), characterized by microaneurysms, retinal hemorrhages, and increased vascular permeability.[2] Without therapeutic intervention, NPDR can progress to diabetic macular edema (DME), and proliferative diabetic retinopathy (PDR), distinguished by neovascularization and vitreous hemorrhages, essentially critically compromising the structural and functional integrity of the retina.[3]

Upregulation of vascular endothelial growth factor (VEGF)-A_{165} is one of the key events in DR, which leads to vascular-associated pathologies, including neovascularization and vascular leakage.[4,5] Therapeutic anti-VEGF-A interventions have demonstrated the efficacy in reducing retinal alterations and improving vision in patients with DR.[6,7] However, patient response variability and the need for frequent injections encourages the ongoing investigation of novel anti-VEGF-A therapies. Therefore, there is an urgent need for VEGF-A-induced animal model development, as they provide a platform to study the underlying molecular mechanisms of VEGF-mediated pathologies and to test therapeutic alternatives. Intravitreal injections (IVT) of recombinant VEGF-A result in retinal vascular abnormalities, but does not replicate DR-like retinal neovascularization[8–10], or the effects of administered proteins are transient.[11] Similarly, intraocular implantation of VEGF-A-releasing pellets fail to stimulate retinal neovascularization in primates, and vascular responses to released VEGF-A in rabbits are temporary.[12] To overcome these limitations, transgenic mouse models that express VEGF-A within the retina have been generated, which develop DR phenotypes, including vascular leakage,[13,14] retinal neovascularisation,[13–15] and retinal detachment.[14,15] Nevertheless, these

models may be surpassed by viral vector-mediated expression of VEGF-A, which can offer enhanced control over gene expression levels and location, as well as it being applied across a wider range of species.

Adeno-associated virus (AAV) vectors are well-known for their long-term transgene expression and low pathogenicity.[16] AAV vectors have been engineered to target and transduce specific cell types, by using different capsid serotypes. For example, the ShH10 variant of AAV selectively targets Müller glial cells within the rodent retina.[17] When delivered via subretinal injection, AAV vectors encoding human *Vegf-a* induces choroidal neovascularization (CNV) in rats,[18,19] confirming its effectiveness and safety *in vivo*. In contrast, IVT injection of AAV-VEGF in nonhuman primates is associated with retinal neovascularization, however, the occurrence of iris neovascularization in this study limited the ability to conduct detailed *in vivo* investigations (such as FA or OCT).[20] In a recent study by Weigelt et al.[21], AAV-mediated expression of human VEGF-A in the murine retina resulted in retinal leakage and neovascularization — an approach that has shaped the framework of our current study. Nevertheless, their analysis was limited to retinal function assessment and did not include evaluation of anti-VEGF-A interventions. Therefore, our study extends beyond these limitations by investigating long-term expression of intravitreally injected AAV vectors encoding *Vegf-a* in Brown Norway rats and including the assessment of aflibercept (Eylea®) as a therapeutic intervention, aiming to determine the translational potential of this novel DR rat model.

5.3 Materials and Methods

Animal Experiments

All animal experiments were approved and monitored by the Animal Welfare Ethical Review Board of Lithuania (Experimentica UAB animal license number G2-216) and performed in accordance with the ARVO Statement for the Use of Animals in Ophthalmic and Vision Research and the EC Directive 2010/63/EU. No power calculations were performed to determine group sizes, but the numbers of animals used were based on previous experiments in similar designs. Animals were randomly assigned to treatment groups and experimenters were masked to the treatment conditions. Seven-week-old male Brown Norway rats (weighing 150–170 g) were purchased from Charles River (Sulzfeld, Germany) and housed at a constant temperature (22±1°C) in a light-controlled environment (lights on from 7 am to 7 pm) with *ad libitum* access to food and water. For all surgical procedures, animals were anesthetized with ketamine (45 mg/kg; Ketamidor, Richter Pharma, Wels, Austria) and medetomidine (0.6 mg/kg; Sedator, Eurovet Animal Health, Bladel, Netherlands) mixture. Anesthesia was reversed by the α2-antagonist for medetomidine, atipamezole (2.5 mg/kg; Atipam, Eurovet Animal Health). At the end of the experiment (week 6), rats were euthanized by cervical dislocation under a non-recovery deep anesthesia and eyes were enucleated. The retinas were either snap-frozen in liquid nitrogen for gene expression analysis, or whole eyes and retinal flat-mounts were fixed in 4% paraformaldehyde (PFA) and prepared for immunohistochemical staining. (N = 6-19 eyes/group).

Adeno-associated Virus (AAV)

Plasmids encoding human DNA sequences of VEGF-A_{165} (AAV/ShH10-CAG-hVEGF165.V5, hereafter referred to as “AAV-hVEGF”) were custom-designed by Vector Biolabs (Malvern,

PA, USA). These plasmids were engineered to be regulated by a CAG promoter, with the addition of a V5-tag at the C-terminus of each protein. AAVs were packaged into the AAV viral capsid variant - ShH10, which is well-known for its predominant transduction of Müller glia.[17] Müller glia cells span the whole retina and make contact with nearly all retinal cell types; therefore, we anticipated that the secreted VEGF-A would be distributed throughout the entire retina. As for negative controls, AAV/ShH10-CAG-Stuffer construct (hereafter referred to as "AAV-stuffer") was employed, representing a non-coding DNA packaged within the same viral capsid.

Intravitreal Injection (IVT)

In the pilot dose-depend10/17/24 12:10:00 PMent study, we evaluated the effects of low (1×10^{10} viral genomes (vg)/eye)) and high (5×10^{10} vg/eye) doses of AAV-hVEGF. Following the study results, we arrived at the conclusion to proceed with a high dose, as it demonstrated the most robust induction of DR-related phenotypes. Intravitreal (IVT) injections were performed under ketamine/medetomidine anesthesia as previously outlined, wherein 5×10^{10} vg/eye of AAV-hVEGF were unilaterally administered into the right eye (OD) of randomly selected rats. AAV-stuffer, used as negative control, was diluted in filtered 1 × phosphate-buffered saline (PBS) and injected at the same dosage of 5×10^{10} vg/eye. The injections of AAVs were delivered at a volume of 5 µl using a 5 µl glass microsyringe (Hamilton Bonaduz AG, Bonaduz, Switzerland) on day 0 of the study. Subsequently, at week 2 and week 3 following imaging, a unilateral IVT injection of aflibercept (Eylea®) (Bayer AG, Leverkusen, Germany) was administered at a dose of 200 µg per eye (a dosage based on previous preclinical models for angiogenesis[21]). In the case of the aflibercept vehicle group, a solution consisting of 100 mM Sodium phosphate, 400 mM sodium chloride, 50% sucrose, and Polysorbate 20, with a pH of

6.2, was prepared and used. Injections, both of aflibercept and the vehicle, were delivered at a volume of 5 µl using a 5 µl glass microsyringe (Hamilton Bonaduz AG).

In Vivo Imaging

AAV-hVEGF-mediated retinal changes in rat eyes were assessed using fluorescein angiography (FA) and spectral-domain optical coherence tomography (SD-OCT). After anesthesia (described above) pupils were dilated with 10 mg/ml tropicamide solution (Alcon-Couvreur, Bornem, Belgium), and the optic nerve head was aligned at the retina level using an infrared reflectance camera. Then a 10% sodium fluorescein solution (Sigma-Aldrich, Steinheim, Germany) was administered as a subcutaneous injection (50 µl/100 g), and images were taken at retinal and choroidal focus levels 5 minutes after injection, using a Spectralis HRA/OCT device (Heidelberg Engineering, Heidelberg, Germany). Following FA, SD-OCT imaging was conducted using the Bioptigen Envisu R2210 device (Leica Microsystems, Mannheim, Germany). The scanned area encompassed a 1.8 x 1.8 mm region of the retina, centered around the optic nerve. Each scan consisted of 100 B-scans, each of which was composed of 1000 A-scans. Inner retinal, outer nuclear layer, and total retinal thickness were measured at 25 different points, with the center point aligned with the optic nerve head, using InVivoVue Diver software (Bioptigen, Morrisville, NC, USA).

Vitreous Fluorophotometry (VFP)

Vitreous fluorophotometry (VFP) — the measurement of fluorescence across the anatomical axis of the eye was conducted using an FM-2 Fluorotron Master (OcuMetrics Inc., Mountain View, CA, USA). The presence of retinal leakage was discerned by a reduction in the calculated slope extending from the retinal peak to the midpoint in the vitreous region (a methodology based on our previous preclinical models featuring retinal leakage). After FA imaging, the rats

remained under anesthesia, and VFP was performed 30 minutes post-administration of the previously described fluorescein injection. VFP was performed at weeks 3 and 6 after AAV injection.

Flash Electroretinography (fERG)

Standard scotopic flash electroretinography (fERG) measurements were conducted at baseline and week 6 with animals dark-adapted overnight (at least 12 hours) in their home cages, with *ad libitum* access to food and water. Rats were anesthetized and their pupils were dilated as described above. Before recording, a lubricant solution (Lakripos, Ursapharm, Saarbrücken, Germany) was applied to maintain corneal moisture and ensure electrical contact between the cornea and recording electrode. A thin silver/silver-chloride wire ring was used as the recording electrode, placed on the cornea. A stainless-steel needle electrode was inserted in the contralateral cheek to serve as a reference electrode, and the ground electrode was placed on the tail. The animals were placed onto a low-noise heating plate (37°C) during the measurements to keep their body temperature constant. All preparations were performed under dim (3 lux) red light. The ERG recordings were taken under complete darkness. Recordings were taken from the right (OD) eyes. An AC/DC differential amplifier (Model 3000; A-M Systems, Sequim, WA, USA), analogue filters set to bandpass of 0.1 Hz to 1 kHz, and a data acquisition interface (C.E.D., Power140, Cambridge, UK) were used for the recordings. Flash stimuli, 3 ms in duration, were administered via LED stimulator at five different intensities, in ascending order: -1.4, -0.12, 0.6, and 1.7 [log (cd.s.m-2)], with respective inter-stimulus intervals of 5, 5, 20 and 60 s. The responses at each intensity were recorded ten consecutive times for the two lowest intensities and 4 and 3 for the two highest. The individual responses were averaged, and further used to manually identify the amplitudes (μV) for both a- and b-

waves. Amplitudes of a-waves were measured from the baseline to the peak of the a-wave and b-wave amplitudes were measured from the peak of the a-wave to the peak of the b-wave.

Tissue Lysis and Gene Expression

For the analysis of both human and rat *Vegf-a* gene expression, frozen retinal tissues were homogenized, and total RNA was extracted using a commercially available RNA/DNA Purification Kit (Norgen Biotek, Thorold, Canada) following the manufacturer's instructions. The RNA was quantified using a Multiskan Sky spectrophotometer (Thermo Fisher Scientific, Waltham, MA, USA) and complementary DNA (cDNA) was synthesized following the established protocols outlined in the High-Capacity RNA-to-cDNA Kit (Thermo Fisher Scientific). The resulting cDNA underwent a real-time quantitative PCR (RT-qPCR) (QuantStudio™, Thermo Fisher Scientific) for human VEGF-A (Hs00900055_m1; Thermo Fisher Scientific) and rat VEGF-A (Rn01511602_m1; Thermo Fisher Scientific) expression, with rat GAPD (GAPDH; Thermo Fisher Scientific) serving as endogenous control. The assays were conducted in triplicates for each sample.

Immunohistochemistry of Eye Cup Cross-Section

Eyes were enucleated and fixed in 4% PFA overnight at 4°C. Subsequently, tissues were washed in 1x Tris-Buffer Saline (TBS) for 15 minutes at room temperature, and eye cups were carefully prepared for further analysis. Eye cups then underwent a series of rinses with sucrose solutions, progressively transitioning through concentrations of 10%, 20%, and 30% to prevent the formation of ice crystals. After this step, the eye cups were embedded in optimal cutting temperature (O.C.T.) compound (Sakura, Torrance, CA, USA), frozen, and cut at 7 μm sections. For antigen retrieval, eye cup cross-sections were exposed to heat at 100°C for 10 minutes in a citrate buffer with a pH of 6.0 and 0.05% Tween 20 (Sigma-Aldrich). Sections were then

washed in 1x TBS at room temperature for 10 minutes and blocked with ready-to-use blocking solution (Life Technologies, Carlsbad, CA, USA). After this step, eye cup cross-sections were washed in 1x TBS again, and incubated with rabbit anti-CD31 primary antibody (1:500 dilution, AB222783; Abcam, Cambridge, UK) overnight at 4°C. Sections were then washed in 1x TBS for 10 minutes and incubated with F(ab')2-goat anti-rabbit IgG (H+L) secondary antibody (1:500 dilution, A-21069; Invitrogen, Carlsbad, CA, USA) for 3 hours in the dark. After further washes in 1x TBS, sections were counterstained with DAPI (1:10 000, 6843.1; Carl Roth, Karlsruhe, Germany) and mounted with Fluoroshield (F6937-20ML; Sigma-Aldrich). Images of the eye cup cross-sections were captured using an upright microscope (DM6 B; Leica Microsystems) by an investigator masked to the treatment conditions.

Immunostaining of Retinal Flat-mounts

For preparation of retinal flat-mounts, eyes were fixed in 4% PFA at room temperature for 30 minutes. Retinas were dissected, flattened with four radial cuts, and further fixed in 4% PFA overnight at 4°C. Flat-mounts then were washed in 1x TBS overnight at 4°C and blocked with blocking solution (10 % horse serum and 0.5 % Triton [Sigma-Aldrich] in 1x TBS). After this step, tissues were washed with washing solution (1 % horse serum and 0.1 % Triton in 1x TBS) for a period of 10 minutes and incubated with the following primary antibodies: goat anti-Iba-1 (1:200, NB100-1028; Novus Biologicals, Centennial, CO, USA), rabbit anti-glial fibrillary acidic protein (GFAP) (1:1000 dilution, PA516291; Invitrogen), and Isolectin B_4 (1:200, FL-1201; Vector, Newark, CA, USA) overnight at 4°C. Retinal flat-mounts were then washed with washing solution and incubated with secondary antibodies: donkey anti-goat AF568 IgG (H+L) (1:500, A11057, Invitrogen) and goat anti-rabbit IgG (H+L) F(ab')2 AF647 (1:500, A21246;

Invitrogen) before washing with washing solution, counterstained with DAPI (1:10 000, 6843.1, Carl Roth), washed and mounted with Fluoroshield (F6937-20ML, Sigma-Aldrich).

Slides were imaged using an upright microscope (DM6 B, Leica Microsystems) by an investigator masked to the treatment conditions. For GFAP and Iba-1 analysis, twelve images were taken from each retinal flat-mount at 12 different locations (4 in the periphery, 4 in the middle and 4 in the central parts). GFAP and Iba-1 positive cells were calculated for each image, using a proprietary algorithm that combines a convolutional neural network (CNN), that has been trained to recognize and quantify cell bodies using a transfer learning approach. The results generated by the model were reviewed and adjusted, if required, by a scientist masked to the treatment conditions.

For Isolectin B_4 analysis, we applied semantic segmentation using U-Net neural network algorithm on panoramic Isolectin B_4-positive flat-mount images (5x/0.15 HC PL FLUOTAR, Leica Microsystems) to generate blood vessel segmentation masks and calculate the vascular area. We also calculated the total length of blood vessel and blood vessel branching points, where segmentation masks were skeletonized and the skeleton vertex points were processed with Dijkstra's algorithm for graph length calculation, and morphological hit-or-miss transformations were performed with different kernels to mark the branching points of a vessel. The analysis was performed using the algorithm written in Python (version 3.8.12), which implements a neural network model built using the fast.ai library (version 2.0.13). For subsequent image analysis steps, the OpenCV library (version 4.5.4.60) was used.

Statistical Analysis

Statistical analysis was performed using GraphPad Prism (version 10.0.2, GraphPad Software, La Jolla, CA, USA). Data were analyzed using unpaired two-tailed t-test, one-way, or two-way

ANOVA, followed by Dunnet's or Šídák's multiple comparisons tests as appropriate, and presented as mean ± standard error of mean (SEM). Significance was determined according to the *P* value: * $P < 0.05$, ** $P < 0.01$, and *** $P < 0.001$.

5.4 Results

Expression of Vegf-a gene in AAV-injected Rat Retinas

Our primary objective in this study was to validate human *Vegf-a* gene expression within retinal tissues of rats which received AAV-hVEGF. To achieve this, we performed IVT injections of AAV's, collected eyes at 2-, 4-, or 6-weeks post-injection, and assessed human *Vegf-a* mRNA concentrations within rat retinal tissues. Quantitative PCR analysis showed notable augmentation in human *Vegf-a* mRNA levels at weeks 2, 4 and 6, with no detectable human *Vegf-a* mRNA observed in neither the AAV-stuffer nor in the naïve groups (Figure 1A). Human *Vegf-a* mRNA upregulation demonstrates a successful delivery of the AAV-hVEGF constructs within rat retinas. Additionally, we aimed to investigate the potential of exogenous human VEGF-A to mediate endogenous mechanisms in rat retinas, which might result in rat *Vegf-a* mRNA expression level changes. Indeed, at week four post-AAV-hVEGF injection a 20% increase in rat *Vegf-a* mRNA expression was found when compared to the levels observed in naïve rats ($P < 0.01$; Figure 1B).

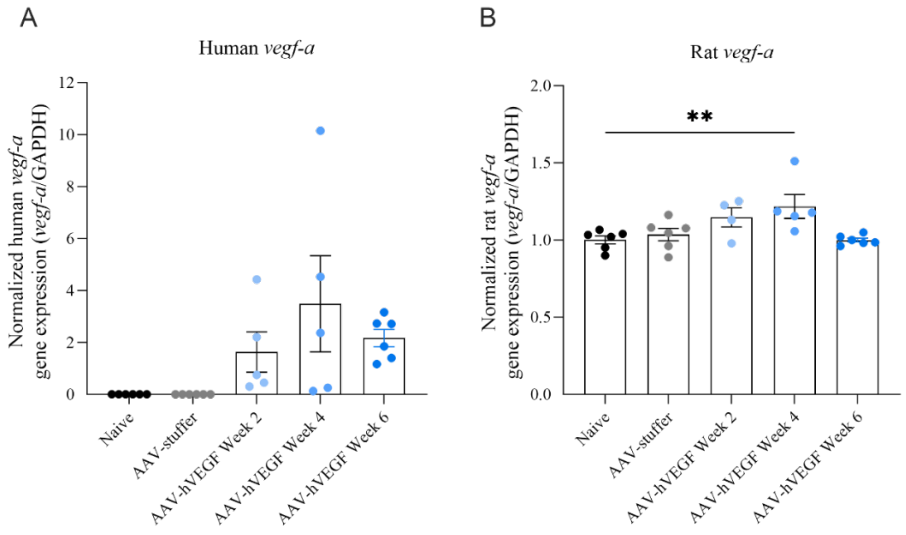

Figure 1. Human and rat *Vegf-a* mRNA expression in AAV-injected rat retinas at different timepoints. (**A**) Increased human *Vegf-a* mRNA levels were detected by qPCR 2, 4, and 6 weeks after IVT injection of AAV-hVEGF; No detectable human *Vegf-a* mRNA levels were observed in AAV-stuffer nor in the naïve groups (n = 5-6). (**B**) At week 4 rat retinas that received AAV-hVEGF injection exhibited a 20% increase in rat *Vegf-a* mRNA levels as compared to naïve rats. ** $P < 0.01$ (n = 4-6). Data were normalized using the GAPDH endogenous control. Statistical analysis was done by one-way ANOVA followed by Dunnett's multiple comparison test. Data are presented as mean ± SEM.

AAV-hVEGF Injection Led to Vascular Pathologies in Rat Eyes

Two weeks post-IVT injection of AAV-hVEGF, FA images revealed the presence of vascular tortuosity and changes in vessel diameter, which were attributed to mild DR phenotypes (Figure 2A, arrowheads). Additionally, AAV-hVEGF-injected rats exhibited distinct white spots next to blood vessels, signifying microaneurysms, corresponding to a moderate DR phenotype (Figure 2A, circles). Severe DR phenotype was observed in 52% of the rats, where changes in vascular tortuosity, increased blood vessel diameter, appearance of microaneurysms were

accompanied with increased areas of fluorescein outside of the blood vessels, suggesting fluid extravasation from the vasculature due to increased vascular permeability (Figure 2B, arrows). No vascular changes were observed in the AAV-stuffer group (Figure 2C).

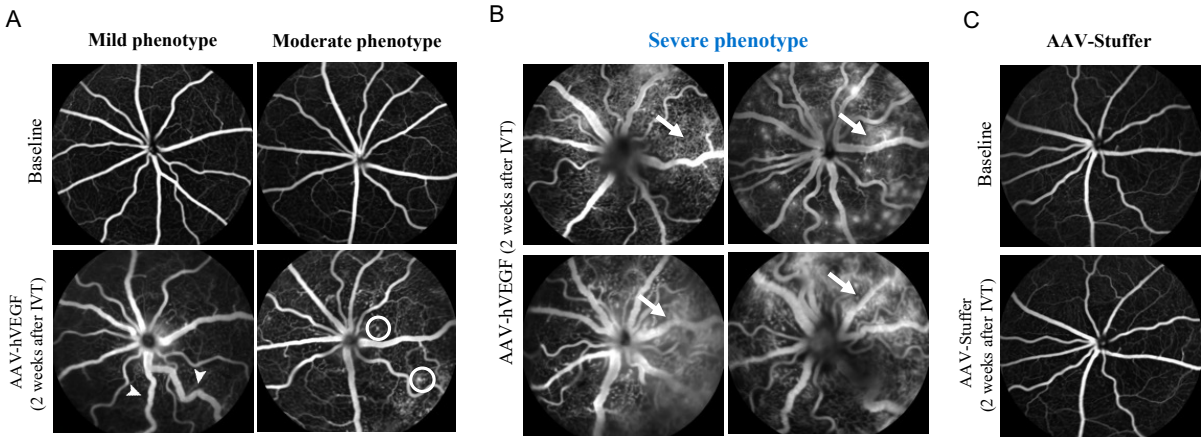

Figure 2. AAV-hVEGF injection led to vascular pathologies in rat eyes. (**A**) IVT injection of AAV-hVEGF led to vascular tortuosity, focally dilated or constricted vessels (mild DR phenotype, *arrowheads*), and microaneurysms (moderate DR phenotype, *circles*) 2 weeks after injection as seen by FA images. (**B**) Increased vascular leakage was observed in 52% of AAV-hVEGF injected rats 2 weeks post-AAV administration (severe DR phenotype, *arrows*). (**C**) No vascular changes were observed in the AAV-Stuffer group.

Furthermore, we aimed to explore the potential of aflibercept in halting AAV-hVEGF-induced retinal leakage. Administration of aflibercept at weeks 2 and 3, effectively arrested retinal leakage in AAV-hVEGF-injected rats, as observed by FA (Figure 3, top row). In contrast, progressive retinal leakage started at week 2 and persisted until week 6 in the vehicle-treated rats (Figure 3, bottom row).

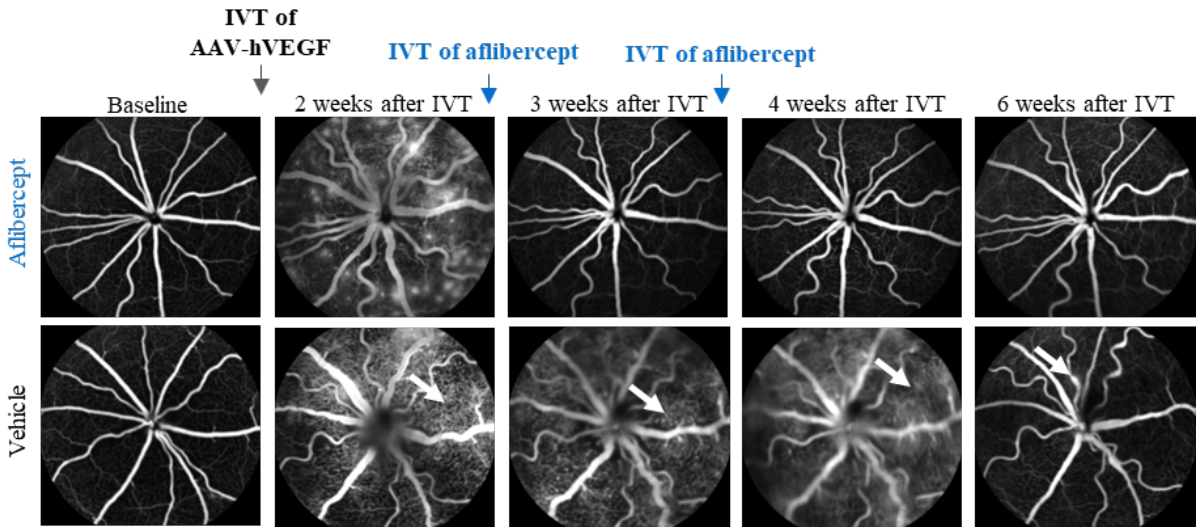

Figure 3. Treatment of aflibercept halted AAV-hVEGF-induced retinal leakage in rat eyes. IVT injections of aflibercept at weeks 2 and 3 stopped AAV-hVEGF-mediated retinal leakage as seen by FA images at different timepoints (*top row*). Progressive retinal leakage (*arrows*) was found in vehicle-treated rats starting from week 2 and persisting until week 6 (*bottom row*).

In the quantitative assessment of retinal leakage using vitreous fluorophotometry (VFP), AAV-hVEGF-injected rats had a significantly decreased VFP slope at week 3 post-injection, when compared to baseline measurements, indicating retinal leakage ($P < 0.05$; Figure 4A). Herein administration of aflibercept demonstrated beneficial effect by ameliorating retinal leakage, and the absolute VFP slope decrease from baseline at week 3 was significantly different between aflibercept and vehicle-treated rats. However, retinal leakage was diminished at week six post-AAV injection in both vehicle and aflibercept groups.

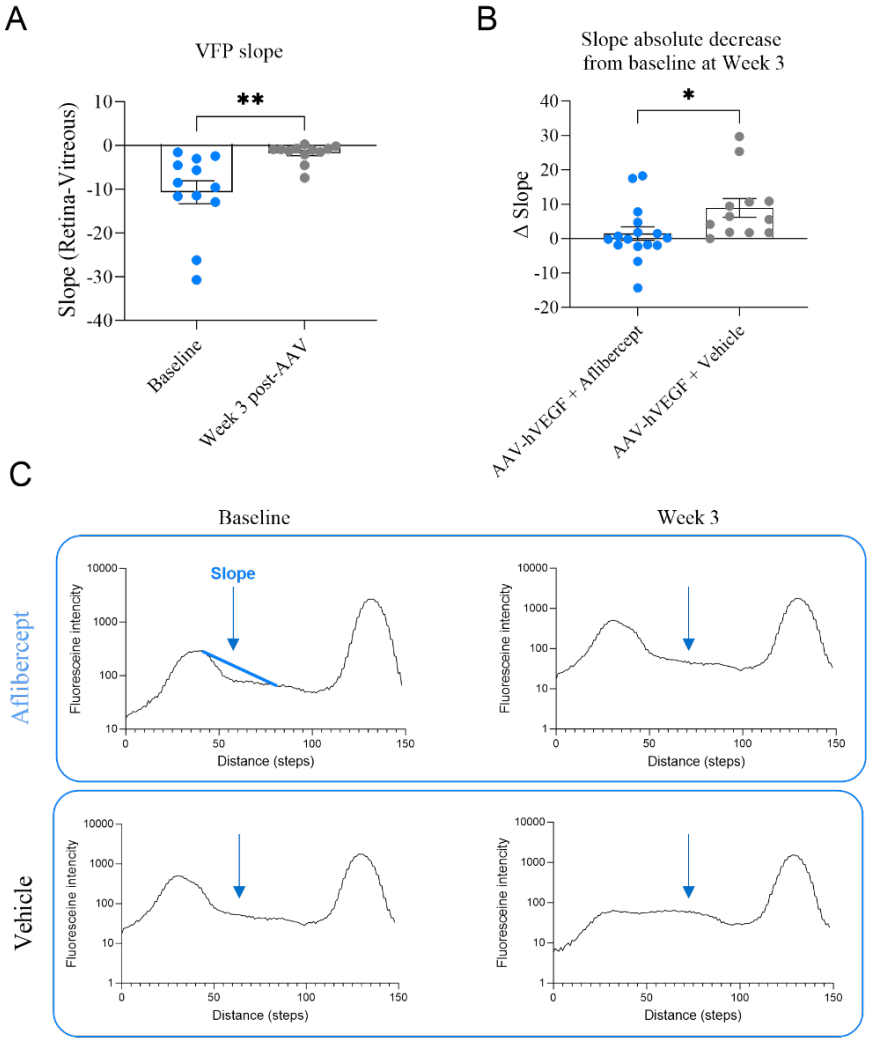

Figure 4. IVT administration of AAV-hVEGF mediated retinal leakage in rat eyes. (**A**) At week 3 VFP slope significantly decreased in AAV-hVEGF-injected rats compared to their baseline measurements, indicating retinal leakage. ** $P < 0.01$ (**B**) Aflibercept demonstrated a therapeutic effect, as VFP slope absolute decrease from baseline was significantly different between aflibercept and vehicle treated rats at week 3. * $P < 0.05$. Statistical analysis was done by unpaired two-tailed t-test. Data are presented as mean ± SEM, n = 12-16 eyes per group. (**C**) Graphic representation of a VFP scan in aflibercept and vehicle groups at baseline and week 3. The line between the retina peak and vitreous mid-point were used to calculate the slope, which is added to the VFP measurement graph as *blue* line.

AAV-hVEGF Administration Induced Structural Changes in Rat Retinas

SD-OCT scans revealed alterations in the structural integrity of the retina, characterized by retinal swelling (Figure 5A, white arrow) and the presence of presumably inflammatory cells within the vitreous (Figure 5A, arrowheads) 2 weeks post-AAV-hVEGF administration. Notably, SD-OCT fundus microscopy confirmed AAV-hVEGF-mediated vascular tortuosity as previously observed by FA (Figure 5A, blue arrow). More in-depth analysis of SD-OCT scans revealed a notable increase in total, inner, and outer nuclear layer thickness, which became evident at week 2 post-AAV injection, suggesting the development of retinal edema in AAV-hVEGF injected eyes ($P < 0.001$, $P < 0.001$, and $P < 0.05$, respectively; Figure 5B). Treatment of aflibercept demonstrated therapeutic effect by reducing retinal thickness: at weeks 3 and 4 following AAV-hVEGF injection, significant reductions in total retinal thickness ($P < 0.01$ and $P < 0.001$, respectively), inner retinal thickness ($P < 0.001$ and $P < 0.001$, respectively), and outer nuclear layer thickness ($P < 0.05$ and $P < 0.001$, respectively) were observed between aflibercept-treated rats and vehicle group (Figure 5C).

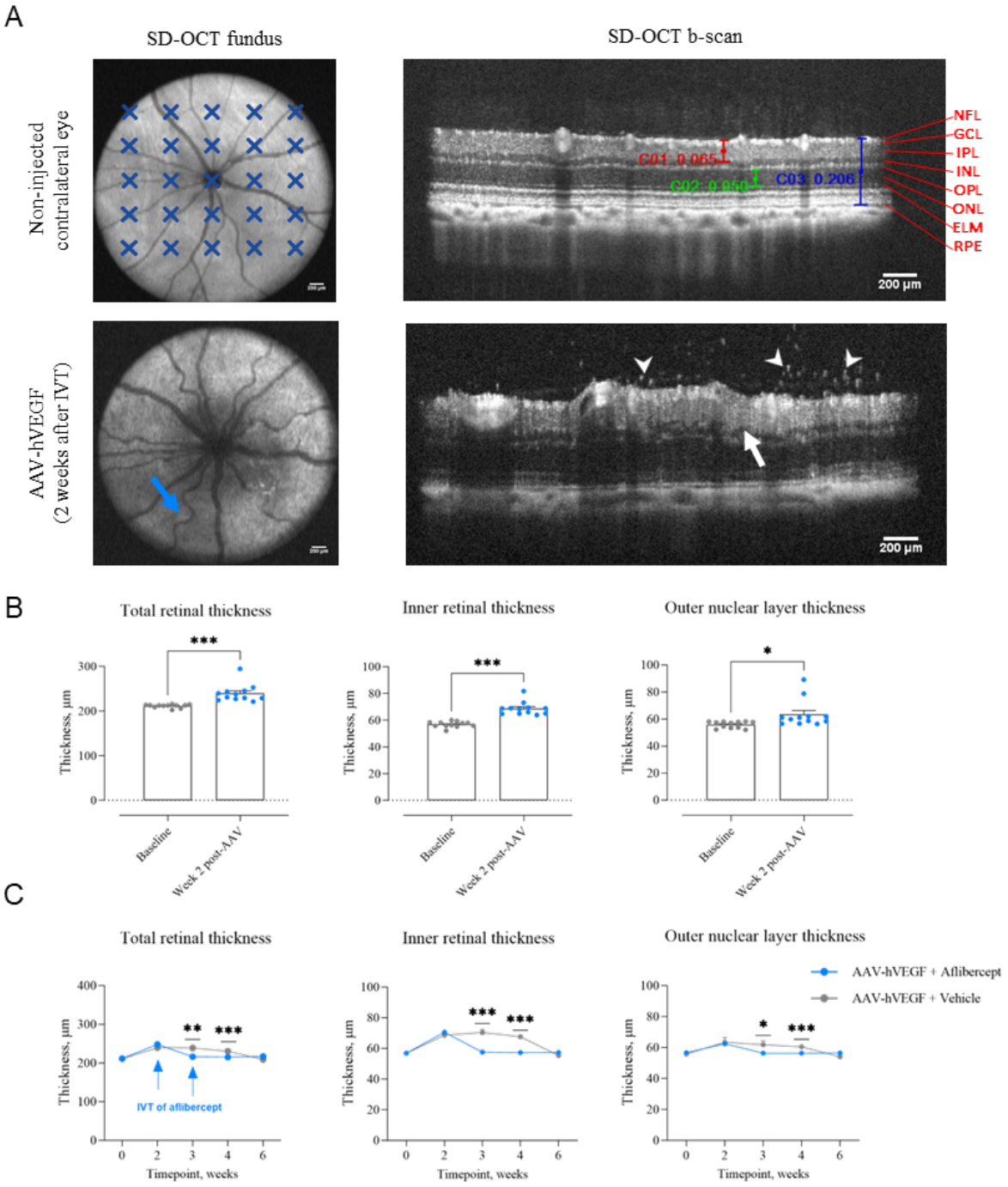

Figure 5. Injections of AAV-hVEGF resulted in structural changes in rat retinas. (**A**) Representative SD-OCT images: SD-OCT fundus image displays blue crosses indicating locations where retinal thickness measurements were taken (*left panel*), while SD-OCT b-scan features a red caliper indicating inner retinal thickness measured region, green – outer nuclear

layer, and blue representing total retina's measured area (*right panel*); AAV-hVEGF injection mediated vascular tortuosity (*blue arrow*), retinal edema (*white arrow*), and the infiltration of inflammatory cells within vitreous body (*arrowheads*) 2 weeks after IVT. (**B**) Total retinal thickness, inner retinal thickness, and outer nuclear layer thickness significantly increased in AAV-hVEGF injected eyes at week 2 compared to their baseline measurements. * $P < 0.05$; *** $P < 0.001$ (**C**) Retinal thickness was significantly reduced by treatment with aflibercept compared to vehicle-treated rats at weeks 3 and 4. * $P < 0.05$; ** $P < 0.01$; *** $P < 0.001$. Statistical analysis was performed using an unpaired two-tailed t-test. Data are presented as mean ± SEM, n = 12-16 eyes per group. GCL – ganglion cell layer, IPL – inner plexiform layer, INL – inner nucleus layer, OPL – outer plexiform layer, ONL – outer nucleus layer, ELM – external limiting membrane, RPE – retina pigment epithelium. Scale bars in (A) = 200 μm.

Reduced Retinal Activity in AAV-hVEGF-injected eyes

To explore the potential of AAV-hVEGF-induced effects on retinal function, we performed fERG. Six weeks post-induction, we observed a significant 22% decline in a-wave and 28% decline in b-wave amplitudes (1.7 [*log* (cd.s.m-2)] stimulus intensity, $P < 0.001$ and $P < 0.001$, respectively; Figure 6), indicating decreased retinal activity. Administration of aflibercept significantly prevented AAV-hVEGF-mediated reduction of a-wave amplitudes compared to vehicle-treated rats (0.6 [*log* (cd.s.m-2)] stimulus intensity, $P < 0.01$; Figure 6C), but did not show any significant effects on AAV-mediated reduction of b-wave amplitudes (0.6 [*log* (cd.s.m-2)] stimulus intensity, $P = 0.41$; Figure 6D).

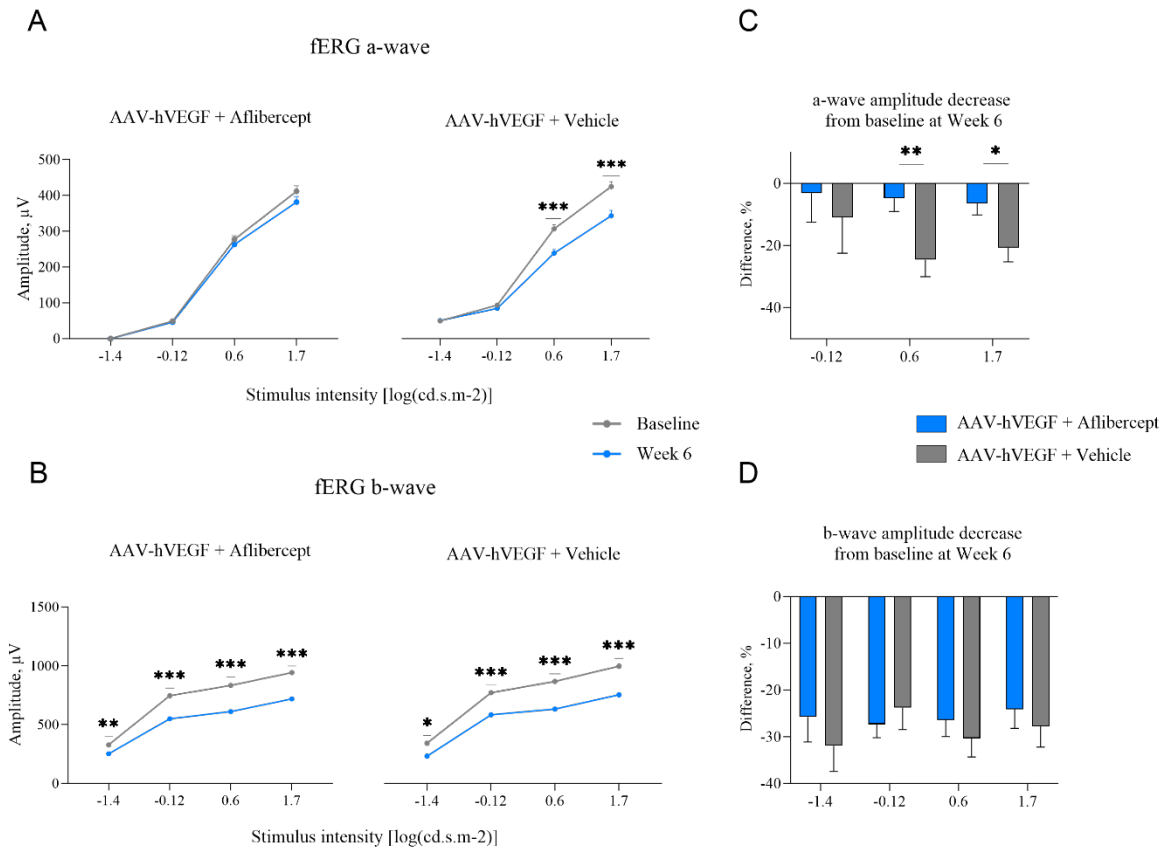

Figure 6. AVV-hVEGF injection reduced retinal activity. AAV-hVEGF injections led to (**A**) a-wave and (**B**) b-wave amplitude decrease by week 6. * $P < 0.05$; ** $P < 0.01$; *** $P < 0.001$. (**C**) Treatment of aflibercept significantly prevented a-wave amplitude decrease from baseline at week 6. * $P < 0.05$; ** $P < 0.01$. (**D**) Aflibercept administration did not have a significant impact on b-wave amplitudes. Retinal function was analyzed by fERG at following stimulus intensities -1.4, -0.12, -0.6, 0.6, 1.7 [log (cd.s.m-2)]. Statistical analysis was performed using two-way ANOVA followed by Šídák's multiple comparisons test. Data are presented as mean ± SEM, n = 12-16 eyes per group.

AAV-hVEGF-mediated Retinal Angiogenesis

To assess AAV-hVEGF-mediated retinal angiogenesis, Isolectin B_4 stained retinal flat-mounts were analyzed using semantic segmentation via the U-Net neural network algorithm for blood

vessel segmentation masks generation and vascular area identification (Figure 7A). Analysis of Isolectin B_4-labeled vasculature revealed a 22% increase of vascular area in AAV-hVEGF-injected eyes at week 6, as compared to contralateral eyes ($P < 0.001$; Figure 7C). We also calculated total vessel length by skeletonizing segmentation masks and processing skeleton vertex points with Dijkstra's algorithm for graph length calculations (Figure 7B). Six weeks post-induction we observed a significant increase in total vessel length ($P < 0.001$; Figure 7D) when compared to contralateral eyes. To identify the vessel branching points, morphological hit-or-miss transformations with various kernels were employed (Figure 7B). The number of branching points exhibited a significant increase in rats subjected to AAV-hVEGF ($P < 0.001$; Figure 7E) when compared to contralateral eyes. This augmentation in vascular area, total vessel length, and branching points collectively indicates AAV-hVEGF-induced retinal angiogenesis. Eyes treated with aflibercept showed no significant differences in the vascular area, total vessel length, or vessel branching points when compared to the vehicle group ($P > 0.99$, $P = 0.91$, and $P = 0.77$, respectively).

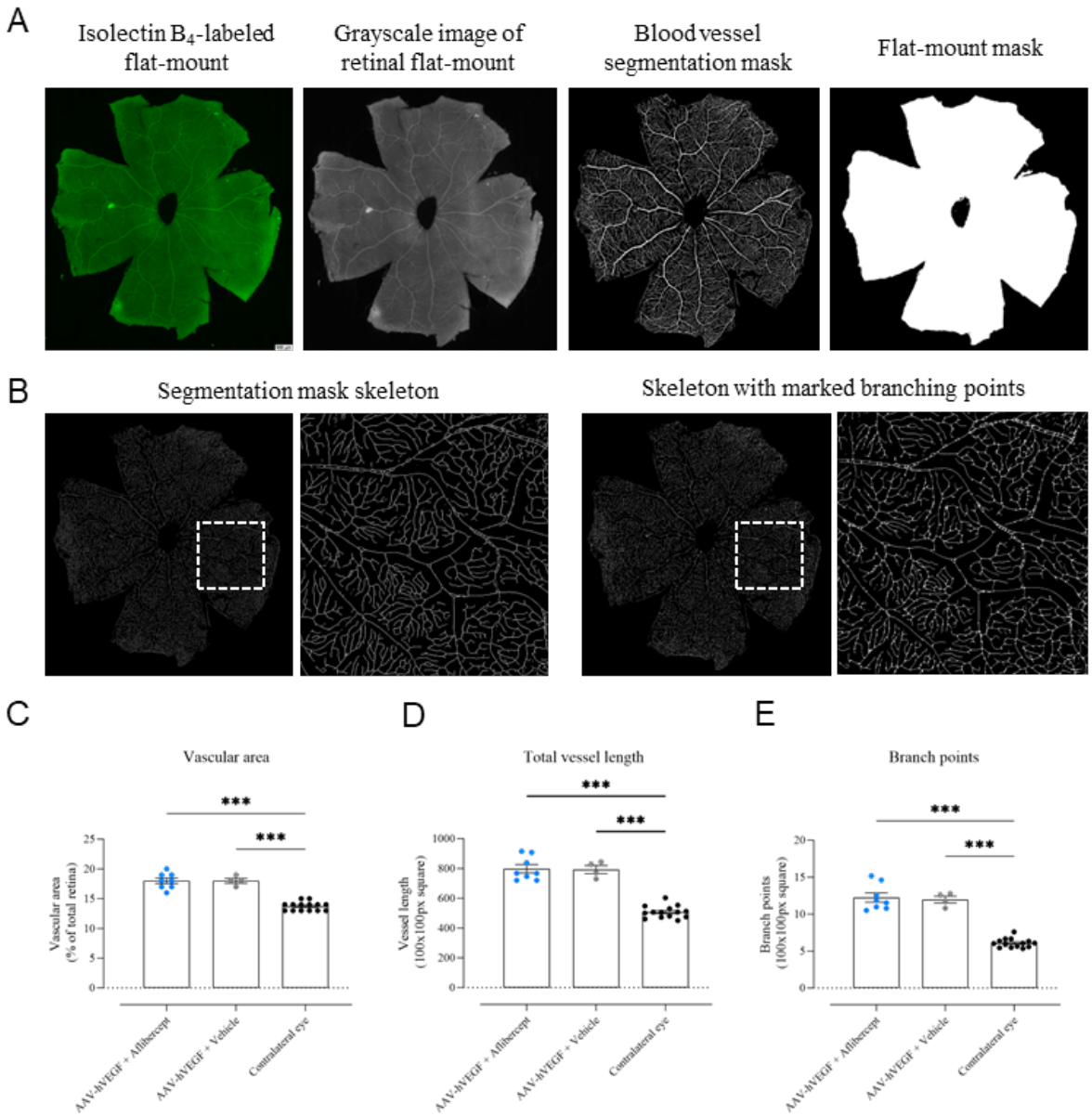

Figure 7. AAV-hVEGF injection led to retinal angiogenesis. (**A**) Representative images of Isolectin B_4-labeled retinal flat-mount, grayscale image of retinal flat-mount, blood vessel segmentation mask and retinal flat-mount mask, used for calculations of vascular area. (**B**) Representative images of segmentation mask skeleton and the same skeleton with marked branching points, used for total vessel length and branching point calculations. A significant increase was found in (**C**) vascular area, (**D**) total vessel length, and (**E**) branching points 6 weeks post-AAV-hVEGF administration, as compared to non-injected eyes. *** $P < 0.001$.

Branching points and total vessel length are presented per 100x100 px square. Statistical analysis was done by two-way ANOVA followed by Tukey‘s multiple comparisons test. Data are presented as mean ± SEM, n = 4 -14 eyes per group. Scale bar = 500 μm for the Isolectin B_4-labeled retinal flat-mount.

Immunofluorescent staining of CD31, a marker for endothelial cells, was used to qualitatively verify angiogenesis in AAV-hVEGF-injected eyes. The anticipated presence of normal vasculature was observed in the central retinal region and periphery areas of non-injected contralateral eyes (Figure 8A). Conversely, within eyes subjected to AAV-hVEGF, blood vessels with enlarged diameter were found (Figure 8B, white arrows), indicating abnormal blood vessel growth. Additionally, in the far peripheral regions of the AAV-hVEGF-injected eyes, we observed an increased presence of CD31-positive cells, suggesting increased proliferation of endothelial cells (Figure 8B, white arrowheads). In summary, examination of Isolectin B_4 and CD31 staining provided conclusive evidence of retinal angiogenesis in eyes administered with AAV-hVEGF.

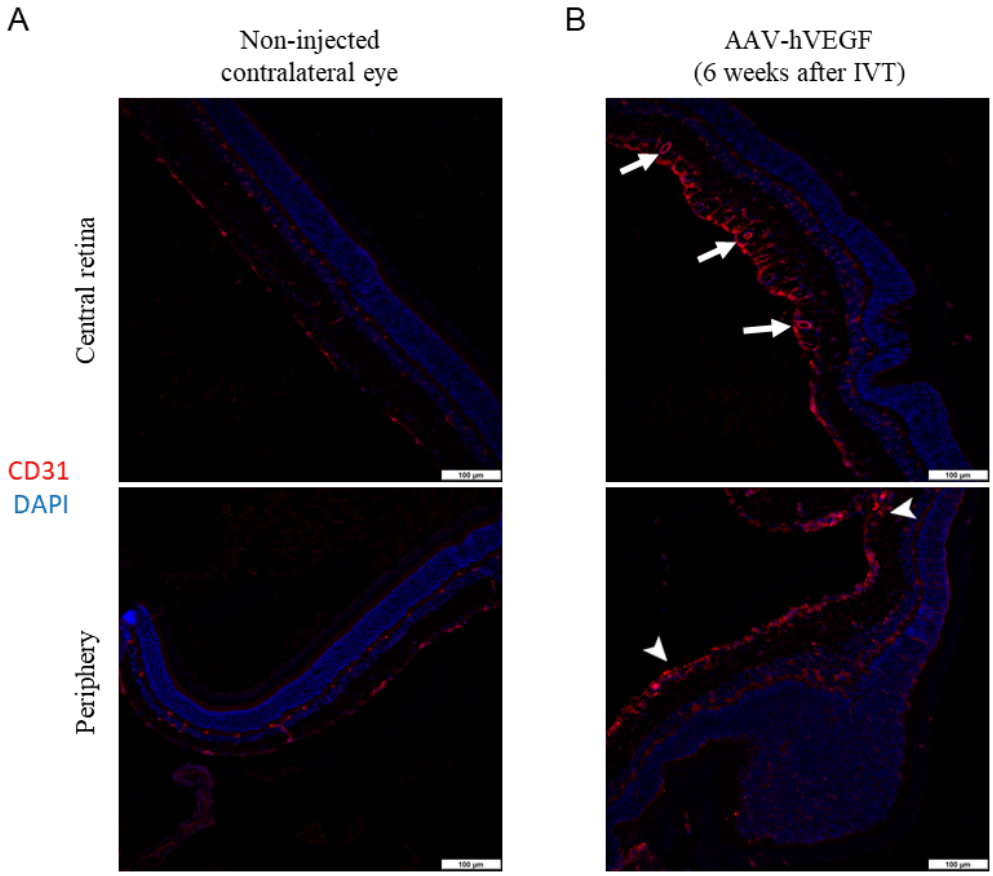

Figure 8. Abnormal blood vessel growth and endothelial cell proliferation in AAV-hVEGF-injected eyes. (**A**) Immunostaining with endothelial cell marker CD31 (*red*) and counterstain with DAPI (*blue*) demonstrates normal vasculature in non-injected contralateral healthy eyes. (**B**) Administration of AAV-hVEGF led to enlarged blood vessels (*white arrows*) in the central retina, which was accompanied by increased presence of endothelial cells in far periphery (*white arrowheads*) (CD31 = *red*, DAPI = *blue*). Scale bar = 100µm.

Activation of Microglia and Reactive Gliosis in AAV-hVEGF-injected eyes

To investigate reactive gliosis and evaluate microglial activation in AAV-hVEGF-injected eyes, retinal flat-mounts were stained with glial marker GFAP and microglial marker Iba-1. Six weeks after IVT injection of AAV-hVEGF, retinas were largely disorganized, accompanied by an increased number of GFAP-positive cells in AAV-hVEGF-injected eyes as compared to non-

injected contralateral eyes ($P < 0.001$; Figure 9A and B). Aflibercept treatment had no effect on GFAP-immunoreactive cell number (aflibercept *vs.* vehicle, $P = 0.32$; Figure 9A). Furthermore, an increased number of total Iba-1-labeled cells was detected in the retina of AAV-hVEGF-injected eyes ($P < 0.001$; Figure 9C), which suggests microglial activation. More detailed qualitative analysis of cellular morphology revealed that the vast majority of Iba-1-immunoreactive cells had hypertrophic cell bodies and nearly complete disappearance of cellular processes, indicating microglial activation (Figure 9F, arrow). Notably, AAV-hVEGF-injected eyes showed a higher number of active Iba-1-positive cells as compared to non-injected contralateral healthy eyes ($P < 0.001$; Figure 9D). Administration of aflibercept significantly reduced the number of Iba-1-immunoreactive cells in the activated state compared to vehicle-treated eyes ($P < 0.05$; Figure 9E).

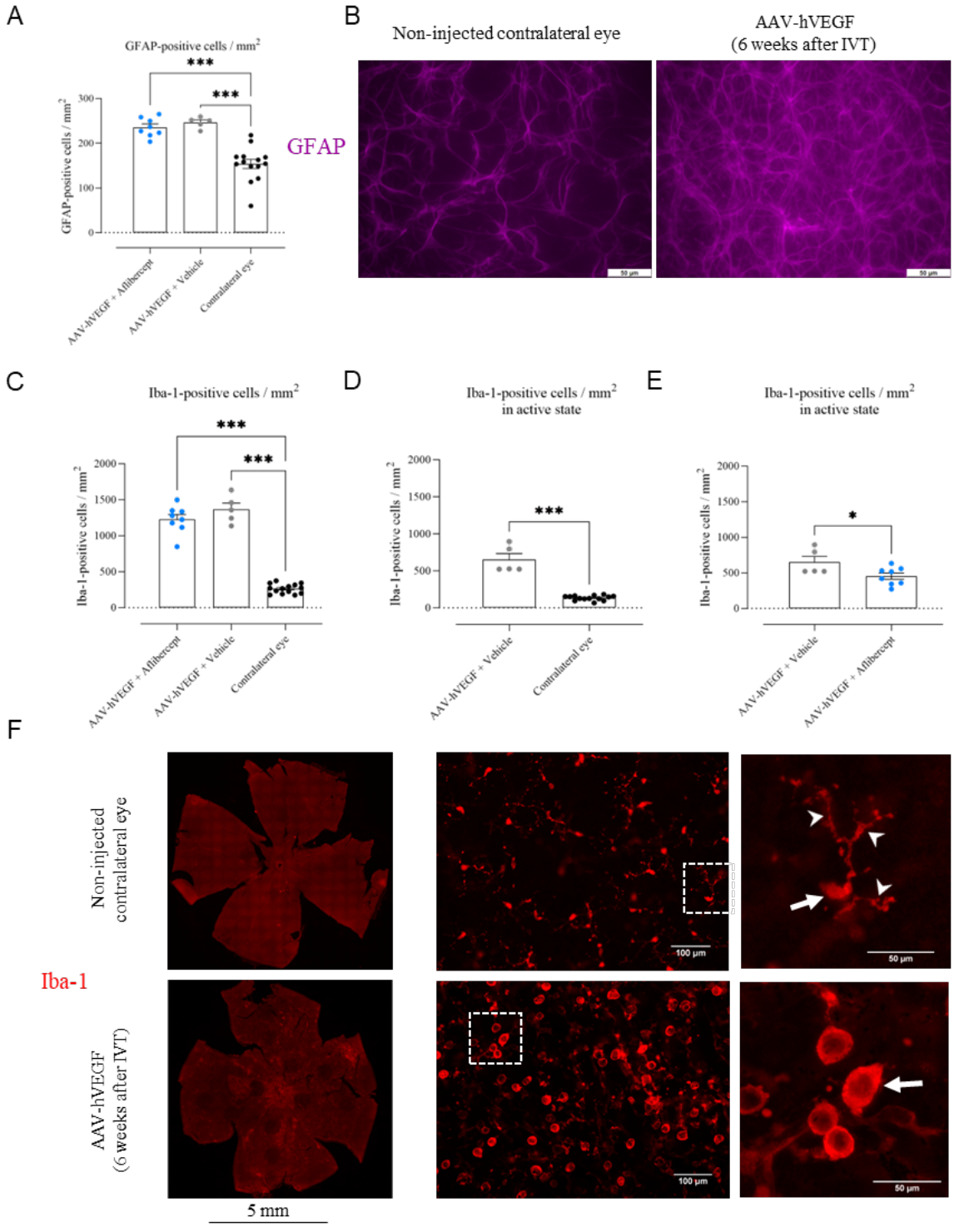

Figure 9. AAV-hVEGF injections induced microglial activation and reactive gliosis in rat eyes. (**A**) GFAP-positive cell number per retinal area (1 mm^2). There was a statistically significant increase of GFAP-positive cells in AAV-hVEGF-injected eyes as compared to contralateral

healthy eyes. *** $P < 0.001$. (**B**) Representative images of GFAP (*purple*) labeled flat-mount from AAV-hVEGF and contralateral eye groups. Statistically significant increase of (**C**) total and (**D**) active Iba-1-positive cell number was detected in AAV-hVEGF-injected eyes as compared to contralateral eyes. *** $P < 0.001$. (**E**) Treatment of aflibercept decreased activated microglia as compared to the vehicle-injected eyes. * $P < 0.05$. (**F**) Retinal flat-mounts stained with Iba-1 (*red*) revealed increased density of Iba-1 cells as compared to non-injected contralateral healthy eyes (*left panel*). As observed in higher-magnification images (*right panel*), activated Iba-1 cells had specific hypertrophic cell body (*arrow*) and retracted cellular processes (AAV-hVEGF-injected eye retina). In contrast, silent microglia (*arrowheads*) had ramified cellular morphology with small cellular body (*arrow*) (non-injected contralateral eye retina). For statistical analysis we used two-way ANOVA followed by Tukey's multiple comparisons test, and unpaired two-tailed t-test. Data are presented as mean ± SEM, n = 8-14 eyes per group. Scale bars in (**B**) = 50 μm; in (**F**) = 50 μm, 100 μm and 5 mm, as indicated.

5.5 Discussion

This study presents a comprehensive evaluation of DR-like pathology in Brown Norway rats, induced using AAV viral vectors expressing human VEGF-A. Our AAV-based VEGF rat model resembles several DR-related features, including retinal angiogenesis, vascular leakage, retinal edema, functional impairment, and inflammatory responses. These effects were partially ameliorated by the administration of aflibercept (Eylea®), confirming the translational applicability of AAV-hVEGF-induced rat model.

We successfully achieved long-term expression of human *Vegf-a* mRNA in rat retinas through AAV-hVEGF injection, confirming the efficacy of AAV variant ShH10, which is known to selectively transduce Müller cells.[17] Müller cell-derived VEGF plays a causative role in major

pathologic changes during DR, such as vascular leakage and retinal inflammation.[23] Additionally, Müller cells processes transverse the entire thickness of the retina, representing an ideal target for achieving widespread expression of human VEGF-A after a single intravitreal administration. To further validate the transduction of Müller cells using the ShH10 variant, our future investigations will involve administering AAV-ShH10 construct expressing green fluorescent protein (GFP), which would enable us to visualize and confirm the selective transduction of Müller glia. In addition to this, we found an increase in endogenous rat *Vegf-a* mRNA levels in eyes that received AAV-hVEGF administrations, which suggests a possible feedback mechanism, that might have augmented such pathology. However, to precisely understand the mechanisms behind the interplay between exogenous and endogenous VEGF-A expression, further investigation would be needed.

Intravitreal injections of AAV-hVEGF in Brown Norway rats led to a range of retinal vascular abnormalities such as vascular tortuosity, changes in vessel diameter, microaneurysm formation, and and significant retinal leakage — findings comparable to those observed in transgenic mouse models.[13,14] However, transgenic mice rapidly develop severe disease phenotypes shortly after birth, whereas the AAVs used in our study were administered to a fully developed adult rats, offering a more controlled onset of the disease. Additionally, the analysis of Isolectin B_4-stained retinal flat-mounts using neural network-based algorithm provided direct evidence of retinal angiogenesis, a hallmark of proliferative diabetic retinopathy.[3] This observation contrasts with transgenic mice models, where new blood vessel formation typically occurs in the outer retina or choroid, raising concerns about the model's relevance to human DR.[13,15] One explanation for these discrepancies may be the different cellular targets of VEGF expression: in transgenic mice, VEGF is typically expressed in photoreceptors,[14,15] while in our study, the AAV-ShH10 construct selectively transduced Müller cells, which span the entire

retina.[17] Additionally, although subretinal delivery of AAV-VEGF in mice has been shown to induce retinal angiogenesis, neovascularization was limited to the outer retinal layers, close to the injection site.[24] In our study, AAVs were delivered intravitreally and induced angiogenesis in the inner layers, suggesting that the route of AAV delivery may influence the location of neovascularization within the retina. Retinal neovascularization in our study was further confirmed through immunofluorescent staining of endothelial cells, which revealed abnormal vessel growth and increased presence of endothelial cells in the eyes subjected to AAV-hVEGF, consistent with previous studies using intravitreal AAV-mediated human VEGF in murine eyes.[21] However, quantification of CD31-positive cells would strengthen our findings and clarify the extent of pathology.

In vivo imaging, specifically SD-OCT, revealed increased retinal thickness in AAV-hVEGF-injected rats, suggesting retinal edema — a frequent complication observed in DR patients.[25] Similar signs of retinal edema have been reported in Kimba and Akimba mice,[26] and in rats subjected to VEGF-A protein injections.[10] Moreover, in SD-OCT scans we noticed signs of retinal inflammation, indicated by accumulation of presumably inflammatory cells in the vitreous. Indeed, retinal inflammation was identified by immunohistochemistry analysis of retinal flat-mounts, indicating activation of microglia and manifestation of retinal gliosis in AAV-hVEGF-injected eyes, both of which are also observed in DR patients.[27,28]

In this study, we implemented a novel analysis of Isolectin B_4-stained retinal flat-mounts using neural network-based algorithms to quantitatively assess retinal vasculature. Algorithm provided valuable insights into vascular area, total vessel length, and vessel branching points. These read-outs significantly increased after AAV-hVEGF injection indicating retinal angiogenesis. However, further validation of this algorithm is necessary to ensure the accuracy and reliability of the results. Validation could be achieved by comparing its output to well-

established tools such as AngioTool,[29] assessing its consistency across multiple datasets, and ensuring it accurately accounts for three-dimensional effects, such as overlapping vessels appearing as branching points.

The observed vascular and structural retinal changes in AAV-hVEGF-injected eyes were accompanied by a decrease in retinal activity, as identified by flash electroretinography. By the sixth week post-injection, a significant reduction in both a-wave and b-wave amplitudes was observed. Most studies involving transgenic mice[13–15,26,30] or AAV-VEGF injections [21,24] which report severe DR-related vascular changes have primarily concentrated on vascular alterations, often overlooking the impact on visual function. However, visual deficits have been reported in streptozotocin-injected Sprague Dawley rats following VEGF-A protein injections,[10] aligning with our finding, although it remains unclear whether these deficits were a result of STZ-induced diabetes, VEGF-A protein excess, or STZ's potential to cause neurotoxic effects on neurons.[31,32] Therapeutic intervention with aflibercept, an FDA-approved anti-VEGF-A treatment for wet age-related macular degeneration, diabetic macular edema and DR,[33] partially halted AAV-hVEGF-induced vascular pathologies, restoring retinal vasculature to the levels comparable to healthy eyes. These findings are in line with clinical studies reporting the benefits of anti-VEGF-A therapy in DR management,[7] supporting the translational potential of our rat model for DR. Interestingly, although aflibercept significantly prevented the AAV-hVEGF-mediated decrease in a-wave amplitude, it had no effect on the b-wave amplitude. This difference may be due to aflibercept's more potent effect on the outer retinal layers, impacting photoreceptor function (a-wave), rather than affecting the function of retinal interneurons (b-wave). This observation could be further explained through immunohistochemical analysis of photoreceptors and interneurons. Further exploration is necessary to define if this therapeutic

anti-VEGF effect on the function of different retinal cell populations is specific for AAV-inducible model or is applicable to other VEGF-related models as well.

Our easy-to-induce AAV-based DR rat model that replicates major pathological features of DR, also has several limitations that need to be considered. Fistly, AAV-hVEGF-induced vascular leakage and retinal swelling were diminished at six weeks post-AAV, although retinal angiogenesis, decreased retinal function, and inflammation were still evident. Subretinal injection of AAV-VEGF has been demonstrated to induce long-lasting CNV-like pathology in rats, with Liu et al.[18] reporting effects for a period of 9 weeks, and Wang et al.[19] indicating pathology persisting for up to 20 months post-injection. Intravitreal delivery of AAV-VEGF in non-human primates has been shown to induce DR-like pathology for a period of 3 weeks, but the occurrence of iris neovascularization limited longer follow-up time.[20] Diminished vascular leakage six weeks post-AAV administration in our study could be explained by decline in AAV-induced gene expression, adaptive immune responses, or the influence of endogenously regulated factors. Secondly, AAV-hVEGF administration resulted in variable DR-related phenotypes within the same group of animals with some rats exhibiting mild to moderate vascular changes, while others showing severe ones. This variability observed via FA imaging corresponded to variable *Vegf-a* mRNA expression levels in the retinal tissue. The variability might be attributed to the distribution of intravitreally injected AAV vectors across the retina or differences in individual immune responses to the injected AAVs. Given that most drugs fail during clinical trials despite demonstrating efficacy and safety in animal models,[34–36] employing human transgenes in animal studies provides valuable insights into potential human responses in clinical trials.[37] However, the use of humanized transgenes can trigger different immune responses in animals due to species-specific differences, which potentially complicate the interpretation of drug efficacy. In our study, the overexpression of humanized VEGF may have

influenced inflammatory rat profiles, contributing to the observed phenotype variability and loss of pathology, specifically diminished vascular leakage, by week six following AAV administration. In light of these considerations, as well as ethical concerns surrounding animal research, alternative non-animal models such as organoids, bioengineered tissue constructs, and organs-on-chips could be valuable tools for preclinical testing of new therapeutic agents prior to using our proposed animal model.[34] In future studies, standardizing AAV-hVEGF dosages and monitoring AAV distribution could help to reduce variability, ensuring more consistent transgene expression and DR phenotypes across treated animals. Finally, similarly to other VEGF models, our AAV-hVEGF-induced rats are not hyperglycaemic, lacking insights into the sequence of events leading to VEGF upregulation in diabetic retinopathy. Therefore, our future directions will involve testing inducible VEGF-A overexpression in Müller cells on diabetic background, reflecting the entire spectrum of DR.

In conclusion, AAV-mediated expression of human VEGF-A in rat retinas, coupled with the observed therapeutic effects of aflibercept, demonstrates an easy-to-use AAV-based model that recapitulates several aspects of DR pathology and serves as an attractive approach to gain valuable insights into the underlying molecular mechanisms of VEGF-mediated pathologies and for testing novel anti-angiogenic therapies.

5.6 Acknowledgments

This work was funded by the European Union's Horizon 2020 Research and Innovation Programme under the Mari Sklodowska-Curie Actions (grant agreement – No 813440).

5.7 Contributions

The project was conceptualized by I.L, Z.A., and G.K. Intravitreal injections were performed by S.R. In vivo imaging, VFP measurements, and fERG were performed by I.L, with support

from S.R., T.P., and other members of the Experimentica team (not included in the author list). Histology and immunohistochemistry analysis were performed by I.L with support from D.L. and other members of the Experimentica team (not included in the author list). Data analysis was performed by I.L. Original draft was written by I.L. Work was reviewed, edited, and supervised by G.K. and Z.A.

5.8 Disclosures

Employment: G.K., S.R., T.P., D.L. and I.L. (Experimentica Ltd.); Stock/equity ownership: G.K. (Experimentica Ltd.). S.K. conducts academic research in areas of interest like the business interests of K&P Scientific LLC. The terms of this arrangement have been reviewed and approved by Loyola University Chicago in accordance with its conflict-of-interest policy. The funders had no role in the study. Z.A. declare no conflicts of interest.

5.9 References

1. Teo ZL, Tham YC, Yu M, Chee ML, Rim TH, Cheung N, et al. Global Prevalence of Diabetic Retinopathy and Projection of Burden through 2045. Ophthalmology. 2021 Nov;128(11):1580–91.

2. Gomułka K, Ruta M. The Role of Inflammation and Therapeutic Concepts in Diabetic Retinopathy—A Short Review. Int J Mol Sci. 2023 Jan 5;24(2):1024.

3. Glassman AR, Beaulieu WT, Maguire MG, Antoszyk AN, Chow CC, Elman MJ, et al. Visual Acuity, Vitreous Hemorrhage, and Other Ocular Outcomes After Vitrectomy vs Aflibercept for Vitreous Hemorrhage Due to Diabetic Retinopathy: A Secondary Analysis of a Randomized Clinical Trial. JAMA Ophthalmology. 2021 Jul 1;139(7):725–33.

4. Aiello LP, Wong JS. Role of vascular endothelial growth factor in diabetic vascular complications. Kidney International. 2000 Sep 1;58:S113–9.

5. Gupta N, Mansoor S, Sharma A, Sapkal A, Sheth J, Falatoonzadeh P, et al. Diabetic Retinopathy and VEGF. Open Ophthalmol J. 2013 Feb 1;7:4–10.

6. Gupta MP, Kiss S, Chan RVP. Reversal of retinal vascular leakage and arrest of progressive retinal non-perfusion with monthly anti-vascular endothelial growth factor therapy for proliferative diabetic retinopathy. Retina. 2018 Sep;38(9):e74–5.

7. Kim YJ, Yeo JH, Son G, Kang H, Sung YS, Lee JY, et al. Efficacy of intravitreal Aflibercept injection For Improvement of retinal Nonperfusion In diabetic retinopathy (AFFINITY study). BMJ Open Diabetes Res Care. 2020 Oct 19;8(1):e001616.

8. Tolentino MJ, Miller JW, Gragoudas ES, Chatzistefanou K, Ferrara N, Adamis AP. Vascular endothelial growth factor is sufficient to produce iris neovascularization and neovascular glaucoma in a nonhuman primate. Arch Ophthalmol. 1996 Aug;114(8):964–70.

9. Tolentino MJ, Miller JW, Gragoudas ES, Jakobiec FA, Flynn E, Chatzistefanou K, et al. Intravitreous injections of vascular endothelial growth factor produce retinal ischemia and microangiopathy in an adult primate. Ophthalmology. 1996 Nov;103(11):1820–8.

10. Clermont AC, Murugesan N, Aiello LP. Vascular endothelial growth factor (VEGF) induces retinal edema and neuroretinal dysfunction in diabetic rats. Investigative Ophthalmology & Visual Science. 2020 Jun 10;61(7):1385.

11. Edelman JL, Lutz D, Castro MR. Corticosteroids inhibit VEGF-induced vascular leakage in a rabbit model of blood-retinal and blood-aqueous barrier breakdown. Exp Eye Res. 2005 Feb;80(2):249–58.

12. Ozaki H, Hayashi H, Vinores SA, Moromizato Y, Campochiaro PA, Oshima K. Intravitreal sustained release of VEGF causes retinal neovascularization in rabbits and breakdown of the blood-retinal barrier in rabbits and primates. Exp Eye Res. 1997 Apr;64(4):505–17.

13. Okamoto N, Tobe T, Hackett SF, Ozaki H, Vinores MA, LaRochelle W, et al. Transgenic mice with increased expression of vascular endothelial growth factor in the retina: a new model of intraretinal and subretinal neovascularization. Am J Pathol. 1997 Jul;151(1):281–91.

14. Lai CM, Dunlop SA, May LA, Gorbatov M, Brankov M, Shen WY, et al. Generation of transgenic mice with mild and severe retinal neovascularisation. Br J Ophthalmol. 2005 Jul;89(7):911–6.

15. Ohno-Matsui K, Hirose A, Yamamoto S, Saikia J, Okamoto N, Gehlbach P, et al. Inducible Expression of Vascular Endothelial Growth Factor in Adult Mice Causes Severe Proliferative Retinopathy and Retinal Detachment. Am J Pathol. 2002 Feb;160(2):711–9.

16. Ail D, Malki H, Zin EA, Dalkara D. Adeno-Associated Virus (AAV) - Based Gene Therapies for Retinal Diseases: Where are We? Appl Clin Genet. 2023 May 30;16:111–30.

17. Klimczak RR, Koerber JT, Dalkara D, Flannery JG, Schaffer DV. A Novel Adeno-Associated Viral Variant for Efficient and Selective Intravitreal Transduction of Rat Müller Cells. PLoS One. 2009 Oct 14;4(10):e7467.

18. Liu S, Biesemeier AK, Tschulakow AV, Thakkar HV, Julien-Schraermeyer S, Schraermeyer U. A new rat model of treatment-naive quiescent choroidal neovascularization induced by human VEGF165 overexpression. Biol Open. 2020 Jun 11;9(6):bio048736.

19. Wang F, Rendahl KG, Manning WC, Quiroz D, Coyne M, Miller SS. AAV-Mediated Expression of Vascular Endothelial Growth Factor Induces Choroidal Neovascularization in Rat. Investigative Ophthalmology & Visual Science. 2003 Feb 1;44(2):781–90.

20. Lebherz C, Maguire AM, Auricchio A, Tang W, Aleman TS, Wei Z, et al. Nonhuman Primate Models for Diabetic Ocular Neovascularization Using AAV2-Mediated Overexpression of Vascular Endothelial Growth Factor. Diabetes. 2005 Apr 1;54(4):1141–9.

21. Weigelt CM, Fuchs H, Schönberger T, Stierstorfer B, Strobel B, Lamla T, et al. AAV-Mediated Expression of Human VEGF, TNF-α, and IL-6 Induces Retinal Pathology in Mice. Transl Vis Sci Technol. 2021 Sep 14;10(11):15.

22. Kaja S, Ragauskas S, Vähätupa M, Cerrada-Gimenez M, Mering S, Hakkarainen JJ, et al. Standardization and validation of intravitreal and systemic administration of aflibercept in preclinical models for angiogenesis. Investigative Ophthalmology & Visual Science. 2019 Jul 22;60(9):1629.

23. Wang J, Xu X, Elliott MH, Zhu M, Le YZ. Müller cell-derived VEGF is essential for diabetes-induced retinal inflammation and vascular leakage. Diabetes. 2010 Sep;59(9):2297–305.

24. Rakoczy PE, Brankov M, Fonceca A, Zaknich T, Rae BC, Lai CM. Enhanced Recombinant Adeno-Associated Virus-Mediated Vascular Endothelial Growth Factor Expression in the Adult Mouse Retina: A Potential Model for Diabetic Retinopathy. Diabetes. 2003 Mar 1;52(3):857–63.

25. Ciulla TA, Amador AG, Zinman B. Diabetic Retinopathy and Diabetic Macular Edema: Pathophysiology, screening, and novel therapies. Diabetes Care. 2003 Sep 1;26(9):2653–64.

26. Rakoczy EP, Rahman ISA, Binz N, Li CR, Vagaja NN, de Pinho M, et al. Characterization of a Mouse Model of Hyperglycemia and Retinal Neovascularization. Am J Pathol. 2010 Nov;177(5):2659–70.

27. Rübsam A, Parikh S, Fort PE. Role of Inflammation in Diabetic Retinopathy. Int J Mol Sci. 2018 Mar 22;19(4):942.

28. Yu Y, Chen H, Su SB. Neuroinflammatory responses in diabetic retinopathy. Journal of Neuroinflammation. 2015 Aug 7;12(1):141.

29. Zudaire E, Gambardella L, Kurcz C, Vermeren S. A Computational Tool for Quantitative Analysis of Vascular Networks. PLoS One. 2011 Nov 16;6(11):e27385.

30. Can Eeden PE, Tee LBG, Lukehurst S, Lai CM, Rakoczy EP, Beazley LD, et al. Early Vascular and Neuronal Changes in a VEGF Transgenic Mouse Model of Retinal Neovascularization. Investigative Ophthalmology & Visual Science. 2006 Oct 1;47(10):4638–45.

31. Shoham S, Bejar C, Kovalev E, Weinstock M. Intracerebroventricular injection of streptozotocin causes neurotoxicity to myelin that contributes to spatial memory deficits in rats. Exp Neurol. 2003 Dec;184(2):1043–52.

32. Genrikhs EE, Stelmashook EV, Golyshev SA, Aleksandrova OP, Isaev NK. Streptozotocin causes neurotoxic effect in cultured cerebellar granule neurons. Brain Res Bull. 2017 Apr;130:90–4.

33. Inc RP. EYLEA HD (aflibercept) Injection 8 mg Approved by FDA for Treatment of Wet Age-related Macular Degeneration (wAMD), Diabetic Macular Edema (DME) and Diabetic Retinopathy (DR) [Internet]. GlobeNewswire News Room. 2023 [cited 2023 Nov 8].

34. Loewa A, Feng JJ, Hedtrich S. Human disease models in drug development. Nat Rev Bioeng. 2023 May 11;1–15.

35. Golding H, Khurana S, Zaitseva M. What Is the Predictive Value of Animal Models for Vaccine Efficacy in Humans? The Importance of Bridging Studies and Species-Independent Correlates of Protection. Cold Spring Harb Perspect Biol. 2018 Apr 2;10(4):a028902.

36. Franco R, Cedazo-Minguez A. Successful therapies for Alzheimer's disease: why so many in animal models and none in humans? Front Pharmacol. 2014;5:146.

37. Houdebine LM. Transgenic animal models in biomedical research. Methods Mol Biol. 2007;360:163–202.

CHAPTER 6

GENERAL DISCUSSION

6.1 Main findings, limitations, and future investigations

Existing animal models fall short of reflecting the entire spectrum of pathological features of diabetic retinopathy, particularly its late-stage. This research project attempted to establish a novel rat animal model that recapitulates the pathophysiology of both proliferative and non-proliferative DR. To summarize already existing data on the rodent STZ-induced DR model, a systematic literature review was performed. Different factors leading to structural and functional changes in the STZ-induced rat model were analyzed and compared. Following that, a study using the Brown Norway rat STZ-induced DR model was undertaken to characterize changes in the ocular structure and functional activity. In the pursuit of developing preclinical model relevant to DR, the feasibility of cumate-inducible LV vectors mediating VEGF-A expression was explored in ARPE-19 cells. Cumate tolerability was assessed in Wistar rat eyes after intravitreal delivery. However, due to the observed cumate toxicity in rat eyes, the focus of model development shifted to the use of AAV vectors. This direction led to an investigation into the long-term expression of intravitreally injected AAV vectors encoding *Vegf-a* in Brown Norway rats. Additionally, an assessment of aflibercept (Eylea®) as a therapeutic intervention was explored in this model.

We conducted a systematic review on STZ-induced animal models and performed a study using STZ-induced Brown Norway rats as a strategic step toward developing our new rat DR model. The rationale behind this approach was to gain a deeper understanding of the most commonly used DR model and evaluate how well it replicate key features of diabetic retinopathy. The first finding of this research underscored the significance of ERG as the most consistent functional readout in the rodent STZ model (Chapter 2), corroborating previous research that reports visual function decline in diabetic rodents.[1–4] However, studies have demonstrated that STZ has a neurotoxic effect on neurons, which can lead to non-specific neuronal damage.[5,6] This

neurotoxicity may exaggerate the extent of neurodegeneration beyond what is typically observed in human DR, raising concerns about the STZ model's ability to accurately mimic the disease's progression in humans. In addition, the absence of quantitative data for various outcome measures in most of the studies resulted in a significant challenge to interpret obtained results. Additionally, risk of bias assessment revealed that all analyzed STZ studies exhibited a high risk of bias, either due to the lack of reporting or correctly following the procedures. To mitigate reporting shortcomings, we have encouraged researchers to adhere to reporting guidelines, such as ARRIVE,[7,8] and in response to this we have implemented these recommendations in our future experiments as well. Despite these limitations, the systematic review offered valuable insights into key factors, such as STZ dosing, glucose thresholds, follow-up durations, and main readouts, which guided the design of our future STZ study (Chapter 3).

Detailed analysis of the structure-function relationship in the Brown Norway rat DR model revealed consistent morphological changes and visual deficits following streptozotocin injection (Chapter 3). Neovascularization, a key feature of proliferative DR,[9,10] has been variably reported in STZ-induced animals.[11,12] While some studies claim the presence of neovascularization, the methods used to confirm new blood vessel formation are often insufficient.[13] In our study, STZ-induced Brown Norway rats recapitulated the known phenotypes of early DR, however, the absence of any severe vascular abnormalities, such as vascular leakage, vascular tortuosity, and neovascularization in STZ-induced Brown Norway rats, suggests that this particular model mimics only early stages of DR, further encouraging our aim to develop a novel rat model, which recapitulates late-stage DR-related phenotypes. Moreover, although the introduction of anti-VEGF antibody treatment ameliorated STZ-induced vascular changes, it had no impact on STZ-mediated retinal function decline. In

contrast, anti-VEGF treatment in STZ-induced animals led to an additional decline in retinal function. This aligns with previous research highlighting VEGF's role as a neurotrophic factor,[14,15] and with research presenting that inhibition of VEGF with anti-VEGF therapies can result in significant retinal neurodegeneration in diabetic animals.[16,17] However, a key limitation in our STZ-induced Brown Norway study was a lack of IgG control and a non-treated STZ control group, which would have ensured that the observed effects were directly attributable to the anti-VEGF antibody and STZ, respectively, rather than other experimental variables. Modeling the late-stage DR-related pathology is crucial for the development of novel therapeutic strategies. Consequently, our next aim was to develop a novel rat model that mimics both early and late-stage complications observed in DR. To achieve this, we have decided to use inducible system that offers titratable and finely tuned control over gene expression. Specifically, we utilized a cumate-inducible lentiviral vector, which allows controlled expression of VEGF-A upon exposure of cumate (Chapter 4). While the cumate-inducible gene expression system has shown promise across various cell lines,[18–20] it has not yet been applied in ophthalmic research. Therefore, first, we tested cumate-inducible LV mediating VEGF-A expression on ARPE-19 cells. Although ARPE-19 cells are not directly relevant to the clinical manifestation of diabetic retinopathy, our findings demonstrated that VEGF-A expression can be successfully induced using the cumate-inducible system, and that the produced VEGF-A is biologically active. This system offers advantages over other inducible platforms, such as rapamycin-inducible system,[21] light-sensitive system,[22] and the tetracycline system,[23] which face limitations like metabolic disruption,[24] oxidative stress,[25,26] and leaky expression without inducers.[27] Furthermore, our findings suggest that the cumate-inducible system could be valuable for studying other ocular conditions, like age-related macular degeneration, where upregulated VEGF-A expression in RPE cells contributes to the development of choroidal

neovascularization.[28,29] However, in this study as well, a key limitation was the absence of both a negative control and a no-treatment group, ensuring that any observed effects are specifically due to LV mediated VEGF-A expression and not to other experimental variables. Taken together, these results suggest that cumate-inducible LV-mediated VEGF-A expression could be valuable in preclinical cellular drug discovery studies targeting VEGF-A related pathways. Future work may include the development of stably expressing cell lines, wherein VEGF-A expression could be titratable by adjusting the concentrations of cumate.

While cumate is generally considered as non-toxic molecule,[30,31] our animal experiments provide strong evidence that even low doses of cumate exert a toxic effect and induce retinal degeneration in Wistar rats. Like our *in vitro* studies, other investigations have also reported no cellular toxicity associated with the cumate-inducible system.[18,20,32] However, a study by Park et al.[30] observed cell toxicity in cumate-GFP-transduced quail cells, although this was not the case in chicken cells. Interestingly, research by Azed et al.[33] demonstrated that oral administration of cumate is safe and feasible. However, it remains unclear whether cumate can effectively cross the blood-retinal barrier in our study, which is crucial for transgene expression in the retina. We might consider administering lower concentrations of cumate, however, this approach would likely necessitate multiple low-dose intravitreal injections to achieve the required transgene expression. This cumate toxicity in rat eyes could be attributed to various factors, including potential disruptions in cellular homeostasis and complex interactions with specific retinal components. Nonetheless, recognizing that the use of cumate-inducible LV is not a feasible approach to model DR *in vivo,* our focus shifted towards adeno-associated virus vectors.

Although the AAVs we chose do not allow control over transgene expression via an inducer, we selected them for their well-known long-term transgene expression, low pathogenicity, and the confirmation of their effectiveness and safety in previous *in vivo* studies.[34–36] Our approach was further informed by the study of Weigelt et al., which found that AAV-mediated expression of human VEGF-A in the murine retina resulted in late-stage DR related phenotypes. However, their analysis was limited to retinal function assessment and did not evaluate anti-VEGF-A interventions, allowing us to expand upon their findings.

Our AAV-based VEGF rat model resembles several DR-related features, including retinal angiogenesis, vascular leakage, retinal edema, functional impairment, and inflammatory responses. These effects were partially ameliorated by the administration of aflibercept (Eylea®). Our model presents several advantages over existing DR animal models. While neovascularization, a hallmark of proliferative DR, was observed in our AAV-based VEGF rat model, it is often either absent in other diabetic models or confirmed using methods that lack reliability.[13,37–39] Additionally, our AAV-VEGF model demonstrated neovascularization in the inner rat retina, closely resembling human DR, rather than the outer retina or choroid, as typically observed in transgenic mouse models.[40–42] Moreover, our approach of delivering AAV-VEGF via intravitreal injection, as opposed to subretinal injection utilized in other AAV-based models,[43,44] facilitated inner retinal neovascularization, rather than new blood vessel formation in outer retinal layers. Additionally, compared to the study by Weigelt et al.,[45] which reported late-stage DR phenotypes resulting from AAV-mediated expression of human VEGF-A in murine retinas, our work expands on their findings by assessing retinal function and evaluating the efficacy of anti-VEGF-A interventions in AAV-VEGF-induced rats.

However, while our AAV-based DR rat model recapitulates several pathological features of DR, it is important to acknowledge its limitations. Firstly, the retinal swelling and vascular leakage induced by AAV-hVEGF were significantly reduced by six weeks post-administration. This contrasts with findings from other studies that report prolonged transgene expression lasting over two months[35] or even twenty months.[36] In our study, the diminished vascular leakage six weeks after AAV administration could potentially be attributed to several factors, including a decline in AAV-induced gene expression, the onset of adaptive immune responses, or the influence of endogenously regulated factors. Secondly, AAV-hVEGF administration resulted in variable DR-related phenotypes within the same group of animals with some rats exhibiting mild to moderate vascular changes, while others showing severe ones. This phenotypic variability, observed through FA imaging, corresponded to differing levels of *Vegf-a* mRNA expression in the retinal tissue. The variability might be attributed to the distribution of intravitreally injected AAV vectors across the retina or differences in individual immune responses to the injected AAVs. To address these limitations in our future investigations, we aim to explore methods to enhance the consistency of transgene expression and reduce phenotypic variability. This may involve optimizing AAV-hVEGF dosages, monitoring AAV distribution throughout the retina, and investigating inflammatory responses in rats. Finally, similarly to other VEGF models, our AAV-hVEGF-induced rats are not hyperglycaemic, limiting our insights into the sequence of events leading to VEGF upregulation in diabetic retinopathy. Therefore, future studies will also focus on testing inducible VEGF-A overexpression in Müller cells within a diabetic context to better reflect DR pathology. By addressing these limitations and refining our model, we hope to enhance its utility for studying the mechanisms underlying DR and evaluating potential therapeutic interventions more effectively.

6.2 Conclusions

The findings described in this thesis explore the prevalent STZ-induced DR animal model and successfully culminate in the development of a novel rat model replicating the main pathophysiological features of DR. The newly established easy-to-use AAV-induced rat model recapitulates several DR-related phenotypes and serves as an attractive tool to gain valuable insights into the underlying molecular mechanisms of DR pathologies and for testing novel therapeutic strategies.

6.3 References

1. Clermont AC, Murugesan N, Aiello LP. Vascular endothelial growth factor (VEGF) induces retinal edema and neuroretinal dysfunction in diabetic rats. Investigative Ophthalmology & Visual Science. 2020 Jun 10;61(7):1385.

2. Han Z, Guo J, Conley SM, Naash MI. Retinal Angiogenesis in the Ins2Akita Mouse Model of Diabetic Retinopathy. Invest Ophthalmol Vis Sci. 2013 Jan;54(1):574–84.

3. Hombrebueno JR, Chen M, Penalva RG, Xu H. Loss of synaptic connectivity, particularly in second order neurons is a key feature of diabetic retinal neuropathy in the Ins2Akita mouse. PLoS One. 2014;9(5):e97970.

4. Gaucher D, Chiappore JA, Pâques M, Simonutti M, Boitard C, Sahel JA, et al. Microglial changes occur without neural cell death in diabetic retinopathy. Vision Research. 2007 Mar 1;47(5):612–23.

5. Genrikhs EE, Stelmashook EV, Golyshev SA, Aleksandrova OP, Isaev NK. Streptozotocin causes neurotoxic effect in cultured cerebellar granule neurons. Brain Res Bull. 2017 Apr;130:90–4.

6. Shoham S, Bejar C, Kovalev E, Weinstock M. Intracerebroventricular injection of streptozotocin causes neurotoxicity to myelin that contributes to spatial memory deficits in rats. Exp Neurol. 2003 Dec;184(2):1043–52.

7. Percie du Sert N, Ahluwalia A, Alam S, Avey MT, Baker M, Browne WJ, et al. Reporting animal research: Explanation and elaboration for the ARRIVE guidelines 2.0. PLoS Biol. 2020 Jul;18(7):e3000411.

8. Percie du Sert N, Hurst V, Ahluwalia A, Alam S, Avey MT, Baker M, et al. The ARRIVE guidelines 2.0: Updated guidelines for reporting animal research. PLoS Biol. 2020 Jul;18(7):e3000410.

9. Ishibazawa A, Nagaoka T, Yokota H, Takahashi A, Omae T, Song YS, et al. Characteristics of Retinal Neovascularization in Proliferative Diabetic Retinopathy Imaged by Optical Coherence Tomography Angiography. Investigative Ophthalmology & Visual Science. 2016 Nov 16;57(14):6247–55.

10. Josifova T, Plestina-Borjan I, Henrich PB. Proliferative diabetic retinopathy: predictive and preventive measures at hypoxia induced retinal changes. EPMA J. 2010 Mar;1(1):73–7.

11. Naderi A, Zahed R, Aghajanpour L, Amoli FA, Lashay A. Long term features of diabetic retinopathy in streptozotocin-induced diabetic Wistar rats. Exp Eye Res. 2019 Jul;184:213–20.

12. Liu G, Chen L, Cai Q, Wu H, Chen Z, Zhang X, et al. Streptozotocin-induced diabetic mice exhibit reduced experimental choroidal neovascularization but not corneal neovascularization. Mol Med Rep. 2018 Nov;18(5):4388–98.

13. Jiang N, Chen XL, Yang HW, Ma YR. Effects of nuclear factor κB expression on retinal neovascularization and apoptosis in a diabetic retinopathy rat model. Int J Ophthalmol. 2015 Jun 18;8(3):448–52.

14. Froger N, Matonti F, Roubeix C, Forster V, Ivkovic I, Brunel N, et al. VEGF is an autocrine/paracrine neuroprotective factor for injured retinal ganglion neurons. Sci Rep. 2020 Jul 24;10(1):12409.

15. Martínez-Vacas A, Di Pierdomenico J, Gómez-Ramirez AM, Vidal-Sanz M, Villegas-Pérez MP, García-Ayuso D. Dose-Related Side Effects of Intravitreal Injections of Humanized Anti-Vascular Endothelial Growth Factor in Rats: Glial Cell Reactivity and Retinal Ganglion Cell Loss. Investigative Ophthalmology & Visual Science. 2024 Apr 4;65(4):10.

16. Park HYL, Kim JH, Park CK. Neuronal Cell Death in the Inner Retina and the Influence of Vascular Endothelial Growth Factor Inhibition in a Diabetic Rat Model. The American Journal of Pathology. 2014 Jun 1;184(6):1752–62.

17. Hombrebueno JR, Ali IH, Xu H, Chen M. Sustained intraocular VEGF neutralization results in retinal neurodegeneration in the Ins2Akita diabetic mouse. Sci Rep. 2015 Dec 16;5(1):18316.

18. Mullick A, Xu Y, Warren R, Koutroumanis M, Guilbault C, Broussau S, et al. The cumate gene-switch: a system for regulated expression in mammalian cells. BMC Biotechnology. 2006 Nov 3;6(1):43.

19. Poulain A, Perret S, Malenfant F, Mullick A, Massie B, Durocher Y. Rapid protein production from stable CHO cell pools using plasmid vector and the cumate gene-switch. Journal of Biotechnology. 2017 Aug 10;255:16–27.

20. Choi JS, Kim K, Lee DH, Cho S, Ha JD, Park BC, et al. cIAPs promote the proteasomal degradation of mutant SOD1 linked to familial amyotrophic lateral sclerosis. Biochemical and Biophysical Research Communications. 2016 Nov 18;480(3):422–8.

21. Rivera VM, Clackson T, Natesan S, Pollock R, Amara JF, Keenan T, et al. A humanized system for pharmacologic control of gene expression. Nat Med. 1996 Sep;2(9):1028–32.

22. Yamada M, Suzuki Y, Nagasaki SC, Okuno H, Imayoshi I. Light Control of the Tet Gene Expression System in Mammalian Cells. Cell Rep. 2018 Oct 9;25(2):487-500.e6.

23. Gossen M, Bujard H. Tight control of gene expression in mammalian cells by tetracycline-responsive promoters. Proc Natl Acad Sci U S A. 1992 Jun 15;89(12):5547–51.

24. Abu-Remaileh M, Wyant GA, Kim C, Laqtom NN, Abbasi M, Chan SH, et al. Lysosomal metabolomics reveals V-ATPase- and mTOR-dependent regulation of amino acid efflux from lysosomes. Science. 2017 Nov 10;358(6364):807–13.

25. Nakashima Y, Ohta S, Wolf AM. Blue light-induced oxidative stress in live skin. Free Radic Biol Med. 2017 Jul;108:300–10.

26. Lee JB, Kim SH, Lee SC, Kim HG, Ahn HG, Li Z, et al. Blue light-induced oxidative stress in human corneal epithelial cells: protective effects of ethanol extracts of various medicinal plant mixtures. Invest Ophthalmol Vis Sci. 2014 Jun 12;55(7):4119–27.

27. Costello A, Lao NT, Gallagher C, Capella Roca B, Julius LAN, Suda S, et al. Leaky Expression of the TET-On System Hinders Control of Endogenous miRNA Abundance. Biotechnol J. 2019 Mar;14(3):e1800219.

28. Wang H, Han X, Wittchen ES, Hartnett ME. TNF-α mediates choroidal neovascularization by upregulating VEGF expression in RPE through ROS-dependent β-catenin activation. Mol Vis. 2016;22:116–28.

29. Spilsbury K, Garrett KL, Shen WY, Constable IJ, Rakoczy PE. Overexpression of vascular endothelial growth factor (VEGF) in the retinal pigment epithelium leads to the development of choroidal neovascularization. Am J Pathol. 2000 Jul;157(1):135–44.

30. Park TS, Kim SW, Lee JH. Efficient transgene expression system using a cumate-inducible promoter and Cre-loxP recombination in avian cells. Asian-Australas J Anim Sci. 2017 Jun;30(6):886–92.

31. Yuan S, Zhang R, Cao Y, Guo J, Xian M, Liu W. New expression system to increase the yield of phloroglucinol. Biotechnology & Biotechnological Equipment. 2020 Jan 1;34(1):405–12.

32. Qi Z, Wilkinson MN, Chen X, Sankararaman S, Mayhew D, Mitra RD. An optimized, broadly applicable piggyBac transposon induction system. Nucleic Acids Res. 2017 Apr 20;45(7):e55.

33. Azad T, Rezaei R, Singaravelu R, Pelin A, Boulton S, Petryk J, et al. Synthetic virology approaches to improve the safety and efficacy of oncolytic virus therapies. Nat Commun. 2023 May 26;14(1):3035.

34. Ail D, Malki H, Zin EA, Dalkara D. Adeno-Associated Virus (AAV) - Based Gene Therapies for Retinal Diseases: Where are We? Appl Clin Genet. 2023 May 30;16:111–30.

35. Liu S, Biesemeier AK, Tschulakow AV, Thakkar HV, Julien-Schraermeyer S, Schraermeyer U. A new rat model of treatment-naive quiescent choroidal neovascularization induced by human VEGF165 overexpression. Biol Open. 2020 Jun 11;9(6):bio048736.

36. Wang F, Rendahl KG, Manning WC, Quiroz D, Coyne M, Miller SS. AAV-Mediated Expression of Vascular Endothelial Growth Factor Induces Choroidal Neovascularization in Rat. Investigative Ophthalmology & Visual Science. 2003 Feb 1;44(2):781–90.

37. Barber AJ, Antonetti DA, Kern TS, Reiter CEN, Soans RS, Krady JK, et al. The Ins2Akita Mouse as a Model of Early Retinal Complications in Diabetes. Investigative Ophthalmology & Visual Science. 2005 Jun 1;46(6):2210–8.

38. Su L, Ji J, Bian J, Fu Y, Ge Y, Yuan Z. Tacrolimus (FK506) prevents early retinal neovascularization in streptozotocin-induced diabetic mice. Int Immunopharmacol. 2012 Dec;14(4):606–12.

39. Feit-Leichman RA, Kinouchi R, Takeda M, Fan Z, Mohr S, Kern TS, et al. Vascular damage in a mouse model of diabetic retinopathy: relation to neuronal and glial changes. Invest Ophthalmol Vis Sci. 2005 Nov;46(11):4281–7.

40. Okamoto N, Tobe T, Hackett SF, Ozaki H, Vinores MA, LaRochelle W, et al. Transgenic mice with increased expression of vascular endothelial growth factor in the retina: a new model of intraretinal and subretinal neovascularization. Am J Pathol. 1997 Jul;151(1):281–91.

41. Ohno-Matsui K, Hirose A, Yamamoto S, Saikia J, Okamoto N, Gehlbach P, et al. Inducible Expression of Vascular Endothelial Growth Factor in Adult Mice Causes Severe Proliferative Retinopathy and Retinal Detachment. Am J Pathol. 2002 Feb;160(2):711–9.

42. Rakoczy EP, Rahman ISA, Binz N, Li CR, Vagaja NN, de Pinho M, et al. Characterization of a Mouse Model of Hyperglycemia and Retinal Neovascularization. Am J Pathol. 2010 Nov;177(5):2659–70.

43. Rakoczy PE, Brankov M, Fonceca A, Zaknich T, Rae BC, Lai CM. Enhanced Recombinant Adeno-Associated Virus-Mediated Vascular Endothelial Growth Factor Expression in the Adult Mouse Retina: A Potential Model for Diabetic Retinopathy. Diabetes. 2003 Mar 1;52(3):857–63.

44. Lebherz C, Maguire AM, Auricchio A, Tang W, Aleman TS, Wei Z, et al. Nonhuman Primate Models for Diabetic Ocular Neovascularization Using AAV2-Mediated Overexpression of Vascular Endothelial Growth Factor. Diabetes. 2005 Apr 1;54(4):1141–9.

45. Weigelt CM, Fuchs H, Schönberger T, Stierstorfer B, Strobel B, Lamla T, et al. AAV-Mediated Expression of Human VEGF, TNF-α, and IL-6 Induces Retinal Pathology in Mice. Transl Vis Sci Technol. 2021 Sep 14;10(11):15.